THE UNIVERSITY *of* EDINBURGH

This thesis has been submitted in fulfilment of the requirements for a postgraduate degree (e.g. PhD, MPhil, DClinPsychol) at the University of Edinburgh. Please note the following terms and conditions of use:

- This work is protected by copyright and other intellectual property rights, which are retained by the thesis author, unless otherwise stated.
- A copy can be downloaded for personal non-commercial research or study, without prior permission or charge.
- This thesis cannot be reproduced or quoted extensively from without first obtaining permission in writing from the author.
- The content must not be changed in any way or sold commercially in any format or medium without the formal permission of the author.
- When referring to this work, full bibliographic details including the author, title, awarding institution and date of the thesis must be given.

Inhibition of protein-peptide interactions by small molecules

A thesis

Submitted for the Degree of

Doctor of Philosophy

by

Li-Hsuan Yen, Msc (Bsc)

Structural Biochemistry Group

Institute of Structural and Molecular Biology

School of Biological Sciences

University of Edinburgh

Scotland

United Kingdom

April 2014

Abstract

In all kinds of disease models, many proteins involved in protein-protein interactions (PPIs) are mutated and do not function properly. The important role of PPIs in disease makes the design of small molecule inhibition an interesting proposition. This project looks at mouse double minute 2 (MDM2) and mouse double minute X (MDMX) which binds and inhibits the tumour suppressor protein p53. MDM2 and MDMX are therefore attractive therapeutic targets due to their role in tumour progression. The aim is to identify small molecule dual inhibitors that are able to disrupt MDM2 and MDMX from binding to p53.

Both N-terminal MDM2 and MDMX were successfully expressed and purified with high purity and decent yield. These proteins were used to develop Fluoresence Polarization (FP) and Capillary Electrophoresis (CE) assays for small molecule inhibitors screening. This work has successfully developed FP and CE assays for detecting weakly interacting fragments. The CE assay is a novel method for detecting weak fragments for protein-protein interactions, which are a challenging target.

Two approaches were employed to identify small molecule inhibitors for MDM2-N/p53 interaction. At first, small molecules were identified using *in silico* screening and these hits were verified using FP and CE assays. Second, analogue exploration was applied to identify fragments from the small molecule inhibitors discovered from the *in silico* screening.

Diphenylamine and oxindole fragments were identified as the most potent. However, diphenylamine fragment was discovered to aggregate MDM2-N and was ranked as a false positive hit. No protein aggregation was found when incubated with the oxindole fragment. Therefore oxindole can provide a good starting point for the design of higher affinity analogues.

Studying the interaction of MDMX has only recently been undertaken. MDMX contains a high homology binding site with MDM2. Hence, developing a dual MDM2/MDMX inhibitor has become an attractive target to focus on. FP and CE assays were developed to screen compounds against MDMX-N. *In silico* screening against MDM2-N and MDMX-N found several hits. One compound was discovered as a dual binder to MDM2-N and MDMX-N with low μM affinity. This novel hit is potentially a good starting point for the design of higher affinity analogues.

Declaration

The work presented in this thesis is the original work of the author. This thesis has been composed by the author and has not been submitted in whole or in part for any other degree.

Li-Hsuan Yen

Acknowledgements

I would like to thank my first supervisor Professor Malcolm D. Walkinshaw for providing me with the degree of Doctoral of Philosophy and his kind support, encouragement and advices. I would like to thank all the members on the Swann third floor, in particular Sandra Bruce, Dr. Matthew Nowicki, Dr. Martin Wear and Simon Varzandeh.

Beside my supervisor, I would like to thank Dr. Paul Taylor and Dr. Sander Granneman to be in my PhD committee and giving ideas and supports.

A special thanks to Professor Kathryn Ball and Dr. Maria Concepcion Sanchez Perez for the full length MDM2, MDMX and the N-terminal domain of MDM2, MDMX constructs.

I was fortunate to be sponsored by Selcia as part of a BBSRC CASE studentship. I would like to thank my industrial supervisors Dr. Carol Austin and Dr. Simon Pettit for their guidance and insightful advices. In addition, I would like to thank Dr. Martin Walker for his support, guidance and helping me with setting up the CE.

I thank Dr. Dallas Hughes, Dr. Yuriy Dunayevskiy, Dr. Alexy Korneev and Dr. Leonid Rashkovetsky from Selcia US for developing the MDM2/p53 CE protocols and answering my technical queries.

I would like to thank Sarah Martin for performing the solubility test on the compounds and I also like to thank everyone in the Selcia Biology department and Dr. Cyrille Landreau for their help during my visits in Selcia.

Lastly, I would like to thank my family for their support and encouragement during my studies.

Abbreviation list

ABC	Ammonium bicarbonate
ACE	Affinity capillary electrophoresis
ACN	Acetonitrile
ATM	Ataxia telangiectasia mutated
BSA	Bovine serum albumin
CE	Capillary Electrophoresis
CHCA	a-cyano-4-hydroxycinnamic acid
CODASS	COmbine Docking And Similarity Search
CPS	Counts per second
DLS	Dynamic Light Scattering
DMSO	Dimethyl sulfoxide
DNA	Deoxyribonucleic acid
DNA-PK	DNA dependent protein kinase
DTT	Dithiothreitol
E. coli	Escherichia coli
EDULISS	Edinburgh University Ligand Selection System
FAM	Fluorescein amidite
FBDD	Fragment Based Drug Discovery
FP	Fluorescence Polarization
HEPES	4-(2-hydroxyethyl)-1-piperazineethanesulfonic acid
IAA	Iodoacetamide
IC50	Half maximal inhibitory concentration
ITC	Isothermal Titration Calorimetry
IMAC	Immobilised Metal Affinity Chromatography
IPTG	Isopropyl β-D-1thiogalactopyranoside
Kd	Equilibrium dissociation constant
kDa	Kilodalton
Ki	Binding affinity of the inhibitor
LB	Luria-Bertani broth
LE	Ligand Efficiency
LIDAEUS	LIgand Discovery At Edinburgh UniverSity

LIF	Laser induce fluorescence
MALDI MS	Matrix Assisted Laser Desorption Ionization Mass Spectrometry
MDM2	Mouse double minute 2
MDMX	Mouse double minute X
NBS	Non-binding surface plate
NES	Nuclear export signal
NLS	Nuclear localisation signal
NMR	Nuclear magnetic resonance
P53-F	Fluorescently labelled p53 peptide
PCR	Polymerase chain reaction
PDB	Protein Data Bank
pI	Isoelectric point
PPI	Protein-protein interaction
PVA	Polyvinyl alcohol
RMSD	Root mean square deviation
RING	Really Interesting New Gene
SDS-PAGE	Sodium Dodecyl Sulphate-Polyacrylamide Gel Electrophoresis
SPR	Surface plasmon resonance
TAPS	N-tris(Hydroxymethyl)methyl-3-aminopropanesulfonic acid
TB	Terrific broth
TEV	Tobacco Etch Virus
UFSRAT	Ultra Fast Shape Recognition Atom Type

Table of Contents

Tables and Figures

Chapter 1 Introduction

1.1 The importance of protein-protein interactions (PPI)

Proteins are responsible for many biological systems in the cell. Some proteins perform their functions independently but most proteins perform their functions by interacting with others (Gadek and Nicholas, 2003, White et al., 2008). Many of the fundamental processes in cells are controlled by protein-protein interactions (PPI) which play key roles in the signal transduction pathway. **Figure 1.1** shows one part of the signal network driven by the protein-protein interaction to control cell proliferation and apoptosis.

Living cells are constantly exposed to signals from the environment. These signals are detected by receptors on cell surfaces which are processed and transduced through a signalling cascade. The proteins translocate in the cell through PPI (**Figure 1.1**) and uncontrolled protein-protein interactions may lead to diseases such as cancer. In cancer the oncogenic and tumour suppressor proteins are overexpressed and mutated respectively which leads to uncontrolled cell proliferation (Ivanov et al., 2013). Therefore the design of small molecules to inhibit specific protein-protein interactions has become a major focus of current biomedical and pharmaceutical research.

1.2 Challenges of designing small molecule inhibitors for protein-protein interactions

Designing a small molecule to bind to a protein-protein interaction site holds many challenges because naturally occurring small molecules that bind to PPI sites are rare, unlike enzymes which mostly have substrates that can be used as template for drug design. Peptide inhibitors are often used to target protein-protein interactions, however peptides are considered poor drug candidates due to the low oral bioavailability or short half-life. One possible starting point to design small molecules for a particular protein-protein interface is to create a small peptide from one of the proteins and understand the mode of binding. Another challenge of small molecule design for PPI is that the interaction sites are often flat with a large surface area which is many times larger than a small molecule, therefore making it difficult to develop high affinity

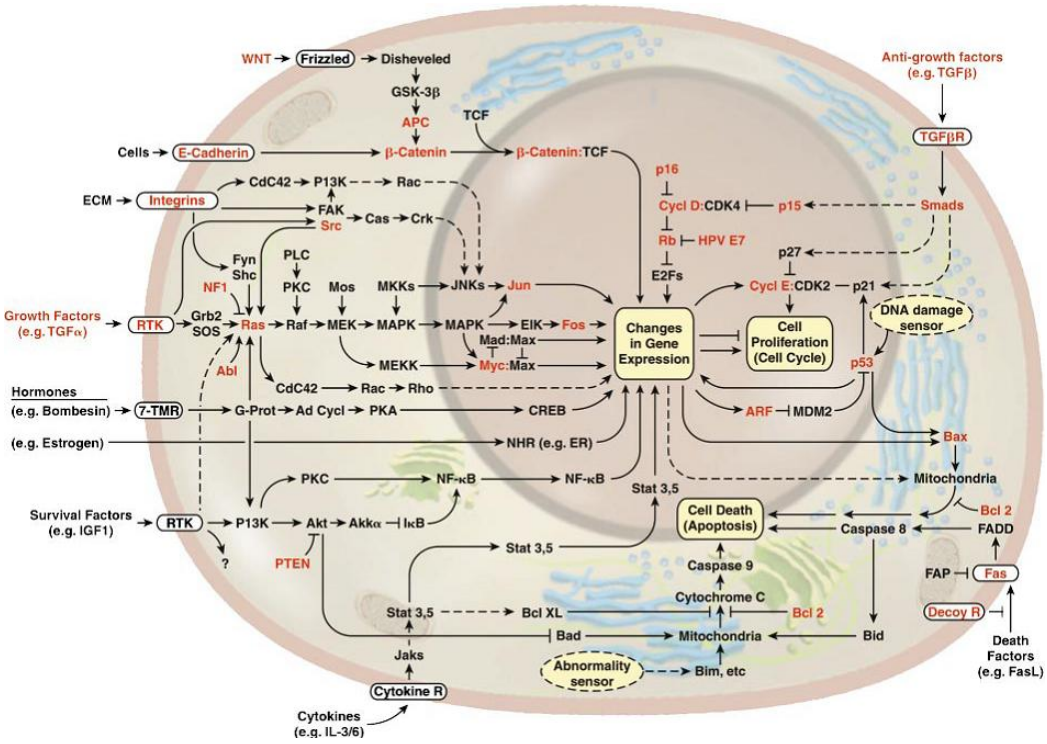

Figure 1.1 Signalling transduction pathways to control cell proliferation and apoptosis (Hanahan and Weinberg, 2000).

When a stress signal is detected the cell converts the signal from the environment and transports from the cell surface into the nucleus through protein-protein interactions.

inhibitors (Arkin and Wells, 2004, White et al., 2008). As well as the shallow interface the protein-protein interaction site commonly contains a deep hydrophobic groove. The inhibitor design often ended up with a large complex structure to fill up the whole PPI site which resulted in the inhibitors to be hydrophobic and insoluble (White et al., 2008). However, by combining X-ray crystallography with computer-aided drug discovery it is now possible to design small molecules to target the crucial interaction spots in the PPI site and generate high affinity inhibitors (**Table 1.1**). In **Table 1.1** these non-peptide inhibitors were discovered using different approaches. IL-2/IL-2α inhibitor was designed using combination of X-ray crystallography, NMR and structural activity studies (Tilley et al., 1997). LFA-1/ICAM, Bak-BH3/Bcl-x_L, MDM2/p53 and HIV1/CCR5 inhibitors were identified by high throughput screening from a diverse library of compounds (Vassilev et al., 2004, Alexei et al., 2001, Baba et al., 1999, Kelly et al., 1999).

	Target protein	Protein partner	Binding affinity	Reference	Methods of Identification
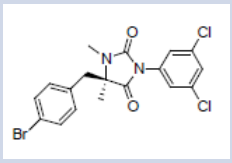	LFA-1	ICAM	Kd = 26nM	(Last-Barney et al., 2001)	HTS
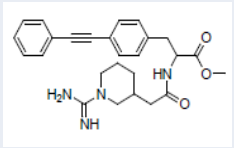	Interleukin-2 (IL-2)	IL-2 receptor α	IC_{50} = 3μM	(Braisted et al., 2003)	Combine crystallography, NMR and structural activity studies
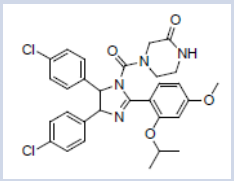	MDM2	p53	IC_{50} = 90nM	(Vassilev et al., 2004)	HTS
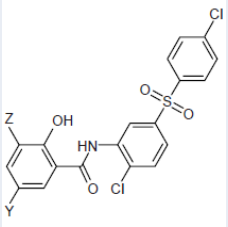	Bak-BH3	Bcl-x_L	Ki = 3.3μM	(Alexei et al., 2001)	HTS
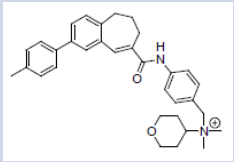	HIV1	CCR5	Ki = 1.1nM	(Baba et al., 1999)	HTS

Table 1.1 Examples of PPI inhibitors (Pagliaro et al., 2004).

The table shows some examples of small molecule inhibitors capable of inhibiting protein-protein interactions.

1.3 Fragment based drug design (FBDD)

Fragment based drug design is a new emerging approach for drug discovery (Hajduk and Greer, 2007). The method uses small molecular weight molecules (<250Da) to interact in the binding grooves. These fragments are more soluble and provide a good starting point for subsequent lead optimisation. FBDD is gradually used in developing inhibitors of PPIs because the hits identified from the conventional high throughput screening (HTS) often brings large and insoluble molecular weight molecules (> 400Da). Therefore FBDD provides a higher chance of finding soluble hits for optimisation. However these weak binding affinity fragments (μM to mM) require highly sensitive techniques in order to detect weak interactions (**Table 1.2**).

Capillary electrophoresis (CE) is one of the few techniques that is able to detect the weak fragment interaction (**Table 1.2**). **Table 1.2** shows the advantages and disadvantages of several techniques that were used in FBDD. CE possesses several advantages over other common techniques (SPR, NMR or ITC) such as there is no protein size limit and the protein does not need to be modified or tethered and the assay development time is relatively fast. CE is applicable for studying protein-protein and protein-ligand interactions and requires little sample consumption. It should be noted that occasionally false positive can occur when the protein is aggregated by the compounds and there are some techniques that are able to detect protein conformation change listed in **Table 1.2**.

Technique	Advantages	Disadvantages	Throughput
capillary electrophoresis (CE)	*solution phase *Fast assay development time *Low protein consumption *No protein size limit *Applicable to protein-protein interaction *Can obtain IC50 value *Label free technique	*Cannot determine on/off rate	medium
Microscale thermophoresis (MST)	*Solution phase *Label free and fluorescent machine avalaible *High salt tolerance *Can obtain IC50 value *Can be used for membrane proteins	*Label free not usable with PPI *Not automated *Cannot determine on/off rate	low
Surface plasmon resonance (SPR)	*High information binding data (on/off rates and stoichiometry of binding) *Low protein consumption *fast screening time *Can obtain Kd value *Automated	modified/tethered-may affect activity *High ligand concentrations can give high false positive *Protein size limit *Long assay development time *High instrument entry cost *Protein needs to be stable for days	medium
Nuclear magnetic resonance (NMR)	*Clear binding information/interaction with key residues obtained *No modification of protein required *Ligand and protein state monitored *Site localisation *Automated *Can detect protein conformation change	*High protein consumption *Protein size limit (<~30kDa) *Expensive instrumentation *Resource intensive - interpretation requires NMR expert Labelling of protein required	medium
X-ray crystallography	*Full site specific structural information *Screening of mixtures possible *No need for immobilising/labelling *Can obtain Kd value *Can detect protein conformation change	*soakable crystal form required: Not all target crystallise *Require specialist equipment. *Requires intensive time for data interpretation	low
Isothermal titration calorimetry (ITC)	*High information binding data (stoichiometry of binding, enthalpy/entropy driven binding *No need for immobilising/labelling *Can obtain Kd value *Can detect protein conformation change	*High protein consumption *Low automation throughput	low
Hydrogen/Deuterium exchange (H/D)	*Low protein consumption *Can detect protein conformation change	*Require specialist equipment. *Requires intensive time for data interpretation	low
FRET	*Can be used for HTS *Low sample consumption *Easily adapted to any intruments	*Must incorporate the distance of spacers and limit the range of fluorophores *Changing the environment can alter the fluorescent properties of the probe	high
Ramen spectroscopy	*Solution phase *Low sample consumption *No sample preparation needed *Ramen spectra are acquired quickly	*Sample heating through intense laser can destroy the sample	medium

Table 1.2 The advantages and disadvantages of the techniques that can be used in FBDD

1.3.1 Capillary electrophoresis for small molecule screening

In CE, electrophoresis is carried out in the interior of a narrow glass capillary. CE has the ability to separate ions based on their electrophoretic mobility with the use of the applied voltage. The electrophoretic mobility will be affected by the differences in the charge to size ratio of the analyte ion (Coulter, 1994). Therefore it is possible to separate mixtures of various ions by mass and charge ratio under the same electric field strength. Affinity capillary electrophoresis (ACE) is a technique that is used to monitor the migration patterns of the interacting molecules in the capillary and can be used in protein-ligand study (Austin et al., 2012). Hence CE was applied in this work to identify small molecule inhibitors to inhibit protein-protein interactions (See **Chapter 5**).

1.4 MDM2/p53 interaction as a promising cancer therapeutic target

1.4.1 The role of p53

Cell replication is carried out in an event called the cell cycle where the cell duplicates into two daughter cells. The cell cycle consists of four stages. During Gap 1 (G1) phase the cell grows and organises chromosomes ready for replication. This is followed by DNA duplication in the Synthesis (S) phase. The cell then prepares for mitosis in Gap 2 (G2) phase followed by the mitosis (M) phase in which the cell divides into two identical cells. During cell replication there are multiple checkpoint proteins that constantly monitor the replication process and ensure the fidelity of the replication. If the checkpoint detects damage then the cell cycle is postponed until the repairs are made or if the damage cannot be repaired then the activation of the p53 protein is triggered. p53 functions as a transcription factor that simultaneously activates proteins to inhibit the cell cycle progression and sequentially targets the cell for destruction via apoptosis (**Figure 1.2**). This protects cell populations from harbouring mutations and thus p53 has been recognised as “the guardian of the genome” (Lane, 1992).

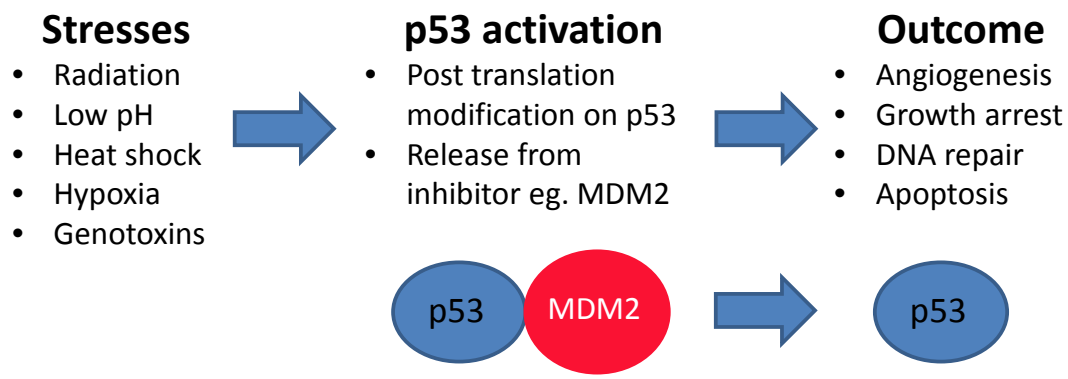

Figure 1.2 Activation of p53

In the cell p53 is activated upon stresses and various pathways will result in the release of p53 from the MDM2 binding. Activation of p53 leads to cell cycle arrest to repair damaged DNA or apoptosis to destroy the damaged cell.

The activity of p53 is tightly regulated by post translational modification and interaction with other proteins (Prives and Hall, 1999). It was shown that over 50% of cancers involved a mutation in the p53 gene in order to evade the p53 apoptotic and growth arrest activities and hence manifest its role as a tumour suppressor (Petitjean et al., 2007). Even when certain tumours retain wild type p53, it may also show mutations in other proteins that inhibit p53 activities (Oliner et al., 1992a).

Multiple studies have demonstrated that reactivation of the p53 protein is destructive to cancer cells and hence reactivation of p53 in cancer becomes an attractive therapeutic approach (Teodoro et al., 2007). There are studies showing that in some cancer models p53 has retained the wild type form but the activities have been inhibited by p53 degradation (Reifenberger et al., 1993) (See **section 1.9**).

Huge efforts have been put into restoring the p53 activities and one of these is the use of small molecules to inhibit MDM2 that has been known to be a major negative regulator of p53 (Zhao et al., 2013). MDM2 binds to the N-terminal domain of p53 in the cell and carries p53 to the proteasome (**Figure 1.4**). Recent research shows that MDM2 also contain another p53 binding site where the acidic domain of MDM2 interacts with the DNA binding domain of p53 (Hernychova et al., 2013). Hence the

instability of p53 is largely caused by MDM2 and results in p53 with a short life time in a normal cell (Vogelstein et al., 2000).

1.4.2 MDM2 regulates the tumour suppressor p53

MDM2 along with another two MDM genes were originally isolated from the transformed mouse cell line 3T3-DM (Cahilly-Snyder et al., 1987). MDM2 has been discovered to be amplified and overexpressed along with other oncogenes and is therefore associated with tumour progression. This supports the role of MDM2 as an oncogene. Transgenic mice overexpressing MDM2 demonstrated a 100% incidence of tumour formation with amplification in over one-third of osteosarcomas and other soft tissue sarcomas (Jones et al., 1998).

To determine the relationship of MDM2 with p53 in humans, a co-immunoprecipitation experiment was carried out on MDM2 with p53 and confirmed the formation of the MDM2-p53 complex (Oliner et al., 1992b).

Further studies have discovered that MDM2 is an E3 ubiquitin ligase and has been confirmed as a key regulator of the tumour suppressor p53 protein in the cell and responsible for p53 degradation (Momand et al., 1992).

Not only being responsible for the ubquitination of p53, MDM2 also disrupts p53 activity through binding to the N-terminal transactivation domain of p53 (Moll and Petrenko, 2003). In the stressed condition that leads to an increase of p53 level, p53 also induces the expression of MDM2 through an autoregulatory feedback loop and hence p53 in the cell is maintained at low levels (**Figure 1.4**). Through this autoregulatory loop MDM2 expression is also reduced to control its expression levels in the cell. The p53 protein activity and level in unstressed cells is regulated by the MDM2-ubiquitin-proteasome degradation pathway (Moll and Petrenko, 2003, Alarcon-Vargas and Ronai, 2002). MDM2 promotes p53 degradation through the E3 ligase function on the RING finger domain located at the C-terminal end of the protein. **Figure 1.3** shows the domain organisation of MDM2 and p53 and studies have shown that there are two interaction sites between MDM2 and p53. The first interaction site is at the hydrophobic site of MDM2 and the N-terminal transactivation domain of p53. The second interaction site is between the acid domain of MDM2 and the DNA binding domain of p53 (Hernychova et al., 2013).

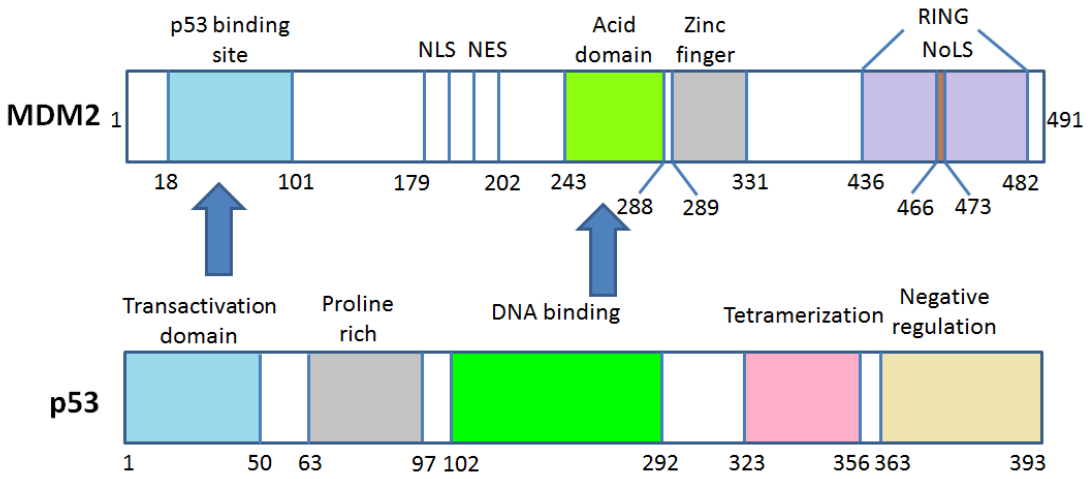

Figure 1.3 Domain structure of MDM2 and p53.

There are two interaction sites between MDM2 and p53 that are indicated using arrows and the domains are coloured in light blue and green in the structures.

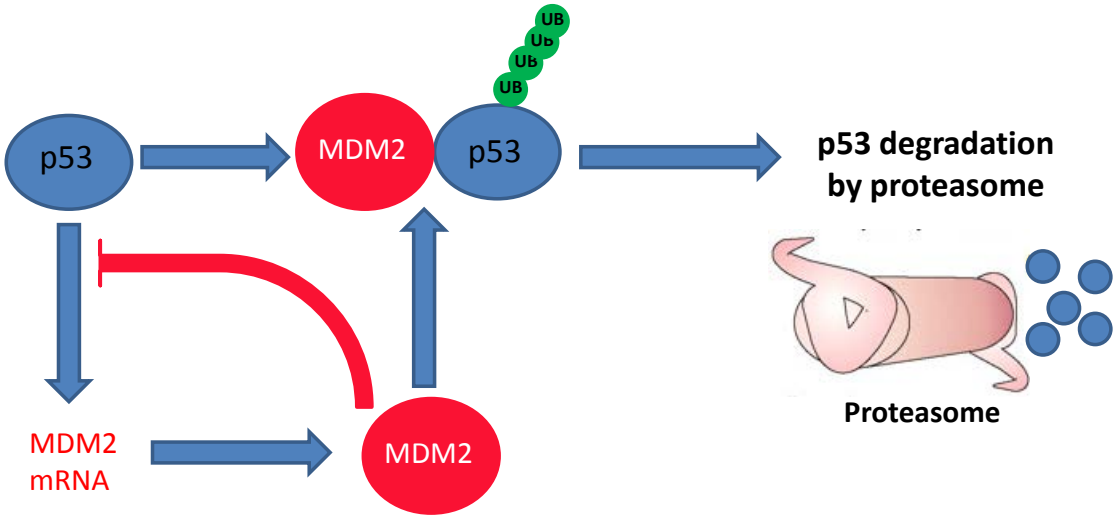

Figure 1.4 MDM2/p53 autoregulatory feedback loop

The levels of MDM2 and p53 in cells are regulated by the autoregulatory feedback loop. The increase in the level of p53 will also trigger the expression of MDM2 leading to p53 degradation in the proteasome.

1.5 Ligand and peptide binding induce MDM2-N conformational changes

There are many studies suggesting the presence of a 'lid' at the N-terminal domain of MDM2 that may be involved in controlling the stability of the MDM2-p53 complex (Shimizu and Hupp, 2003, Schon et al., 2004).

In 2005, Uhrinova S. et al. was able to solve the first apo-MDM2 structure using solution NMR and revealed the open conformation of the MDM2-lid (PDB structure 1Z1M) (Uhrinova et al., 2005). In the open conformation the lid moved outward from the hydrophobic pocket (**Figure 1.5 top**) to allow interaction with the p53 protein.

In 2008, Showalter S. A. et al. used NMR to demonstrate the difference in the lid state upon binding to p53 peptide and Nutlin-3. When MDM2 bound to the p53 peptide the lid is competed out from the cleft and becomes more dynamic (Showalter et al., 2008). Whereas when MDM2 bound to the Nutlin-3, the surface of the cleft is not fully occupied which allows the lid to interact and resulted in semi-closed state (Showalter et al., 2008).

The structure solved by Michelsen K. et al. (PDB structure 4HBM) was the first structure of MDM2-lid with ligand bound and the structure shows that in the presence of inhibitor piperidinones the lid closes the hydrophobic pocket by fitting over it (Michelsen et al., 2012). This conformationally flexible MDM2-lid is a highly ordered structural element which contains a β sheet (Thr10 – Thr16 (coloured yellow in **Figure 1.5 bottom**)) and β turn (Ser17 – Pro20). In the closed state the lid is stabilized using Thr16 to form a hydrogen bond with the imidazole functional group on His96.

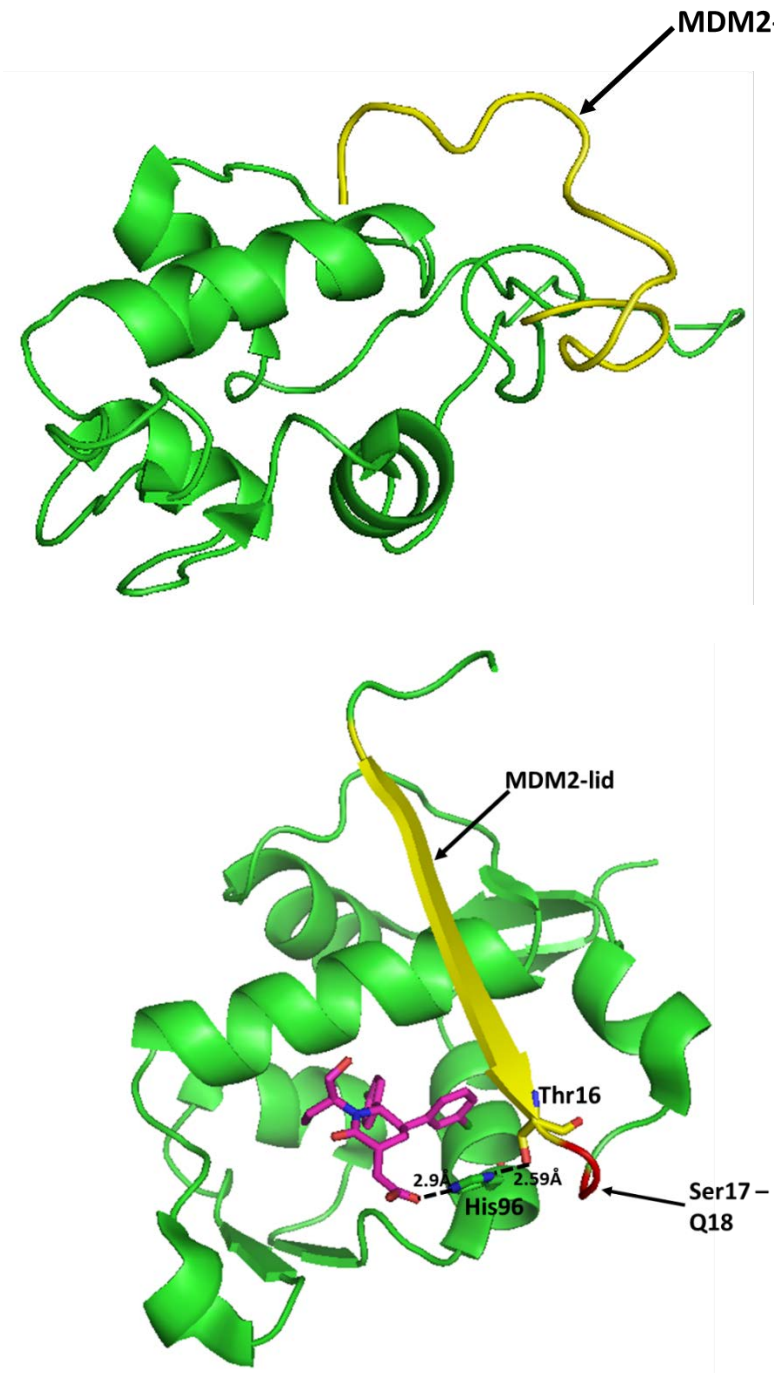

Figure 1.5 Structures of MDM2-lid

Top) NMR structure of MDM2-lid in open state (1Z1M). The lid is coloured in yellow which swings away from the binding site.

Bottom) The crystal structure of MDM2-lid with piperidinones inhibitor bound (4HBM). Piperidinones is shown as stick and coloured in pink while the lid is coloured in yellow. The lid covers the binding pocket and His96 residue has oriented for interaction with the lid. The phosphorylation site $S^{17}Q^{18}$ is coloured in red.

It was found that DNA dependent protein kinase (DNA-PK) and ataxia telangiectasia mutated (ATM) were involved in activating p53 pathway through phosphorylation of p53 causing release of the bound MDM2 (McCoy et al., 2003, Shimizu and Hupp, 2003). DNA-PK and ATM are both able to recognize and phosphorylate serine on the sequences that contain “SQ”.

The MDM2-lid contains a $S^{17}Q^{18}$ sequence at the β loop and phosphorylation of Ser17 causes a conformational shift of the lid towards the hydrophobic pocket (Shimizu and Hupp, 2003).

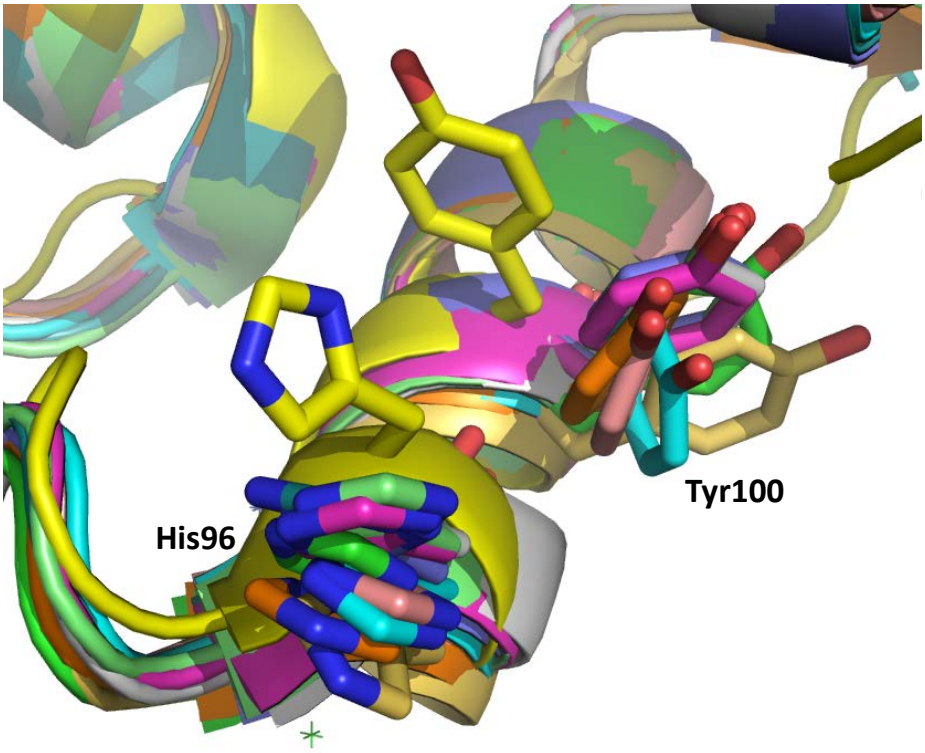

Figure 1.6 Position of MDM2 Tyr100

Apo-MDM2 structure is shown in yellow (1Z1M), MDM2 with piperidinones bound is shown in blue (4HBM), MDM2 with MI63 inhibitor (3LBL) is shown in green, MDM2 interaction with Nutlin-2 (1RV1) is shown in light blue, MDM2 with Nutlin-3a (4HG7) bound is shown in grey, MDM2 with benzodiazepine inhibitor (1T4E) is shown in magentas, MDM2 with central valine inhibitor (4DIJ) is shown in lime green, MDM2 bound with chlorobenzyl inhibitor (3TJ2) is shown in dark blue, MDM2 interaction with D-peptide (3IWY) is shown in tints, MDM2 interaction with stapled peptide (3V3B) is shown in orange and MDM2/p53 peptide complex is shown in pale yellow (1YCR). For clarity ligands are not shown in the figure.

In the apo-MDM2 structure (**Figure 1.6**) it has been discovered that the binding site is rather dynamic and flexible (Schon et al., 2004, Uhrinova et al., 2005). The binding site may undergo chemical shift upon binding to p53 peptide.

Certain residues in the binding site can be affected when the binding site is occupied. The conformation change of these residues can open or close the binding site. X-ray crystal structures also showed that Tyr100 may also pose as intermediate position upon binding to small molecules and peptide inhibitors (**Figure 1.6**). There are several papers suggesting that Tyr100 is flexible and can exist as a closed and open conformation (Uhrinova et al., 2005). When the different states of MDM2 structure are superimposed a clear positional difference can be seen in His96 and Tyr100 (**Figure 1.6**).

In the unbound structure (yellow in **Figure 1.6**) the residues His96 and Tyr100 are in a closed position where the side chains tilt into the binding site. In the presence of small molecule and peptide inhibitors the side chain of Tyr100 rotates outward by 6.4 – 7.5 Å and the side chain of His96 rotates outward by 3.8 – 4.9 Å (**Figure 1.6**).

Upon binding to p53 peptide (pale yellow in **Figure 1.6**) the side chain of Tyr100 rotates outward by 10 Å whereas the imidazole ring of His96 has tilted outward by 5 Å. In the presence of the ligand the side chain of Tyr100 and His96 becomes semi-open and tilted outward by 6 Å and 3 Å respectively. The imidazole ring of His96 also rotates by 90° to provide π-π interaction and hydrogen bond interaction with the ligand (**Figure 1.7**).

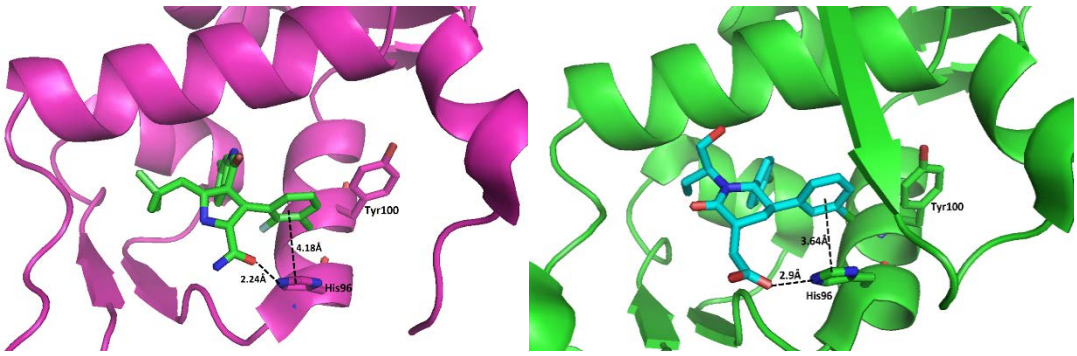

Figure 1.7 Side chain movement of His96 and Tyr100 in the presence of ligands

Left) MI63 ligand in the MDM2 binding site induces His96 and Tyr100 side chain movement (PDB structure of 3LBL).

Right) Piperidinones (light blue stick) interacts with MDM2 and induces side chain movement on His96 and Tyr100 (PDB structure 4HBM). Upon binding to piperidinones the lid move and sit beside the binding pocket.

1.6 MDM2 and MDMX coordinate to regulate p53 in the cell

Several studies have identified that MDM2 is not the only negative regulator to inhibit p53 tumor suppressor activity in both unstressed and cancer cells. MDMX (also known as MDM4) is a homolog of MDM2 which also binds to the N-terminal transactivation domain of p53 but it does not contain E3 ubquitin ligase function and the expression level is not p53 dependent. MDM2 contains 491 residues and MDMX contains 490 residues. They contain three well conserved regions: the p53 binding site at N-terminal domain (residues 18-101), a zinc finger domain (residues 289-331) and a RING domain (residues 436-482) (**Figure 1.8 bottom**).

The N-terminal domains of MDM2 and MDMX are structurally related with a high similarity of 54% and the amino acids required to interact with p53 are highly conserved.

MDM2 also contains a nuclear localisation signal (NLS) (residues 179-185) and nuclear export signal (NES) (residues 190-202) which is absent in MDMX. Therefore MDM2 is able to travel in between the nucleus and the cytoplasm. Through binding to p53 protein MDM2 exports p53 from nucleus into the cytoplasm for degradation.

MDMX however does not contain NLS and NES in the sequence and hence its subcellular localisation depends on the interaction with other proteins.

There is evidence to indicate that the RING domain at the C-termini of MDM2 and MDMX is essential for heterodimer and homodimer formation (Tanimura et al., 1999). Dimerization of MDM2-MDMX or MDM2-MDM2 is required for E3 ubiquitin ligase activity. There is no MDMX-MDMX homodimer found *in vitro* or *in vivo* studies which suggest that free MDMX may be monomeric or heterodimeric with MDM2 (Wade and Wahl, 2009). MDMX heterodimerization with MDM2 helps to stabilize MDM2 from auto-ubiquitination (Gu et al., 2002).

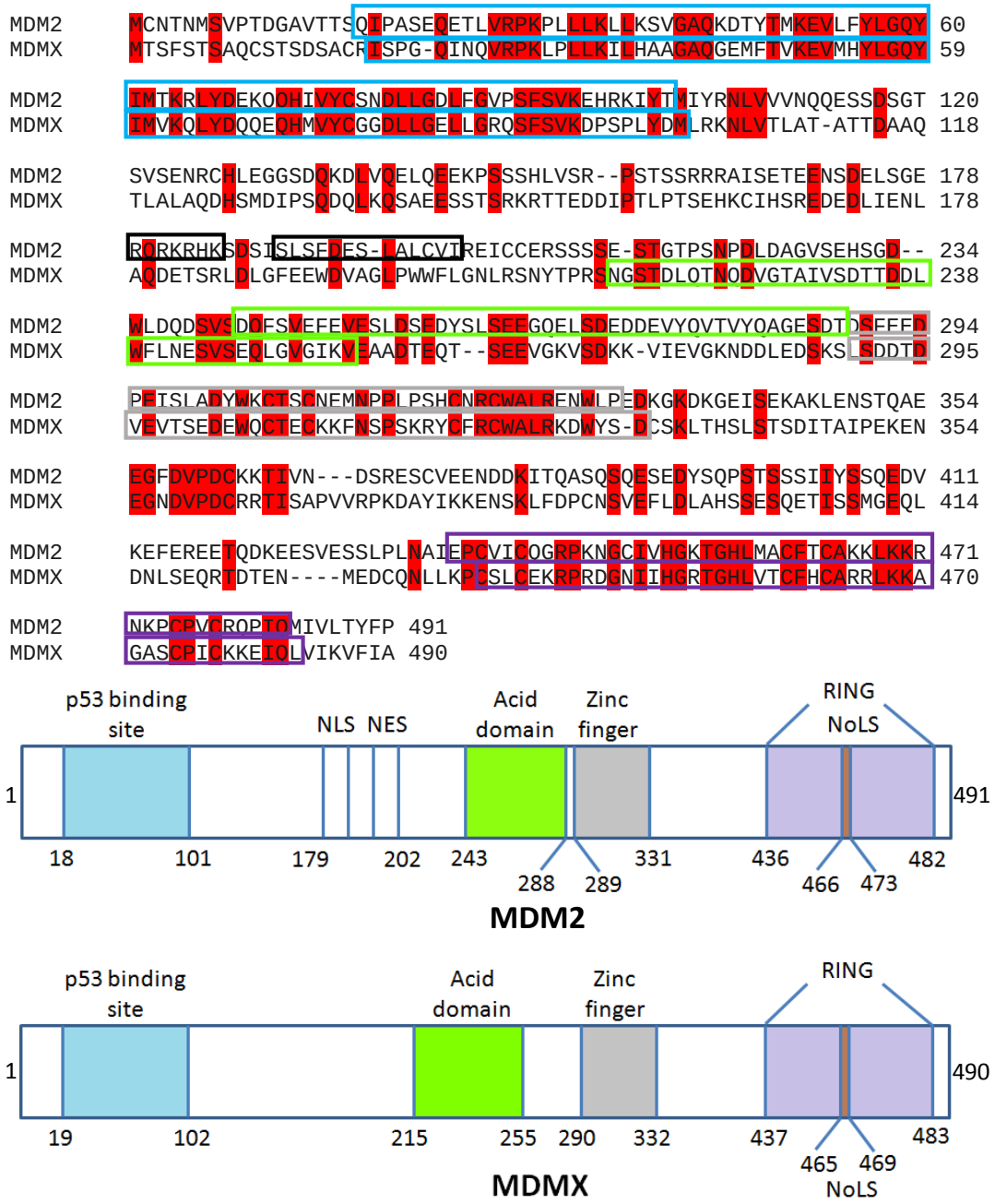

Figure 1.8 Sequence comparison of MDM2 and MDMX

Top) Sequence alignment on MDM2 and MDMX. The identical residues are highlighted in red. Most conserved residues are located at the N-terminal and C-terminal. The sequences of p53 binding site, Nuclear Localisation signal/Nuclear export signal, acid domain, zinc finger, Nucleolar localisation signal and RING domains are circled in light blue, black, green, grey, brown and purple respectively.

Bottom) Comparison of MDM2 and MDMX structure. High conserved regions of MDM2 and MDMX p53 binding site, Acid domain, Zinc finger, Nucleolar localisation signal and RING domains are coloured in light blue, green, grey, brown and purple respectively.

1.7 Structure of the N-terminal domain of MDM2

The N-terminal domain of MDM2 (MDM2-N) is the most studied because it is directly involved in the interaction with the p53 transactivation domain and inhibits its tumour suppressor activities. The crystal structure of the N-terminal domain of MDM2 solved by Kussie et al. confirmed MDM2-N can bind to the transactivation domain of p53 (Kussie et al., 1996). The crystal structure of the 109 residues of MDM2-N reveals two highly similar structure of portions that consist of two helices and two beta strands in each portion (**Figure 1.9 left**). Each portion contains a short α helix named α1, a long α helix, α2 and two β strand, β1 and β2. The other portion uses the apostrophe symbol to distinguish. The α1 and α1' helices sit antiparallel to each other at the bottom of the hydrophobic cleft while the α2 and α2' form the left and right side of the cleft (**Figure 1.9 right**).

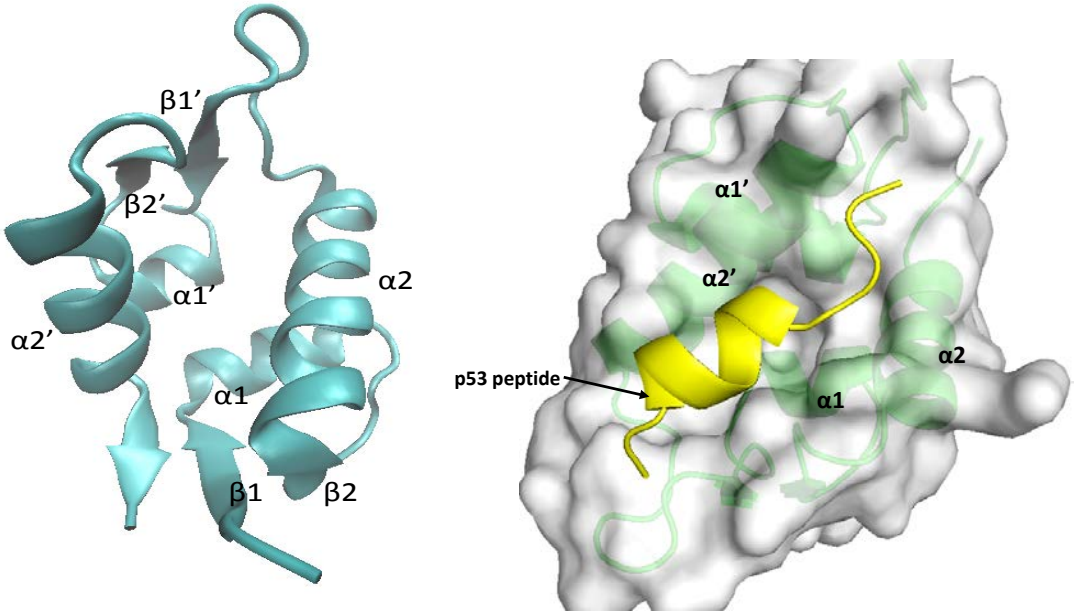

Figure 1.9 The structure of MDM2-N showing two highly similar portions

Left) The crystal structure of MDM2-N solved by Kussie et al. (PDB: 1YCR) is displayed in cartoon form (light blue colour). The second repeat of the α and β strands are distinguished using the apostrophe symbol. The picture is generated using VMD software (Humphrey et al., 1996).

Right) The structure of MDM2-N is displayed in surface form with 20% transparency (grey colour) and the secondary structure is displayed in green colour. The α helices have been labelled. The p53 peptide bound to the MDM2-N binding site is coloured in yellow. The picture was generated using PyMOL (Delano, 2002).

The sequence of MDM2-N is shown in **Figure 1.10 top** and the residues highlighted in grey are the residues that form the MDM2-N binding pocket. The sequence reveals that the binding site is mainly comprised of hydrophobic residues. A hydrophobicity surface generated using Discovery Studio 4.0 shows the binding site is highly hydrophobic; hydrophilic residues can be seen on the exterior of the pocket (**Figure 1.10 bottom**).

```
          10          20          30          40          50
SQIPASEQET LVRPKPLLLK LLKSVGAQKD TYTMKEVLFY LGQYIMTKRL
          60          70          80          90         100
YDEKQQHIVY CSNDLLGDLF GVPSFSVKEH RKIYTMIYRN LVVVNQQESS

DSGTSVSEN
```

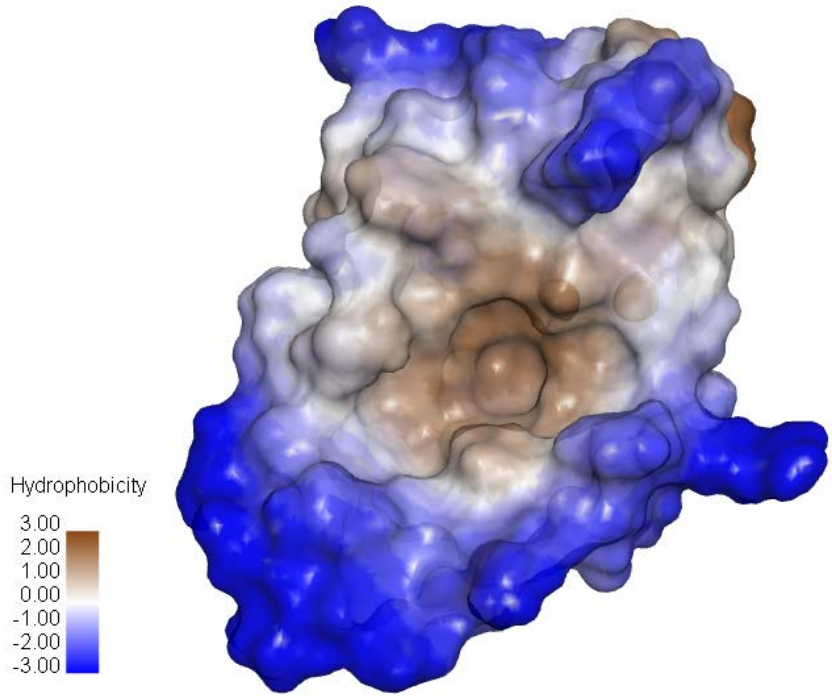

Figure 1.10 The hydrophobicity of MDM2-N binding site.

The hydrophobic binding site is formed by various hydrophobic residues. The hydrophobicity of the binding site is generated using Discovery Studio 4.0 (Accelrys, 2013). Brown colour is ranked as hydrophobic and blue colour is ranked as hydrophilic.

1.8 MDM2-N binds to a p53 helical stretch

The p53 peptide that binds to MDM2-N in the crystal structure is 13 residues long (residues 17 – 29) and fills the whole entrance of the binding site (**Figure 1.11**). The position of the p53 peptide allows the hydrophobic side chains of Phe19, Trp23 and Leu26 to insert deep into the hydrophobic pocket (**Figure 1.11**). The deepest hydrophobic groove lies in the middle accommodating the Trp23 side chain, whereas the Phe19 and Leu26 side chains bind into the other two shallower hydrophobic grooves on the flank.

Phe19 of p53 forms van der Waals interactions with Gly58 and Ile61 of MDM2-N while Trp23 forms van der Waals interaction with Phe86. The Leu26 of p53 also forms van der Waals interaction with Ile99. Additionally there are also tight hydrogen bond interactions present between the amide backbone of Phe19 of p53 with the oxygen atom of side chain Gln72 and the nitrogen atom of p53 side chain of Trp23 with the oxygen atom on the backbone carbonyl of Leu54. These three residues, Phe19, Trp23 and Leu26 are the three principle residues that contribute to the binding. The three hydrophobic grooves that are occupied by these residues are therefore named after these residues.

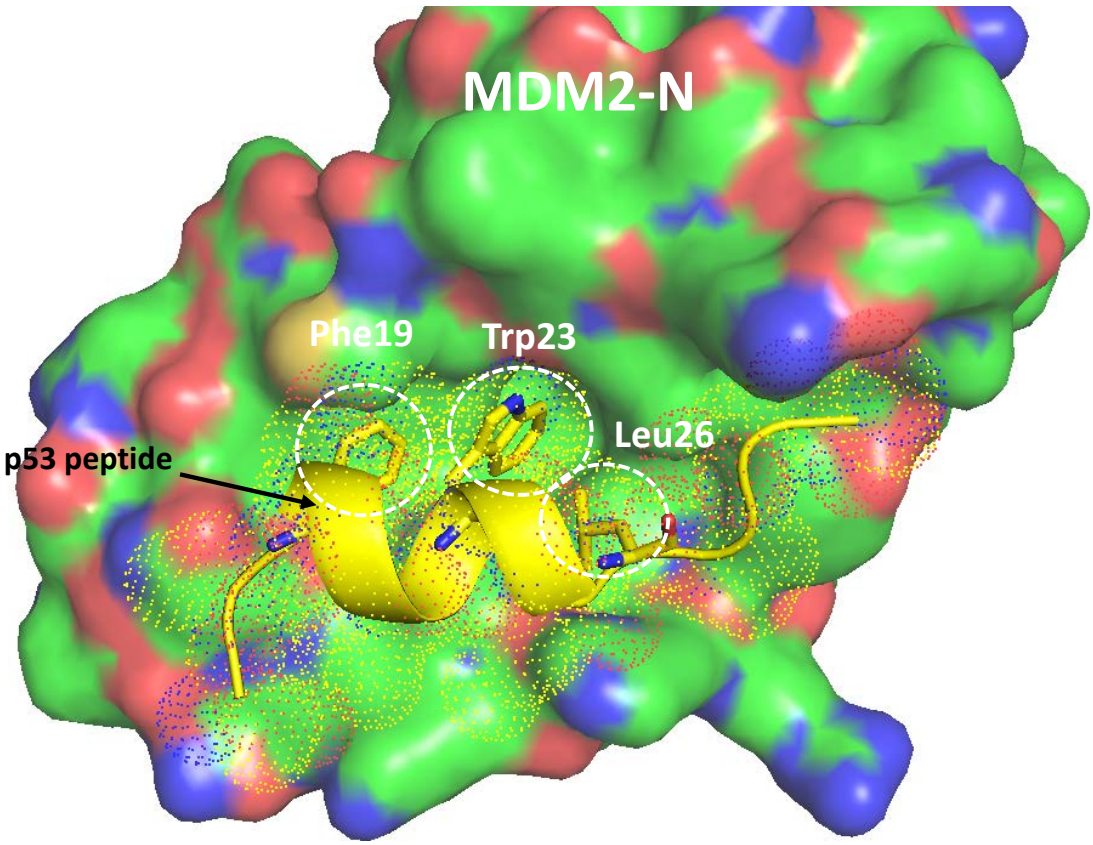

Figure 1.11 p53 peptide binds to the MDM2-N cleft.

The helix of p53 peptide[17-29] (coloured in yellow) binds to a deep MDM2-N hydrophobic pocket using Phe19, Trp23 and Leu26 residues. Dots are displayed for the p53 peptide to show that the peptide has filled up the pocket.

1.9 Drug discovery on disrupting the MDM2/p53 interaction

In the initial MDM2/p53 small molecule drug discovery the work focused on using known inhibitors with anti-tumour effects, however this was unsuccessful (Stoll et al., 2001).

The first crystal structure of p53 peptide interaction with MDM2 (1YCR) has unveiled a deep hydrophobic pocket in MDM2. More importantly the p53 peptide filled the three hydrophobic grooves in MDM2 using the side chains of Phe19, Trp23 and Leu26 residues (**Figure 1.12**). This provides a novel strategy for designing potent MDM2 inhibitors. Many known published inhibitors eg. Nutlin-3, Mi63, isoindolinones, benzodiazepinediones and WK298 mimic the binding of p53.

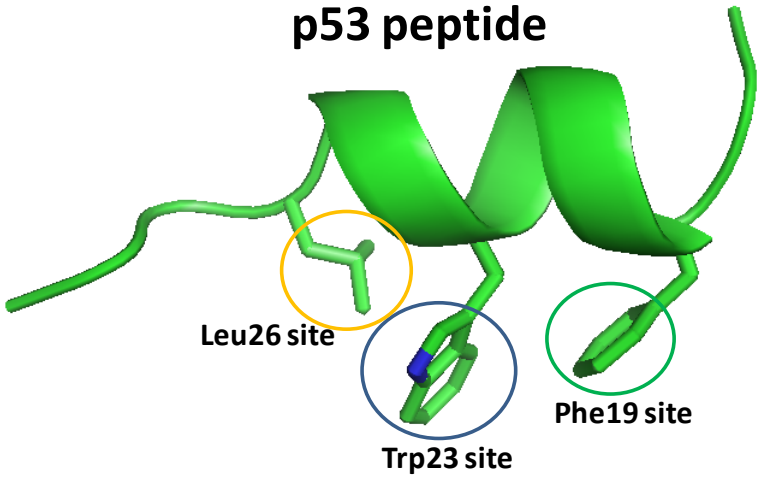

Figure 1.12 p53 peptide[17-29] uses three hydrophobic residues to interact with MDM2.

The helix of p53 peptide is displayed and the three residues that bind to the three hydrophobic pockets of MDM2-N are circled using yellow for the Leu26 site, blue for the Trp23 site and green for the Phe19 site.

1.9.1 Nutlin series

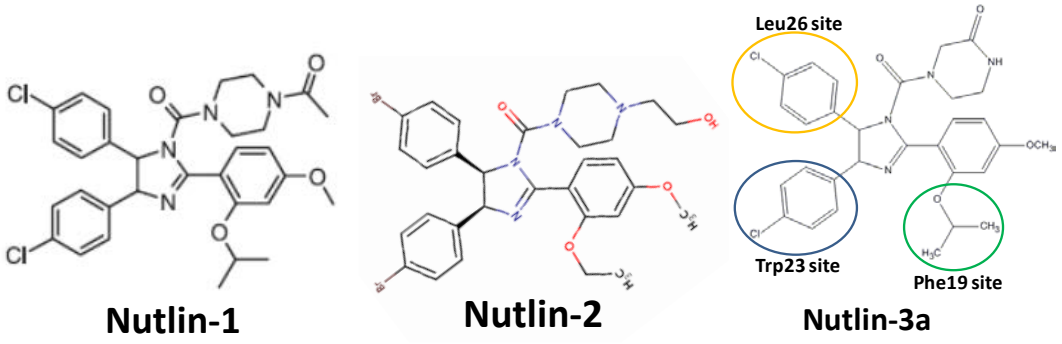

Figure 1.13 Chemical structures of Nutlin series

The structure of Nutlin1, Nutlin-2 and Nutlin-3a are displayed. The subgroups of Nutlin-3a that occupy the three hydrophobic sites are circled in different colours.

The Nutlin series is the most studied inhibitor of MDM2 and it was identified in high throughput screening (Vassilev et al., 2004). There are three analogues; Nutlin-1, Nutlin-2 and Nutlin-3, with IC_{50}s ranging from 100nM to 300nM and the most potent inhibitor for the Nutlin series is Nutlin-3a (**Figure 1.13**) with an IC_{50} of 90nM (Vassilev et al., 2004). The crystal structure of MDM2-Nutlin-2 complex (PDB structure: 1RV1) was the first inhibitor bound MDM2 structure available (Vassilev et al., 2004). Due to the flexible structure of MDM2 it was not until 2013 that a MDM2-Nutlin-3a complex was made (PDB structure: 4HG7) (Anil et al., 2013). Nutlin-3a contains an imidazoline group as the core to connect four hydrophobic groups and it is posed at the centre of the MDM2 binding site. In Nutlin-3a there are two 4-chlorobenzyl groups, the first 4-chlorobenzyl group inserts deep into the Trp23 pocket and the second 4-chlorobenzyl group fits into the Leu26 pocket. The chlorine atom on the 4-chlorobenzyl is positioned at the bottom of the Trp23 pocket which provides a tight interaction with the side chain residues in the pocket. The dimethyl ether group on the Nutlin-3a occupies the third pocket (Phe19). As seen in **Figure 1.14**, the side chain residues that surround Nutlin-3a are highly hydrophobic which suggest that the tight binding interaction may be driven by the hydrophobic interactions. Disrupting the interaction between MDM2 and p53 by Nutlin-3a enables the stabilization and accumulation of p53. Both *in vitro* and *in vivo* studies showed that Nutlin-3a is able to re-activate p53 tumour suppressor activity and results in suppressed tumour growth (Tovar et al., 2006). Currently the Nutlin inhibitor has progressed to Phase I clinical trial (Hoe et al., 2014).

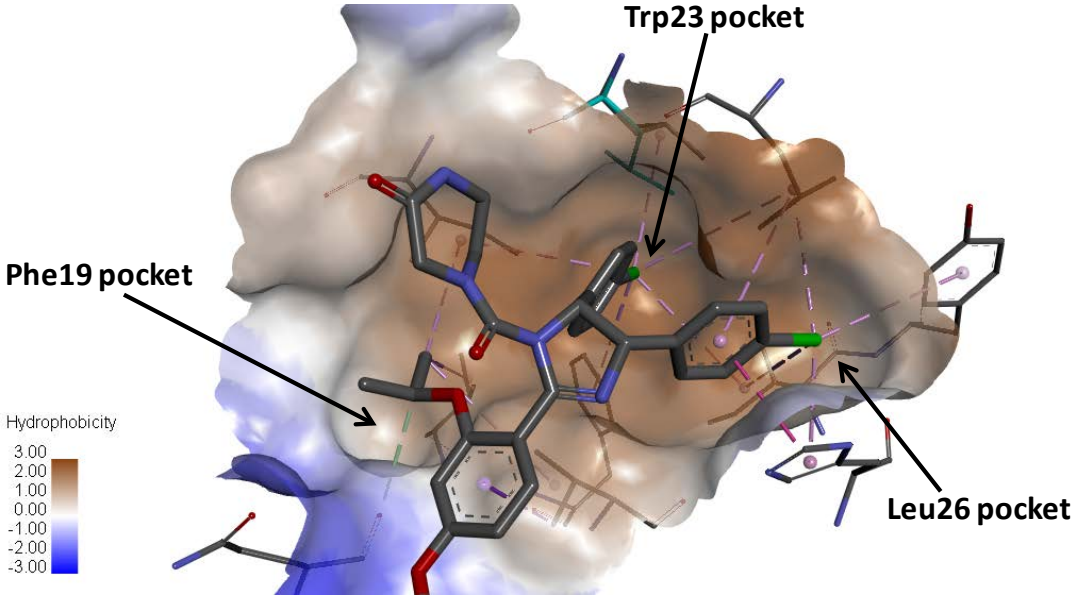

Figure 1.14 Nutlin-3a interaction in the MDM2-N binding groove

Nulin-3a interaction with MDM2 is presented using Discovery studio (Accelrys, 2013) and the protein hydrophobicity surface is shown where brown is hydrophobic and blue is hydrophilic.

1.9.2 MI families

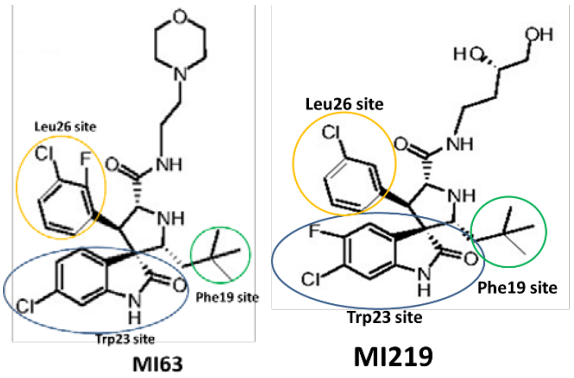

Figure 1.15 Chemical structures of MI63 and MI219.

The structures of MI63 and MI219 are displayed and the subgroups that occupy the three hydrophobic sites are circled in different colours.

The MI series is the second most studied group of MDM2 inhibitors which were developed by Shaomeng Wang's group (Ding et al., 2006). Structure based de novo design was employed to design compounds based on the spiro-oxindole group. The oxindole group originated from the indole ring of tryptophan to mimic the interaction of Trp23 on p53 (Ding et al., 2005). Both MI63 and MI219 bind tightly to MDM2 with Kis of 3nM and 5nM respectively (Shangary et al., 2008). MI63 has poor pharmacokinetic properties therefore MI219 was developed with improved solubility and hence better bioavailability. Similar to the Nutlin series the MI family of inhibitors also uses a core structure that stretches the subgroup to fit into the Phe19, Trp23 and Leu26 pockets (**Figure 1.16**).

MI63 and MI219 contain 2-morpholin-4-yl-ethylamine and 1, 2-pentanediol groups respectively (**Figure 1.15**) that extend to the region between Glu72 and Lys94. This provides additional interactions as well as improving the water accessibility of the compound (Ding et al., 2006). The MI63 bound MDM2 crystal structure 3LBL did not contain this 2-morpholin-4-yl-ethylamine probably due to its flexible structure making it difficult to crystalize (**Figure 1.16**). The tighter interaction of MI63 may be owing to the hydrogen bond interactions present in the nitrogen atom on the oxindole group with the Leu54 backbone and the oxygen atom on the 2-morpholin-4-yl-ethylamine with His96 (green dash line in **Figure 1.16**). These hydrogen bond interactions are absent in the Nutlin-3a/MDM2-N interaction.

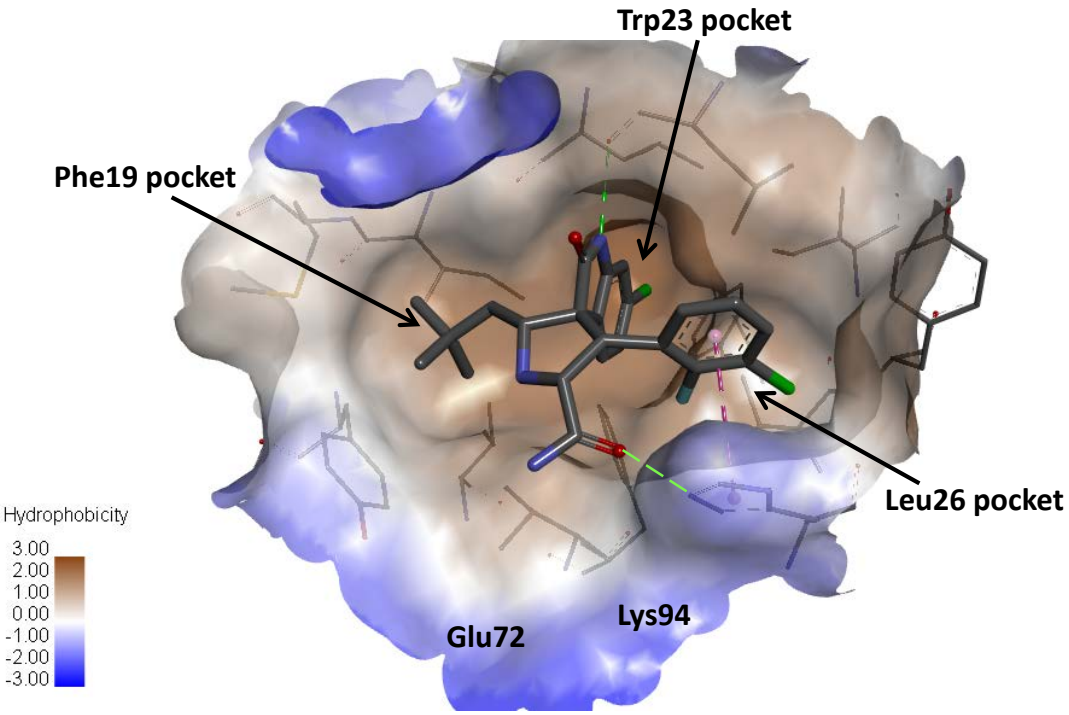

Figure 1.16 MI63 interaction in the MDM2-N binding groove.

MI63 (grey stick) binds to the MDM2-N binding groove is shown. The hydrogen bond interaction is displayed using green dash and pie-pie interaction is displayed using purple dash. The protein surface is presented by hydrophobicity where brown is hydrophobic and blue is hydrophilic.

1.10 MDMX as a target to design a dual inhibitor

It has been confirmed that MDM2 and MDMX are both negative regulators of the tumour suppressor p53. These proteins use their highly similar N-terminal domains to bind to the N-terminal transactivation domain of p53 and inhibit p53 transcriptional activity. The N-terminal domain is therefore an attractive target for drug design (Brown et al., 2009, Brown et al., 2011, Wade and Wahl, 2009).

As of now there are no effective dual inhibitors developed to target both MDM2 and MDMX. There are multiple classes of inhibitors developed to disrupt the MDM2/p53 complex which have proceeded to clinical trials, however they bind at least 1000 times weaker to MDMX (**Table 1.3**).

	MDM2	MDMX	Reference
	Ki (nM)	Ki (μM)	
Nutlin-3a	36	9.3	(Shangary et al., 2008)
MI63	3	55	(Shangary et al., 2008)
MI219	5	55	(Shangary et al., 2008)
WK298	109	11	(Popowicz et al., 2010)

Table 1.3 Binding constants of MDM2 and MDMX inhibitors

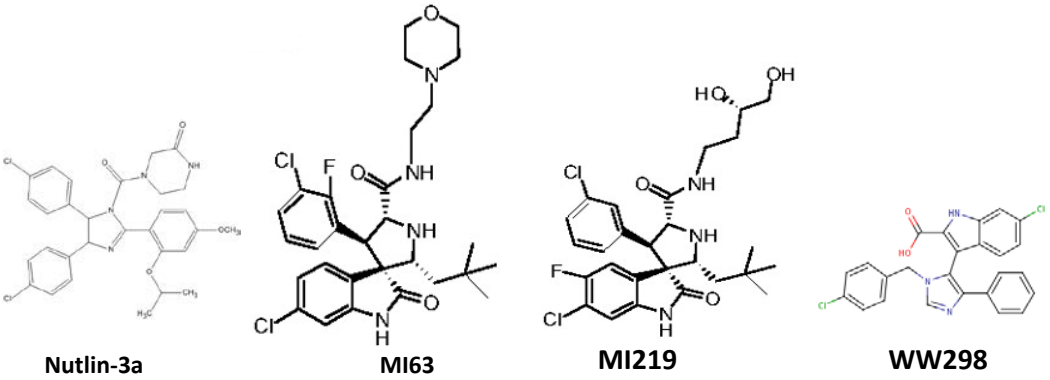

There has been several approaches for developing dual inhibitors using phage display and staple peptide to design peptide inhibitors (Bernal et al., 2010, Pazgier et al., 2009, Chang et al., 2013). Pazgier et al. have used phage display to identify a peptide inhibitor with Kd values of 3nM and 4nM affinity for MDM2 and MDMX respectively. However *in vitro* studies showed this peptide inhibitor is only active in the cell free systems (Pazgier et al., 2009). Bernal F. et al. and Chang Y. et al. have designed stapled peptide named SAH-p53-8 and ATSP-7041 to inhibit both MDM2 and MDMX. ATSP-7041 has progressed into clinical trials but SAH-p53-8 designed by Bernal F. et al. is unable to disrupt p53-MDM2 binding effectively (Bernal et al., 2010, Chang et al., 2013).

It was not until 2012 when Graves B. et al. identified a new class of small molecule inhibitor RO-2443 that is capable of inhibiting both the MDM2-p53 and MDMX-p53 interaction with 33nM and 41nM affinities respectively (Graves et al., 2012). RO-2443 was identified using HTS on a diverse library comprising ~1 million of organic compounds. Examining RO-2443 (**Figure 1.17**) we see that its structure is very different from the known MDM2 inhibitors. It does not contain a central group to connect multiple hydrophobic rings together to fit into all three hydrophobic pockets. In fact, when viewing the crystal structure of the MDM2 and MDMX complex with RO-2443, RO-2443 only fits into the Phe19 and Trp23 pocket (**Figure 1.18 A and C**).

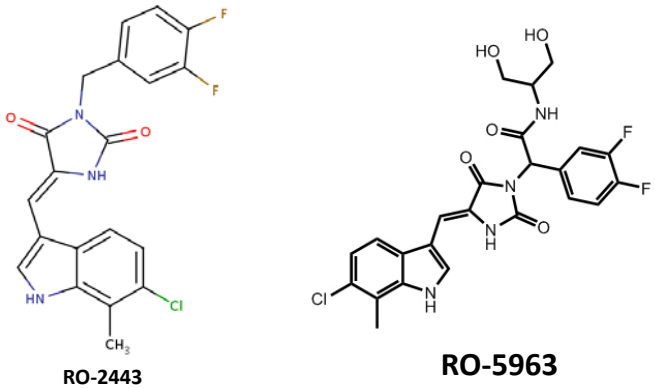

Figure 1.17 Structure of RO-2443 (left) and RO-5963 (right).

RO-2443 is able to bind to both MDM2 and MDMX with high potency through a unique mode of binding. It occupies two out of three hydrophobic pockets on the surface of MDM2 and MDMX. Dimerization of the protein occurs when the indolyl hydantoin group forms an aromatic stacking interaction. The indolyl hydantoin also forms a stacking interaction with a tyrosine ring (Tyr67 in MDM2 or Tyr66 in MDMX) and creates four π-π stacked rings (**Figure 1.18 B, D**). The di-fluoro-phenyl group inserts deep into the Trp23 pocket.

Further chemical optimisation has yielded the inhibitor RO-5963 with improved water solubility and potency (**Figure 1.17**). Testing RO-5963 in *in vitro* has been shown to re-activate the wild type p53 signalling pathway (Graves et al., 2012).

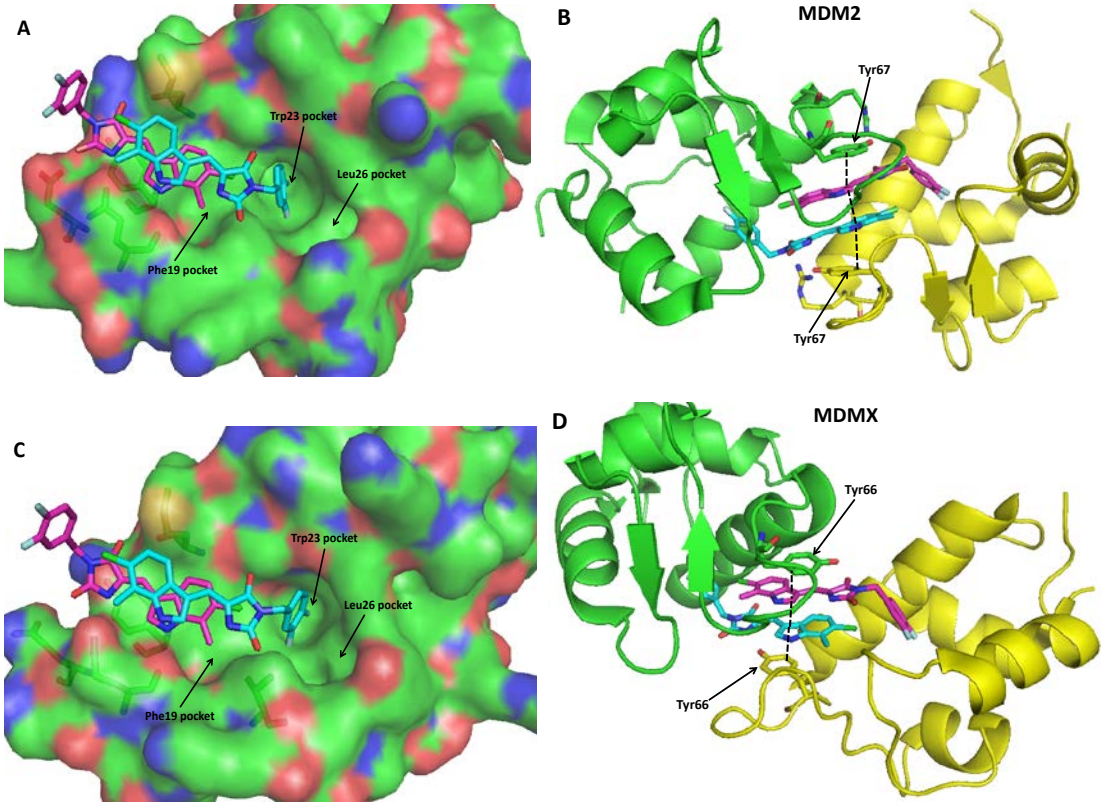

Figure 1.18 Crystal structure of RO-2443 bound to MDM2 and MDMX

A and C) Co-crystal complex structure of RO-2443 bound to MDM2 (**A**) (3VBG) and MDMX (**C**) (3U15) in surface representation. There are two RO-2443 compounds which stack together in the binding pocket as shown in in pink and light blue sticks.

B and D) MDM2 (**B**) and MDMX (**D**) dimer are displayed using cartoon to reveal how RO-2443 assists the dimerization on both MDM proteins.

At the moment the most advanced MDM2/X dual inhibitor is the stapled peptide inhibitor ATSP-7041 developed by Chang Y. S. et al. with Kd values of 0.91nM and 2.31nM against MDM2 and MDMX (Chang et al., 2013). *In vitro* and *in vivo* studies have shown activation of p53 signalling pathway in the MDM2 and MDMX overexpressed cancer models. Whereas for the small molecule inhibitors, the most potent Nutlin family and MI series have advanced into phase I clinical trial and the recently discovered dual action inhibitor RO-5963 is still at the stage of optimisation of the potency and pharmacological properties (Graves et al., 2012, Hoe et al., 2014). The discovery of these small molecule inhibitors has demonstrated that it is possible to use small molecule inhibitors to target both MDM2/p53 and MDMX/p53

interactions and it is clear that the most potent inhibitors have > 1000 times higher affinity than the p53 peptide. These inhibitors provide a new approach to design potent dual MDM2/MDMX inhibitors.

1.11 Insight into the MDMX/p53 interaction site

Early studies have discovered MDMX as another key gatekeeper of the genome and huge effort has recently been placed into studying MDMX because of its high similarity with MDM2 (Marine et al., 2007). The sequence comparison carried out in **Section 1.6** showed that the p53 binding site at the N-terminal domains of MDM2 and MDMX are highly conserved. Popowicz G. et al. have determined the crystal structure of the MDMX-N/p53 (residues 15 – 29) complex (PDB structure 2Z5S) and reveals several features in the MDMX-N structure that restrict the known MDM2-N inhibitors from binding (Popowicz et al., 2007).

The MDMX-N structure is also comprised of two highly similar portions consisting of two α helices and two β strands (**Figure 1.19 left**) that is similar to the MDM2-N structure (**Figure 1.9**). The short α helices (α1, α1') in both portions form the bottom of the binding site and the long α helices from both portions form the side of the binding site.

The surface of MDMX-N is also shown to be highly hydrophobic in the binding site with three hydrophobic grooves similar to the MDM2-N binding pocket (**Figure 1.19 right**).

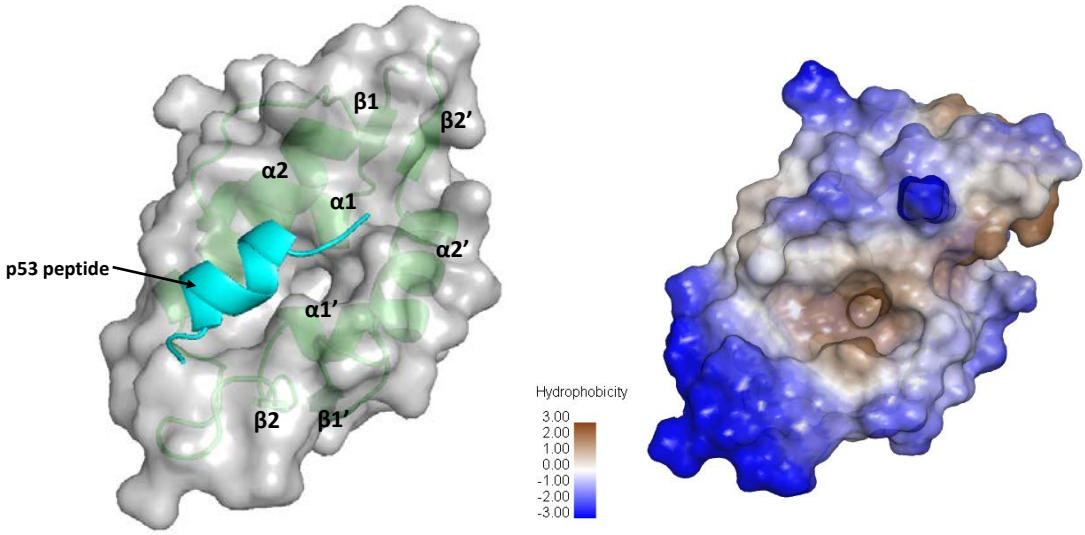

Figure 1.19 The secondary structure of MDMX-N (Left) and the hydrophobicity surface of MDMX-N (Right).

Left) The crystal structure of MDMX-N solved by Popowicz G. et al. (PDB: 2Z5S) is displayed. The structure is presented in surface form with 20% transparency (grey colour) and the secondary structure is displayed in green colour. The p53 peptide binds to the MDMX-N binding site and is coloured in light blue. The second repeat of the α and β strands are distinguished using apostrophe symbol. The picture is generated using PyMOL (Delano, 2002). **Right)** The hydrophobic binding site of MDMX-N is comprised of various hydrophobic residues and the hydrophobicity of the binding site is generated using Discovery Studio 4.0 (Accelrys, 2013). Brown is ranked as most hydrophobic and blue is ranked as hydrophilic.

The crystal structure shows that the p53 peptide also binds to MDMX-N using the same hydrophobic residues Phe19, Trp23 and Leu26 from a 15 amino acid helical stretch (**Figure 1.20**). These residues are able to fully occupy the hydrophobic grooves in MDMX-N using the same binding mode as with MDM2-N. The interaction of the p53 peptide with MDMX-N is mainly driven by the hydrophobic contacts that are also observed in the MDM2-N/p53 interaction. The same hydrogen bonds present in the MDM2-N/p53 interaction have also been identified with the MDMX-N/p53 complex, namely p53 Trp23---MDM2/X Leu54 and p53 Phe19---MDM2 Gln72 (MDMX Gln71). At the C-terminal end of p53 peptide there is a different number of hydrogen bonds formed between MDM2-N/p53 and MDMX-N/p53 complexes. In the MDM2-

N/p53 complex there are hydrogen bonds formed at p53 Asn29---MDM2 Tyr100, Tyr104 and Thr26. Whereas in the MDMX-N/p53 complex there is only one hydrogen bond formed at p53 Pro27---MDMX Tyr99.

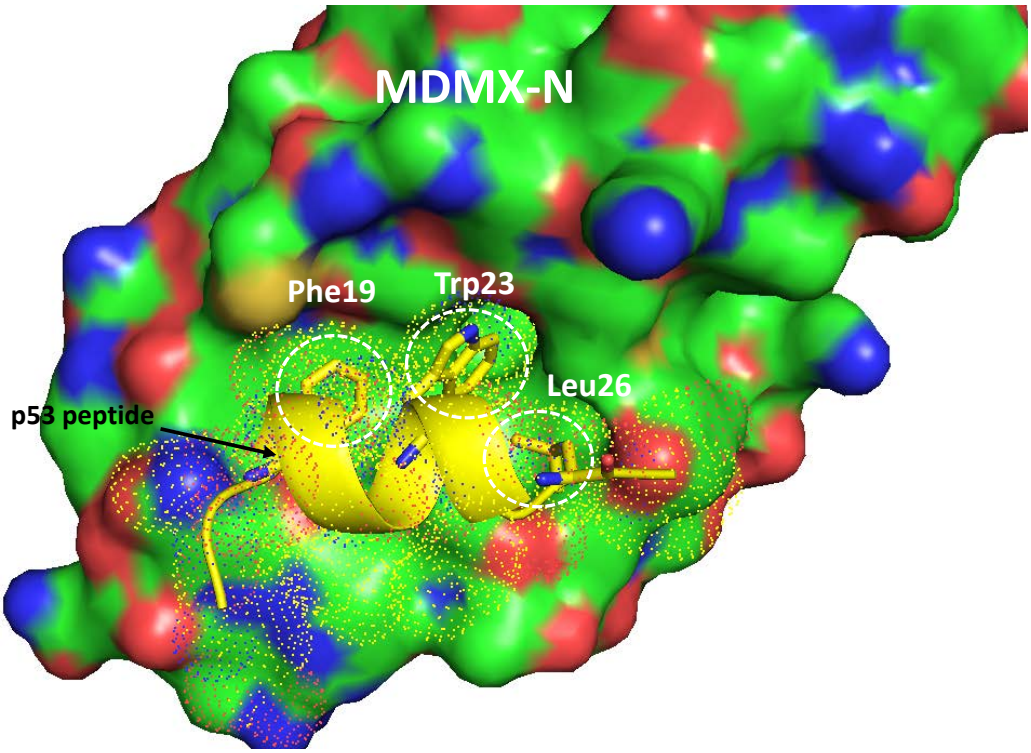

Figure 1.20 p53 peptide binds to MDMX-N using three hydrophobic residues.
Crystal structure of 2Z5S with p53 peptide binding to MDMX-N. The p53 peptide uses three hydrophobic side chains, residues Phe19, Trp23 and Leu26 to interact with MDM2 and MDMX. Dots are displayed for the p53 peptide to represent the peptide has filled up the pocket.

Despite the high level of similarity between the MDM2-N and MDMX-N structures there are still two differences that result in a shallower binding pocket in MDMX-N. First, Leu54 on MDM2-N has been substituted by the Met53 in MDMX-N where the side chain of Met53 is pointed towards the binding site (**Figure 1.21**). The second variation is the helix loop of His96-Arg97-Lys98-Ile99-Tyr100 in MDM2-N which has been substituted by Pro95-Ser96-Pro97-Leu98-Tyr99 in MDMX-N (**Figure 1.21**). This helix is situated at the rim of the Leu26 pocket and the Tyr99 residue protrudes into the binding pocket and fixes the closed conformation which results in a shallow Leu26 pocket (**Figure 1.22**).

With the assistance of high resolution crystal structures we are able to understand the major differences between the MDM2-N and MDMX-N binding grooves and consequently this will assist in the rational development of greater affinity inhibitors toward MDMX-N.

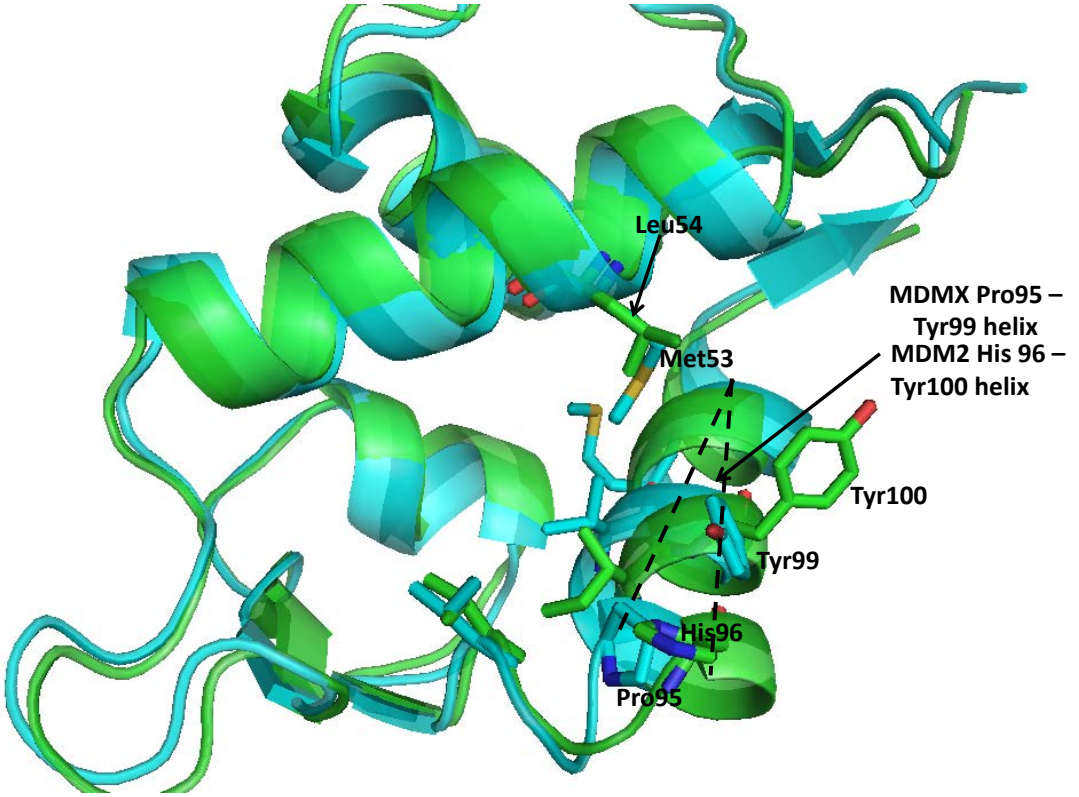

Figure 1.21 An overlap of MDM2 and MDMX N-terminal binding site.

p53 peptide bound MDMX structure (2Z5S) (light blue) is superimposed onto p53 peptide bound MDM2 structure (1YCR) (green) with a RMS fit of 1.01Å.

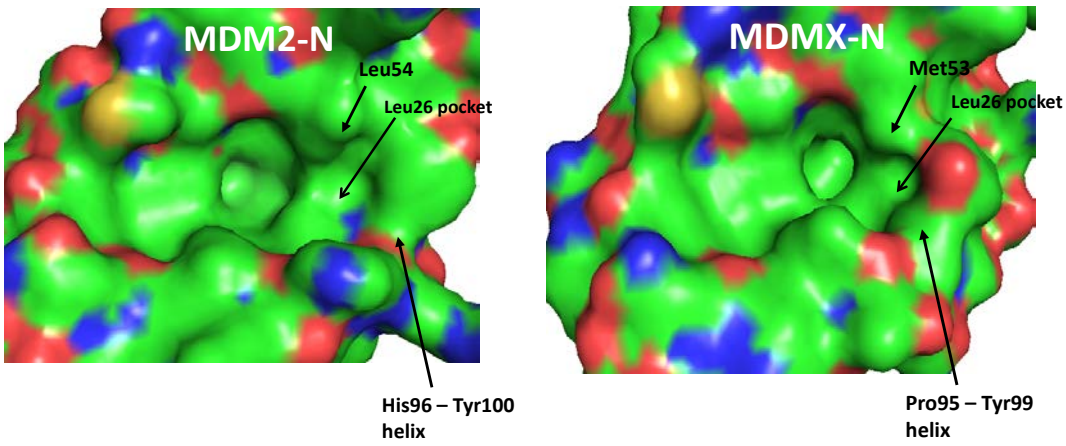

Figure 1.22 The p53 binding site MDM2-N and MDMX-N.

Surface representation of MDM2-N (left) and MDMX-N (right) to highlight the size difference in the Leu26 pocket.

1.12 Aim of project

The aim of this project is to identify small molecules to prevent MDM2 and MDMX from binding to the tumour suppressor p53. This is aided using the in house virtual screening script CODASS to search through millions of commercially available compounds in the EDULISS database. There are also other papers that use virtual screening approach in small molecules identification, however the CODASS employed in this project is a combined docking and ligand based virtual screening method which increased the hit rate even when targeting protein-protein interfaces.

The interaction of the small molecules will be validated by fluorescence polarization and capillary electrophoresis assays.

The currently identified inhibitors have high complexity and hydrophobicity which results in poor solubility, preventing further optimization. This project will explore analogues of the virtual screening hits to aid in identifying small molecular weight fragments with higher solubility.

In order to provide a sufficient amount of protein needed for the assays an optimised scale up for protein purification and storage conditions has been developed.

Chapter 2 Protein expression and purification

The expression and purification strategies of MDM2-N and MDMX-N will be discussed in this chapter. In **Figure 2.1**, a sequence alignment was done on the published structures with the MDM2-N^{11-130}. The published structures of MDM2-N were shorter than the MDM2-N^{11-130} construct used in the studies. The MDM2-N^{11-130} construct contains an unstructured tail at the C-terminal end and lid at the N-terminal end which are not present in the published structures and this makes the protein uncrystallizable. Therefore a short MDM2-N^{18-111} construct was designed for a crystallization trial.

When comparing the sequence of MDMX-N^{14-111} with the published structures' sequences in **Figure 2.2**, the alignment showed that MDMX-N^{14-111} has more residues at the N-terminal domain. To maximise the chance that the MDMX-N would be crystallisable a short MDMX-N^{23-109} construct was designed from MDMX-N^{14-111}.

We have also aligned the sequence of MDM2-N^{11-130} with MDMX-N^{14-111} using PRALINE sequence alignment tool. The alignment showed MDM2-N^{11-130} and MDMX-N^{14-111} has an identity of 54% with only **two residue** difference in the binding sites of MDM2-N and MDMX-N (**Figure 2.3**). Therefore designing dual inhibitors against MDM2-N and MDMX-N becomes highly attractive.

The purified MDM2-N^{11-130} and MDMX-N^{14-111} were used for biophysical studies and screening against small molecules identified from the *in silico* screening.

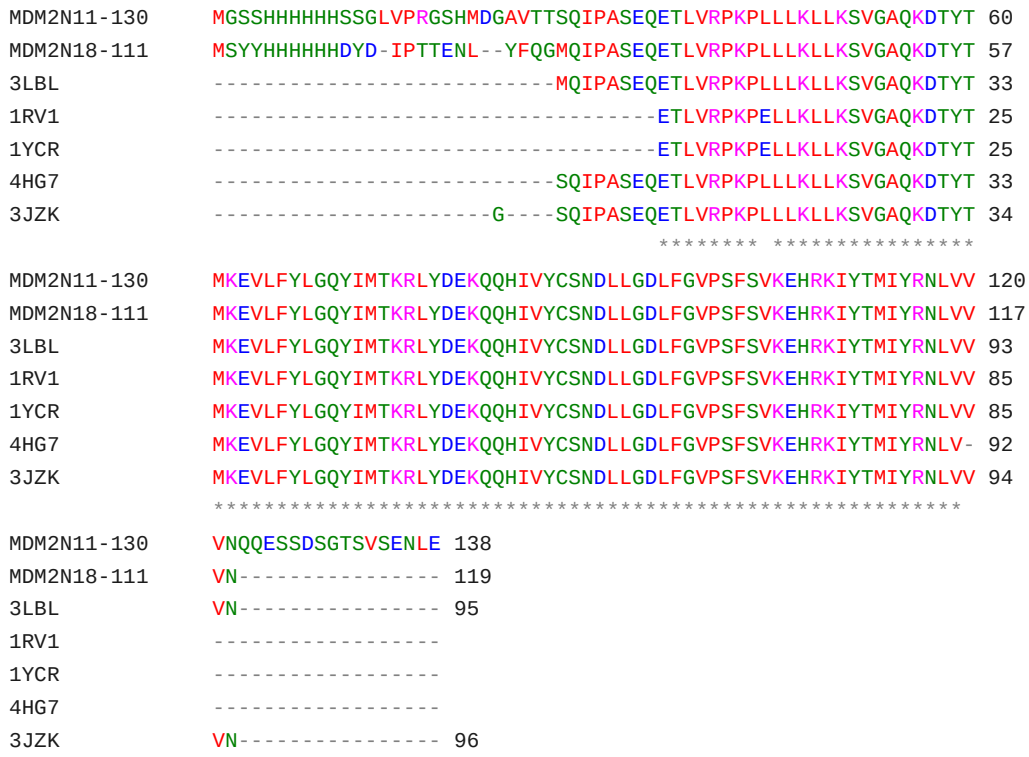

Figure 2.1 MDM2-N sequence alignment.

Sequence alignment of MDM2-N$^{11\text{-}130}$ and MDM2-N$^{18\text{-}111}$with other published structures' sequences. The star sign below the sequences indicate that the residues are identical. The sequences are aligned using ClustalW2 (http://www.ebi.ac.uk/Tools/msa/clustalw2/).

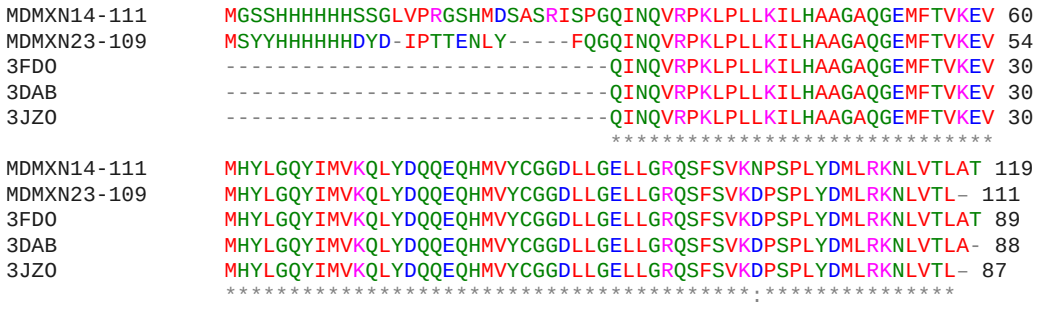

Figure 2.2 MDMX-N sequence alignment.

Sequence alignment of MDMX-N$^{14\text{-}111}$ and MDMX-N$^{23\text{-}109}$ with other published structures' sequences. The sequences are aligned using ClustalW2 (http://www.ebi.ac.uk/Tools/msa/clustalw2/).

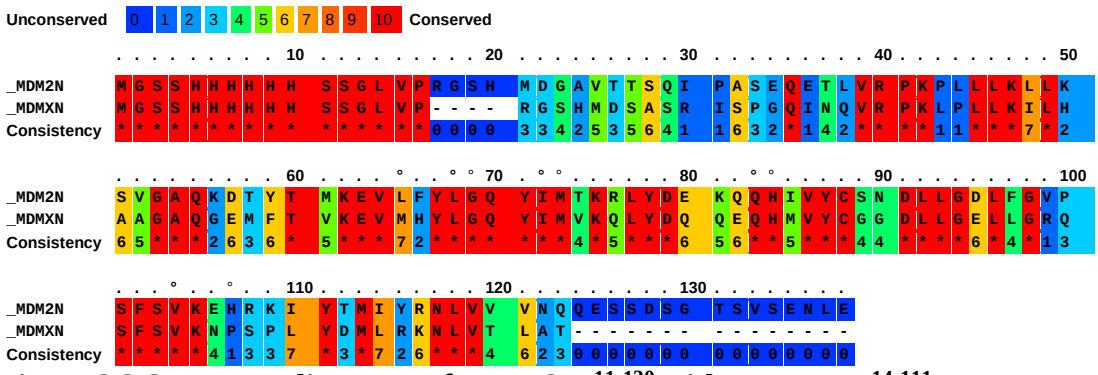

Figure 2.3 Sequence alignment of MDM2-N$^{11\text{-}130}$ with MDMX-N$^{14\text{-}111}$.

The sequences of MDM2-N11-130 and MDMX-N14-111 are aligned using PRALINE alignment (http://www.ibi.vu.nl/programs/pralinewww/). The conserved sequences are highlighted in different colours from red as highly conserved to blue as unconserved. The clear circle above the sequences are the residues in the binding site of MDM2-N and MDMX-N. The percent sequence identity of MDM2-N$^{11\text{-}130}$ and MDMX-N$^{14\text{-}111}$ is 54%.

2.1 Methods

2.1.1 Cloning of MDM2-N and MDMX-N

2.1.1.1 MDM2-N$^{18-111}$ and MDMX-N$^{23-109}$ cloning

For cloning the MDM2 N-terminal region (Residues 18-111) and MDMX N-terminal region (Residues 23-109), the DNA sequence from Dr. Maria Sanchez's MDM2-N$^{11-130}$ and MDMX-N$^{14-111}$ constructs were used as template. Forward and reverse primers were designed to amplify the DNA coding sequence as shown below.

Primer Name	Description	Sequence 5' - 3'
MDM2-N$^{18-111}$		
MDM2-N F1	TEV	CCGAAAACCTGTATTTTCAGGGCT CTCAGATTCCGGCGAGCGAA
MDM2-N F2	AttB1, RBS, ATG, 6x His, TEV	GGGGACAAGTTTGTACAAAAAAG CAGGCTTCGAAGGAGATATACAT ATGTCGTACTACCATCACCATCA CCATCACGATTACGATATCCCAA CGACCGAAAACCTGTATTTTCAG GGC
MDM2-N R	AttB2, CTA	GGGGACCACTTTGTACAAGAAAG CTGGGTCCTAGTTCACCACCACC AGGTTACG
MDMX-N$^{23-109}$		
MDMX-N F1	TEV	CCGAAAACCTGTATTTTCAGGGC ACAAATCAATCAGGTACGACCAA AAC
MDMX-N F2	AttB1, RBS, ATG, 6x His, TEV	GGGGACAAGTTTGTACAAAAAAG CAGGCTTCGAAGGAGATATACAT ATGTCGTACTACCATCACCATCA CCATCACGATTACGATATCCCAA CGACCGAAAACCTGTATTTTCAG GGC
MDMX-N R	AttB2, CTA	GGGGACCACTTTGTACAAGAAA GCTGGGTCCTAGCTAAAGTGAC AAGATTCTTTCTTAGC

Two PCR reactions were required to attach the His-tag onto the N-terminal sequence. The first reaction required a forward primer with TEV recognition sequence which was recognised by the second PCR reaction forward primer. The second forward primer contains AttB1, RBS, ATG, 6x His tag and TEV recognition site.

Only one reverse primer was used with an AttB2 and a stop codon.

The gateway entry vector contained attL recombination site allowing PCR products that contained attB sites to recombine with the entry vector.

PCR cloning

In PCR reactions the templates were a plasmid containing the full length MDMX and N-terminal MDM2 gene which was a gift from Prof. Kathryn Ball and Dr. Maria Sanchez.

The PCR reaction mixtures contained the components in **Table 2.1** and Elongase enzyme mix kit (Invitrogen) was used.

Component	Volume (Total 50µl)
dNTP mix (0.5mM)	20µl
Forward primer (10µM)	1µl
Reverse primer (10µM)	1µl
Template DNA (≥100ng)	1µl
Elongase enzyme mix	1µl
5x Buffer A	5µl
5x Buffer B	5µl
Water	17µl

Table 2.1 Reaction set up for PCR Elongase enzyme mix.

PCR reaction conditions were:

1. Pre amplification denaturation 94°C for 2min.
2. Thermal cycling: Denaturation; 94°C for 1min
   Annealing; 50 - 55°C for 30sec
   Extension; 68°C for 1min
   ⎫ 35 cycles
3. 68°C for 10min.

When the first PCR reaction was finished the PCR products were verified on a 1.2% agarose gel. This separated the PCR products from the mixtures. The band at the expected size was cut out from the agarose gel and purified using a PCR purification kit (QIAquick).

Purified PCR product was used as the template DNA in the second PCR reaction. The second PCR reaction attached the His-tag onto the N-terminal end of the sequence. The PCR reaction was performed by adding the same mixtures and performed in the same reaction conditions. The PCR reaction mix was loaded onto an agarose gel and

the band purified using the PCR purification kit. The purified PCR product contained the specific gene sequence with the attB sites attached on both end of sequence which allows insertion into the gateway entry vector.

Gateway cloning

The Gateway cloning technology enables transfer of DNA sequence into different cloning vectors. First, the sequence was inserted into the donor vector using BP clonase enzyme mix.

The following components were added into a sterile tube:

	Volume (µl)
attB-PCR product (15-150ng)	1-7µl
pDONR221 vector (150ng/µl)	1µl
TE buffer pH 8.0	To 10µl
BP clonase enzyme mix	2µl

The reaction mixture was incubated at 25°C for 1h. To terminate the reaction 1µl of Proteinase K was added into the mixture and incubated at 37°C for 10min. Following the BP clonase reaction mixtures were transformed into the DH5α competent cell for plasmid production. 2µl BP reaction was added into 50µl DH5α cells, incubated on ice for 30min followed by heat shock at 42°C for 30seconds. S.O.C. medium (250µl) was then added and the mixture incubated in the shaking incubator at 37°C for 1h. The competent cells were spread onto a LB agar plate (30µg/ml Kanamycin) and incubated at 37°C overnight. A single colony was grown in a 5ml LB medium (30µg/ml Kanamycin) overnight and the plasmid was harvested using the QIAprep Miniprep kit (Qiagen).

The donor vector containing the gene of interest was subcloned into the destination vector pDEST14. This was done by LR clonase enzyme mix (Invitrogen). The mixture was made and incubated at 25°C for 1h:

	Volume (µl)
pDONR221 (15-150ng)	1-7µl
pDEST14 vector (150ng/µl)	1µl
TE buffer pH 8.0	To 10µl
BP clonase enzyme mix	2µl

The reaction was terminated with Proteinase K and transformed into the DH5α cell for plasmid production.

Sequences of all the constructs designed were verified by sequencing in GenePool.

2.1.2 Protein concentration determination

The protein concentration was measured using a NanoVue spectrophotometer measuring the absorbance at 280nm using molar extinction coefficient and molecular weight of the protein. The extinction coefficient and molecular weight of each construct are listed below:

Constructs	Extinction coefficient (M^{-1} cm^{-1})	Molecular weight (Da)
MDM2-N^{11-130}	10430	15601.7
MDM2-N^{18-111}	16390	14153.3
MDMX-N^{14-111}	7450	13313.3
MDMX-N^{23-109}	13410	13001.9

2µl of protein buffer was used as a blank and 2µl of protein sample was used to measure the concentration. The protein was measured in triplicate and the average concentration was calculated.

2.1.3 Transformation and expression

The construct along with optimised expression and purification protocols for MDM2-N^{18-111} and MDMX-N^{14-111} were obtained from Dr. Maria Sanchez in the School of Chemistry, University of Edinburgh. All the constructs contain a His-tag and thrombin or TEV cleavage site at N-terminus. The vector used is PET28b and expression is in E. *coli* BL21 STAR strain.

All the agar plates and mediums contain the specific antibiotics for the constructs.

Constructs	Antibiotics used
MDM2-N^{11-130}	50µg/ml Kanamycin
MDM2-N^{18-111}	100µg/ml Carbenicillin
MDMX-N^{14-111}	50µg/ml Kanamycin
MDMX-N^{23-109}	100µg/ml Carbenicillin

Single colonies of cells were picked up from Luria Bertani (LB) plates and used to inoculate 50ml of Terrific Broth (TB) media. Cultures were grown for ~5 hours at 37°C with shaking (250rpm). This culture was transferred to 1L of TB media and grown at 37°C with shaking (250rpm). When the one litre cultures were grown to OD_{600} = 0.3 the temperature was reduced to 25°C. Expression was induced with 0.1mM IPTG when OD_{600} reached 0.6 and the culture was incubated overnight at 25°C. The cells were harvested by centrifugation at 8000rpm for 30min at 4°C. One litre cell pellet (weight around 9 grams) was frozen in liquid nitrogen and stored in -80°C freezer.

2.1.4 Preparation of cell lysate

The cellular pellet was resuspended in 5ml lysis buffer (50mM HEPES pH 8.5, 300mM NaCl, 1mM DTT, 20mM Imidazole, 1mg/ml Lysozyme, 2.5 units/ml benzonase, 10% glycerol) per 1gram cell pellet and incubated on ice for 30min. The cells were passed through a constant system cell disruptor twice to break open the cells. After lysis the lysate was centrifuged at 16000rpm for 45minutes at 4°C. The supernatant was collected and filtered through 0.2µm filter.

2.1.5 Purification strategies for MDM2-N & MDMX-N

All purifications were performed using AKTA purifier system (10ml/min) at 6°C. Two steps of purifications were applied.

2.1.5.1 Immobilized metal ion affinity chromatography (IMAC)

In the IMAC purification a HisTrap column containing an immobilized chelating group which can be charged with metal ions such as Ni, Co, Zn Fe and Cd was used.

Several amino acids bind to divalent metals when exposed on the protein surface. To improve the affinity of binding the protein has fused with a 6xHis tag and this makes the His tag protein the strongest binder. The His tag protein can then be eluted by high concentration of imidazole.
All the constructs that were used in this work have 6xHis-tag fused on the N-terminal for IMAC purification.

Buffer A

50mM HEPES pH8.5, 300mM NaCl, 1mM DTT, 20mM Imidazole (pH 7.5 with 10% (v/v) glycerol when purifying MDMX-N^{14-111} and MDM2-N^{18-111}).

Buffer B

50mM HEPES pH8.5, 300mM NaCl, 1mM DTT, 500mM Imidazole (pH 7.5 with 10% (v/v) glycerol when purifying MDMX-N^{14-111} and MDM2-N^{18-111}).

The supernatant was loaded onto a pre-packed 5ml Ni^{2+} HiTrap IMAC HP Sepharose column (column was pre-charged with Ni^{2+} and equilibrated with Buffer A) at a flow rate of 5ml/min. The flow rate was maintained at 5ml/min throughout the purification process.
The column was washed with 20 column volumes of Buffer A to remove unbound proteins. Then contaminant was removed by washing with 10 column volumes of 15% Buffer B. The protein was eluted through a linear gradient (0% - 100%) at 25 column volumes using Buffer B. The purity of the fractions was confirmed in SDS-PAGE gel and the fractions containing the desired proteins were pooled together.

2.1.5.2 Size exclusion chromatography (SEC)

Size exclusion chromatography is a technique that can separate molecules based on its molecular size in the solution. SEC uses various columns that contains different matrices to provide diverse separation ranges.
HiPrep 16/60 Sephacryl S-100 HR column was used to purify MDM2-N^{11-130} and MDM2-N^{18-111}, while MDMX-N^{14-111} was purified using HiLoad 16/60 Superdex 200 pg. The column was pre-equilibrated with 2 column volumes of gel filtration buffer. The eluted fractions were confirmed by 18% SDS-PAGE gel. Pure MDM2-N^{11-130}

fractions were pooled and concentrated to 1mg/ml using vivaspin column [Molecular weight cut off = 5kDa] and stored at -80°C. Purified MDM2-N^{18-111} and MDMX-N^{14-111} were concentrated to ~0.5mg/ml and stored at -80°C.

Gel filtration buffer
50mM HEPES pH 7.5, 100mM NaCl, 0.1mM EDTA and 2mM DTT (10% (v/v) glycerol was added when purifying MDMX-N^{14-111} and MDM2-N^{18-111}).

2.1.6 Matrix Assisted Laser Desorption Ionization Mass Spectrometry (MALDI MS)

MALDI MS is a technique that was first introduced in 1988 by Franz Hillenkamp and Michael Karas for analysing biomolecules (proteins, peptides or DNA) and large organic molecules (polymer and other macromolecules) (Karas and Hillenkamp, 1988, Tanaka et al., 1988). In MALDI MS the molecule is co-crystallized with matrix compound, sinapinic acid for proteins or a-cyano-4-hydroxycinnamic acid (CHCA) for peptides. As the laser is fired onto the crystallized matrix, the matrix strongly absorbs the energy and undergoes desorption and ionization which function to ionize the molecule. In MALDI Time of Flight (TOF) MS, the ionized molecules are accelerated into the tube and can be separated by the mass to charge ratio. Smaller mass molecules reach the detector first and large molecule takes longer time to reach the detector.

A MALDI-TOF MS experiment was used to compare the mass of the MDM2-N^{11-130} after the His-tag cleavage. The sample was prepared by dropping 0.5µl protein onto the Gold plate and then adding 0.5µl of sinapinic acid. The plate was fitted onto the robot arm and scrolled into the voyager DE STR MALDI-TOF MS (Applied Biosystem Ltd.).

2.1.6.1 In-Gel digest for mass spectrometry

MS was also used as an analytical technique to identify protein from the gel. The protein band was digested using trypsin into many small pieces of peptides. Trypsin cuts at the C-terminal side of lysine and arginine.

The protein band was cut out from the gel and incubated in 300µl NH_4HCO_3 (ABC, 200mM) in 50% acetonitrile (ACN) at room temperature for 30min. The washing was repeated twice to remove the SDS from the band. The band was then incubated in 300µl DTT (20mM), ABC (200mM), ACN (50%) at room temperature for 1hour and followed by washing three times with 300µl ABC (200mM), ACN (50%). The next step is to alkylate cysteines in 100µl iodoacetamide (IAA, 50mM), ACN (50%) at room temperature for 20min. The band was washed three times with 500µl ABC (20mM), ACN (50%). The band was centrifuged at 13,000rpm for 2min and covered with ACN for 5min until the band turned white. The band was extracted and allowed to dry before adding 29µl of ABC (50mM) and 1µl trypsin. The band was incubated with trypsin at 32°C overnight to digest. The sample was sonicated for 10min prior to MS analysis as described above.

2.2 Results and Discussion

2.2.1 Expression & purification of MDM2-N^{11-130}

2.2.1.1 Expression of MDM2-N^{11-130}

E. coli BL21 STAR cells were transformed with pET28b vector containing the MDM2-N^{11-130} gene. The expression of MDM2-N was induced with 0.1mM IPTG at OD_{600} of 0.6 and incubated overnight at 25°C.

An expression trial was carried out in LB and TB media to confirm if the expression can be improved in TB medium. Cells were grown using the same conditions and SDS-PAGE was run to compare the expression level of MDM2-N in LB and TB. The gel showed there was more MDM2-N produced in TB than in LB (**Figure 2.4**). This could be because TB medium is more nutritious and provides better cell growth, so the higher biomass in TB gives more protein than in LB.

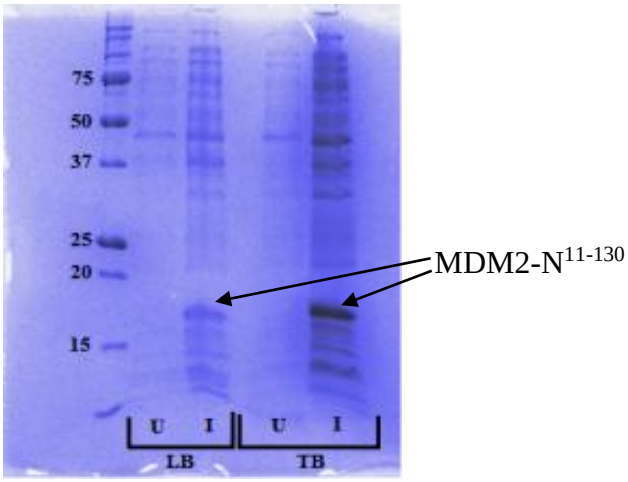

Figure 2.4 Expression trial of MDM2-N in LB and TB medium.

In the gel, a band is present between 15-20kDa markers, indicating presence of MDM2-N^{11-130}. The band in TB medium is more intense than LB showing more MDM2-N^{11-130} produced in TB medium.

2.2.1.2 Purification of His_6-tag MDM2-N^{11-130}

After optimum storing conditions were found (**section 2.2.1.3**) it was possible to purify MDM2-N^{11-130} in large scale so that purification did not have to be repeated so often. 4X 1L of MDM2-N pellets were purified and passed through the cell disruptor at 25KPSI. After purifying using Ni^{2+} HisTrap column, fractions from peak 1 and peak 2 were run on SDS-PAGE gel to confirm MDM2-N presence (**Figure 2.5**).

MDM2-N was present in peak 2 and concentration was determined to be 1mg/ml in 100ml. The yield was ~100mg from 4X 1L pellet.

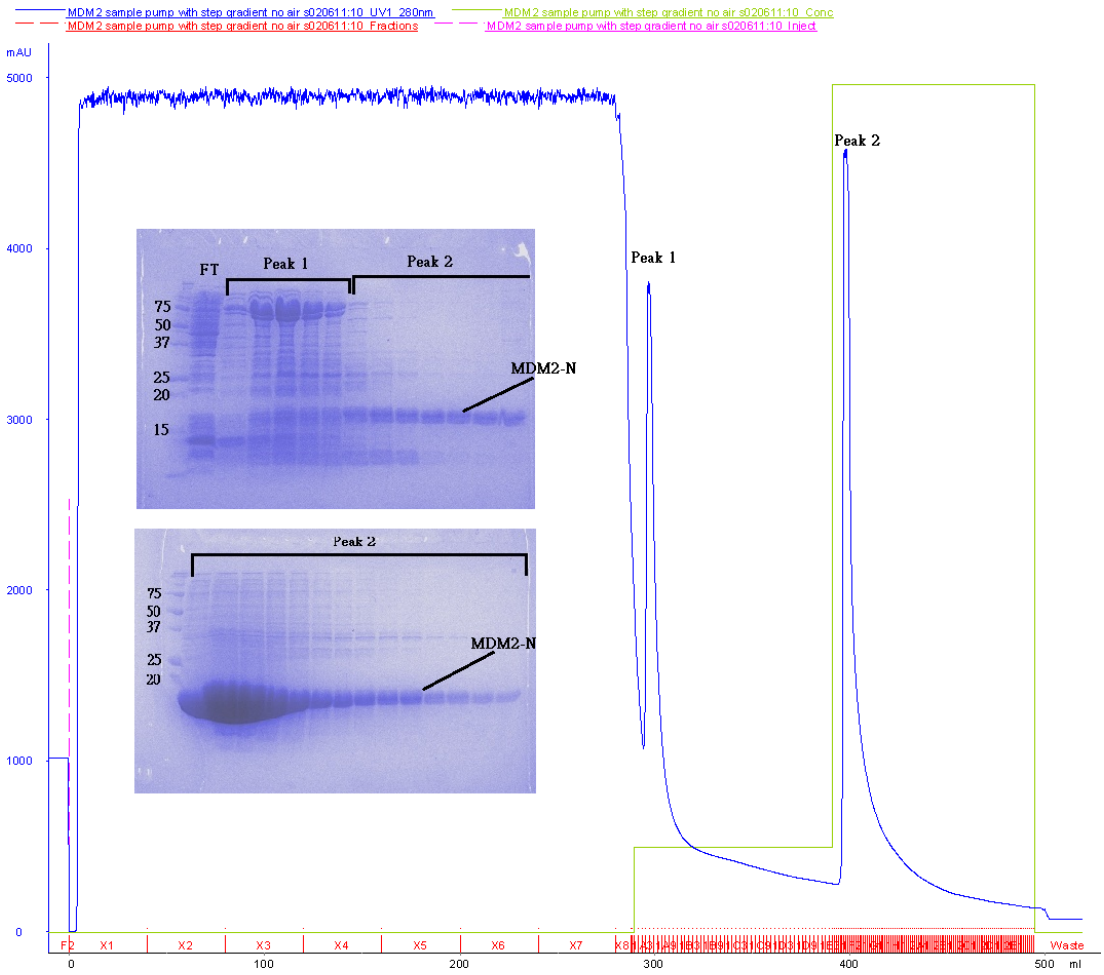

Figure 2.5 First step of purification of MDM2-N.

The soluble fraction was pumped onto a 5ml Ni^{2+} His-Trap column attached to an AKTA system. Two step gradients were applied that elute the contaminant at 7% buffer B, then elute MDM2-N at 100% buffer B.

MDM2-N sample purified from IMAC column was further run through a 26/60 S200 gel filtration column (**Figure 2.6**). Two peaks eluted at 200ml and 340ml. A SDS-PAGE gel was run on the peaks to confirm the presence of MDM2-N and the purity. MDM2-N was found to be present in peak 1 as can be seen on the gel with pure His-tag MDM2-N present only.

The two batches of MDM2-N purified from gel filtration were concentrated and the concentration was measured. The yield from each gel filtration was 18mg and 16mg so the total yield is 34mg. More than half of the protein was lost in gel filtration. One possibility could have been that the protein precipitated during loading onto the

column, becoming stuck in the column. Another possible reason for the protein to precipitate could have been that the buffer was not suitable. The pH has decreased from 8.5 to 7.5 and the salt concentration has dropped from 300mM down to 100mM. These rapid changes may have caused the protein to become unstable and prone to precipitate.

Even though half of the protein was lost ~34mg of MDM2-N was obtained. The purified MDM2-N was concentrated to 1mg/ml and storing conditions explored.

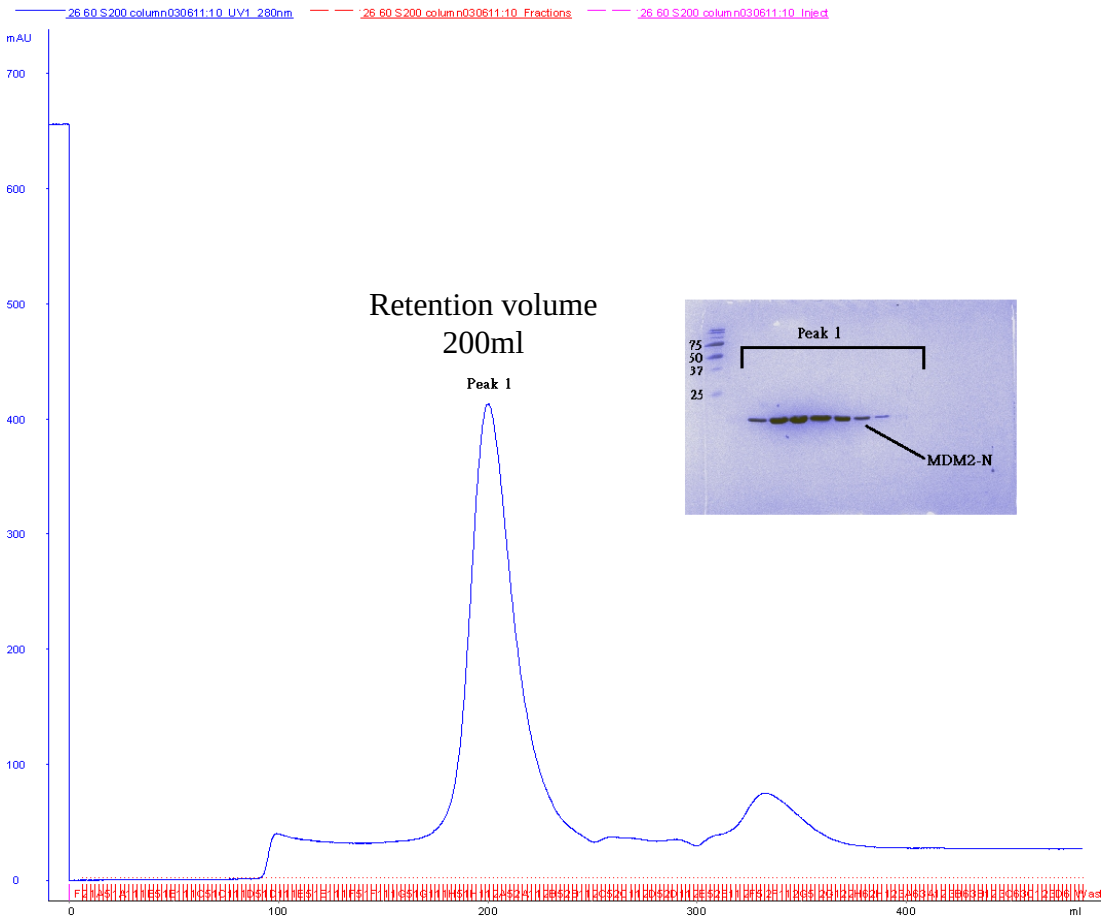

Figure 2.6 Second step purification of MDM2-N.

MDM2-N was run through a 26/60 S200 Gel filtration column. 1 single peak was eluted out at 200ml in the elution profile and confirmed to be MDM2-N from SDS-PAGE gel.

2.2.1.3 Finding storing condition for MDM2-N

Purification of MDM2-N was shown to be successful with pure His-tag MDM2-N obtained but currently there was no long term storing condition available. MDM2-N precipitated within one week and purification had to be carried out every week which was very inconvenient. Therefore a storing condition has to be identified for storing MDM2-N long term.

Two storing trials were tested. The first sample of 200µl MDM2-N was stored in the freezer for two days and the second sample of 200µl MDM2-N was flash frozen using liquid Nitrogen and then stored in the -20℃ freezer. These frozen MDM2-N were thawed and tested in Malvern Zetasizer APS Dynamic Light Scattering (DLS) to confirm if the protein was still folded properly.

Dynamic Light Scattering (DLS) is used to measure hydrodynamic sizes, polydispersities and aggregation effects of protein samples. DLS measures the laser light scattered from the macromolecules in solution. The macromolecules in solution fluctuate due to the Brownian motion so the scattering intensity can be observed. These fluctuations are directly related to the rate of diffusion of the molecules in the solution (Jachimska et al., 2008).

The protein was centrifuged at 12000rpm for 10min to remove any precipitant.

Blank was run using Protein Buffer (50mM HEPES pH 7.5, 100mM NaCl, 1mM DTT).

50µl of protein was added into well and the sample was measured three times.

Since small molecules diffuse faster, they lead to a faster decay in the measured correlation function.

2.2.1.3.1 DLS on fresh MDM2-N sample

Figure 2.7 shows the size distribution results and there were different peaks present in the size distribution. The peaks present in 0.43 and 0.88nm were small particles in the buffer solution. The peaks at the hydrodynamic radius of 5.3nm was MDM2-N and the DLS estimates the molecular weight to be 15.7kDa. The molecular weight of MDM2-N is 15.6kDa so DLS has accurately estimated the molecular weight of MDM2-N. Multiple peaks were found in hydrodynamic radius over 100nm and this indicates that there were aggregates present in the solution.

Intensity Distribution Results

	%Int	Mean (d.n...	Mode (d.n...	StD (d.n...	%Pd	MW (kDa)*	Polydispers...
Peak ...	63.9	4.657	4.665	1.174	25.2	24.3	Polydisperse
Peak ...	24.4	105.3	98.47	28.54	27.1	3.59e4	Polydisperse
Peak...	6.6	0.4625	0.4221	0.07625	16.5	0.109	Monodisperse

Mass Distribution Results

	%Ma...	Mean (d.n...	Mode (d.n...	StD (d.n...	%Pd	MW (kDa)*
Peak...	92.6	0.4328	0.4030	0.06838	15.8	0.0937
Peak ...	6.3	0.8846	0.8442	0.1366	15.4	0.499
Peak 3:	1.1	3.859	3.376	0.9764	25.3	15.7

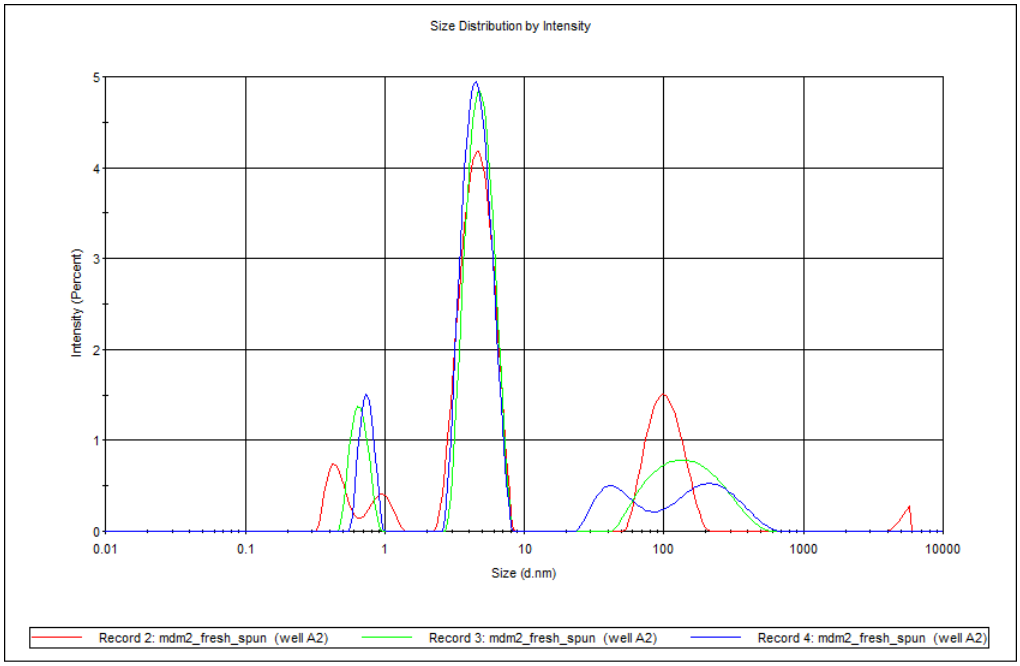

Figure 2.7 Size distribution by intensity of fresh MDM2-N protein.

DLS was performed three times on the same sample and multiple peaks were present in the size distribution profile. The peaks at ~5.3nm size is the MDM2-N which estimates the molecular weight to be 15.7kDa.

2.2.1.3.2 DLS on frozen MDM2-N

MDM2-N protein that had been frozen in -20°C for two days was analysed in DLS to confirm if the protein is still active. The size distribution in **Figure 2.8** showed a similar trend to the size distribution as found in **Figure 2.7** of fresh MDM2-N sample. The peaks at ~5.3nm were MDM2-N and DLS estimated the molecular weight to be 17.9kDa. The molecular weight of MDM2-N is 15.6kDa so this means that MDM2-N did not form aggregates and was stable to use after freezing with only a small amount of aggregate present. However in the MDM2-N protein that was flash frozen using

liquid Nitrogen the size distribution profile showed large aggregates present in the solution (**Figure 2.9**). This suggests that flash freeze is not an ideal method for storing MDM2-N and storing MDM2-N in -20°C freezer is more appropriate.

Intensity Distribution Results

	%Int	Mean (d.n...	Mode (d.n...	StD (d.n...	%Pd	MW (kDa)*	Polydispers...
Peak ...	58.3	4.548	4.455	0.8885	19.5	23.0	Monodisperse
Peak ...	22.1	198.9	179.5	60.12	30.2	1.59e5	Polydisperse
Peak...	9.2	0.7207	0.7017	0.07707	10.7	0.309	Monodisperse

Mass Distribution Results

	%Ma...	Mean (d.n...	Mode (d.n...	StD (d.n...	%Pd	MW (kDa)*
Peak...	97.2	0.6970	0.6700	0.07756	11.1	0.286
Peak ...	2.8	4.084	3.703	0.7779	19.0	17.9
Peak 3:	0.0	0.000	0.000	0.000	0	0.00

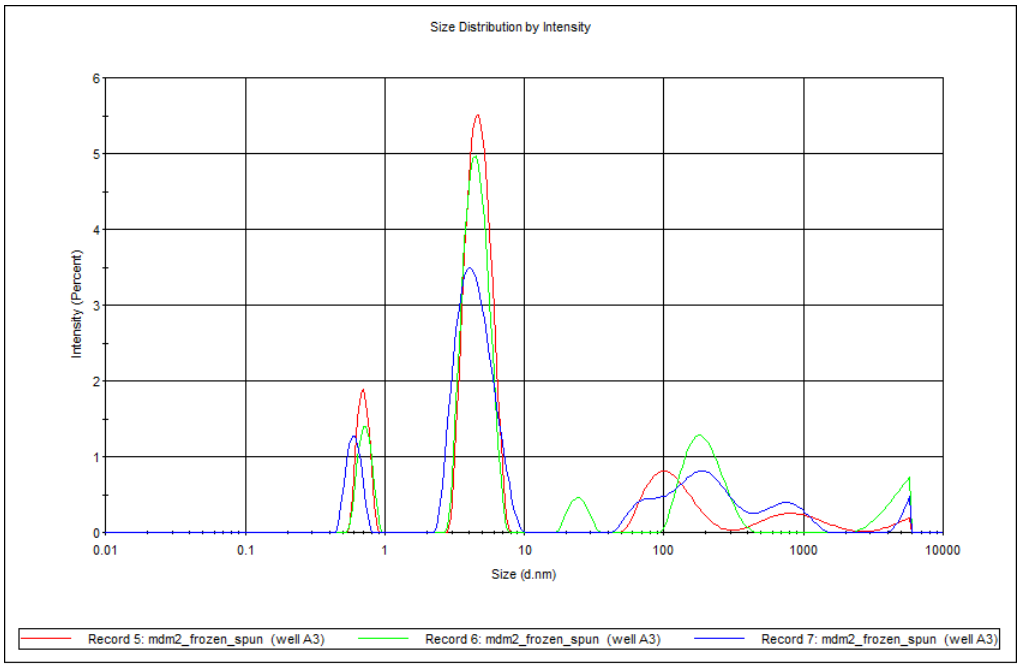

Figure 2.8 Size distribution intensity profile of frozen MDM2-N.

This is the MDM2-N protein frozen in -20°C freezer for two days and analysed in DLS. The sample was analysed in DLS three times. The peaks at ~5.3nm size are the MDM2-N and DLS estimates the molecular weight to be 17.9kDa.

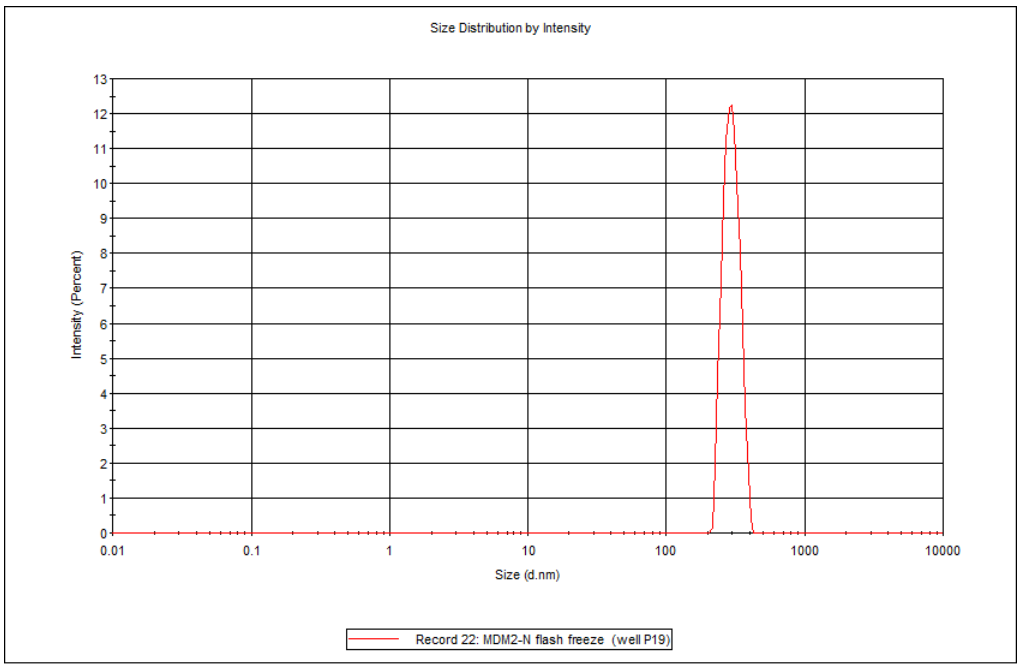

Figure 2.9 Size distribution intensity profile of flash frozen MDM2-N.

MDM2-N protein was frozen using liquid Nitrogen and stored in -20°C freezer. In the profile, there is only a single peak present at hydrodynamic radius >100nm. This suggest the protein has been aggregated.

2.2.1.4 Using thrombin to cleave off His-tag

A thrombin cleavage trial was set up to try cleaving off the His-tag on MDM2-N. The His-tag is located at the N-terminus of the MDM2-N construct near the hydrophobic pocket and this may interfere compounds binding into the pocket. Therefore it was important to cleave off the His-tag to see whether the His-tag had an effect on the assay.

MDM2-N (1mg) was incubated with 2U thrombin (GE healthcare) overnight at 4°C as recommended by the manual. The protein was then loaded back onto the Ni^{2+} HisTrap column and the flow through was collected. From the chromatogram in **Figure 2.10** a large peak was found in the flow through which suggest the His-tag was cleaved off from the MDM2-N and the protein can no longer bind to the HisTrap column. There was only a small peak present in the elution suggesting most of the His-tag was cleaved off from the MDM2-N.

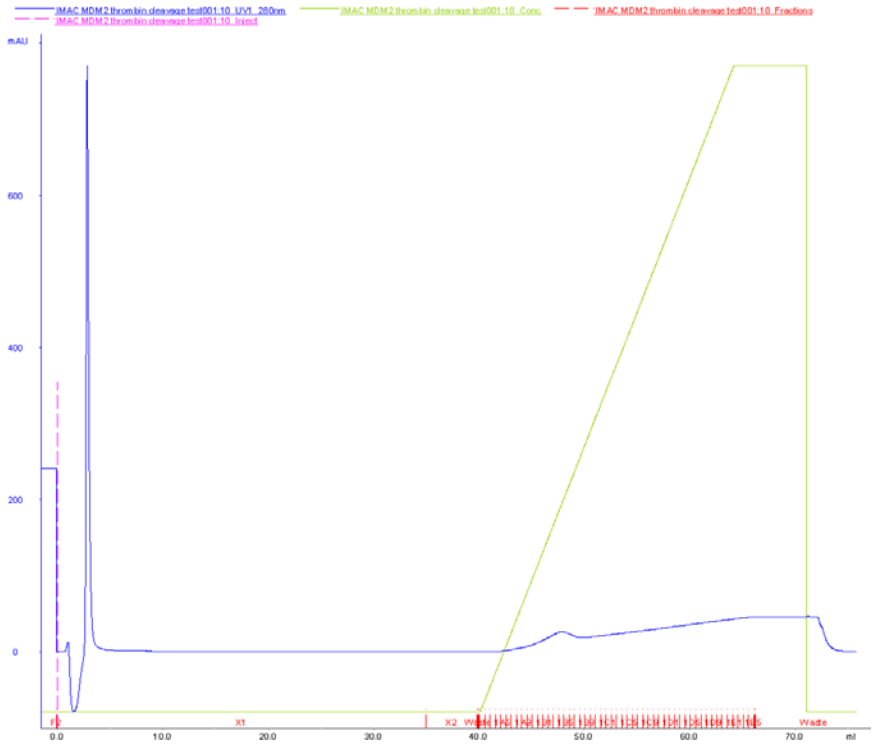

Figure 2.10 MDM2-N incubated with 2U Thrombin was run through Ni2+ IMAC column. A peak came out in the flow through and only a small peak was present in the elution profile indicating that the His-tag was cleaved off and MDM2-N cannot bind to the IMAC column.

2.2.1.5 Matrix assisted laser desorption/ionisation (MALDI) mass spectrometry

His-tag cleavage was further confirmed using MALDI mass spectrometry to identify the molecular weight of MDM2-N sample after incubating with thrombin. Fig. 2.5 shows the results of Mass spectrometry. The top graph shows the control MDM2-N without thrombin incubation and the bottom graph shows MDM2-N after incubating with thrombin. From the mass spectrometry results (**Figure 2.11**) the molecular mass of control MDM2-N detected in the MS was 15473Da and the molecular mass of His-tag MDM2-N is 15601.7Da. In the MS trace after thrombin treatment (**Figure 2.11 bottom**), the molecular mass has change to 13721Da. This change in molecular mass indicated the His tag has been cleaved off from MDM2-N as the His-tag MW is 1900Da.

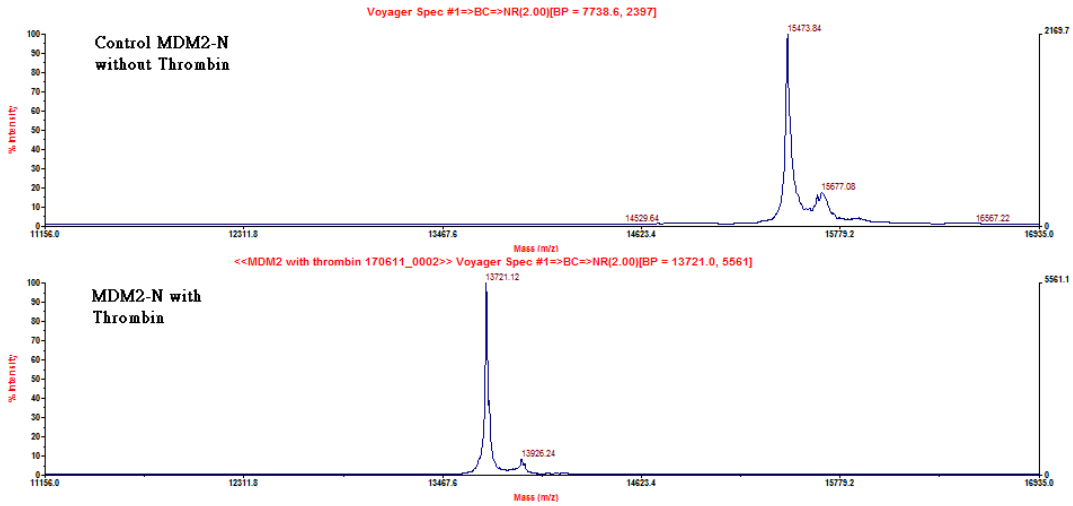

Figure 2.11 Confirm His-tag cleavage by MS.

Mass Spectrometry was run on the control with MDM2-N only and on a sample of MDM2-N incubated with Thrombin. From the profile, MDM2-N incubated with Thrombin changed the molecular weight from 15473Da to 13721Da. This confirms that the His-tag was cleaved.

2.2.2 Expression & purification of MDM2-N$^{18-111}$

A paper published recently by Prof. Martin Noble's group has found a method to enhance the crystallogenesis of the N-terminal domain of MDM2 (Anil et al., 2013). The group has found that residues 109-125 can form a large unstructured tail and disfavour the crystallization process (**Figure 2.1**).

Alignment was performed on the sequences of multiple published structures with the sequence from Martin Noble (4HG7) and the currently used MDM2-N$^{11-130}$ sequence (**Figure 2.1**). As shown below the sequences from the published structures and Martin Noble's structure have the residues 109-125 chopped off. However the construct MDM2-N$^{11-130}$ that was used in the studies has an unstructured tail present and also extra residues on the N-terminal that could be the lid. This could be one of the reasons of no crystal growth in the crystallization trial. Therefore, a new short construct was designed that removed the unstructured tail on residues 109-125 and also the lid residues on the N-terminal.

2.2.2.1 Construct design of MDM2-N$^{18-111}$

The MDM2-N$^{18-111}$ sequence was cloned by PCR using the MDM2-N$^{11-130}$ plasmid as a template. The PCR product was analysed in a 1.2% agarose gel (**Figure 2.12 left**) and extracted using QIAquick gel extraction kit (QIAGEN). The extracted MDM2-N$^{18-111}$ sequence was run through a second PCR reaction to attach a His-tag at the N-terminal end. After attaching the His-tag, the length of the sequence increased by ~100 bases and this difference can be seen from the gel (**Figure 2.12 right**).

The sequence was then inserted into gateway donor vector and destination vector before transforming into the E. *coli* cells.

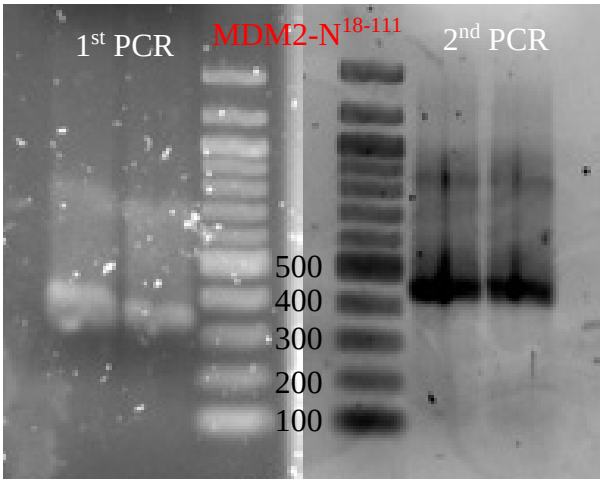

Figure 2.12 MDM2-N18-111 PCR reactions' products in 1.2% agarose gel.
Left gel is the samples from the MDM2-N$^{18-111}$ first PCR reaction and the product is ~350 bases. The right gel is the samples from the second PCR reaction with the His-tag attached and the product length has increased to ~450 bases.

2.2.2.2 Expression of MDM2-N$^{18-111}$

The condition used to express MDM2-N$^{11-130}$ was also used on MDM2-N$^{18-111}$. *E. coli* BL21 (DE3) and BL21 (DE3) STAR cells were investigated. The cells were grown at 37°C until OD_{600} reaches 0.3 and the cells were transferred to 25°C. 0.1mM IPTG was added at OD_{600} = 0.6 to induce the MDM2-N$^{18-111}$ expression.

The cells were harvested by centrifugation at 8000rpm for 30min and the expression was analysed using SDS PAGE. Expression of MDM2-N$^{18-111}$ was present in both

BL21 (DE3) and BL21 (DE3) STAR induced cells (**Figure 2.13**). In the uninduced cells there was also a band present in the same position in both BL21 (DE3) and BL21 STAR uninduced cells which may indicate a leaky expression.

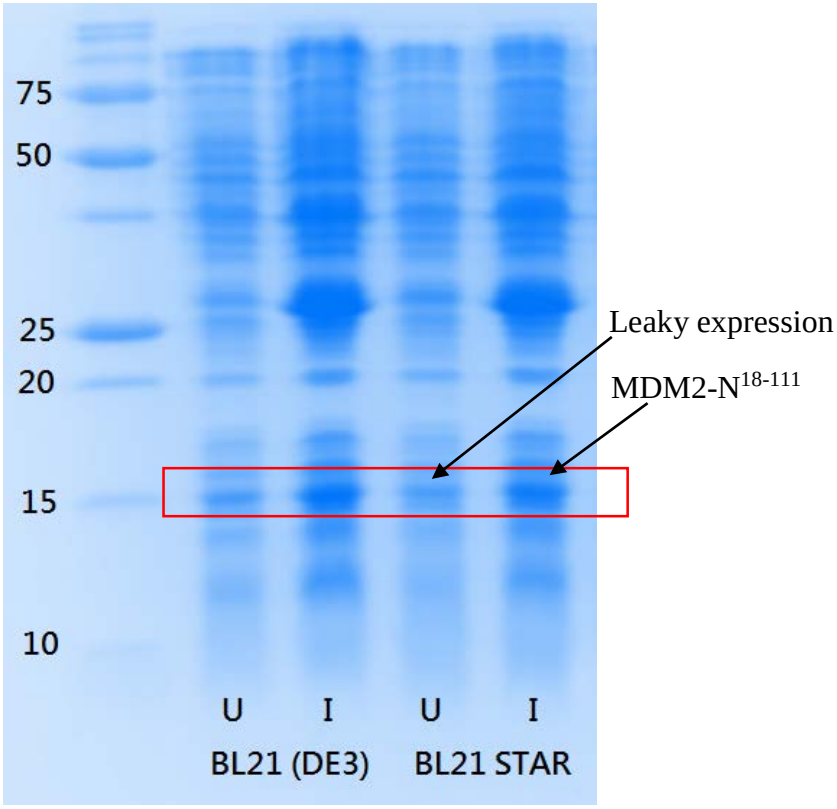

Figure 2.13 The results of an expression trial in two different competent cells.
Cells were induced with 0.1mM IPTG and MDM2-N^{18-111} was expressed in both cell lines.

2.2.2.3 Purification of MDM2-N^{18-111}

To confirm if the protein is expressed in the folded form the pelleted cells were lysed in 30ml lysis buffer and passed through the Constant Systems cell disruptor. The lysate was centrifuged and MDM2-N was mostly present in the soluble fraction (**Figure 2.14**).

MDM2-N was purified using a HisTrap column. Some of the contaminants were eluted at 75mM imidazole elution and the MDM2-N protein was eluted at 120mM concentration. However when looking at the proteins collected in the fraction collector

the MDM2-N proteins precipitated in the fractions. The concentration of the MDM2-N measured in the fractions was ~2mg/ml. This suggested that removing the unstructured tail and the N-terminal sequence from the MDM2-N reduced the solubility of the protein. The MDM2-N became prone to precipitation and the purification step had to be modified to prevent precipitation.

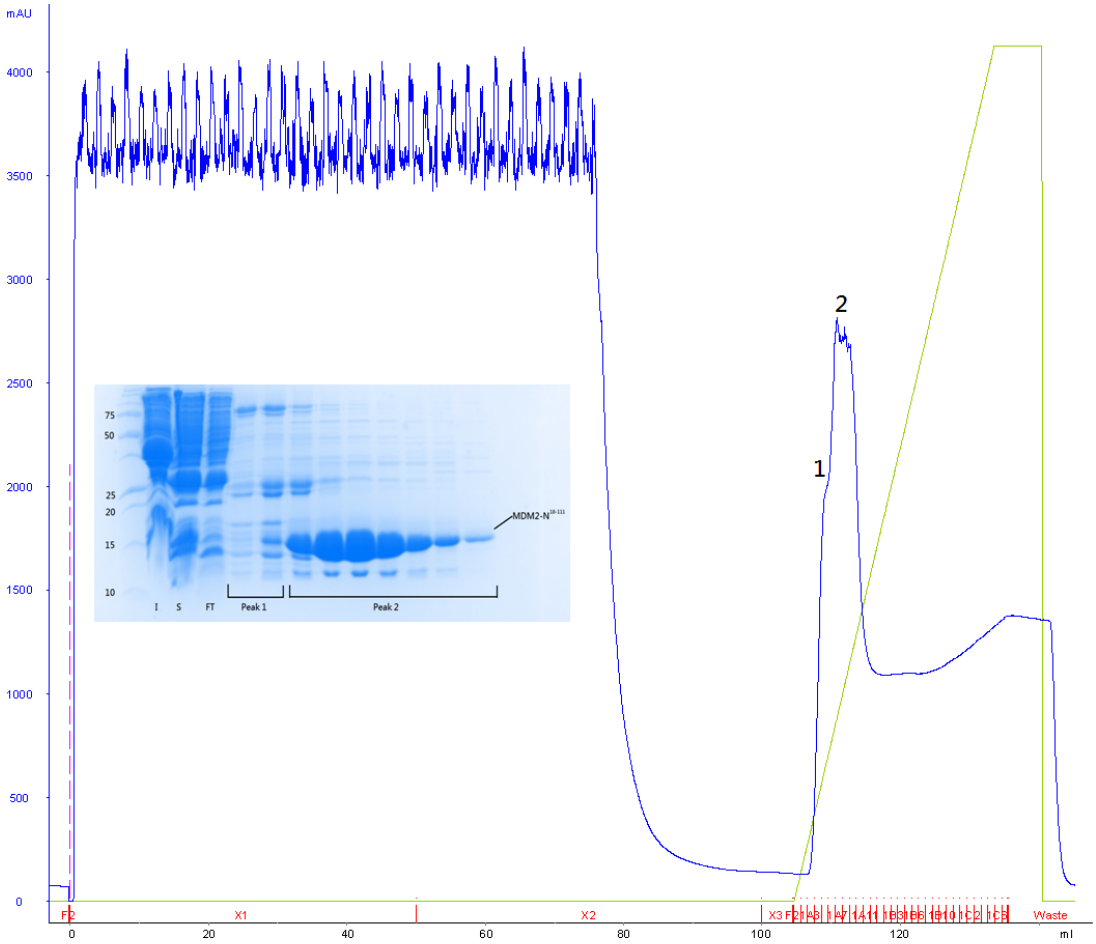

Figure 2.14 First step purification of MDM2-N$^{18-111}$.

MDM2-N$^{18-111}$ was loaded onto a 1ml Ni^{2+} HisTrap column and there were two peaks present in the elution profile. The peaks in the fractions were verified by SDS PAGE gel. MDM2-N$^{18-111}$ was confirmed to be eluted in the 2nd peak.

To help improve the solubility of the protein 10% glycerol was added into all the buffer solutions. The elution step was modified from a linear gradient into a two steps gradient elution. The first step involved eluting with 75mM imidazole to remove contaminants and the second step used 50CV of linear gradient to elute MDM2-N

protein (**Figure 2.15**). Elution with 50CV dilutes the protein to make it less concentrated. Unfortunately the MDM2-N protein eluted in the first 75mM imidazole elution but there was no precipitation in the fraction. The glycerol (10%) must have helped stabilized the protein and prevented the protein from precipitating. The protein was polished using HiPrep 16/60 S100 HR gel filtration column and 6mg/L of pure monomeric MDM2-N^{18-111} was obtained (**Figure 2.16**).

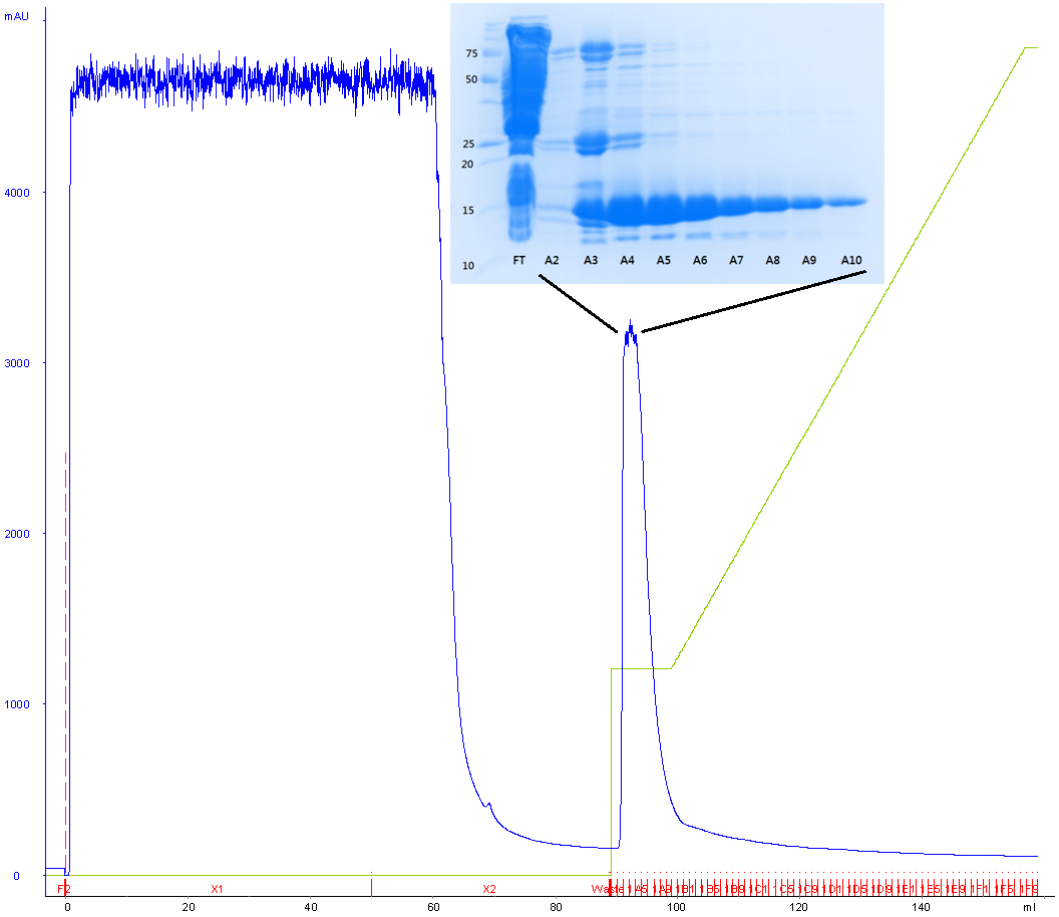

Figure 2.15 MDM2-N18-111 purification in Ni2+ HisTrap column.

MDM2-N^{18-111} was purified on an IMAC column using a buffer solution containing glycerol (10%). The first elution step used a 75mM imidazole step gradient and second step used a 50CV linear gradient from 75mM – 500mM imidazole. The MDM2-N was eluted in the first step of elution.

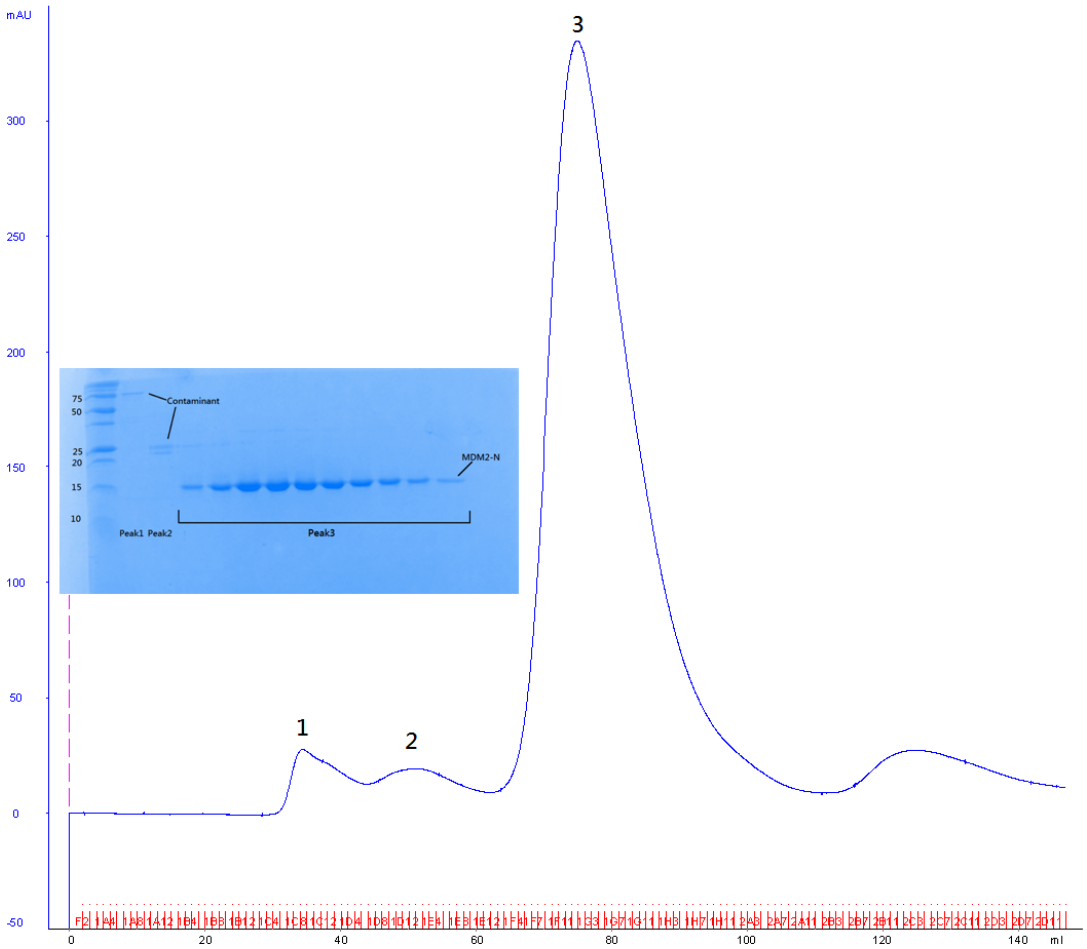

Figure 2.16 MDM2-N$^{18-111}$ purification by SEC.

Size exclusion chromatography purification of MDM2-N$^{18-111}$ using HiPrep 16/60 S100 HR column. Pure MDM2-N$^{18-111}$ was present in peak 3 and separated from the contaminants.

2.2.2.4 Assess MDM2-N$^{18-111}$ in FP binding assay

The purified His tag-MDM2-N$^{18-111}$ was assessed in the FP binding assay with the fluorescent labelled p53 peptide (**Method can be found in Chapter 4**). Detailed principle and method can be found in **Chapter 4**. The results of FP assay in **Figure 2.17** (**A**) showed the His tag-MDM2-N$^{18-111}$ affinity for p53-F has a K_d = 2.79μM. This is seven times weaker than binding with the His tag-MDM2-N$^{11-130}$ (**Figure 2.17 B**). As shown in **Figure 2.1**, the Histag-MDM2-N$^{18-111}$ has seven residues removed from the N-terminal end and the His-tag becomes very close to the binding site. This can

cause the His tag to interfere the p53-F from binding to the binding site and also disrupt the small molecule from binding.

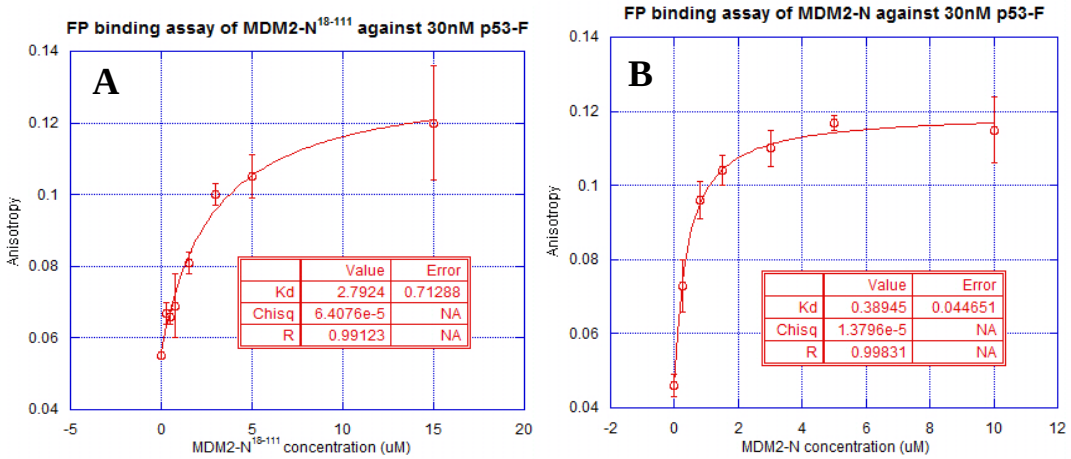

Figure 2.17 Comparing binding affinity of p53-F against MDM2-N$^{18-111}$ and MDM2-N$^{11-130}$.

FP binding assays were performed on MDM2-N$^{18-111}$ (A) and MDM2-N$^{11-130}$ (B) against p53-F. p53-F binds seven times weaker to MDM2-N$^{18-111}$ than MDM2-N$^{11-130}$.

2.2.2.5 His-tag cleavage on MDM2-N$^{18-111}$

A cleavage trial was carried out to cleave off the His-tag attached on the MDM2-N. A TEV recognition site was present between the His tag and MDM2-N so the cleavage trial can be performed using TEV protease enzyme. 100µg of MDM2-N was incubated overnight at 4°C with 1µg, 2µg and 4µg TEV protease. The cleavage trial resulted in around 50% cleavage using 4:100 ratio (**Figure 2.18 left**). When attempting to cleave the His tag from the 1.7mg of MDM2-N using 50µg TEV protease (3:100 ratio), only 50µg of MDM2-N had the His tag cleaved off (**Figure 2.18 right**). The TEV protease cleavage site may have been buried into the binding site and thus hindered the cleavage. Unfortunately the amount of untagged MDM2-N was too small to verify the effect of His tag in the FP assay.

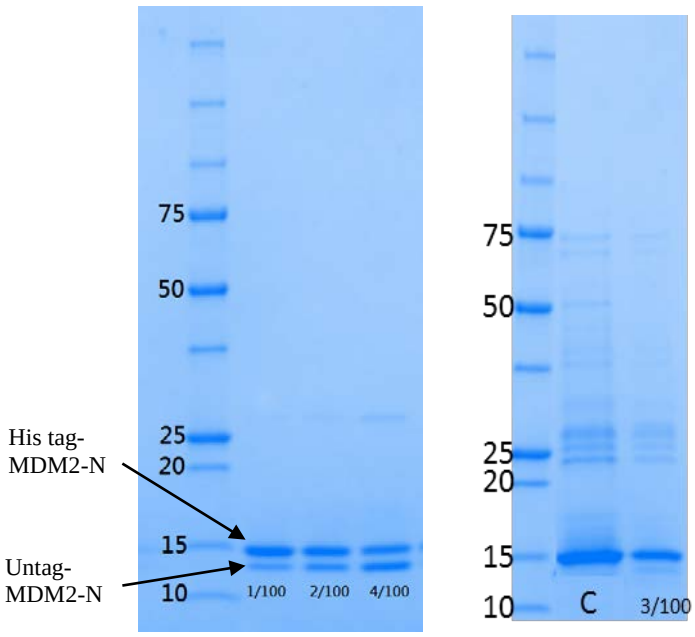

Figure 2.18 SDS-PAGE gel of cleavage trial for His-tag MDM2-N$^{18-111}$.

(Left) Different concentrations of TEV protease were incubated with MDM2-N$^{18-111}$. An increase of cleavage when increased the TEV protease and at 4/100 ratio, the cleavage rate was 50%.

(Right) His-tag-MDM2-N$^{18-111}$ was incubated with TEV protease at a ratio of 3/100.

2.2.3 Expression & purification of MDMX-N$^{14-111}$

MDMX has also been identified as a negative regulator of tumor suppressor p53 protein. Both MDM2 and MDMX binds to a short α helix in the transactivation domain of p53. The N-terminal domain of MDMX contains a p53 binding site that has a high homology as MDM2. Design of a dual inhibitor becomes possible to disrupt both MDM2 and MDMX binding to the p53.

To design a dual inhibitor, high purity MDMX-N had to be purified for small molecules screening in different assays.

2.2.3.1 Expression of MDMX-N$^{14-111}$

MDMX-N$^{14-111}$ plasmid was obtained from Dr. Maria Sanchez (**Figure 2.2**). The construct was expressed in LB, TB and Enpresso mediums. There was no expression found in the Enpresso medium but the MDMX-N$^{14-111}$ was expressed in the LB and

TB mediums (**Figure 2.19**). A higher expression was present in the TB medium than the LB medium.

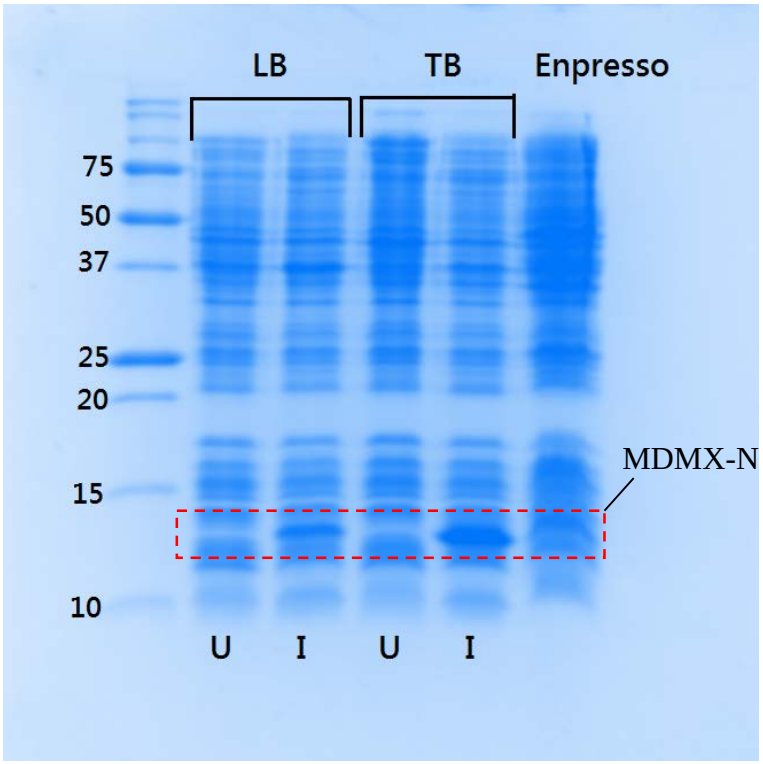

Figure 2.19 Expression trial of MDMX-N$^{14-111}$.
SDS-PAGE gel showing the expression of MDMX-N$^{14-111}$ in *E. coli* BL21 DE3 cells grown in LB, TB and Enpresso mediums. Cells were grown at 25°C and induced with 1mM IPTG when OD_{600} reaches 0.6. The lanes compare the expression level of MDMX-N$^{14-111}$ in the uninduced cells and induced cells grown in the mediums.

2.2.3.2 MDMX-N$^{14-111}$ purification

The *E. coli* cells containing MDMX-N protein were lysed by resuspending the cells in the lysis buffer and passing through the cell disruptor. The lysate was clarified by centrifugation and the His tag-MDMX-N was loaded onto a 1ml Ni^{2+} HisTrap column. The imidazole gradient to elute contaminants was already known from the previous purification trial (data not shown), so a step gradient (75mM imidazole) was applied to remove contaminants before eluting the MDMX-N protein with a linear gradient

(**Figure 2.20**). The truncated MDMX-N was separated at higher imidazole concentration.

The next step purification was to separate the contaminants and the truncated MDMX-N using superdex200 16/60 size exclusion column. The truncated MDMX-N is only 5kDa smaller than MDMX-N but the impurities and truncated MDMX-N was still successfully separated from the MDMX-N yielding 1mg/L culture (**Figure 2.21**).

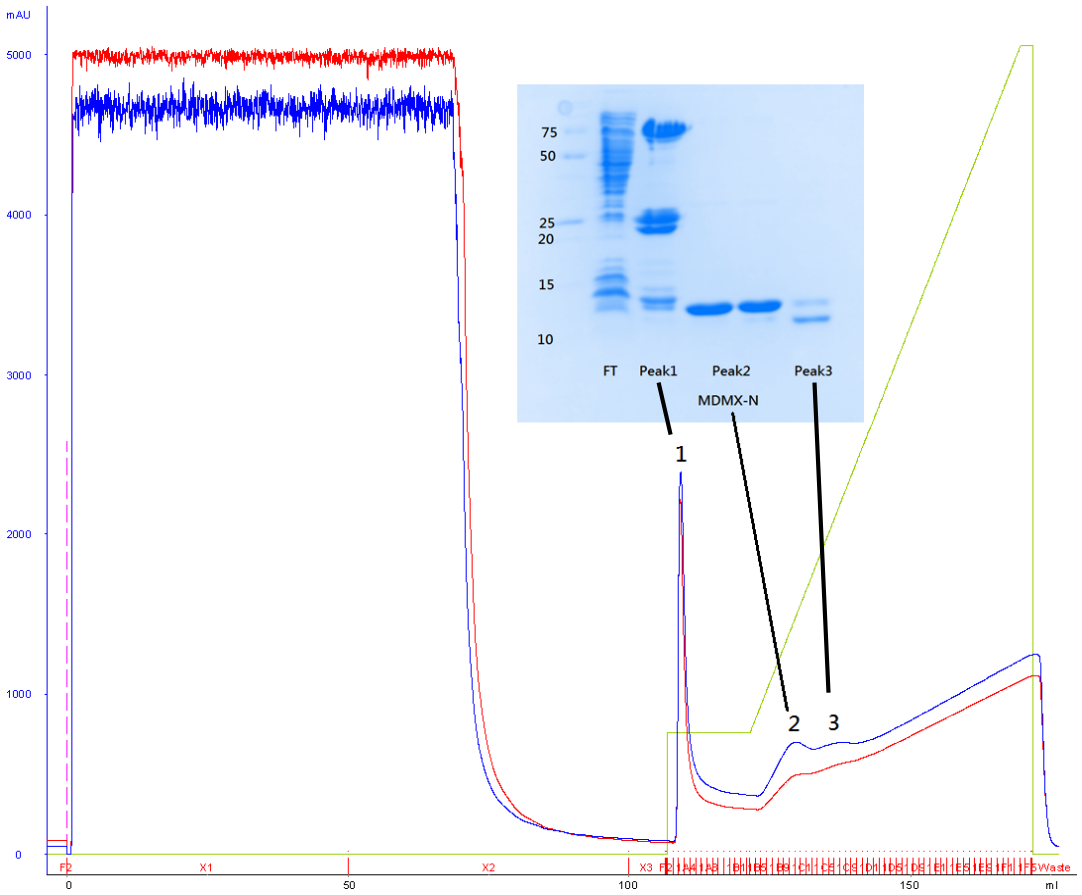

Figure 2.20 IMAC purification of MDMX-N$^{14-111}$.

The lysate containing MDMX-N was loaded onto the 1ml Ni^{2+} HisTrap column as first purification step. First gradient comprised of 75mM imidazole wash and large amount of impurities was washed off. MDMX-N was eluted in the linear gradient elution from 75mM – 500mM imidazole over 30 column volume. The elution also separated truncated MDMX-N at the peak fraction 3.

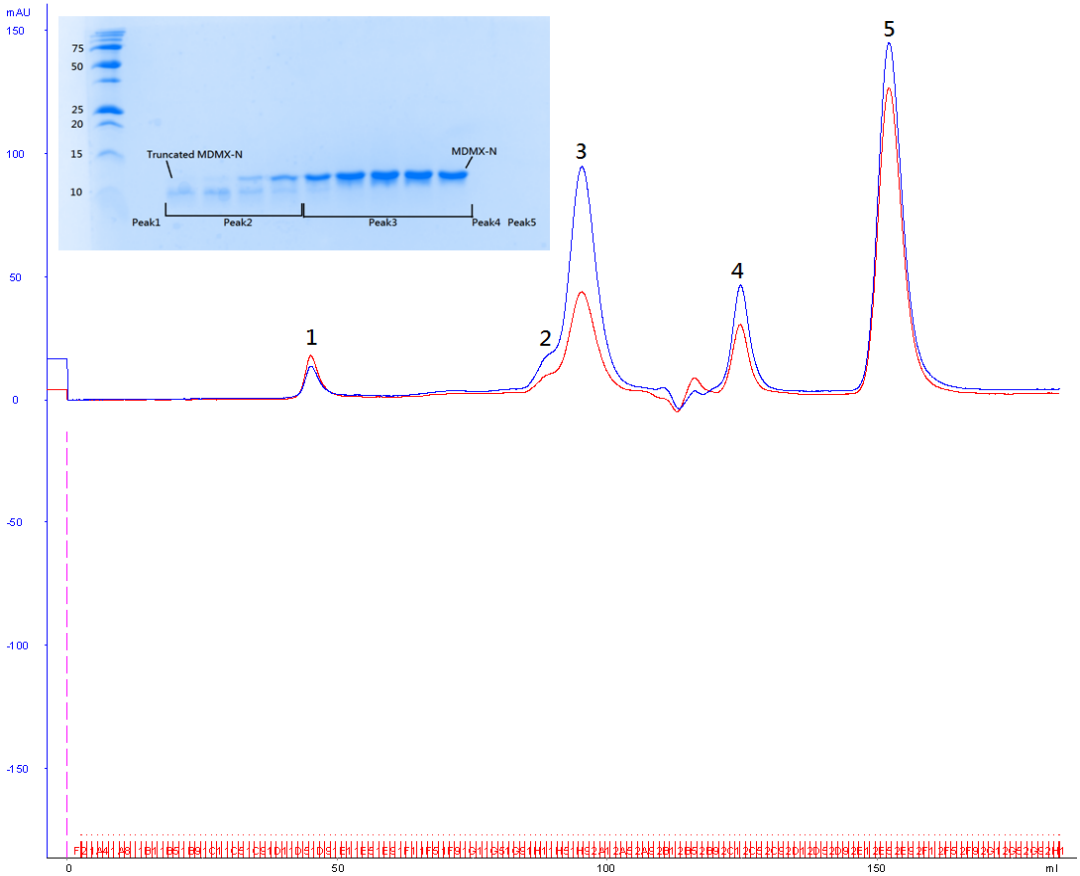

Figure 2.21 Size exclusion chromatography purification of MDMX-N$^{14-111}$.

SEC was performed using Superdex200 16/60 column. The peak fractions were analysed by SDS-PAGE gel. The gel confirmed peak 3 contains the pure MDMX-N and the shoulder peak 2 close to the peak 3 contains truncated MDMX-N.

2.2.4 Expression & purification of MDMX-N$^{23-109}$

2.2.4.1 MDMX-N$^{23-109}$ construct design

In **Figure 2.2**, multiple MDMX-N sequences from the PDB structures were compared with the MDMX-N$^{14-111}$ construct. The MDMX-N$^{14-111}$ sequence has a longer sequence at the N-terminal end and is absent in other published structure sequences. It is not clear whether this extended sequence at the N-terminal will affect the crystallization so a shorter construct was designed. The sequence from 3JZO structure was taken for new construct design.

2.2.4.2 Construct design of MDMX-N^{23-109}

MDMX-N^{14-111} plasmid was used as template to design the MDMX-N^{23-109} construct. Two rounds of PCR reactions were performed to insert the His-tag onto the MDMX-N^{23-109} construct. The length of the sequence has increased to ~400 bases when the His-tag was attached onto the N-terminal of MDMX-N^{23-109} construct (**Figure 2.22**).

The MDMX-N^{23-109} sequence was inserted into the gateway destination vector to be ready to transform into the E. *coli* cells.

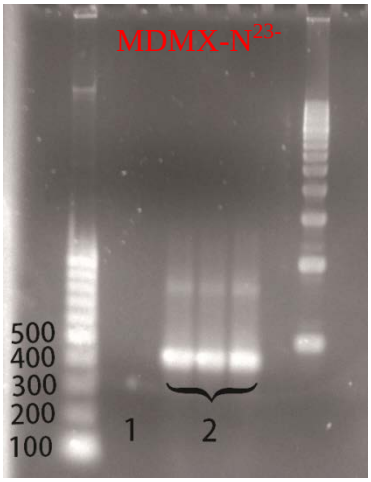

Figure 2.22 MDMX-N^{23-109} PCR reactions' products in 1.2% agarose gel.
Sample 1 is the MDMX-N^{23-109} first PCR reaction product with ~300 bases length and sample 2 is the second PCR reaction product with ~400 bases length.

2.2.4.3 MDMX-N^{23-109} expression

The conditions that were used to express MDMX-N^{14-111} and MDM2-N^{11-130} gave a reasonable yield of soluble proteins so these conditions were also used to express MDMX-N^{23-109}.

The plasmid was transformed into *E. coli* BL21 DE3 and BL21 (DE3) STAR cells. The protein was induced using 0.1mM and 1mM IPTG. The cells were run in the SDS PAGE gel to confirm if there is MDMX-N^{23-109} expression. The MDMX-N^{23-109} molecular weight is 13kDa and should be between 10kDa – 15kDa in the gel but there was no clear indication of MDMX-N^{23-109} expression in this region (**Figure 2.23 Top**).

The plasmid was also transformed into *E. coli* C41 (DE3), C43 (DE3) and Rosetta 2 strains. *E. coli* C41 (DE3) and C43 (DE3) strains were derived from BL21 (DE3) and it has the characteristic that helps to prevent cell death from the expression of toxic protein. Rosetta 2 is derived from BL21 strain with a supply of seven rare codons to enhance the expression of eukaryote proteins in the *E. coli*. The cells were grown using the same condition and the MDMX-N^{23-109} expression was induced using 1mM IPTG. The whole cells were run in the gel and there was still no indication of MDMX-N^{23-109} expression (**Figure 2.23 Bottom**).

Further expression trials will need to be carried out to express MDMX-N^{23-109}.

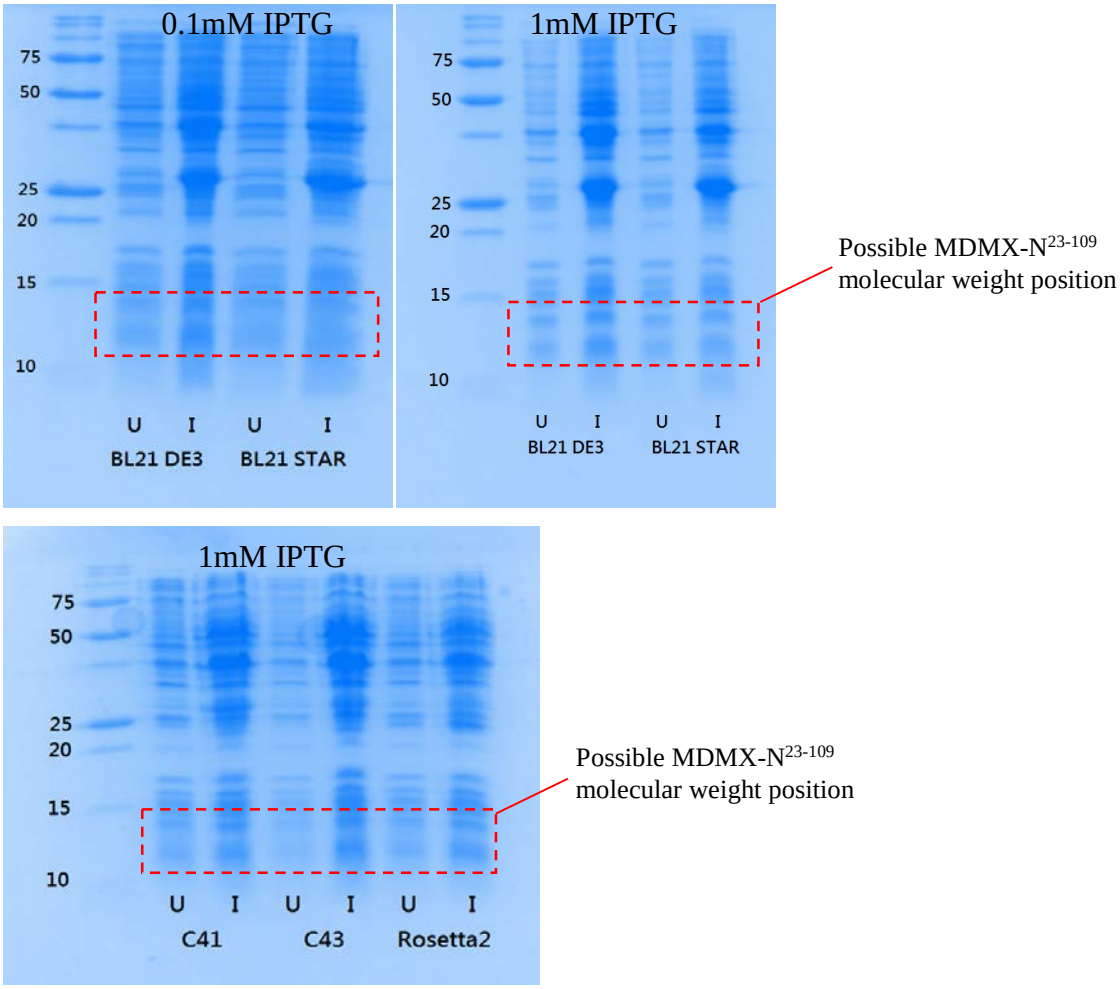

Figure 2.23 SDS PAGE gel showing the trial expression of MDMX-N23-109 construct.

Top) These lanes show different trial expressions in BL21 DE3 and BL21 STAR competent cells, uninduced cells and cells induced with 0.1mM, 1mM IPTG. There is no clear indication of MDMX-N^{23-109} expression at these conditions.

Bottom) This gel shows trial expressions of MDMX-N^{23-109} in C41 (DE3), C43 (DE3) and Rosetta 2 competent cells and induced with 1mM IPTG.

2.3 Conclusion of the purification of MDM2-N and MDMX-N constructs

MDM2-N^{11-130} was successfully expressed and purified with a yield of 34mg/4L and a purity >95%. When MDM2-N^{18-111} construct was expressed and purified we are not sure if the His-tag interfered with the binding site and there were also difficulties with cleaving off the His tag. Due to this problem the MDM2-N^{18-111} construct was not further used in biophysical and structural studies. His-tag MDMX-N^{14-111} was purified but the protein aggregated when the concentration was above 0.5mg/ml. This construct had to be stored at low concentration to prevent aggregation. The His tag of MDMX-N^{14-111} did not interfere the binding site which has been shown in **Figure 4.23** where the Kd value of fluorescently labelled p53 peptide obtained was in agreement with the publication (**Section 4.8.1**).

MDMX-N^{23-109} construct was designed for crystallization trial but the protein was unfortunately not expressed in the expression trial and this construct was discontinued for further study.

MDM2-N^{11-130} and MDMX-N^{14-111} were used for the biophysical studies.

Chapter 3 Screening for hits against MDM2-N and MDMX-N

Over the past few decades high throughput screening (HTS) has been the dominant method in the drug discovery process (Bajorath, 2002, Shoichet, 2004). Millions of compounds were screened through HTS and many lead drugs were identified. Chemists have synthesized large numbers of compounds for HTS. However this is only a small proportion of the possible available compounds and the cost to screen through millions of compounds is high.

An alternative cost effective approach makes use of computer-aided methods. Virtual screening is a computational approach that is able to analyze millions of compounds stored in databases using high throughput computational docking. During the 1970s several investigations were carried out using molecular docking to study intermolecular interactions (Greer and Bush, 1978, Levinthal et al., 1975, Wodak and Janin, 1978, Salemme, 1976). In 1982, Kuntz et al. described a geometric approach to study the receptor-ligand interactions (Kuntz et al., 1982) and numerous computational algorithms were gradually developed and optimised (McInnes, 2007). Virtual screening is becoming an important computational technique for drug discovery.

Even though there are many successful cases in virtual screening there are still many problems which need to be solved. Firstly, the protein flexibility is only partially considered in virtual screening. Further developments are required to address this issue. The participation of water molecules in protein-ligand interaction is also not considered in the docking process. The molecular interactions are difficult to parameterise and the pose scoring and binding energy predictions are imprecise which still require more time to improve.

There are two approaches in virtual screening, one is the structure based approach that uses an X-ray crystal protein structure and a large number of compounds to identify an optimal compound based on docking into a defined binding site on the protein (Reddy et al., 2007, Ghosh et al., 2006). The other approach is the ligand based method that employs compounds or substrates structures which are known to bind to the protein binding site and identify other compounds with similar characteristics (Reddy et al., 2007). These techniques are applied in this chapter to screen for MDM2 ligands.

3.1 Background of database and virtual screening programs employed

In this project I have employed four virtual screening programs to explore compound databases and identify hits. Both structure based and ligand based programmes (**Figure 3.1**) were employed and background for these programs are described.

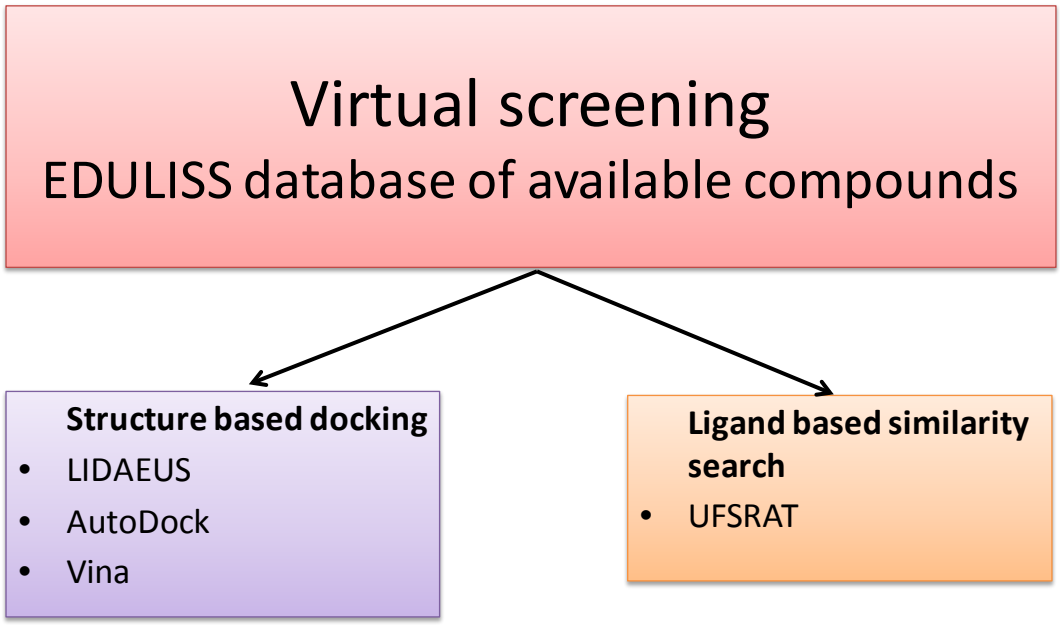

Figure 3.1 Virtual screening programs applied.

A diagram showing a list of virtual screening programs applied in the project to search for small molecule inhibitors.

3.1.1 EDULISS database description

The compound library that we used for database mining is EDULISS which stands for **ED**inburgh **U**niversity **LI**gand **S**election **S**ystem and was developed by Dr. Kun-Yi Hsin (Hsin et al., 2011). The library comprises over 5 millions compounds from 28 different suppliers. The library stores the 3D structure of the compounds for virtual screening and the pharmacophore, physicochemical and structural properties are also stored in the library.

There are over 3.9 millions compounds in the database that fit into the Lipinski's rule of five (Hsin et al., 2011).

In the database there are over 220,000 compounds which fit the Astex rule of three (Hsin et al., 2011) that are suitable for fragment based design (Hsin et al., 2011). When

new compounds are added into the suppliers catalogue they will also be added into the EDULISS library and thus, the library is continuously expanding.

The concept of drug-like or lead-like has been introduced into the drug design to characterise the properties for a drug to be successful. Three well known examples are Lipinski's rule of five, Oprea lead-like criteria and Astex rule of three. These features have often been used in the screening libraries to keep compounds that have smaller molecular weight with higher solubility. However applying these criteria into the search libraries may exclude out some potential hits that don't fit the criteria. One example is the natural products which have been explicitly excluded by the Lipinski's rule but they have contributed to the development of many drugs (Beutler, 2001).

3.1.2 Structure based docking

Structure based docking can be split up into several stages which are illustrated in **Figure 3.2**. The first stage is to identify a protein that has therapeutical interest and can be purified for experimental validation. An X-ray crystal structure of the protein and ligand is required as input for the virtual screening. The results are validated using different biophysical assays.

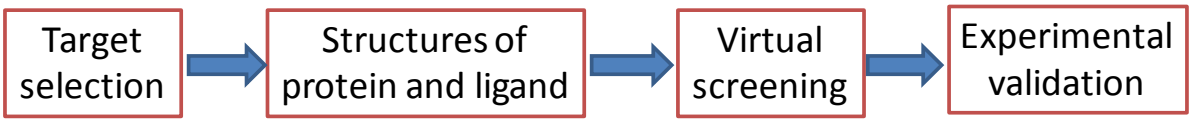

Figure 3.2 Stages involved in Structure based docking.

The diagram represents the pipeline involved in structure based docking. The compounds selected from virtual screening have to be validated using biophysical assays.

3.1.3 LIDAEUS

The first high throughput docking program that we employed was the University of Edinburgh in-house virtual docking program LIDAEUS which stands for **LI**gand **D**esign **A**t **E**dinburgh **U**niver**S**ity (Taylor et al., 2008). LIDAEUS is performed in several steps which are listed in **Figure 3.3**.

In the first stage the pdb structures of the protein and the natural ligand are obtained and used to generate an energy site map. The program MAPGEN is then used to generate the energy map around the binding site. There are three classifications of the site points generated; hydrogen bond donor (blue points), hydrogen acceptor (red) and hydrophobic (white). The site points generated can be manually inspected and modified using PyMOL (Delano, 2002). In POSE, LIDAEUS uses an exhaustive matching algorithm to fit molecules into the binding site by matching atoms with the site points in different positions to find the best poses. Then each compound fitted in the binding site will be scored according to the calculated energies of van der waals, hydrophobic and hydrogen bond interactions. However the desolvation force is not taken into account in LIDAEUS. Finally, the result will be sorted and the top 1000 compounds will be kept and ranked according to the score. In our work the top 50,000 compounds were kept for the next stage.

LIDAEUS is performed in a rigid body docking manner, which means the compounds are treated as rigid during the docking. Different conformations and flexibility in the compounds were not considered: the compounds were unable to change the conformation during docking. In order to partially overcome this problem a multi-conformer library of compounds was generated in which an average of 4 to 5 molecular conformations are stored for each flexible molecule. LIDAEUS is suitable for screening millions of compounds and provides a high throughput first step for virtual screening.

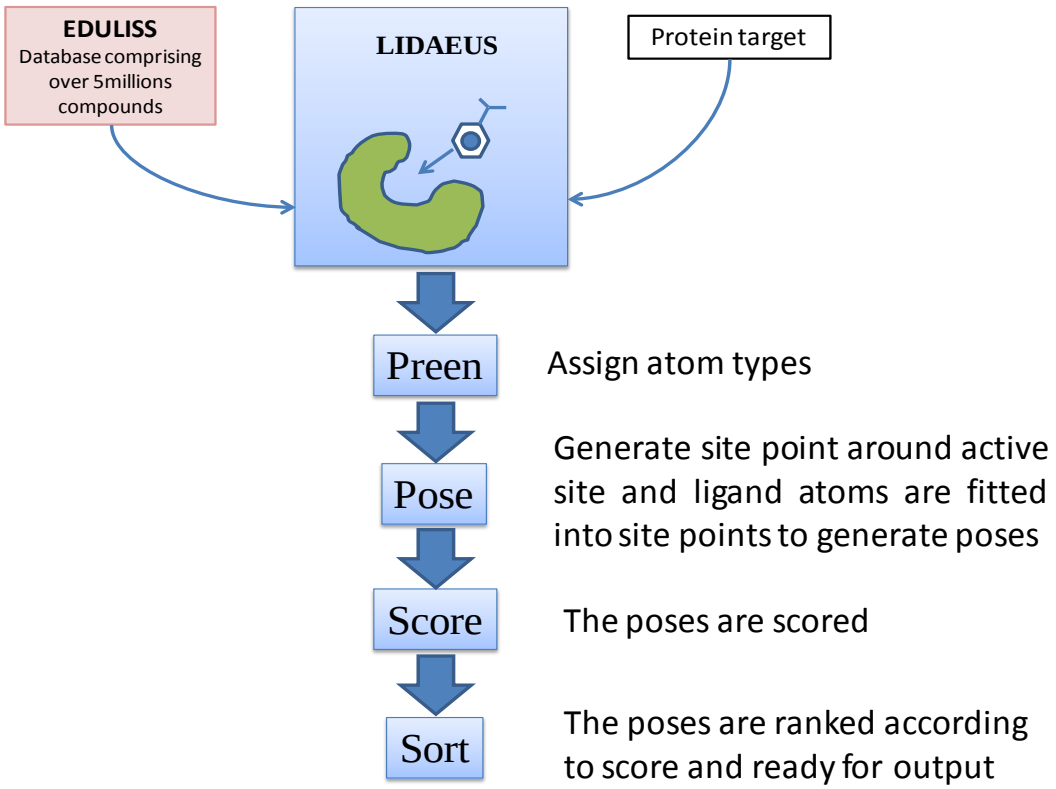

Figure 3.3 LIDAEUS pipline of docking process.

LIDAEUS is a rigid body in-silicon screening program that docks the EDULISS library compounds into the protein binding site through this pipeline. The poses are ranked according to the score and the top 1000 compounds will be kept.

3.1.4 AutoDock & AutoDock Vina

AutoDock and AutoDock Vina (Vina) are both molecular docking tools for protein-ligand docking (Morris et al., 2009, Trott and Olson, 2010). Compared with LIDAEUS that docks the compounds in a single conformation, AutoDock and Vina are able to dock the compounds flexibly in multiple conformations.

AutoDock used the program Autogrid to create an interaction map containing grid points around the binding site of the target protein. Different atom types (hydrophobic, hydrogen bond donor and acceptor) are assigned in the map. These grid points are stored and used in the docking simulation. The ligand atom is sequentially placed in

the grid and the interaction energy between the ligand atom and the protein is calculated.

In AutoDock the algorithm used to predict the conformation is the Lamarckian genetic algorithm (LGA) combined with semi-empirical free energy force field scoring function. In ligand docking the particular arrangement of a ligand and a protein is referred to as a state variable which corresponds to the genotype. The atomic coordinates of the ligand state is referred as the phenotype.

There are five stages involved in the LGA: mapping and fitness evaluation, selection, crossover, mutation and elitist selection.

Mapping reads in the phenotype of each ligand in the population and evaluates the fitness of every ligand. Fitness evaluation involves the calculation of the total interaction energy between the ligand and the protein using a semi-empirical free energy force field. This is the sum of the intramolecular energies of the unbound state ligand and the intermolecular energies between the ligand and the protein. Crossover also occurs in which random pairs of individuals crossover to produce a new genotype. The new genotype will possess genes from both parents. This is followed by selecting the individuals to reproduce depending on the fitness. The conformation with the lowest binding energy is selected.

Vina also employs grid map to calculate the interaction energies between the ligand and protein. However, Vina is able to precalculate the grid map internally and thus decreases the run time (Trott and Olson, 2010).

There are many successful examples of using AutoDock and Vina which can be seen in these papers (Azam et al., 2014, Penta et al., 2014, Gallicchio et al., 2014, Zor et al., 2014).

3.1.5 Ligand based similarity search

Ultra Fast Shape Recognition Atom Type (UFSRAT) is a tool that performs similarity searches on the compound of interest against millions of compounds in the EDULISS library (Shave, 2010).

UFSRAT performs shape recognition first by creating four descriptors from the geometric distribution of the molecule. The four descriptors are defined as points 1 (P1) to 4 (P4) (**Figure 3.4**). P1 is the 3D coordinate of the centre of the volume

occupied by the molecule. The Euclidean distances of all the atoms to P1 position were calculated and stored in a list. From the list, mean, variance and skew were generated. P2 is the atom that is closest to the geometric centre. P3 is the atom that is furthest away from P2 and P4 is the atom that is furthest away from P3. The Euclidean distances were generated between all the atoms and points 1 to 4. From the list of the Euclidean distances; mean, variance and skew were also generated for all distributions. These values allow UFSRAT to recognise the shape of the molecule. Three extra distributions were created to incorporate recognition and distributions of atom types. These are hydrophobic, hydrogen bond acceptor and hydrogen bond donor atom types similar to those used in LIDAEUS. This is used to classify the atoms in the molecule and enables UFSRAT to calculate 12 descriptors for each molecule.

The geometric distribution descriptors for the molecules in the library were previously generated. The geometric distribution descriptors for the query molecules were then compared with the molecules in the library and the similarity score between the two molecules was generated. Using the precalculated descriptors UFSRAT is able to compare the query compound with 1 million compounds within 3 seconds (Shave S. 2010).

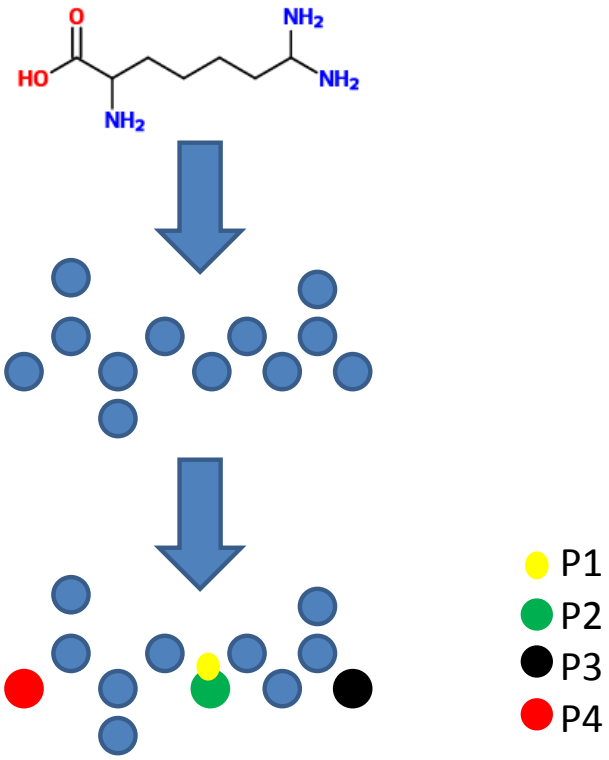

Figure 3.4 UFSRAT descriptors generation process.

The molecule atoms are considered as points and all the atom distances are calculated from the geometric centre (P1). From the list of the Euclidean distances; mean, variance and skew were also generated for all distributions.

3.1.6 Scoring algorithms

After the docking models were generated scoring algorithms were used to estimate the strength of the binding between the protein-ligand complex. Two different types of scoring algorithms, X-cscore and DrugscoreX, were employed in CODASS (as described in **Section 3.1.7**).

X-cscore is an empirical scoring function that estimates the binding affinity of protein-ligand complexes based on calculated energy terms (Huang et al., 2010). It combines three different scoring algorithms to form a consensus scoring strategy and estimates the binding affinity of a given complex. The total binding energy can be dissected into energy of van der waals interaction, hydrogen bonding, hydrophobic effects, desolvation effect and effective rotatable bonds.

Each scoring algorithm has its own advantages and disadvantages. Consensus scoring combines the advantages and reduced the disadvantages which improved the success rate over using a single algorithm (Wang et al., 2002).

DrugscoreX is a knowledge based scoring function which extracts the structural information from crystallographically determined protein-ligand complex data. It uses distance-dependent pair potentials to observe specific interactions between atoms of the protein and ligand.

The protein data bank (PDB) and Cambridge structural database (CSD) were used and the energies between the atoms of protein and ligand at a distance $1.0 \leq d \leq 6.0$ Å were observed. This builds up the knowledge based potential database for statistical observation of intermolecular contacts. Scoring of protein-ligand complexes is calculated as the sum of all occurring atom-atom interactions (Velec et al., 2005).

However, currently there are still some limitations for the scoring algorithms to simulate the binding between protein-ligand complexes (van Gunsteren et al., 2006). The free energy that drives the biomolecular processed is the summation of many atom pairs contributing to the non-bonded interaction. The accuracy decreases when deriving the summation of atom pairs in the large system (such as protein-ligand and protein-DNA etc.). Another problem is that different X-ray crystal structures were obtained using different conditions (such as different temperature, buffer solution or pH) which can affect the conformation of the proteins and the water molecule contribution (solvation and desolvation effect). This results in an entropic effect that plays an important role in the biomolecular systems and brings more difficulties for the computer to simulate the force field parameters.

3.1.7 Combining Docking and Similarity Search (CODASS)

If a protein structure with inhibitor or substrate bound is available, then structure based design may be performed and this involves multiple sequential phases.

CODASS is an integrated virtual screening script developed by Dr. Douglas Houston that combines a multitude of docking algorithms, similarity algorithms and scoring algorithms to search through millions of commercially available compounds in the

EDULISS (Hsin et al., 2011) database. Through combining these virtual screening programmes the run time is minimised while the enrichment is maximised.

Figure 3.5 shows a work flow chart of CODASS. Initially, Oprea lead-like criteria (MW ≤ 460, -4 ≤ LogP 4.2, rotatable bond ≤ 10, number of rings ≤ 4, Hydrogen bond donor ≤ 5 and Hydrogen acceptor ≤ 9) (Hann and Oprea, 2004) was used in order to extract smaller and more soluble compounds. This criteria was used as a filter in the EDULISS library which contains 4 million compounds and 20 million conformers. After this initial screen 1,162,000 compounds and around 4.8 million conformers were identified.

These compounds were fed into LIDAEUS (See **section 3.1.3**), a high throughput rigid body docking program that docked the compounds into the p53 binding site of the MDM2 structure. The results were ranked based on the LIDAEUS score and around 50,000 compounds were selected. These compounds were docked into MDM2 using Vina (Trott and Olson, 2010) which has an improved binding mode prediction and allows flexible docking of the compounds. The docked poses were ranked using Vina and the top 5000 compounds were selected. These 5000 hits were used with UFSRAT to identify compounds with similar structures that was not recognized by LIDAEUS. UFSRAT identify 24,000 compounds from the "Oprea" subset of EDULISS and redocked with Vina. The ranked poses were merged with the original Vina result and duplicates were removed. Ligand based method was used at this stage to pull out analogues to enrich the search results that were not previously identified from the docking programmes. These compounds were then docked using AutoDock. The binding poses predicted by AutoDock and Vina were compared via RMSD (root mean square deviation). AutoDock and Vina uses its own unique algorithm to dock the compound and combining the binding modes predicted by these programmes can significantly increase the success rate (Houston and Walkinshaw, 2013). This is an interesting technique which has proven to generate more reliable docked poses (Houston and Walkinshaw, 2013). Bind poses that were similar with RMSD ≤ 2Å were also scored with X-cscore and DrugscoreX. Final rank list was prepared according to the scores from Vina, AutoDock, X-cscore and DrugscoreX.

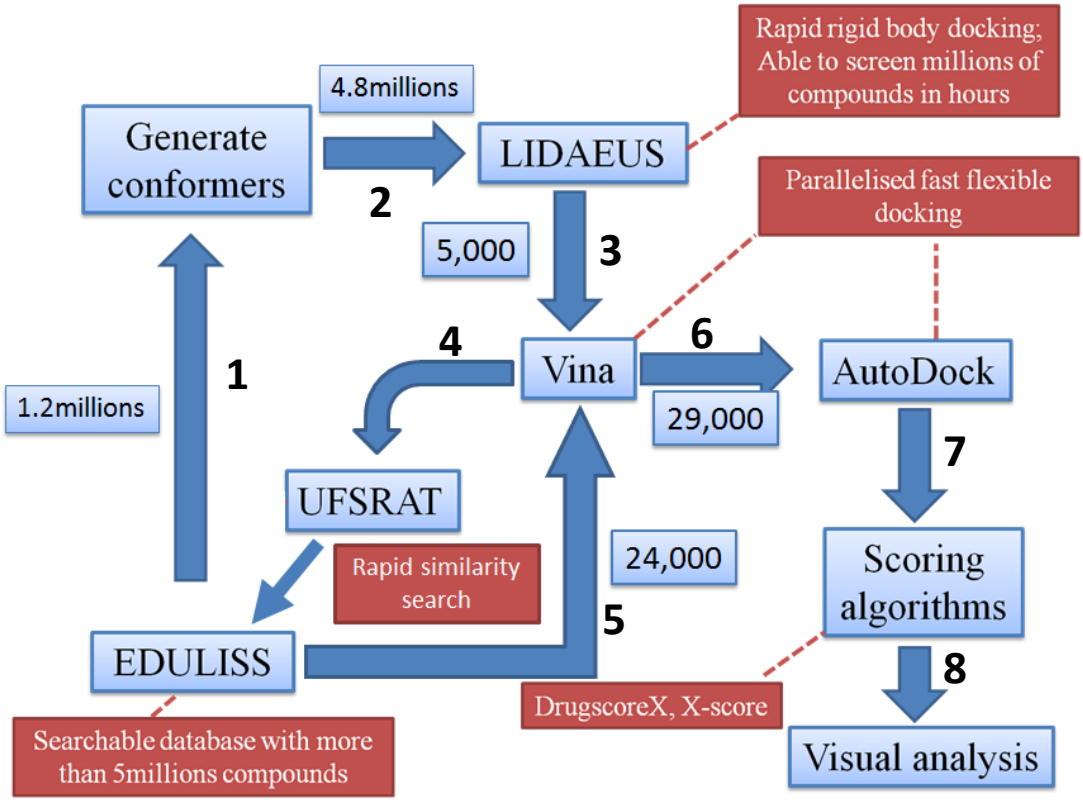

Figure 3.5 Flow chart of CODASS script.

The compounds in the EDULISS library are docked into the protein through multiple virtual screening programs. Numbers were used in the flow chart to indicate the order in the process. Additional similarity search is performed using UFSRAT to enrich the search results. The docked poses predicted by AutoDock and Vina are ranked and scored using DrugscoreX and X-cscore. The top 1000 ranked poses are kept for visual analysis.

3.1.8 Fragment based drug discovery (FBDD)

FBDD focuses on identifying small molecules that are able to fit into binding grooves to achieve efficient binding (Barker et al., 2008). These small molecules tend to be quite soluble and provide good starting points for subsequent chemical modification. This contrasts strongly with the HTS approach in which HTS libraries contain many compounds of high molecular weight with a complex structure. These characteristics cause poor physiochemical properties such as poor solubility and low permeability (Gribbon and Andreas, 2005, Lipinski et al., 1997). Thus, this may result in the genuine hits identified from HTS to be unsuitable as a starting point for lead optimisation.

Fragment design is now well established in many pharmaceutical companies and many successful examples are now published (Hajduk and Greer, 2007, Wyatt et al., 2008). Fragments are low molecular weight molecules (< 250Da) with weak binding affinity ranging from μM – mM. These weak affinity fragments require high sensitive biophysical techniques for detection. Currently the most commonly used techniques for fragment screening are X-ray crystallography (Wyatt et al., 2008, Hartshorn et al., 2004), Nuclear Magnetic Resonance (NMR) (Lepre et al., 2004) and Surface Plasmon Resonance (SPR) (Schulz and Hubbard, 2009). These techniques are highly sensitive but they have constraints on the type of proteins that can be screened.

The rationale of choosing small molecular fragments as the lead-like compounds is that adding sub groups during the optimization stages will result in an increase in molecular mass, complexity and hydrophobicity of the compounds. Using a small molecular weight compound as the starting point is therefore important for drug development.

It is also possible to break down the structure of the known inhibitors into multiple substructures that interact in the binding site (**Figure 3.6**). These substructures can be used to identify higher quality interaction fragments that bind deeply into the binding grooves. Several papers have demonstrated this method to link high quality interaction fragments together to create more potent compounds (Scott et al., 2012).

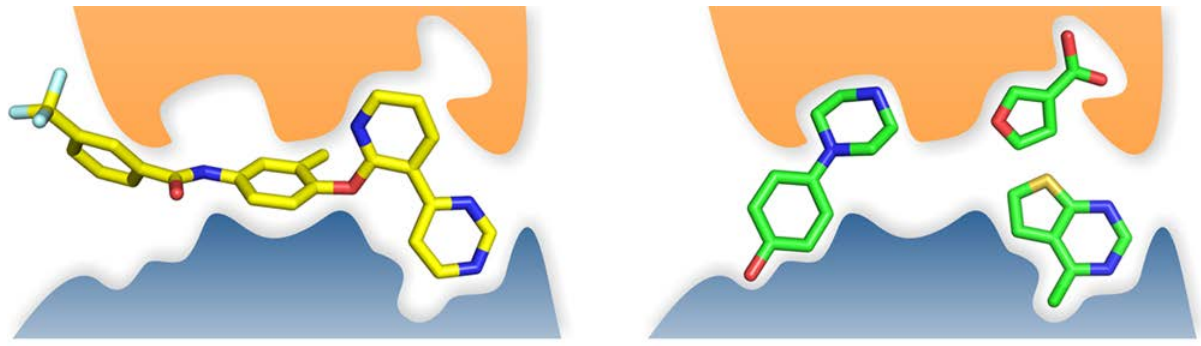

Figure 3.6 Fragment based drug discovery.

Hit identified from screening may interact with multiple binding grooves. When compared with fragment it is more ligand efficient and can provide more optimised interaction. Taken from (Scott et al., 2012).

Ligand Efficiency – an effective index for drug discovery

Ligand efficiency (LE) is a measure of the average binding energy of each heavy atom in a compound to its binding target. **Equation 3.1** (Hopkins et al., 2004) was used to estimate the efficiency of the compound and assess the binding affinity contribution per atom. It is the ratio of binding affinity to molecular size.

$$LE = -\frac{\Delta G}{HA} = \frac{-RT*lnIC50}{HA} \quad \textbf{Equation 3.1}$$

ΔG = Gibbs free energy

R = Gas constant

T = Temperature in Kelvin

HA = Number of heavy atoms

LE has often been used in lead assessment and during the fragment optimisation process. The values are calculated when analogues are synthesized to evaluate the binding efficiency on the added sub group. As the fragment molecular weight grows in optimisation the LE will decrease. A drug like compound should have a LE of ~0.3 (Schultes et al., 2010).

3.1.9 Lipinski's Rule of 5 vs Astex Rule of 3

Lipinski's rule of 5 is a rule that has been widely used by the pharmaceutical companies to evaluate the drug likeliness of a compound and its oral availability into the human body. The rule was proposed by Christopher Lipinski in 1997 and describes the molecular properties of a compound generally required for good pharmacokinetics in the human body (Lipinski et al., 1997). The four pharmacokinetic parameters are Absorption, Distribution, Metabolism and Excretion (ADME). Lipinski predicts compounds that do not obey the rule of five are more likely to have poor absorption and permeability (Lipinski et al., 1997). In Lipinski's rule of five it states orally active drugs should match these criteria:

- Molecular weight ≤ 500Da.
- cLogP ≤ 5.
- Number of Hydrogen bond donors ≤ 5.
- Number of Hydrogen bond acceptors ≤ 10.

cLogP is the calculated LogP that stands for the octanol-water partition coefficient and is a value for measuring the compound hydrophilicity. Low hydrophilic compounds have high cLogP values which leads to a poor absorption and permeability (Lipinski et al., 1997).

Compounds that do not match the rule of five, with 10 or fewer rotatable bonds and polar surface <140 $Å^2$ are less likely to permeate across the membrane bilayer (Lipinski et al., 1997, Veber et al., 2002).

Most of the HTS compounds were selected based on the Lipinski's rule of five. However the compounds that match this rule may be more than 10^{60} (Congreve et al., 2008) and these compounds are more difficult for optimisation. Therefore, an alternative approach has arisen. The Astex rule of three is a more strict criteria compared to the Lipinski's rule of five and it is often used in the fragment selection process (Congreve et al., 2003):

- Molecular weight < 300
- Number of hydrogen bond donors ≤ 3
- Number of hydrogen acceptor ≤ 3
- cLogP ≤ 3

Using the rule of three the compounds in the library can be narrowed down to small molecule fragments that are more chemically diverse and less in number. There are around 10^7 fragments which match the rule of three and this number of compounds is more feasible to be screened and provides a greater chance of finding more diverse hits.

3.2 Virtual screening for MDM2 ligands

3.2.1 Structure model selection

An X-ray protein crystal structure template is vital for computational docking when undertaking structure based virtual screening. An analysis was carried out to review the MDM2 crystal structures available in the PDB website. The structures 3JZK, 3LBK and 3LBL were found to contain chromenotriazolopyrimidine, WK23 and Mi63 analogue bound (**Table 3.1**). From these three structures 3LBL was selected as the template for virtual screening as it had been refined using the highest resolution data with the lowest R-factor.

Structure PDB ID	Ligand name	Ligand structure	Resolution (Å)	R factors -work -free	MDM2 sequence
3JZK	Chromenotriazo-lopyrimidine	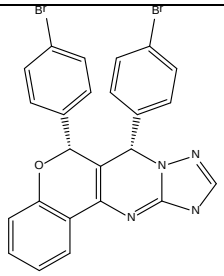	2.10	0.30 0.32	17-111
3LBK	WK23	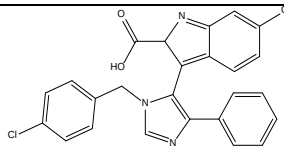	2.30	0.21 0.25	18-111
3LBL	Mi63 analogue	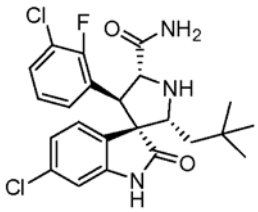	1.60	0.19 0.24	18-111

Table 3.1 Crystal structures of MDM2 with bound small molecules.

An alignment was performed on these three crystal structures to analyze possible side chain movement. **Figure 3.7** shows that in the 3LBL structure the Tyr67 has rotated its side chain into the binding site to form a steeper wall. The Tyr67 – His73 loop in 3LBL

folds differently compared to the other two structures which may be caused by the rotation of Tyr67 side chain.

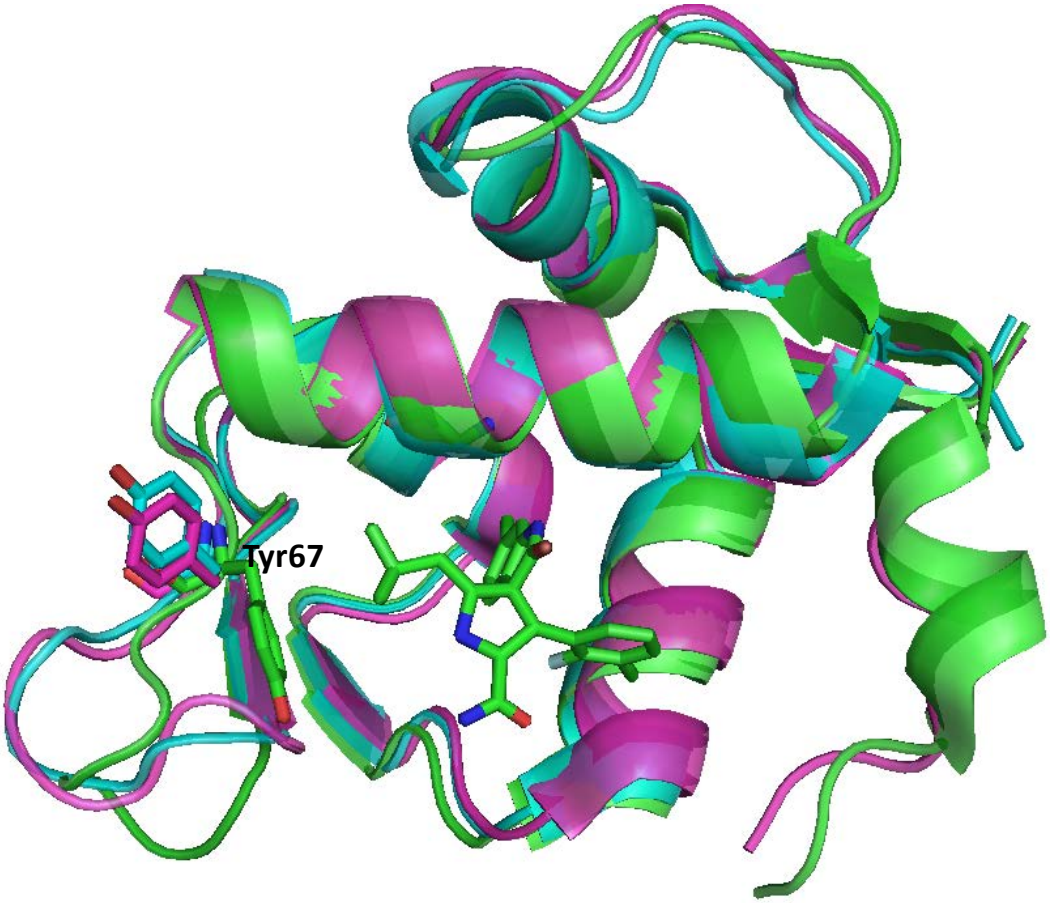

Figure 3.7 Alignment of multi MDM2 crystal structures.

The structure of 3LBL, 3LBK and 3JZK are coloured in green, blue and pink respectively. The Mi63 inhibitor in 3LBL is shown in the binding site and the Tyr67 side chain in 3LBL has rotated into the binding site.

A control docking experiment was carried out using AutoDock and Vina to demonstrate the accuracy of the docking. The control ligand used was Mi63 and the protein model used was the X-ray crystal structure 3LBL pdb file (**Figure 3.9**).

Both AutoDock and Vina have successfully reproduced the crystallographic binding mode of Mi63 with an RMSD of <0.18 Å (**Figure 3.8**). AutoDock predicted the free energy of binding to be -9.38kcal/mol and Ki of 133nM while Vina predicted the free energy of binding to be -6.1kcal/mol. This is relatively close to the experimentally

measured Ki of 36nM (Popowicz et al., 2010) which was not be expected and may be just a relative trends.

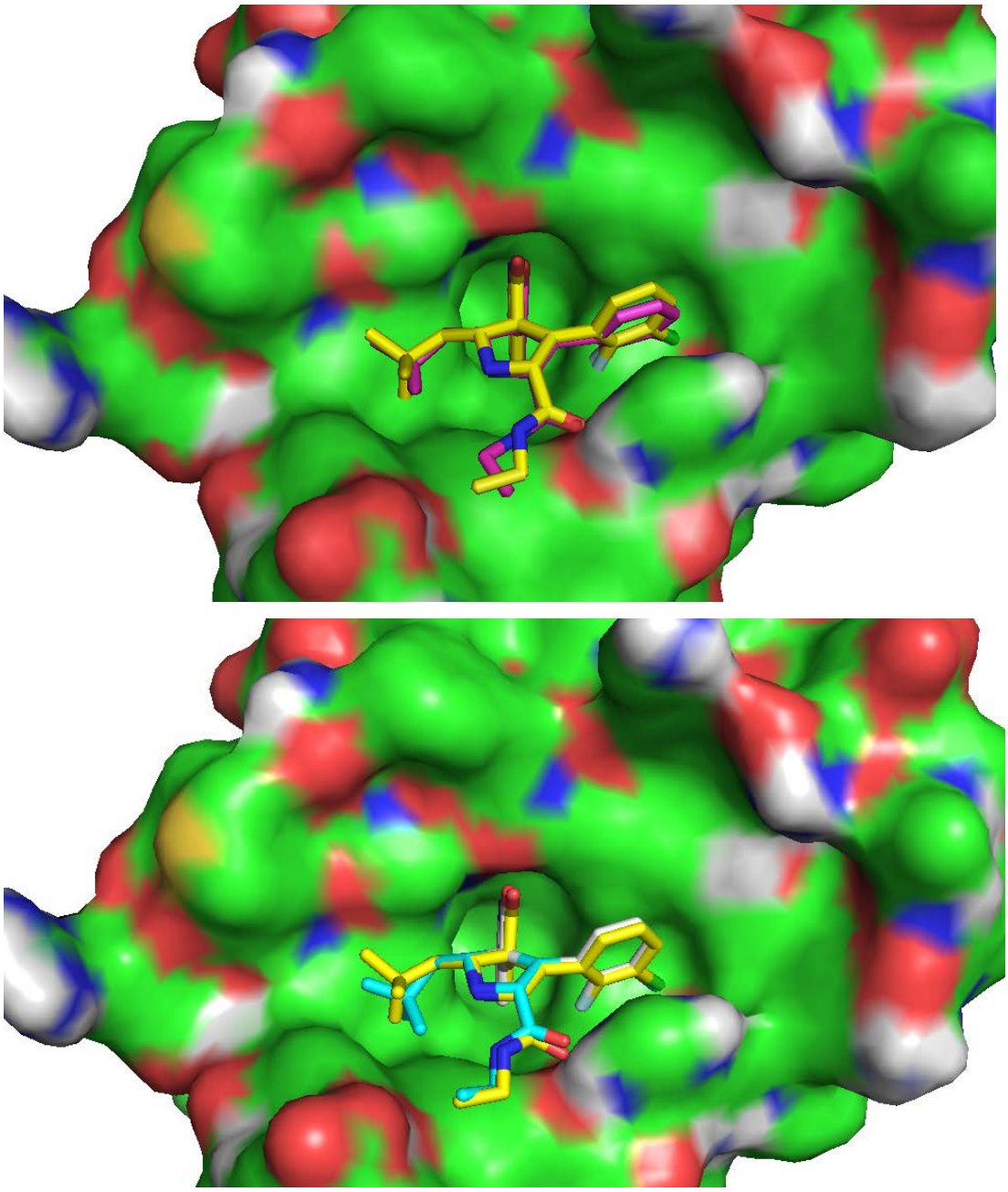

Figure 3.8 Control docking results of Mi63 in MDM2/p53 binding site.
Crystallographic pose of Mi63 in yellow stick is compared with the AutoDock docking pose shown in red (**Top**) and Vina docking pose shown in light blue (**Bottom**). The MDM2 crystal structure used is the 3LBL pdb structure.

3.2.2 First CODASS run with MDM2

As described in **section 3.1.7**, 1.1 million compounds for MDM2-N were screened. The script CODASS was used as the tool for screening (**Figure 3.5**), the X-ray crystal structure from 3LBL pdb file (Popowicz et al., 2010) was used as the protein model and Mi63 inhibitor was used as the template for site points generation around the binding site (**Figure 3.9**).

Analyzing the MDM2/Mi63 interaction revealed that the three side groups of Mi63 were binding into the three hydrophobic pockets in MDM2 which mimic MDM2/p53 interaction. The 6-chlorooxindole group on Mi63 binds into the Trp23 hydrophobic pocket of MDM2 and the NH on the oxindole group is making hydrogen bond contact with Leu54 residue (yellow dashed line in **Figure 3.9**). The other two major groups 2-fluoro-3-chlorophenyl ring and neopentyl have filled into the Leu26 and Phe19 hydrophobic pockets in MDM2 respectively. The amide group on the Mi63 also forms hydrogen bond interaction with the His96 imidazole group.

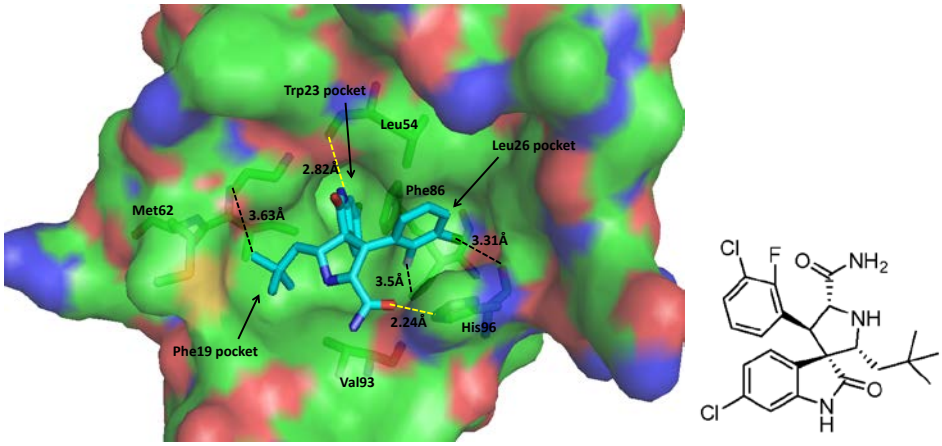

Figure 3.9 The binding of Mi63 in the MDM2-N binding site.

Mi63 binding to MDM2-N is shown in the diagram (Left) and the chemical structure of Mi63 is shown on the right. Mi63 interacts with MDM2 residues using two intermolecular hydrogen bonds as shown in yellow dashes.

After the CODASS run is complete a ranked list of top 266 compounds was generated. These compounds possess multiple hydrophobic rings due to the fact that the MDM2-N binding site is built up by hydrophobic side chain residues.

The docked poses predicted by AutoDock and Vina showed that these compounds use their hydrophobic rings to bind to the three hydrophobic grooves in MDM2-N. The calculated average AutoDock and Vina scoring energies of these 266 hits are between -7.10 to -10.30 and -7.50 to -10.50 respectively. Ligand efficiencies for these compounds were calculated using **equation 3.1** and calculated LE values are between 0.24 to 0.34. These compounds are relatively drug like since the drug like compounds have LE ~0.3 (Schultes et al., 2010).

The 266 top scoring hits from this CODASS run were then screened "visually" by Dr. Simon Pettit (Chemist at Selcia) and 6 compounds were selected (**Table 3.2**) based on the following criteria:

- Good docking score by both methods.
- Drug like structure: no reactive groups (no acid chlorides, no alkyl halides).
- Not too lipophilic (LogP $\leq$ 4).
- When several closely related compounds were selected the final selection was made based on commercial availability and one compound was selected to represent the family.

For the 6 compounds in **Table 3.2** the poses predicted by AutoDock and Vina (**Table 3.2**) showed highly similar docking poses with RMSDs within 2Å. The AutoDock and Vina free energy binding calculated for these compounds are between -7.4 to -8.4kcal/mol and -8.2 to -9.3kcal/mol respectively.

Many of these compound structures were composed of multiple hydrophobic rings that dock into the three hydrophobic grooves of MDM2's binding site. This is relatively similar to the known MDM2 small molecule inhibitors listed in **Table 3.1**.

Compounds 3 and 4 use a pyrrole and imidazole ring as the core to link with three hydrophobic rings. Compound 6 uses a formaldehyde group and compound 2 uses a urea group to link with three hydrophobic rings. These six compounds shared different chemical properties and compounds 1 and 2 appeared more novel and possess little similarities compared to the known inhibitors (**Table 3.1**).

Subsequently these compounds were validated using FP and CE assays (**Section 4.7.3**, **Section 5.4.1.4**). The FP and CE assays results showed 5 out of 6 as active in the competitive binding assays (Discussed in **Section 4.7.3 and Section 5.4.1.4**).

Docked poses from AutoDock and Vina	Chemical structure	Vina (kcal/mol	AD (kcal/mo	Xscore	Drugscore	% Inhibition using CE	% Inhibition using FP
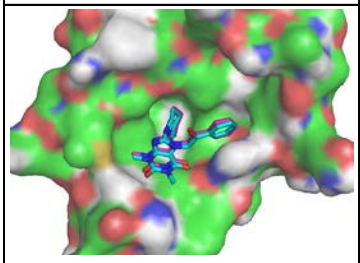	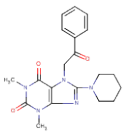	-9	-8.44	6.69	-423197	40% at 300μM	25% at500μM
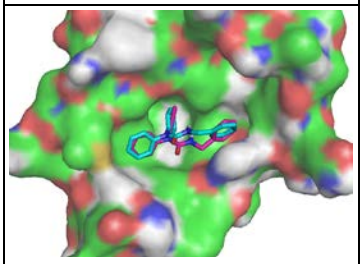	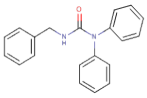	-9	-8.37	7.48	-427206	42% at 300μM	18% at 500μM
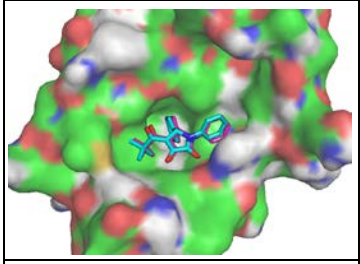	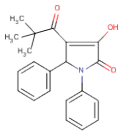	-8.2	-7.79	7.61	-389617	40% at 300μM	37% at 500μM
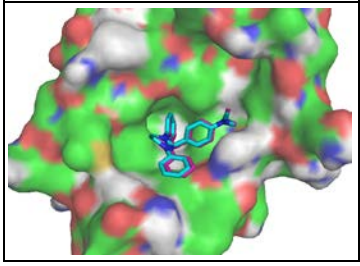	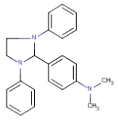	-8.3	-7.42	7.48	-393773	13% at 50μM	0% at 50μM

Docked poses from AutoDock and Vina	Chemical structure	Vina (kcal/mol	AD (kcal/mo	Xscore	Drugscore	% Inhibition using CE	% Inhibition using FP
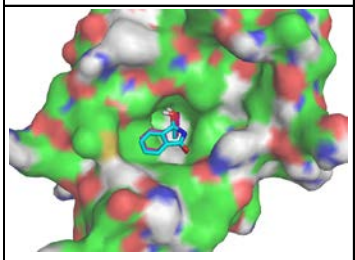	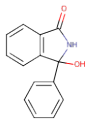	-9	-7.38	7.53	-383764	40% at 300μM	13% at 300μM
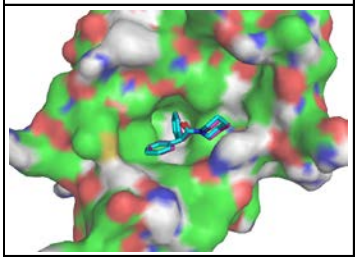	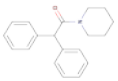	-9	-7.38	7.15	-361414	0% at 50μM	3% at 50μM

Table 3.2 Ligands docking poses predicted by AutoDock and Vina are presented in the table.

Ligands coloured in purple represent docking by AutoDock and ligands coloured in light blue are docked by Vina. The chemical structure, Vina score, AutoDock score, X-score and Drugscore are also listed in the table. The compounds in the table are ranked based on the AutoDock score.

3.3 Second CODASS screening with MDM2 and MDMX

3.3.1 Template structure selection:

With the success from the previous virtual screening run which identified 5 hits against MDM2, a new round of CODASS screening was performed on MDM2 and MDMX to explore the possibility of identifying dual inhibitors. In this virtual screening run a reduced complexity subset of EDULISS library was used in order to obtain compounds that are smaller and more soluble. The subset contains a new criteria (MW 200 – 300Da, -4 ≤ LogP ≤ 4, -4 ≤ LogS ≤*, Rotatable bond ≤ 8, Number of rings ≤ 4, Hydrogen bond donor ≤ 4, Hydrogen bond acceptor ≤ 8, Atoms in largest non-aromatic ring ≤ 6) to filter the EDULISS library. After the screen around 518,000 compounds were identified. A simpler protocol to that described in **section 3.6.2** was used where all compounds (518,000) were docked with Vina without the use of Combisearch.

The MDM2 template used in previous CODASS run (**Section 3.7.2**) was used in this run. The crystal structure 3LBJ (Popowicz et al., 2010) was selected as template for the MDMX run because it was the only crystal structure of MDMX with inhibitor bound (**Figure 3.10**).

WK298 inhibitor binds to MDMX in a similar position as the p53 peptide with a Ki of 11μM (Popowicz et al., 2010). The 6-chloroindole ring on WK298 is posed into the hydrophobic pocket allowing the NH group to form a hydrogen bond interaction with the carbonyl group of Met53. The other 4-chlorobenzyl ring and the phenyl ring on WK298 both fill into the other two hydrophobic pockets in MDMX.

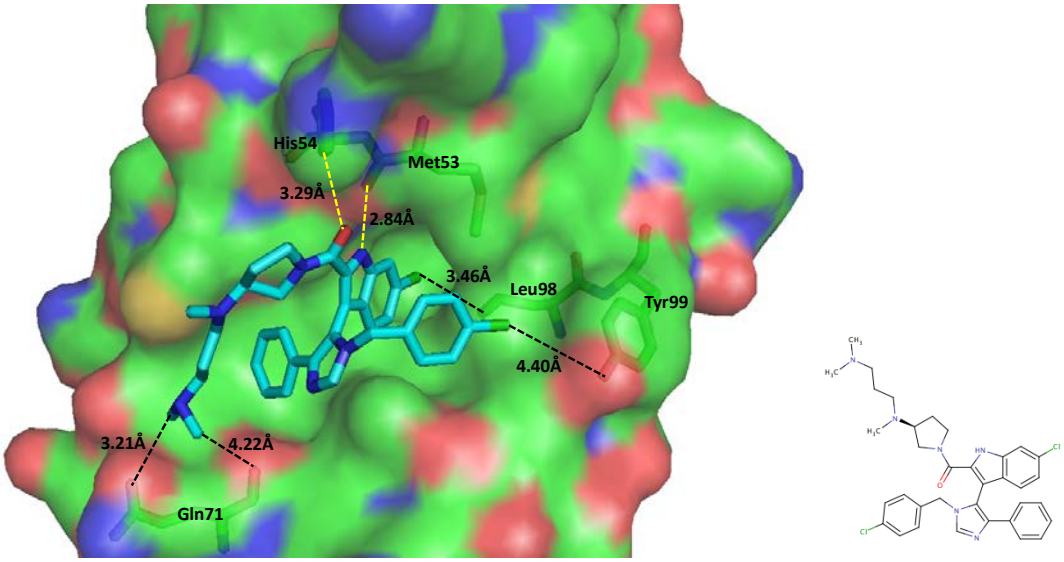

Figure 3.10 The binding of WK298 in the MDMX-N binding site.

On the left is the crystal structure of WK298 binding to MDMX-N (3LBJ) and the chemical structure of WK298 is displayed on the right. WK298 interacts with the MDMX-N residues using two intermolecular hydrogen bonds as shown in yellow dashes.

In order to confirm the accuracy of the docking of AutoDock and Vina control docking experiments of were performed. The control ligand used was WK298 and the protein model used was the X-ray crystal structure 3LBJ pdb file (**Figure 3.10**). Both AutoDock and Vina have successfully reproduced the crystallographic binding mode of WK298 (**Figure 3.11**). AutoDock predicted the free energy of binding to be -

8.33kcal/mol and Ki of 779.48nM while Vina predicted the free energy of binding to be -6.1kcal/mol. It has been noted that AutoDock has docked N,N-dimethylaminopropyl pyrrolidine close to Gln71 residue of MDMX-N for interaction (**Figure 3.11 top**) and Vina has docked 4-chlorobenzyl group out of Leu26 pocket and interact with Pro95 residue of MDMX-N (**Figure 3.11 bottom**).

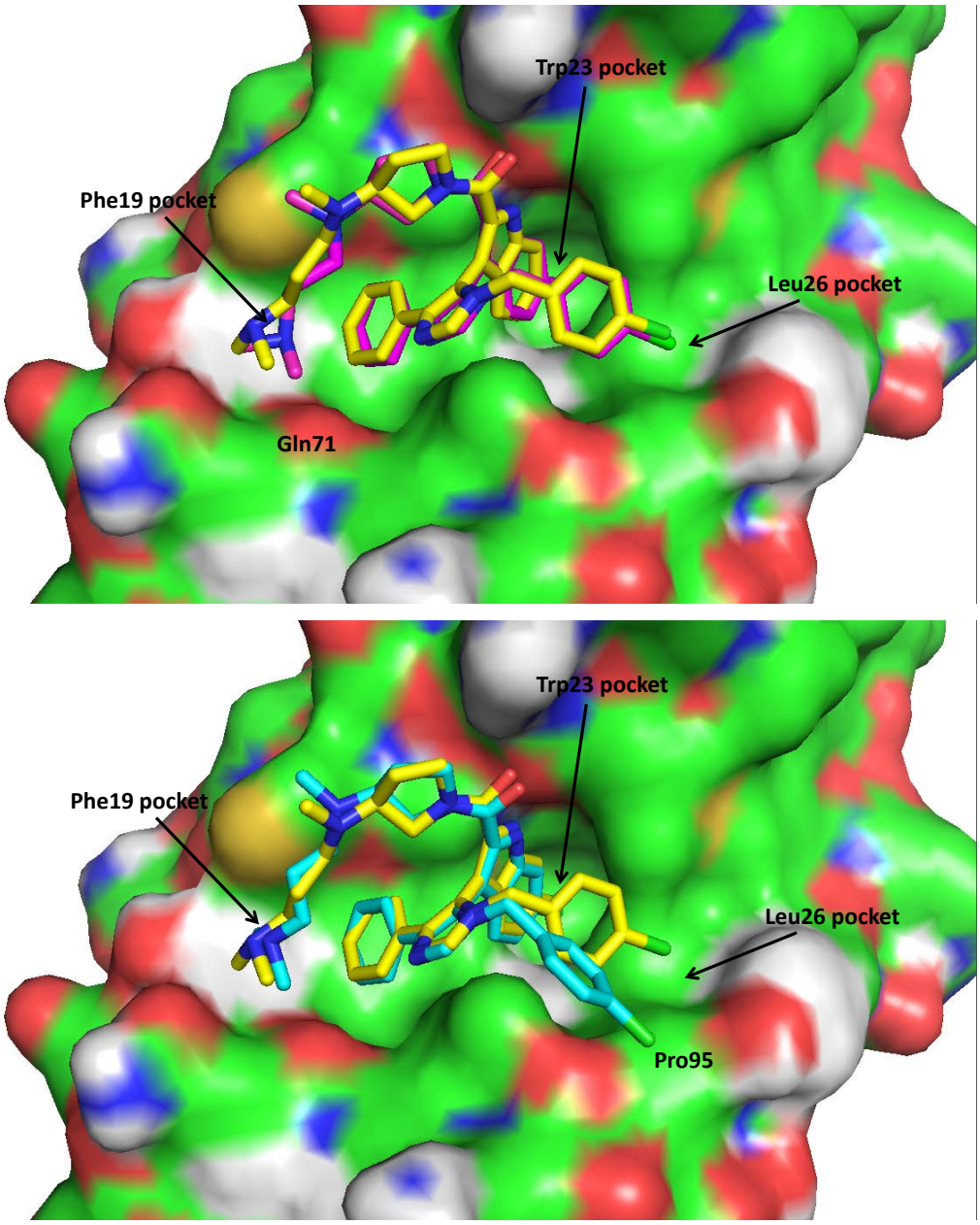

Figure 3.11 Control docking of AutoDock and Vina for WK298 in MDMX-N

WK298 inhibitor is shown as stick, in yellow color is the X-ray crystallographic pose, AutoDock docking pose shown in red (**top**) and Vina docking pose shown in light blue (**bottom**).

3.3.2 Comparison of MDM2/MDMX ligand-amino acid interactions

The co-crystal structures of MDMX-WK298 (3LBJ) and MDM2-WK23 (3LBK) were compared. WK23 inhibitor is an analogue of WK298 but in the absence of N,N-dimethylpropylamine (**Figure 3.12**).

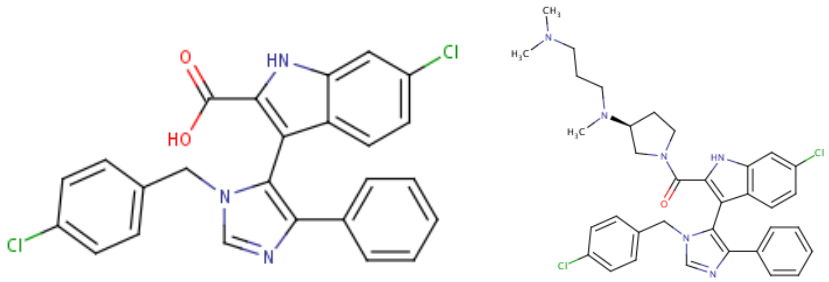

Figure 3.12 Chemical structures of WK23 (Left) and WK298 (Right).

WK23 binds to MDM2 in an identical mode as MDMX-WK298 interaction. WK23 and WK298 both occupy the three hydrophobic pockets using the three aromatic groups in the structure. The 6-chloroindole group on WK23 and WK298 forms hydrogen bonds with Leu54 on MDM2 and Met53 on MDMX respectively.

The two main differences between MDM2 and MDMX are the substitution of Leu53 to Met53 and His96 – Tyr100 helix to Pro95 – Tyr99 helix. These differences resulted in the reduced size in MDMX Leu26 binding pocket and possibly weakens the affinities for the inhibitors (**Figure 3.13**).

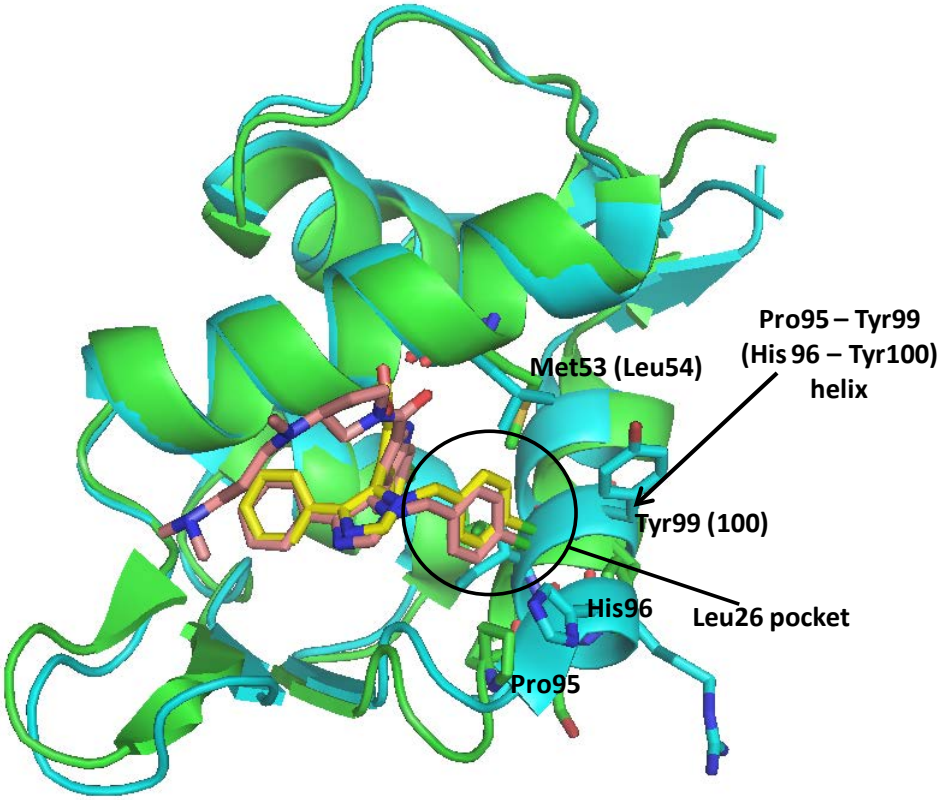

Figure 3.13 Comparison of MDMX-WK298 (3LBJ) structure with MDM2-WK23 (3LBK) structure.

WK298 inhibitor is coloured in salmon stick and WK23 inhibitor is coloured in yellow stick. MDM2 structure is shown as light blue ribbon and MDMX structure is shown as green ribbon. The WK298 and WK23 inhibitors bind to MDMX and MDM2 in an identical mode despite the structural differences between MDM2 and MDMX.

It has also been discovered that the Leu26 binding pocket of MDMX experiences induced fit changes upon binding to the compound (Popowicz et al., 2010) (**Figure 3.14**). When the p53 peptide bound MDMX (2Z5S) is superimposed with WK298 bound MDMX (3LBJ) there are several residues that retract to enable the 6-chlorobenzyl ring to enter (**Figure 3.14)**. The residues Met53, Leu56, Leu98, Tyr99 and Leu102 have retracted to allow binding of WK298 in the binding pocket. However this makes the pocket more shallow and results in WK298 binding more weakly in MDMX (Ki = 11μM) than MDM2 (Ki = 109nM) (Popowicz et al., 2010).

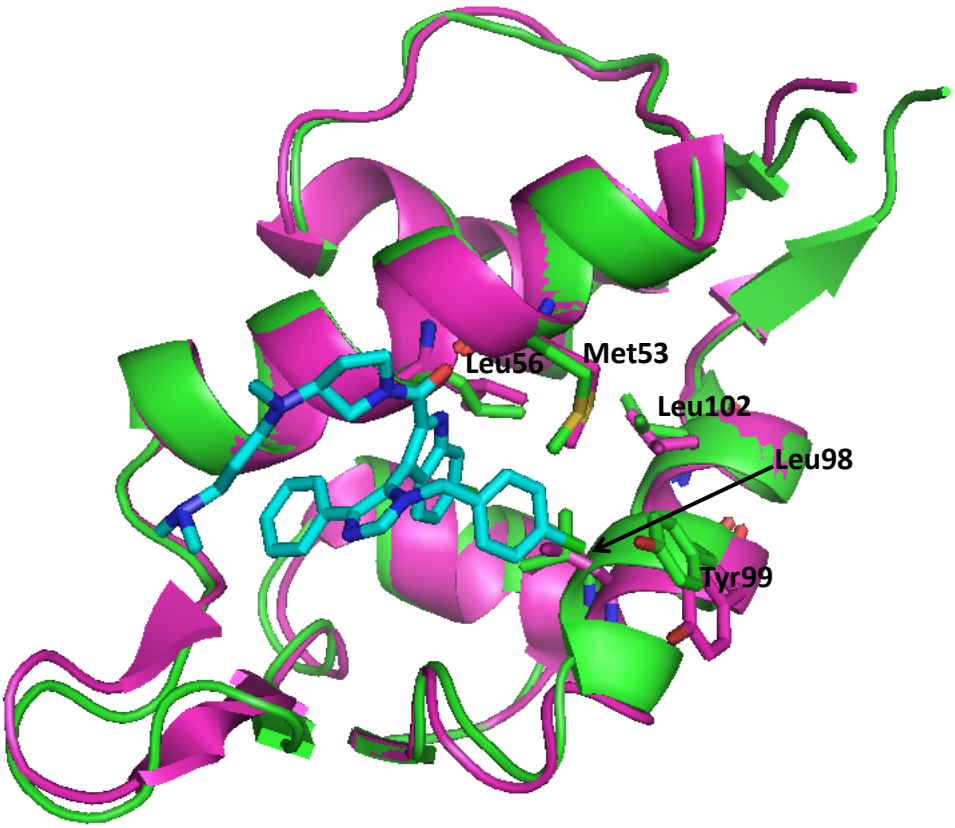

Figure 3.14 Superimposed MDMX-p53 peptide structure with MDMX-WK298 structure. MDMX-p53 peptide complex structure is coloured in green and MDMX-WK298 complex structure is coloured in pink. WK298 inhibitor is coloured in light blue stick.
Met53, Leu56, Leu98, Tyr99 and Leu102 are retracted to allow the inhibitor to enter the pocket.

3.3.3 Results from CODASS screen:

When analysing the binding energies of the compounds between MDM2 and MDMX, the binding energies are generally weaker when binding to MDMX than MDM2. In MDM2 the AutoDock and Vina scoring energies are between -7.2 to -10.02kcal/mol and -8.0 to -9.7kcal/mol. In MDMX the AutoDock and Vina scoring energies are between -6.7 to -8.6kcal/mol and -6.8 to -8.2kcal/mol. There is ~2kcal/mol energy difference between MDM2 and MDMX indicating the compounds bind weaker to MDMX.

The result list contains 1000 compounds from various suppliers and initially these compounds were filtered based on the following two criteria:

- Present in Chembridge supplier catalogue.
- Able to bind to both MDM2 and MDMX binding site.

The reason for chosing compounds from only Chembrige is to reduce the cost and purchase time. However the downside is that this method may miss out some potential hits.

After the initial filter there are 140 compounds from Chembridge and 61 compounds bind to both MDM2 and MDMX. These compounds were then screened visually and 7 compounds were chosen using the same criteria listed in **Section 3.2.2**.

The docking poses of the ligands in MDM2 and MDMX binding sites were shown (**Table 3.3**) and the free binding energies and predicted Ki were also listed. The predicted Ki of these compounds are generally more potent in MDM2 than MDMX. Interestingly, almost all the compounds identified in this virtual screening do not contain the imidazoline core to link three hydrophobic rings. These compounds shared little similiarity with the compounds in the first virtual screening (**Section 3.2.2**) as well as the known MDM2 inhibitors. These compounds were subsequently measured in the FP and CE assays to confirm the interaction (**Section 4.9, Section 5.4.1.7 and Section 5.4.2.3**). The assays have confirmed that 6 out of 7 as hits and in particular compound 2 which has been shown to bind to both MDM2 and MDMX in the assays (Discussed in **Section 4.9, Section 5.4.1.7 and Section 5.4.2.3**).

		MDMX						MDM2				
Predicted docking poses by AD & Vina	Chemical structure	Vina (kcal/mol)	AD (kcal/mol)	PredictedKi	% Inhibition by CE	% Inhibition by FP	Predicted docking poses by AD & Vina	Vina (kcal/mol)	AD (kcal/mol)	Predicted Ki	% Inhibition by CE	% Inhibition by FP
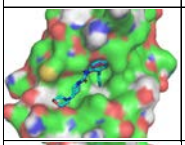	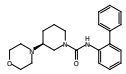	-7.7	-7.12	6.05μM		10% at 50μM	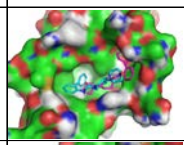	-9.2	-8.41	689.69nM	58% at 100μM	1% at 50μM
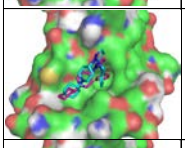	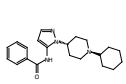	-7.1	-7.02	7.18μM		0% at 50μM	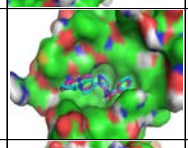	-8.7	-8.1	1.15μM	40% at 50μM	1% at 50μM
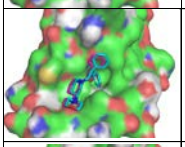	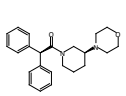	-7.3	-7.38	3.89μM	100% at 50μM	84% at 50μM	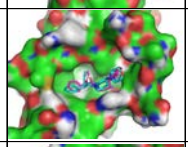	-9.4	-7.85	1.75μM	58% at 50μM	33% at 50μM
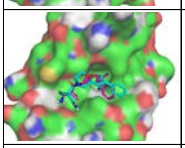	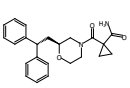	-6.9	-7.23	5.03μM		0% at 200μM	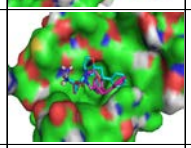	-8.5	-7.84	1.81μM	59% at 100μM	12% at 200μM
		MDMX						MDM2				
Predicted docking poses by AD & Vina	Chemical structure	Vina (kcal/mol)	AD (kcal/mol)	Ki	% Inhibition by CE	% Inhibition by FP	Predicted docking poses by AD & Vina	Vina (kcal/mol)	AD (kcal/mol)	Ki	% Inhibition by CE	% Inhibition by FP
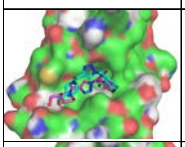	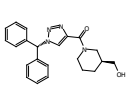	-7.4	-8.13	1.10μM		5% at 200μM	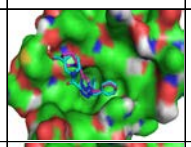	-8.3	-7.78	1.97μM	18% at 50μM	11% at 200μM
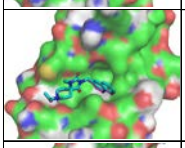	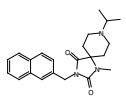	-7.2	-7.37	3.96μM		25% at 50μM	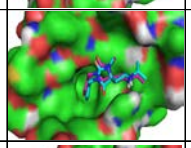	-8.5	-7.77	2.03μM	0% at 100μM	1% at 50μM
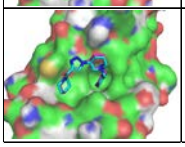	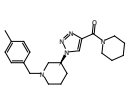	-7.1	-7.51	3.12μM		1% at 200μM	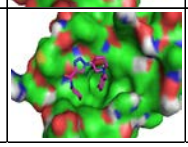	-8.1	-7.31	4.41μM	72% at 50μM	7% at 200μM

Table 3.3 CODASS screen against MDM2 and MDMX.

The listed compounds in the table are ranked based on the AutoDock score of MDM2. The compounds in purple coloured sticks are docked using AutoDock and in light blue coloured sticks are docked using Vina.

3.4 Discussion

This chapter describes the result of two different CODASS virtual screening runs. The first using Oprea's lead like criteria (MW <450Da) contains 1.1million compounds. The second run used the reduced complexity (fragment-like) library of 518,000 compounds with MW <300Da.

These two runs identified very different molecular scaffolds as the best scoring hits. The Oprea hits showed a number of multiple-ring compounds. Some of the most active (**Table 3.2**) have a 5-membered ring core motif which is similar to that found in the Nutlin family of MDM2 inhibitors. Of the top six experimental hits, four have a 5-membered heterocyclic core motif. There is a good correlation between the ranked poses for AutoDock/Vina and the experimental hits and the top 3 scoring hits have the best percentage inhibition values as measured by CE (**Table 3.2**).

For the second CODASS run, the reduced complexity hits showed a more flexible selection of compounds compared to the top hits from the first set and showed little similarity to the currently known Nutlin-like MDM2 inhibitors. In this second set the top hits are generally more active with a top activity of 72% inhibition at 50μM. However there is poorer correlation between the ranked poses for AutoDock/Vina and the experimental hits. The top scoring hit (-8.4kcal/mol) gives 58% inhibition as measured by CE while the best experimental value of 72% inhibition for **7** (**Table 3.3**) only has an AutoDock score of -7.3kcal/mol.

The AutoDock poses for series one has range of scores between -7.4 to -8.4kcal/mol. As only 6 compounds were selected for testing it is not possible to draw a firm conclusion correlating AutoDock score and measured binding affinity. For series two the range of scores for the best hits are -7 to -10kcal/mol which fits with the generally better measured inhibition values for this second series.

In each case (as part of the CODASS routine) there is an excellent agreement between the Vina and AutoDock poses for each compound (RMSD ≤2Å) as can be seen from the closely overlaid final poses from Vina and AutoDock (**Table 3.2 and Table 3.3**). The 3 hydrophobic pockets of MDM2-N (Phe19, Trp23 and Leu26 pockets) are to a greater degree filled by the compounds selected. In the first series, compound **1** and **3**

have a hydrogen bond interaction with Val93 residue. This additional hydrogen bond interaction may explain the higher inhibition shown experimentally for these compounds. For the second series, only compound 7 has a hydrogen bond interaction with Leu54 residue which again may explain the high inhibition found in the CE assay. In the second CODASS run the reduced complexity library was also screened against MDMX protein in parallel with MDM2 in order to identify dual action inhibitors. The AutoDock pose for binding to MDMX has range of scores between -6.7 to -8.6kcal/mol which is relatively lower than the AutoDock scores for MDM2 interaction (-7 to -10kcal/mol). The compounds selected for testing do not fill all the hydrophobic pockets in the MDMX template, in fact five out of seven compounds only interact with the Phe19 and Trp23 pockets (**Table 3.3**). This may be because the MDMX Leu26 pocket is more shallow compared to the MDM2 Leu26 pocket. This constrasts with the same compounds docked into the MDM2 template where in every case (except compound **7**) the binding pose fills each of the available pockets. It has been noted that Compound **1**, **3**, **4** and **5** form hydrogen bond interactions with Gln71 residue in MDMX which is absent in MDM2. This difference in amino acid sequence at the p53 binding site may also explain observed experimental differences in ligand binding. It is however difficult to draw a broad conclusion about the prediction of MDM2 and MDMX binding specificity as the MDMX CE assay is not fully optimised and our test set of compounds are too small to provide reliable correlations between AutoDock/Vina ranked poses and experimental results.

Chapter 4 Development of a fluorescence polarization screening assay for MDM2 inhibitors

4.1 Introduction

The theory of Fluorescence Polarization was first described by Perrin in 1926 and it was first introduced in biological assays by Dandliker in 1970 (Dandliker and de Saussure, 1970, Perrin, 1926). The FP anisotropy assay is based on observing the polarized fluorescence of a fluorescently labelled small molecular weight fluorophore.

The fluorescence polarization (FP) assay is a homogeneous versatile solution based assay that allows rapid and quantitative analysis of the receptor/ligand interaction. The FP assay was chosen as the compound screening method because it offers numerous advantages in studying protein-ligand binding. It is cheap, easy to set up and it is able to screen compounds in a 384 well plate format at high throughput (Owicki, 2000). The FP assay has a lower limit of detection in the sub nanomolar range (Invitrogen, 2006). Binding assays can be carried out to obtain the Kd of labelled peptide and competition assays can also be applied to obtain IC_{50} and Ki values of the compounds.

4.1.1 The principle of Fluorescence Polarization

When plane polarized light excites a "stationary" fluorescent molecule the light will emit in the same polarized plane. However if the molecule rotates out of the plane during excitation then the light will emit in a different plane. The emitted light can be monitored in vertical and horizontal planes. The difference in the emission intensity from the vertical and horizontal planes is dependent on the rotational speed of the fluorescent molecule.

Fluorescence polarization is therefore defined by the equation:

$$P = \frac{I - I\perp}{I + I\perp}$$

I = Intensity with polarizer parallel

I⊥ = Intensity with polarizer perpendicular

The schematic diagram in **Figure 4.1** describes the principle of fluorescence polarization. When excited by polarized light the fluorophore will absorb the photon and undergo rapid tumbling motion and emit light. For low molecular weight compounds emitted light will be largely depolarized due to rapid rotation. When the fluorophore is bound to a high molecular weight protein the rotation speed will be reduced and polarized light will be emitted.

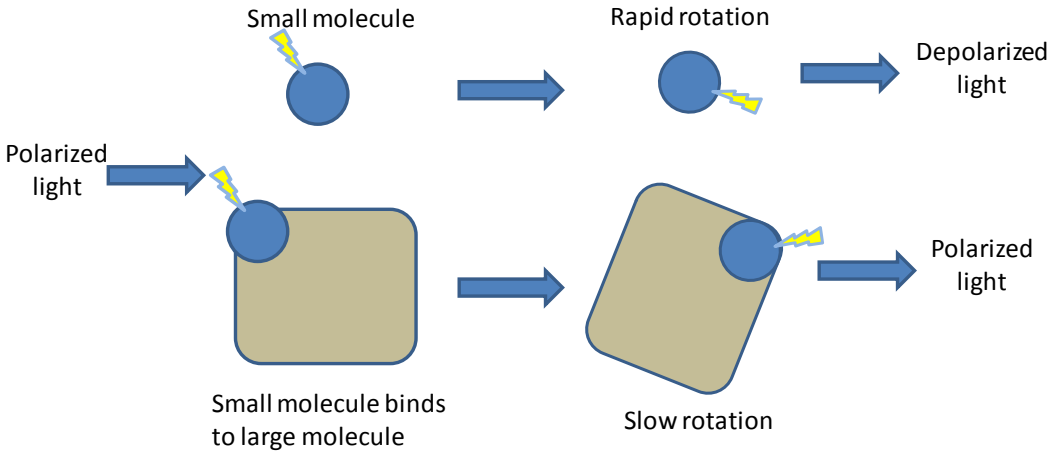

Figure 4.1 Schematic depicting the FP differences between small molecule and large complex.

Fluorophore undergoes rapid rotation when excited by the polarized light. The emitted light is largely depolarized during unbound state. Upon binding to large molecules the rotation speed of the fluorophore is reduced and polarized light is emitted.

4.1.2 Competition FP assay

Many papers and reviews have described the development of FP assays in detecting protein-ligand interactions (Burke et al., 2003, Parker et al., 2000). The competition assay depends on measuring the fluorescence polarization of a labelled substrate molecule in the presence and absence of an (unlabelled) inhibitor molecule. **Figure 4.2** shows a schematic diagram of FP competition. When the fluorescently labelled peptide is bound to a protein it emits a significant degree of FP signal due to the large mass and slow tumbling rate of the protein ligand complex. Ligand interaction with the protein can be detected by measuring the decrease of FP signal when the ligand

competes the fluorescent peptide out from the protein. If there is no interaction then the FP signal from the fluorescent peptide bound to the protein will remain unchanged.

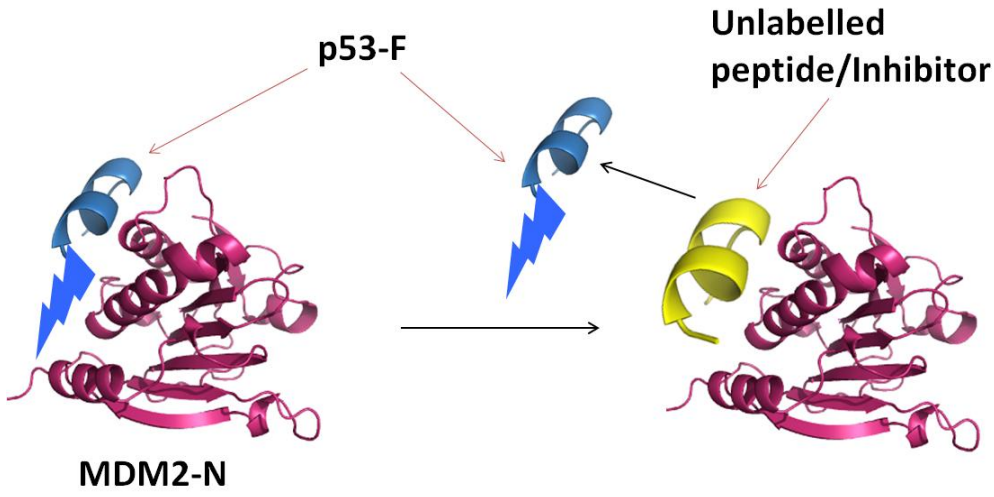

Figure 4.2 Schematic diagram of competition FP assay.

The tumbling rate of fluorescent peptide (p53-F) was monitored. Tumbling rate is reduced when interacting with high molecular weight protein MDM2-N.

4.2 Materials and Methods

In the FP assay the fluorescently labelled p53 peptide (p53-F) used was identical to that described in the paper from C. Brown (Brown et al., 2010). The p53-F peptide (I) was purchased from Biomatik Ltd. and fluorescein amidite (FAM) (II) was labelled at the N-terminus of the peptide.

Fluorescently labelled p53 peptide (p53-F) **(I)**

5-FAM-QETFSDLWKLLP-OH

Fluorescein amidite (FAM) **(II)**

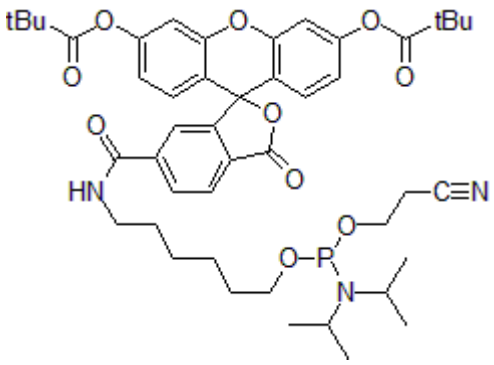

Unlabelled p53 peptide (p53-U) **(III)**

SQETFSDLWKLLPEN

The assay was originally carried out on a SpectraMax M5 multimode plate reader but was replaced with the LJL Biosystems Analyst AD multi-plate reader due to the poor sensitivity. The Biosystems Analyst multi-plate reader contains a dichromatic mirror for fluorescein filter and has the power to reduce the background noise.

The FP assay standard operation procedure (SOP) can be found in the **Appendix A2**

Fluorescence anisotropy

Polarization and anisotropy values are both derived from measured parallel and perpendicular intensities. The values can be interconverted.

$$A = \frac{I - I\perp}{I + 2I\perp} \qquad \textbf{Equation 4.1}$$

A = Fluorescence anisotropy (or “experimental anisotropy”)

I = Intensity with polarizer parallel

$I\perp$ = Intensity with polarizer perpendicular

Kd Equation

At equilibrium, the law of mass action states:

$$Kd = \frac{LF\ X\ RF}{B} \qquad \textbf{Equation 4.2}$$

Where LF is the unbound ligand, RF is the unbound receptor and B is the Receptor: Ligand complex. The equation can be rewritten as:

$$Kd = \frac{LF\ x\ (RT-B)}{B} \qquad \textbf{Equation 4.3}$$

RT = The total receptor concentration

RT – B = Free receptor concentration

In the experiment, the amount of bound ligand is only a small portion of the total ligand concentration. The total ligand concentration can therefore be used to calculate the free ligand concentration. The equation can be rearranged and substitute LF with (LT – B):

$$B = \frac{RT\ x\ (LT-B)}{Kd+(LT-B)} \qquad \textbf{Equation 4.4}$$

Using the quadratic to solve B, the equation is rearranged to:

$$B = \frac{(LT+Kd+RT)-\sqrt{(RT+Kd+LT)^2-4LTxRT}}{2} \qquad \textbf{Equation 4.5}$$

To use the anisotropy data directly, equation 4.5 was used to substitute B:

$$B = LT\ x\ \frac{A-Af}{Ab-Af} \qquad \textbf{Equation 4.6}$$

LT = Total concentration of ligand

Af = Anisotropy of free ligand

Ab = Anisotropy of bound ligand

$$\boldsymbol{A} = A_0 + (A_b - A_0)(\mathrm{Kd} + [\mathrm{L}]_t + [\mathrm{P}]_t) - \sqrt{\frac{(\mathrm{kd}+[\mathrm{L}]_t+[\mathrm{P}]_t)^2 - 4[\mathrm{L}]_t[\mathrm{P}]_t}{2[\mathrm{L}]_t}}$$ **Equation 4.7**

A_0 = anisotropy of free p53-F

A_b = anisotropy of p53-F bound to protein

$[L]_t$ = Total p53-F concentration

$[P]_t$ = Total protein concentration

Where Kd is defined as the concentration of protein at which 50% of the protein is occupied.

IC_{50} Equation

The titration curve was fitted with log (inhibitor) vs. response – variable slope (four parameters) using GraphPad Prism 5 (GraphPad software, San Diego California USA, www.graphpad.com).

$$Y = \frac{Bottom+(Top-Bottom)}{(1+10^{(LogIC50-X)*HillSlope})}$$ **Equation 4.8**

X = Concentration of compound

Bottom = anisotropy of free p53-F

Top = anisotropy of p53-F bound to protein

Hill Slope = Slope factor

As shown in **Figure 4.3.**

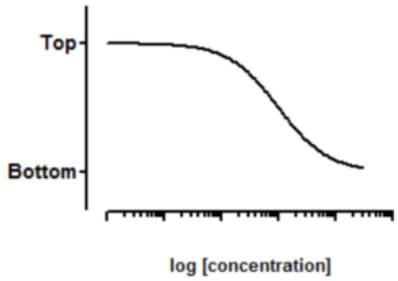

Figure 4.3 Log (Inhibitor) vs response curve.

Ki Equation

The Cheng Prusoff relationship was applied to calculate Ki from the IC_{50} (Lazareno and Birdsall, 1993).

$$Ki = \frac{(IC50-(\frac{[P]}{2}))}{(1+(\frac{[L]}{Kd}))}$$ **Equation 4.9**

[P] = Protein concentration.

[L] = The concentration of p53-F.

Kd = The dissociation constant of the p53-F from the protein.

4.3 Development of an FP binding assay for MDM2-N

A Fluorescence Polarization assay was set up for screening compounds on MDM2-N. In order to implement the assay a fluorescently p53 labelled peptide (p53-F) that binds to MDM2-N was selected. There are a number of references that use fluorescence polarization assays to monitor binding of ligand with MDM2-N (Lai et al., 2000, Brown et al., 2010, Zhang et al., 2004). In these references the labelled peptides (p53-F) bind to the N-terminal pocket in MDM2 with nanomolar affinity (**Table 4.1**); this is too tight to monitor weak fragment binding. Only the p53-F ligand in Brown et al. 2010 has a suitably low affinity of 1.1μM. This p53 derived peptide was labelled with fluorescein FAM dye at the N-terminal of the sequence (FAM)-QETFSDLWKLLP (Brown et al., 2010).

Probe	Kd	Reference
FAM p53 [(FAM)-QETFSDLWKLLP]	1.124μM	Brown C. et al. 2009
Ac-Phe-Arg-Dpr-Ac6c-(6-Br)Trp-Glu-Glu-Leu-NH2 With FAM label With Cy3B label With Texas Red-X label With Cy5 label	 2nM 3nM 20nM 5nM	Zhang R. et al. 2004
5-FAM-LTFEHYWAQLTS	5.6nM	Czarnar A. et al. 2009
5-FAM-βAla-βAla-Phe-Met-Aib-pTyr-(6-Cl-L-Trp)-Glu-Ac3c-Leu-Asn-NH2	6.7μM	Mohammad R. et al. 2009

Table 4.1 List of different labelled peptides synthesised for MDM2-N FP assay in different literatures.

The equilibrium binding of FAM labelled peptide with MDM2-N protein was carried out by adding increasing concentrations of MDM2-N protein to a fixed concentration of labelled peptide. The excitation/emission and cut-off used were 494/530nm and 515nm which were determined in the excitation and emission scan for FAM labelled peptide. These experiments were carried out using three different fixed concentrations of labelled peptide. 60nM, 120nM and 200nM of FAM labelled peptide were used to determine Kd values and to find the optimal concentration for FAM labelled peptide. Each of these three assays were repeated three times and the Kd values were then determined from experimental data (**Figure 4.4**). The Kd value calculated using three

concentrations of peptide were reasonably consistent. 60nM labelled peptide gave a Kd of 0.59µM ± 0.25, using 120nM gave a Kd of 0.7µM ± 0.43 and using 200nM gave a Kd of 0.68µM ± 0.38 (**Figure 4.4**).

In conclusion, different concentrations of p53-F yielded very similar Kd values and all lie within the experimental error range. Therefore 60nM concentration for FAM labelled peptide was used for further FP assay measurements.

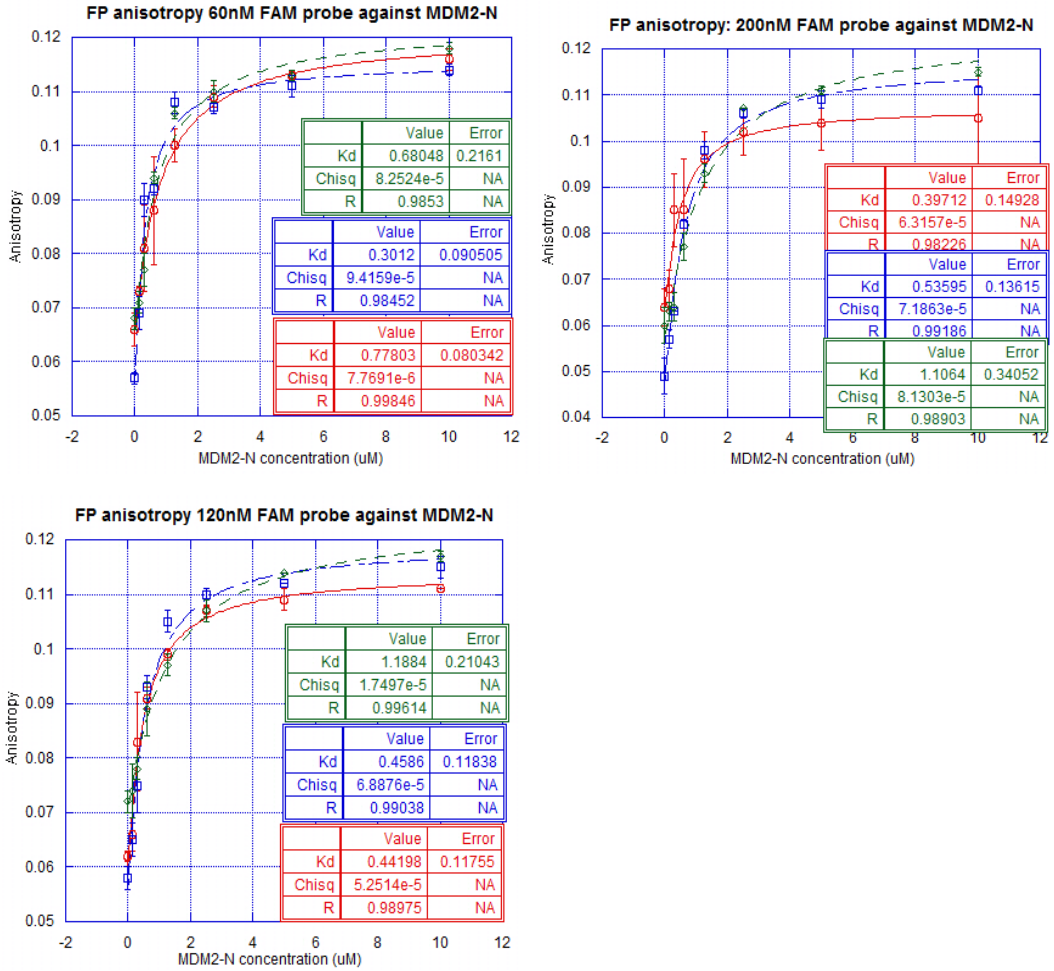

Figure 4.4 60nM, 120nM and 200nM FAM labelled peptide binding curves. Excitation 494nm, Emission 530nm and cut off at 515nm. The assay was repeated three times and the Kd from the three repeats were averaged to be 0.59µM ± 0.25, 0.7µM ± 0.43 and 0.68µM ± 0.38.

4.4 Development of an FP competition assay

Unlabelled p53 peptide titration provides a control for the competition assay:

The unlabelled p53 peptide can also bind to MDM2-N protein and was used for developing the competition binding assay to identify active compounds. The assay works by measuring the decrease of anisotropy caused by a ligand displacing the labelled peptide. Different concentrations of unlabelled p53 peptide were titrated into wells containing a fixed concentration of p53-F and MDM2-N. A solution of 60nM p53-F and 5μM MDM2-N in a total volume of 50μl was chosen for the FP competition assay. In the displacement curve the initial anisotropy value corresponds with fully bound p53-F, and as the unlabelled p53 peptide concentration increases the p53-F is displaced and anisotropy decreases. However the curve in **Figure 4.5** shows there was a trend of increased anisotropy when the unlabelled p53 peptide was over 250μM. It is likely that this increase of anisotropy is caused by formation of oligomer or dimer of p53-F.

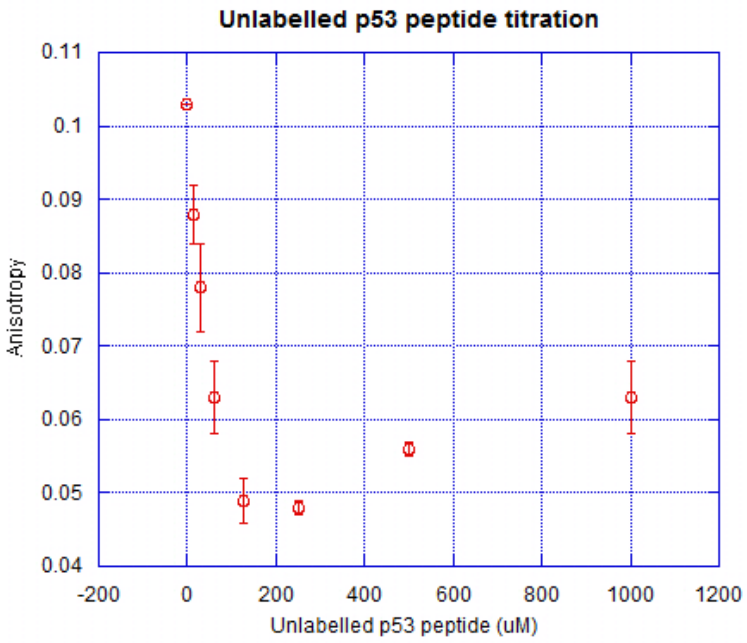

Figure 4.5 Unlabelled p53 peptide titration.

The titration results in an increase in the anisotropy when the unlabelled p53 peptide was above 250μM.

A control was performed to confirm if there was any non-specific interaction. This was done by titrating unlabelled p53 peptide against a fixed concentration of p53-F. If the unlabelled p53 peptide has no effect on p53-F then there will be no change in anisotropy, however, when the unlabelled p53 peptide concentration increased, a decrease of anisotropy was found (**Figure 4.6**). The anisotropy decreases immediately when unlabelled p53 peptide concentration increases and the anisotropy started to increase again as unlabelled p53 peptide concentration increased.

The unexpected and dramatic decrease in anisotropy at low concentration could possibly be explained by oligomerization or aggregation of labelled and unlabelled peptides. However subsequent experiments showed that the absorption of peptide onto the surface of the polystyrene well also affected the anisotropy measurement.

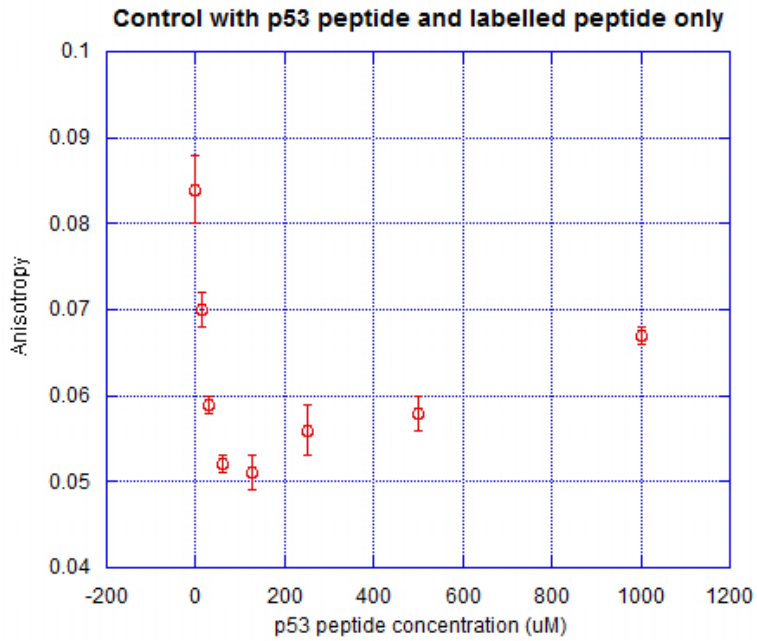

Figure 4.6 Control experiment of unlabelled p53 peptide with p53-F.

FP assay control was performed by titration of unlabelled p53 peptide against a 60nM solution of p53-F peptide.

4.4.1 Effect of detergent on the FP assay

The effect of Tween-20 on peptide solubility:

To address the problem of increased anisotropy at higher concentration of p53-U (as seen in **Figure 4.6**), detergent was added to help improve solubility and help prevent dimerization or aggregation. To determine the effect of Tween-20 on p53-F different concentrations of Tween-20 were added from 0% - 0.25% into wells containing 60nM of p53-F. On addition of Tween-20 a decrease in anisotropy can be seen. From the bar chart in **Figure 4.7**, in the presence of Tween-20 the anisotropy is lower than without Tween-20 suggesting Tween-20 is acting to disrupt the dimerization or oligomerization of the p53-F. The anisotropy decreases to a value of 0.041 at 0.0125% Tween-20.

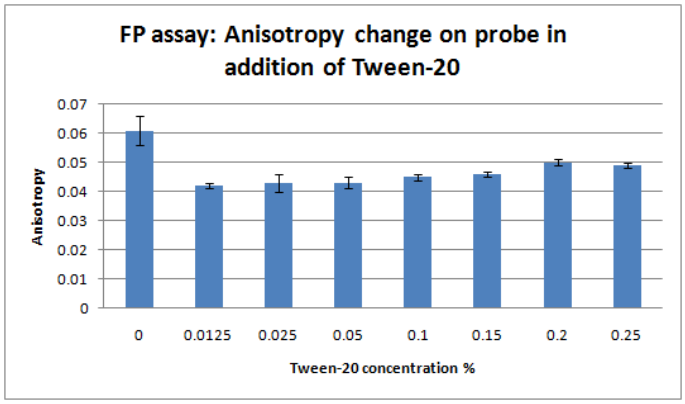

Figure 4.7 FP assay in addition of Tween-20.

Different concentrations of Tween-20 were added into the assay to compare the change in anisotropy.

The critical micelle concentration for Tween-20 is 0.07%. For all subsequent assay measurements a 0.02% concentration of Tween-20 was included.

Repeating the original control experiment in the presence of Tween-20 (**Figure 4.8**) does not show the anomalous drop in anisotropy (**Figure 4.6**). Using the same conditions but in the presence of 0.02% Tween-20, the anisotropy stays constant at ~0.04. This suggests that Tween-20 has helped to solubilise the p53-F.

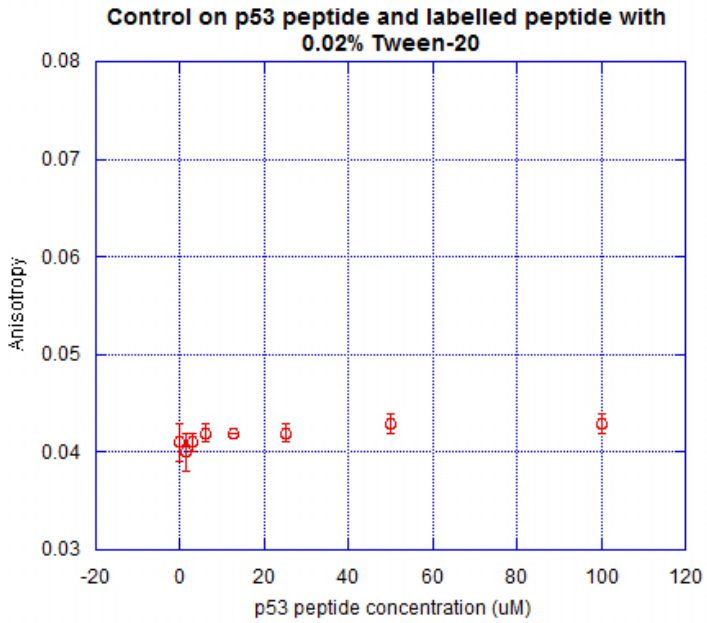

Figure 4.8 Control of FP assay in the presence of 0.02% Tween-20.

A control experiment was carried out on unlabelled p53 peptide with p53-F in the presence of 0.02% Tween-20. The plot showed no change in the anisotropy on titrating the unlabelled peptide when Tween-20 was present.

The effect of Tween-20 on the FP competition assay:

The unlabelled p53 peptide titration was repeated with addition of 0.02% Tween-20. **Figure 4.9** shows the curve of the unlabelled peptide titration and, in contrast with **Figure 4.5**, no increase of anisotropy was observed as peptide concentration increased. The IC_{50} and Ki of unlabelled peptide binding to MDM2-N was calculated using **equation 4.8 and 4.9** respectively and IC_{50} was 23.52μM and the Ki was 18μM. The published IC_{50} of p53 peptide using a similar sequence was 2μM (Phan et al., 2010). The calculated IC_{50} was ten times weaker than the published value but p53-U is one amino acid longer than the p53 peptide used by Phan et al.

```
P53-U  ETFSDLWKLLPEN
       ||||||||||||
Phan   ETFSDLWKLLPE
```

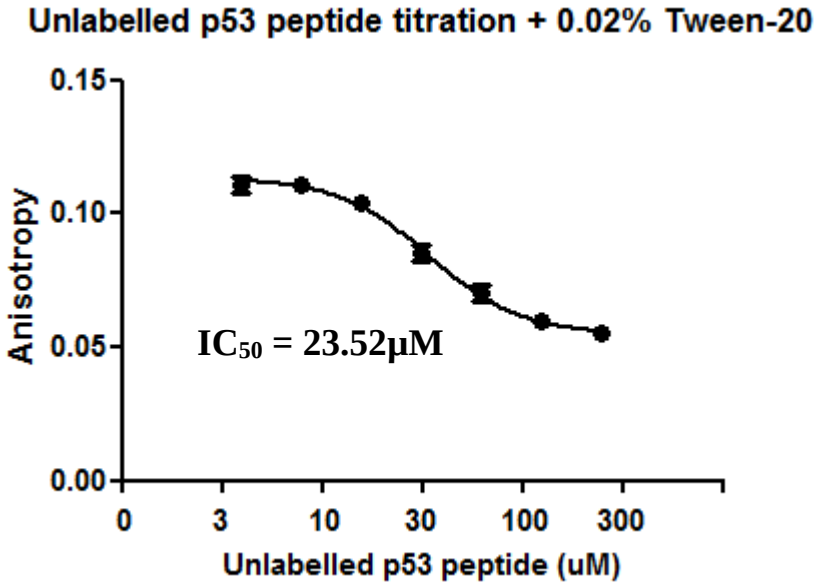

Figure 4.9 FP assay titration curve of unlabelled p53 peptide on addition of 0.02% Tween-20.

The concentrations of p53-F and MDM2-N used were 60nM & 5µM respectively. Tween-20 has solubilised the p53-F and there was no increase of anisotropy at higher concentration of unlabelled p53 peptide.

4.5 Optimising the FP assay using the LJL Biosystem Analyst Multi-plate reader

4.5.1 Determining the optimised labelled peptide concentration for the assay

To improve the sensitivity of the FP assay the protein concentration has to be decreased which means that the p53-F concentration also has to be decreased. The signal in the FP assay depends on the amount of p53-F present. Therefore the lowest concentration of p53-F that can be used has to be assessed.

In order to reduce the p53-F concentration another multi-plate reader was tested. The LJL Biosystem Analyst Multi-plate reader was used. The machine has an optimal signal range between 156,000 to 31,200,000 counts per second. 384 well plates were used for setting up the assay. The total volume in each well is 30µl, so lower volume samples were needed for setting up the assay. The read out from the machine is in counts per second (cps).

The fluorescence signals (ex 485/ex 530) from different p53-F concentrations were examined. A steady increase of signal can be seen when increasing the labelled peptide concentration (**Figure 4.10**). At 5nM concentration the signal has more than 2 million cps which is in the optimal signal range and can be used to test in the FP assay (**Figure 4.10**). If the signal is too low then background noise will interfere with the signal.

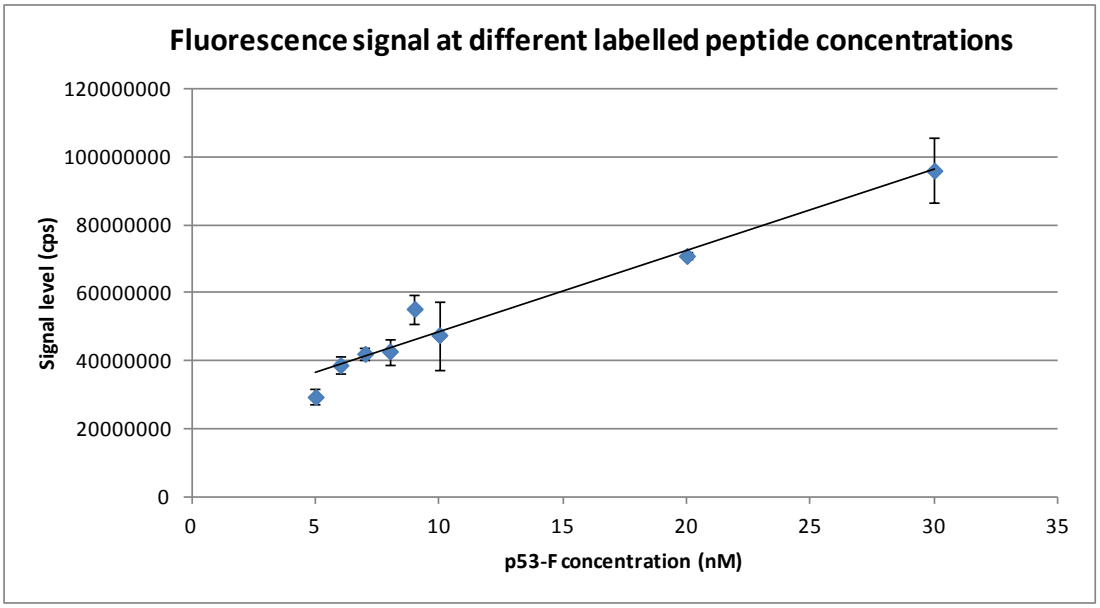

Figure 4.10 Plate reader output as a function of p53-F concentration.

Labelled peptide concentrations tested are from 5nM – 30nM. An increase of signal can be seen when concentration is increased. The signals from these concentrations were in the optimal signal range of the machine.

4.5.2 Determining the optimum MDM2-N concentration for the FP assay

To optimise the sensitivity of the FP assay it is generally desirable to use a p53-F concentration as low as possible, but in the range for the instrument detector. At 5nM p53-F there was background in the anisotropy readings. The noise was subsequently reduced when the p53-F concentration was increased to 8nM (**Figure 4.11**) and this concentration was selected for further assay work.

To determine the optimum MDM2-N concentration to use for the FP competition assay binding experiments were performed in the presence and absence of Nutlin-3. The

binding assay in the presence of Nutlin-3 shows the competition of Nutlin-3 and p53-F and decreases caused by competing out bound p53-F. When compared with the control binding curve without Nutlin-3 an optimal protein concentration was calculated by looking at the gap between the two curves. The curves fitted in **Figure 4.12** show that the optimum protein concentration for seeing the displacement of the curve in the competition assay is 0.5µM.

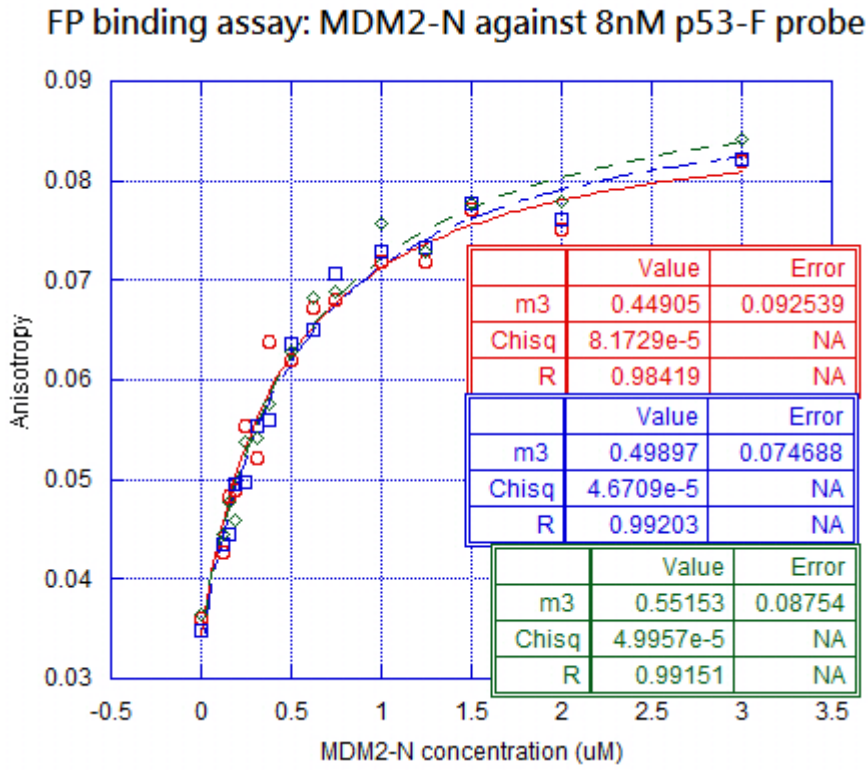

Figure 4.11 FP binding assay of MDM2-N against p53-F (8nM).

Each experiment point was measured in triplicate. Three independent curves are shown to provide a measure for the reproducibility of the assay.

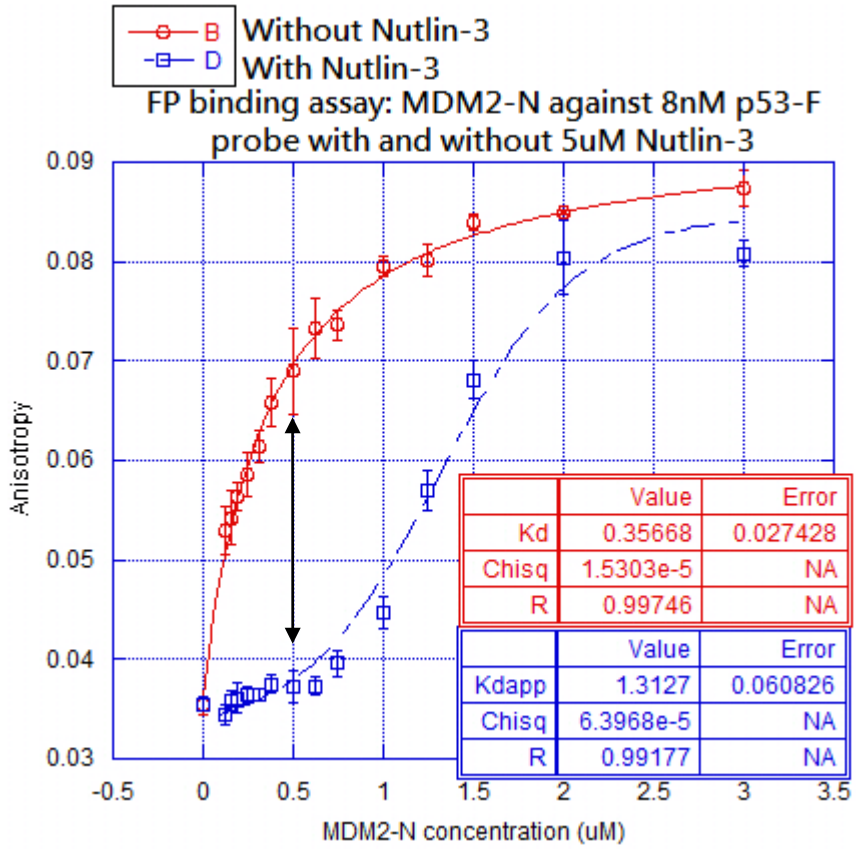

Figure 4.12 FP binding assays of MDM2-N with ± Nutlin-3 (5µM).

The curves are measured in the presence (blue line) and absence (red line) of Nutlin-3. Optimal MDM2-N concentration to use for competition assay was determined as 0.5µM.

4.5.3 Comparison of His_6-tag-MDM2-N and Untagged-MDM2-N

In the construct there is a His_6-tag located at the N-terminal of MDM2-N which is close to the MDM2-N/p53 binding site. Therefore it is crucial to confirm if there is any effect on the MDM2-N binding. His-tag cleaved MDM2-N was tested in the FP binding assay with p53-F to compare the K_d obtained from with the His-tag MDM2-N. His_6-tag cleaved MDM2-N was diluted into different concentrations and titrated into wells with 8nM p53-F. The assay was done in triplicate and the curve was fitted using **equation 4.7**. The average K_d for the p53-F with tag cleaved MDM2-N was calculated to be 0.25µM ± 0.02 (**Figure 4.13A**). The K_d for p53-F when running with tagged MDM2-N was 0.34µM ± 0.02 (**Figure 4.13B**).

Comparing the FP assay results of tag cleaved MDM2-N and un-cleaved MDM2-N shows that there is no significant difference between cleaved and un-cleaved MDM2-

N. This indicates the His-tag at the N-terminal of MDM2-N does not affect labelled peptide or small molecules binding to the binding site.

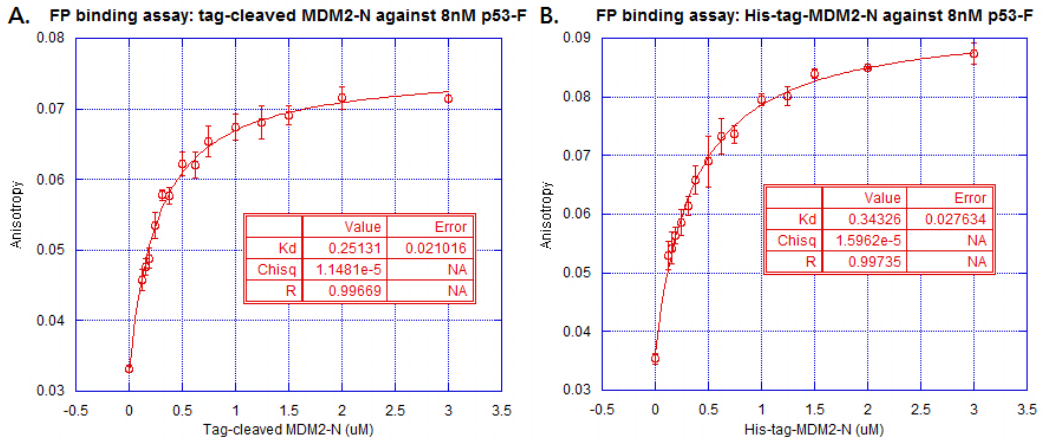

Figure 4.13 FP binding assays of p53-F against His-tag MDM2-N and untagged-MDM2-N.

The binding assays of untagged-MDM2-N (A) and His-tag MDM2-N (B) showed no significant difference in the Kd obtained.

4.5.4 Nutlin-3 titration against MDM2-N

Nutlin-3a is the first known inhibitor for MDM2 and has been commonly used in the biochemical and cell based studies. Nutlin-3a has an affinity of IC_{50} = 90nM and a Ki = 36nM (Shangary et al., 2008, Vassilev et al., 2004) as measured by SPR and fluorescence polarization studies respectively. Initially in our studies we used relatively high concentrations of MDM2-N (5μM) and p53-F (60nM). With these high concentrations it was not possible to obtain a complete titration curve. The assay was optimised and the concentrations of both MDM2-N and p53-F could be significantly reduced to 500nM and 8nM respectively. The Nutlin-3 titration curve using these values gave a good sigmoidal curve (**Figure 4.14**) with an IC_{50} value of 1.18μM and Ki = 0.91μM. However the affinity estimated from this titration was 25 times weaker than the published affinity (36nM). This may be due to the weak sensitivity of the FP assay and further optimisation was carried out in **section 4.6**.

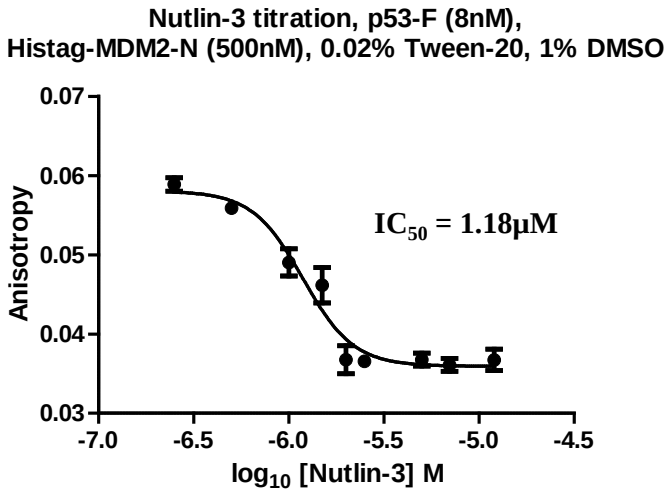

Figure 4.14 Nutlin-3 titration with His-tag MDM2-N.

The titration was performed using MDM2-N (500nM), p53-F (8nM), 0.02% Tween-20 and 1% DMSO. A sigmoidal curve was obtained with an IC_{50} of 1.18µM.

One reason for the discrepancy is due to the fact that Nutlin-3 from Sigma Aldrich (Cat No. N6287) which was used in our assay is a racemic mixture. This means that both active Nutlin-3a and inactive Nutlin-3b are present in equimolar amounts. Interestingly, there was a published paper (Bernal et al., 2010) that also used racemic Nutlin-3 in an FP assay and the IC_{50} obtained from this work was 2.11µM, a value very similar to that obtained in our work.

Another possible reason for the discrepancy between the low published IC_{50} value of 90nM is the presence of the His_6-tag located near the MDM2-N/p53 binding site. In order to examine the effect of this tag on Nutlin-3 binding the protein was treated with thrombin to provide a tag-free construct (as described in **Chapter 2, section 2.2.1.4**). The untagged MDM2-N resulted to an IC_{50} of 1.8µM (**Figure 4.15**). This is nearly identical to the Nutlin-3's affinity with His-tagged MDM2-N and suggests that the His-tag near the MDM2-N/p53 binding site has no effect on the small molecule binding. In all subsequent work the assays were performed using His-tagged-MDM2-N.

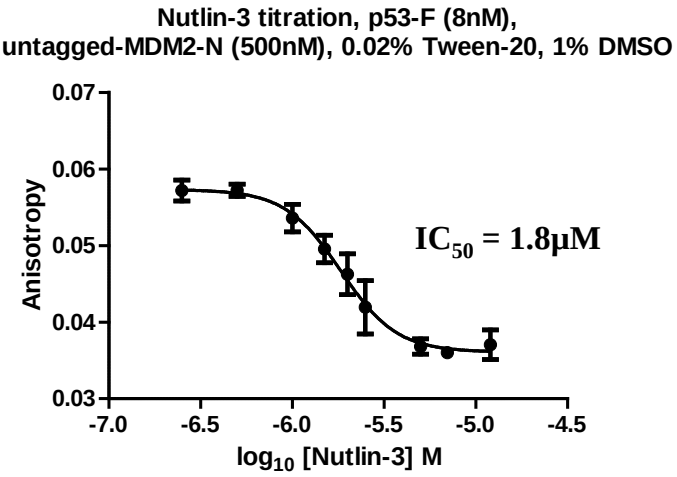

Figure 4.15 Nutlin-3 titration against His-tag cleaved MDM2-N.

Titration of Nutlin-3 with untagged-MDM2-N was carried to confirm if the His-tag interferes the small molecules binding.

4.6 Optimising the FP assay using siliconised equipment

Comparison of two CE runs showed that when unsiliconised tips were used the limit of detection for p53-F peptide was 250nM. When siliconised tips were used the limit of detection was reduced to 500pM. This suggested that p53-F was sticking to the unsiliconised tips and the effective concentration was reduced by a factor of ~1000.

To confirm this effect an experiment was carried out to compare fluorescence after pipetting p53-F into a siliconised plate using a siliconised tip (**Figure 4.16**). For this experiment a non-binding surface plate (NBS) (Corning cat No: 3820) was used. Absorption of p53-F peptide onto unsiliconised plate and tips strongly reduces the fluorescent signal.

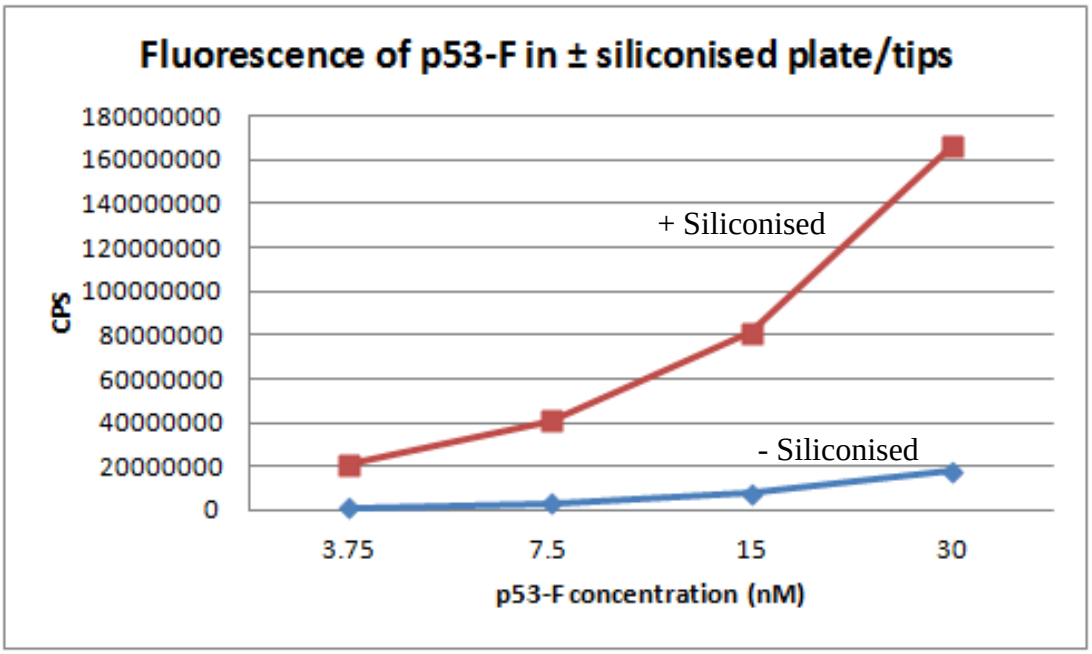

Figure 4.16 Fluorescence of p53-F was measured.

Serial dilution of p53-F with ± siliconised plate/tips and measured fluorescence in Analyst multiplate reader.

4.6.1 Siliconised tips using dimethyldichlorosilane solution

Siliconised tips were identified to be essential in diluting the p53-F. However when setting up the FP assay tips were always used in large quantities and it would have been too expensive to continuously purchase them from the supplier. We developed a way to siliconise tips in-house as described below.

Siliconising the pipette tips was performed in a chemical fume hood. Dimethyldichlorosilane solution was poured into glass bowl and pipette tips were immersed in the siliconising solution. Using the pipette the solution was pipetted into the tips so that the inner surfaces of the tips were fully covered with the siliconizing solution. The tips were taken out from the solution and washed with distilled water then allowed to dry overnight in the fume hood.

In order to compare different siliconised tubes fluorescence measurements on p53-F were carried out by diluting p53-F using commercial siliconised tips, home siliconised tips and normal tips.

From the results in **Figure 4.17**, it can be seen that there are no significant differences between the fluorescence readings of p53-F diluted using commercial siliconised tips and home siliconised tips. There was a 3 fold difference on the fluorescence of p53-F diluted using normal tips.

This verifies that home siliconised tips were also able to prevent p53-F sticking. Therefore home siliconised tips were used for subsequent assay measurements.

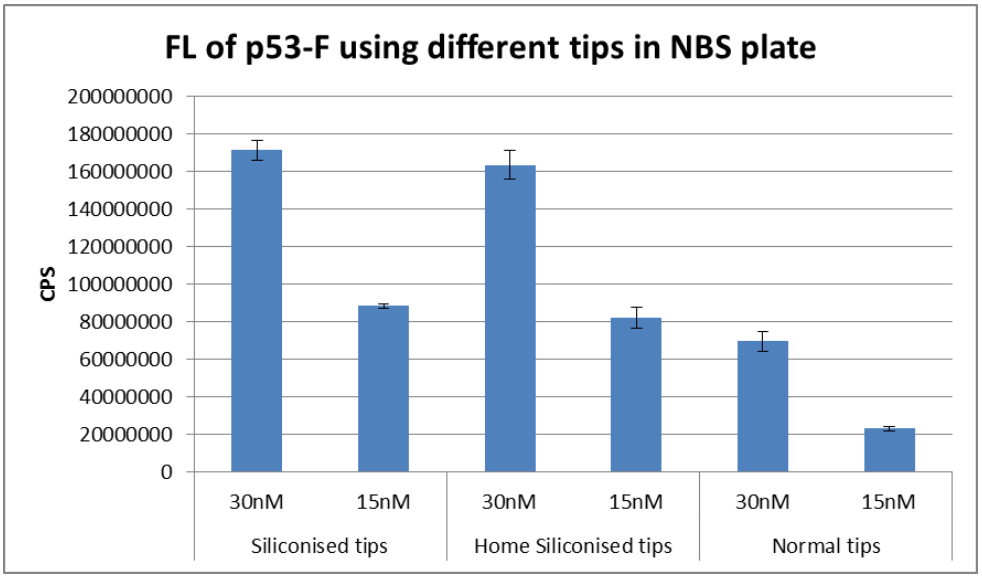

Figure 4.17 Fluorescence of p53-F diluted using different type of tips.

p53-F was diluted using commercially siliconised, home siliconised and normal plastic tips. Fluorescence of p53-F was measured using NBS plate and expressed in counts per second (CPS).

4.6.2 Siliconised equipment allows FP assay using 2nM p53-F

In order to quantify the effect of the p53-F peptide absorption on the plate three binding assays were performed. A lower p53-F concentration of 2nM was used in these trials. The first binding assay in **Figure 4.18A** was set up by diluting the samples using siliconised tips/vials and measured in the NBS plate. A second binding assay was carried out in **Figure 4.18B** using siliconised tips/vials and measured in a black polystyrene plate. In the third a control was set up in **Figure 4.18C** with samples using unsiliconised tips/vials and measured in the polystyrene plate.

As shown in **Figure 4.18A**, the binding assay using siliconised tips/vials and measured in the NBS plate gave a reproducible result. Higher noise was found when setting up the binding assay using siliconised tips/vials in the normal plate (**Figure 4.18B**) and using non-siliconised tips/vials in the polystyrene plate (**Figure 4.18C**). These results show that p53-F binds to the unsiliconised plate. From the binding assay using 2nM p53-F (**Figure 4.18A**) the K_d calculated for p53-F was 0.32µM which was identical to the K_d obtained previously using 8nM p53-F (0.35µM).

This confirms that using siliconised tips with NBS plate can help improve the sensitivity of the FP assay and the p53-F concentration used in the assay can now be significantly reduced.

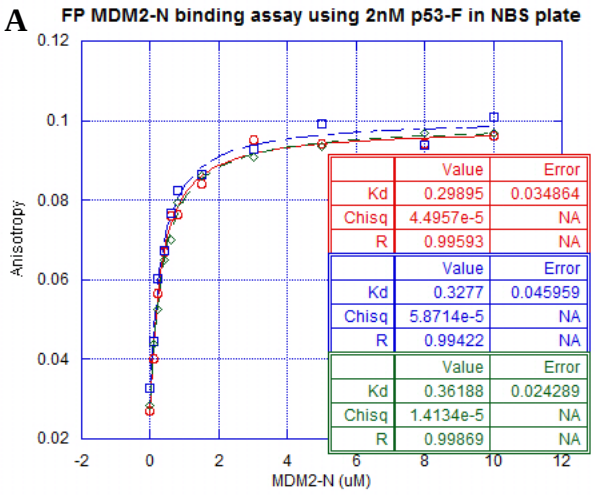

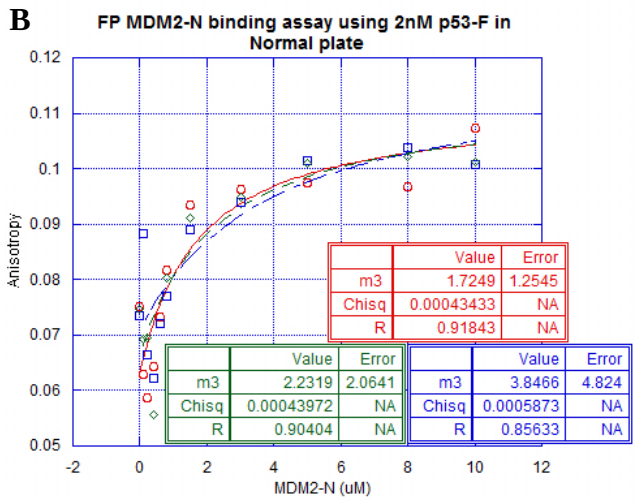

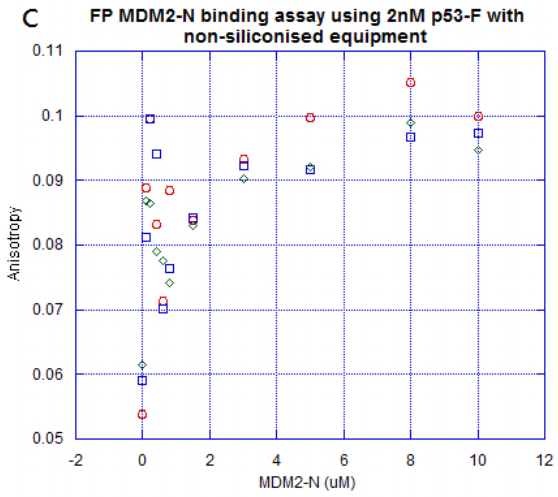

Figure 4.18 Three binding assays were carried out in different conditions.

A) The assay was performed using siliconised equipment and a non-binding surface plate.

B) The samples were diluted in the siliconised equipment and measured in a polystyrene plate.

C) The samples were diluted using non-siliconised equipment and measured in a polystyrene plate.

4.6.3 Effect of siliconised equipment on Nutlin-3 titration

To validate the effect of siliconised equipment the titration of Nutlin-3 was repeated. Competition assay was done on Nutlin-3 from 0-10μM using the condition of p53-F (2nM) and MDM2-N (500nM). Several publications have suggested that fluorescent compounds can cause interference to the fluorescence based assay leading to false positive or false negative results (Owicki, 2000). This interference was often resolved by using a higher concentration of labelled probe but this will reduce the sensitivity for detecting weak ligand interactions. When using low concentration of labelled probes the sensitivity can be increased but this will decrease the signal and make the measurements more sensitive to any fluorescent background. As a control the fluorescence of each compound is measured at the same concentration (but in the absence of peptide and protein) and this reading is subtracted from the assay measurement.

Nutlin-3 titration was repeated and, after compound fluorescence subtraction, the IC_{50} of racemic Nutlin-3 was found to decrease to 266nM (**Figure 4.19**) with a Ki

calculated at 264nM. The sensitivity has been greatly improved compared to the Nutlin-3 titration that was carried out when using unsiliconised equipment (IC_{50} = 1.18µM) (**Section 4.5.4**). However the IC_{50} of enantiomeric Nutlin-3a from the literature is 90nM (Vassilev et al., 2004). The calculated IC_{50} from the FP assay was ~3 times larger than the literature value and this discrepancy is possibly explained by the fact that the Vassilev study used enantiomerally pure Nutlin-3a, although this would only explain 2 fold increase in IC_{50}. The other reason may be that the sensitivity of the FP assay was still not sensitive enough.

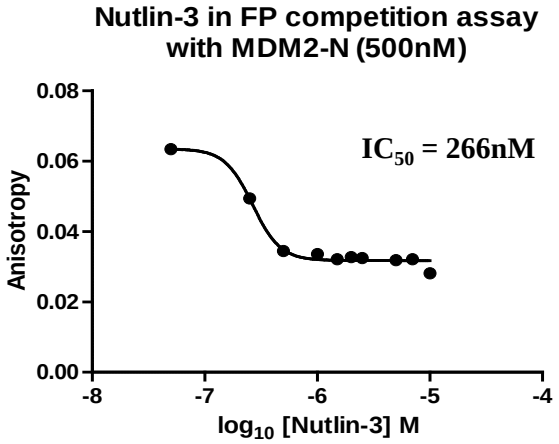

Figure 4.19 Nutlin-3 titration with MDM2-N using siliconised equipment.
The samples were prepared using siliconised tips and vials and titrated into a non-binding surface plate for measurement.

A detailed "SOP" for carrying out a 384 well format FP screen is given in **Appendix A2**.

4.7 FP assay compound screening results

4.7.1 Screening the Selcia fragment library

As described in **Chapter 3** fragment based drug discovery is a relatively new approach in developing leads with good drug like properties (Carr et al., 2005, Neidle and Hubbard, 2006). Fragments are small molecular weight molecules and conform to the Rule of three: molecular weight ≤ 300, hydrogen bond donor ≤ 3, hydrogen bond acceptor ≤ 3 and calculated logP ≤ 3 (Congreve et al., 2003).

The Selcia fragment library contains approximately 1400 compounds that have been selected based on the Rule of three criteria. From the analogues screening, there were 14 fragments selected from the library for screening in the FP assay (**Table 4.2**).

Mi63 and Nutlin-3 inhibitors (**Figure 4.20**) were analysed and 14 fragments were selected based on the substructures of these inhibitors. For simplicity a name was given for each substructure group, **MR1-4** and **NR1-4** for Mi63 and Nutlin-3 respectively (**Figure 4.20**). **Table 4.2** shows the structures of these fragments and many of these fragments selected were analogues of the **MR3** substructure of Mi63 inhibitor (**Figure 4.20**). The SFL001328 fragment is an analogue of the **MR3** group but without the chlorine atom at 6 position and the SFL001303 fragment has moved the chlorine atom from 6 position to 7 position. To assess if the imidazole ring on the **MR3** group has any effect on binding we have replaced the imidazole ring with the pyridine ring on SFL00134 and SFL001397 fragments. In SFL001290, SFL001542, SFL001675 and SFL000829 fragments, we have substituted the chlorine atom on the **MR3** group with different substructures. SFL000576 is an analogue of Nutlin-3 at **NR3** (**Figure 4.20**) and this fragment was also selected to confirm the binding.

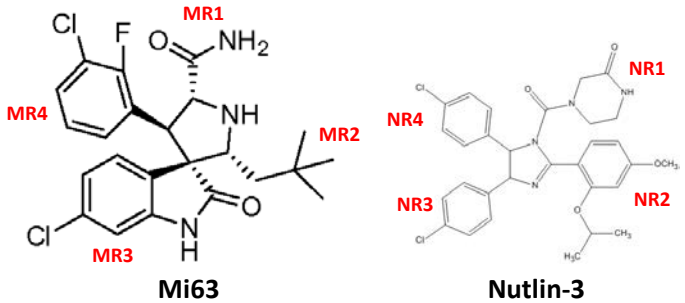

Figure 4.20 Known inhibitors Mi63 (left) and Nutlin-3 (Right) were used for fragment selection.

Fragments	Structure	Fragments	Structure
SFL00134	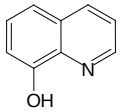	SFL000866	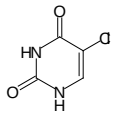
SFL001397	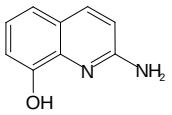	SFL001669	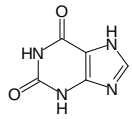
SFL001328	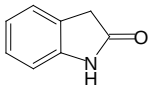	SFL000572	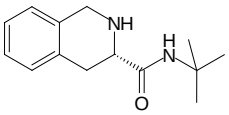
SFL001303	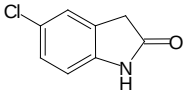	SFL000829	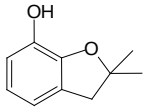
SFL001290	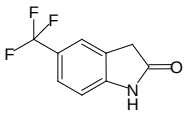	SFL001502	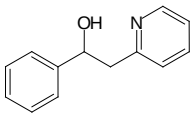
SFL001542	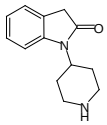	SFL000576	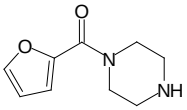
SFL001675	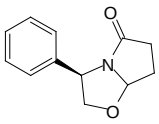	SFL000577	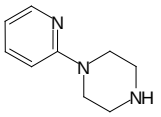

Table 4.2 Fragments selected for FP screening

4.7.2 FP studies on "Selcia fragments"

This initial screen of fragment compounds was carried out before the problem of peptide-absorption onto the plates had been resolved. This assay was therefore less sensitive than in the later work (as described in **Section 4.7.3**) as higher concentration of peptide was used.

The FP assay was set up to screen the fragments at 2mM concentration (as described in **Appendix A2**). SFL001290 and SFL001669 were insoluble so they had to be screened at lower concentrations. Nutlin-3 (5μM) was used as a positive control to

show full inhibition. Most of the fragments showed ~10% inhibition and SFL001669 showed the highest inhibition of 23% at 250μM (**Figure 4.21**). The fragments were also screened in CE at Selcia US which confirmed SFL001328 and SFL001669 to bind at 300μM concentration (Results not shown). Thus SFL001669 was the only confirmed hit from the FP assay; the other fragments screened did not show an appreciable drop in anisotropy. SFL001328 was not active in the FP assay when screening at 2mM concentration.

SFL001290 is possibly insoluble at 2mM and has a higher anisotropy than the anisotropy of MDM2-N on its own. This could be caused by the light scatters from particles of partially dissolved compound present in the solution.

The relatively weak binding of low molecular weight fragments means that screening for binding needs to be carried out at high concentrations. Only SFL001669 was confirmed binding at 250μM. In the hope of identifying more weak binding fragments, further optimization trials are described in the next section to improve the sensitivity of the FP assay.

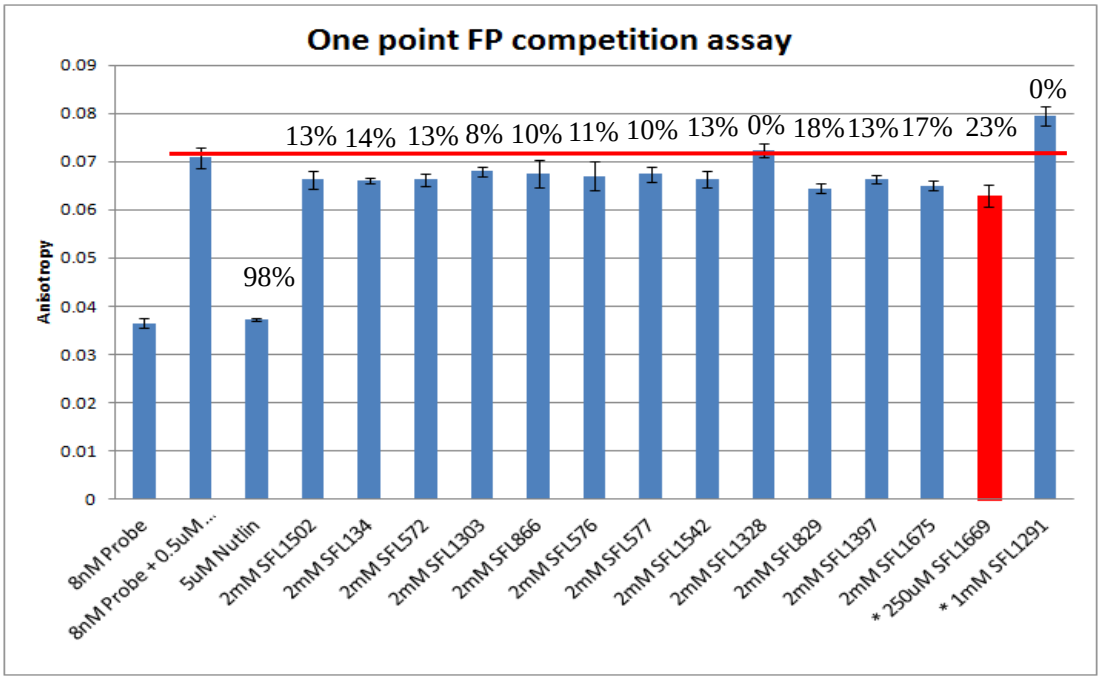

Figure 4.21 Screening of Selcia fragments in the competition FP assay.

The fragments were at 2mM concentration and 250μM for SFL001669 and screened in the presence of MDM2-N (0.5μM), p53-F (8nM) and 2% DMSO. Nutlin-3 (5μM) was used as a positive control.

4.7.3 Validating the virtual screening hits in the FP assay

As described in **Chapter 3**, the CODASS routine was used to rank 1000 hits from a library of 1.1 million compounds. The top 266 ranked hits were examined for substructures of known binding inhibitors. Six compounds (**Table 4.3**) were selected based on the criteria listed in **Section 3.7.2**.

Compounds	CODASS score/ Binding energy	Compounds	CODASS score/ Binding energy
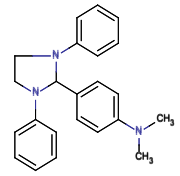 SEL101063	-7.42kcal/mol	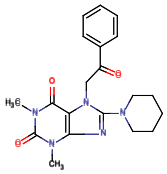 SEL101067	-8.44kcal/mol
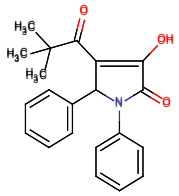 SEL101064	-7.79kcal/mol	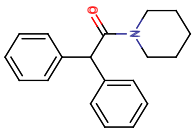 SEL101068	-7.38kcal/mol
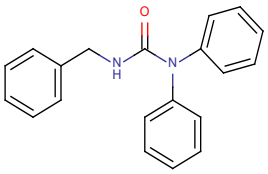 SEL101066	-8.37kcal/mol	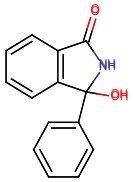 SEL101069	-7.38kcal/mol
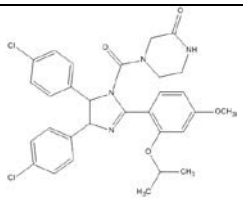 Nutlin-3 Positive control		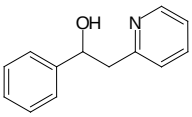 SFL001502 Negative control	

Table 4.3 The structures of the compounds selected from the CODASS ranked list.

The competition assay for these compounds is described in detail in **Appendix 2**. Siliconised equipment was used throughout. Nutlin-3 was used as a positive control and SFL001502 was used as a negative control. The virtual screening hits were initially screened at 500µM with 1% DMSO. SEL101063 and SEL101068 were found to be insoluble at 300µM when screening in the CE assay. Subsequently they were screened at 50µM.

The bar chart in **Figure 4.22** shows the results on the compound screening. SEL101063 showed small (1-2%) increase in anisotropy which may be due to insoluble particles present in the solution. The poorly soluble compound SEL101068 showed only 3% inhibition which may be due to screening at a low concentration. All other virtual screening hits showed inhibition. From the FP assay screen SEL101064 gave the highest inhibition of 37% at 500µM concentration.

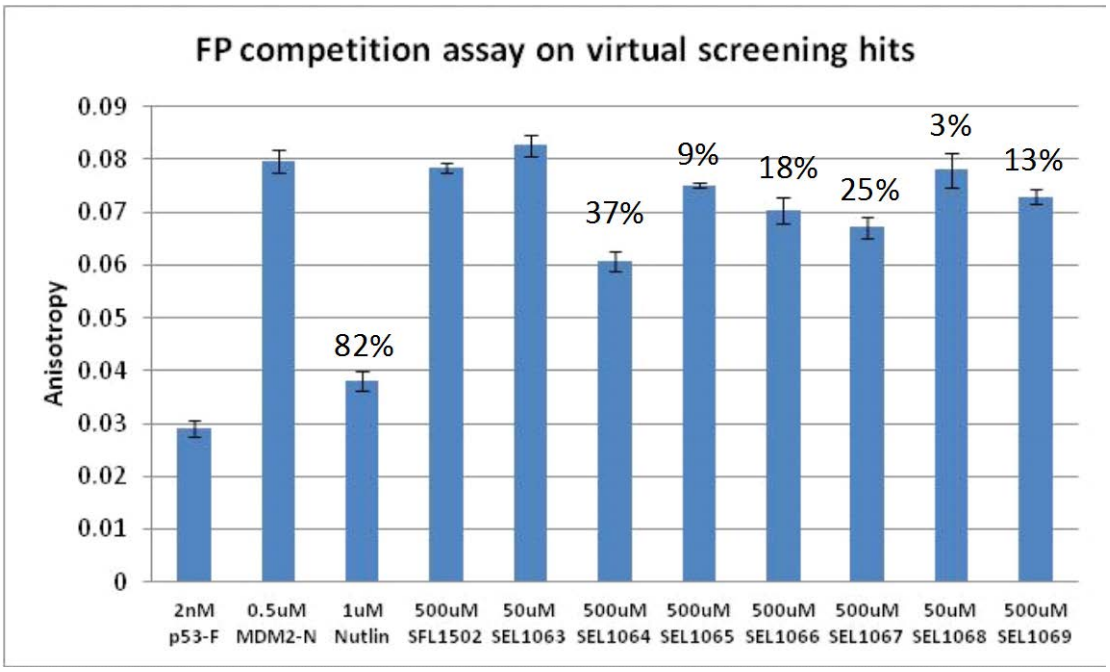

Figure 4.22 Result of FP competition assay on virtual screening hits.

SEL1063 gave an increase of anisotropy which may be due to compound particles present in the solution.

4.8 FP assay studies on MDMX-N

MDMX has also been identified to be a negative regulator of p53 and many studies have demonstrated that MDMX cooperates with MDM2 to ubiquinate p53. The X-ray crystal structure of MDM2 and MDMX showed that they are very similar in the p53 binding site at the N-terminal domain (Popowicz et al., 2010) (**Figure 1.11 and Figure 1.20, Chapter 1**).

4.8.1 FP binding assay of MDMX-N against p53-F

The MDMX-N protein was initially tested in the binding assay against p53-F to validate that p53-F can also bind to MDMX-N. Several literature studies demonstrated p53 peptide was able to bind to MDMX (Popowicz et al., 2007, Phan et al., 2010). The assay was optimised with siliconised plastic ware (**Appendix A2**). MDMX-N was titrated in the presence of p53-F (2nM). The results are shown in **Figure 4.23**. The Kd of the p53-F was calculated as 0.2µM. This result suggests that there is not a significant difference of affinity of p53-F binding to MDM2-N and MDMX-N. This result is in agreement with the results of Popowicz et al. 2007, for the p53 peptide with MDMX-N which gives a Kd value of 0.21µM.

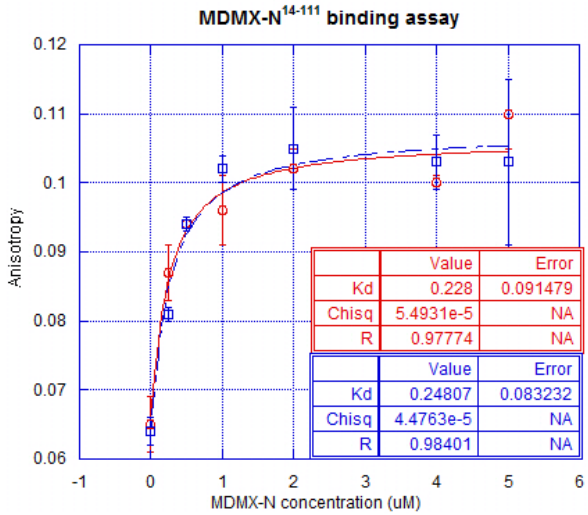

Figure 4.23 FP binding studies of MDMX-N$^{14-111}$.

Titration of MDMX-N into the p53-F (2nM). The binding assay was performed twice. Binding affinity of the p53-F to MDMX-N was ~0.22µM.

4.8.2 Nutlin-3 titration against MDM2-N and MDMX-N

Several studies have revealed that the known tight binding inhibitors of MDM2 bind weakly to the MDMX-N due to the differences in the binding site (Shangary et al., 2008, Popowicz et al., 2008). The side chains Met53 and Tyr99 are pointing into the binding site of MDMX-N thus making the p53 binding cleft smaller (**See Chapter 1 and Figure 4.24**).

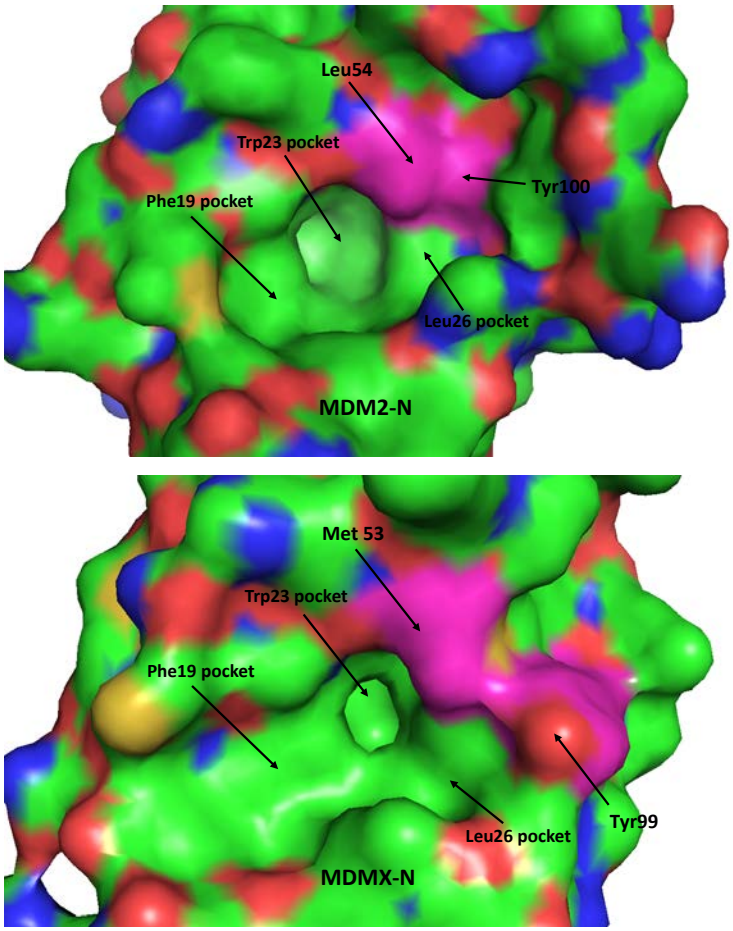

Figure 4.24 The difference in the binding site of MDM2-N (top) and MDMX-N (bottom). Surface representations of MDM2-N (PDB: 3LBL) and MDMX-N (PDB: 3DAC). The residues Met53 and Tyr99 on MDMX-N and Leu54 and Tyr100 on MDM2-N are coloured in magentas. Leu26 pocket in MDMX-N is smaller than MDM2-N due to Met53 and Tyr99 side chains pointing into the binding site.

Titration of the racemic Nutlin-3 was performed to compare the affinity with MDM2 and MDMX. The Nutlin-3 titration against MDMX-N was done using the same conditions as MDM2-N (p53-F (2nM), MDMX-N (500nM), 1% DMSO) as described in **section 4.6.4**.

In this assay Nutlin-3 has a Ki value of 266nM for binding to MDM2-N (**Figure 4.25 Top**) and a Ki value of 2.8µM for binding to MDMX-N (**Figure 4.25 Bottom**). This is consistent with Popowicz who reported a Ki of 70µM and IC_{50} of 221µM for binding to MDMX-N (Popowicz et al., 2010). The other reported value is from Shangary et al. with a Ki of 9µM (Shangary et al., 2008). The conclusion is therefore, that Nutlin-3 binds to MDMX-N with an over ten times weaker affinity than binding to MDM2-N.

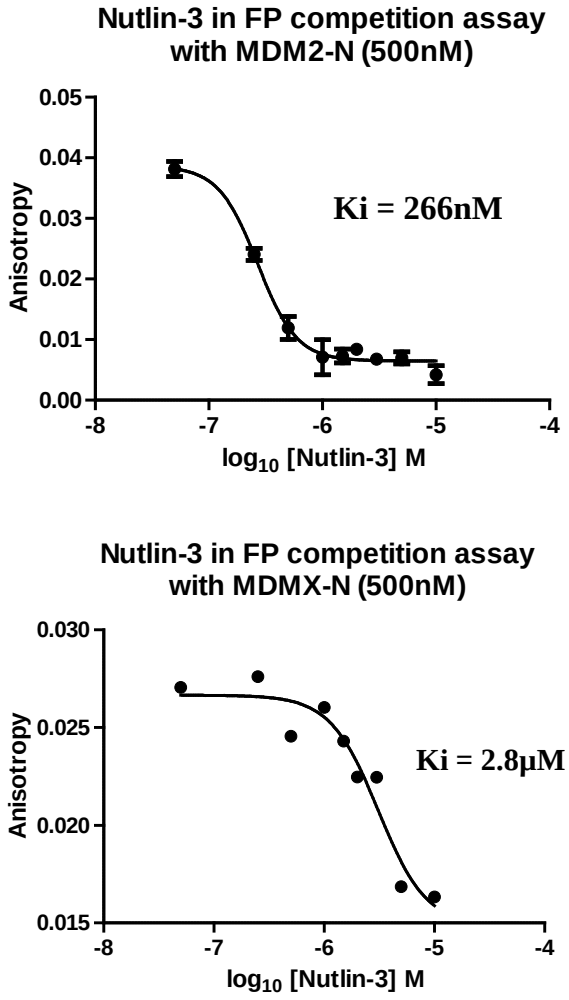

Figure 4.25 Nutlin-3 titration against MDM2-N (Top) and MDMX-N (Bottom).
Competitive binding of Nutlin-3 to MDM2-N and MDMX-N was carried out to examine the affinities of Nutlin-3 in these two highly similar proteins.

4.9 Virtual screening against MDM2-N and MDMX-N FP assay

Given the success of the previous virtual screening, which resulted in the identification of 5 hits against MDM2, a new round of virtual screening was carried out. It would be therapeutically useful to find inhibitors against both MDM2 and MDMX. A reduced complexity library containing 518,000 compounds were therefore screened against both MDM2-N and MDMX-N. The reduced complexity criteria filters the library to identify compounds with smaller molecular weight and therefore improved solubility. The result of this docking score are summarised in **Chapter 3** (**Chapter 3**). Only the compounds supplied by Chembridge were manually viewed in the PyMOL. The docking poses of these compounds in the MDM2-N and MDMX-N binding site were investigated. To maximise chemical diversity seven compounds were selected that contain different chemical scaffolds and chemical properties.

Compounds	Structures	Predicted Ki against MDM2	Predicted Ki against MDMX
SEL101875	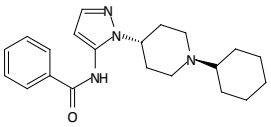	1.15 μM	7.18 μM
SEL101876	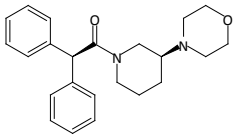	1.75 μM	3.89 μM
SEL101877	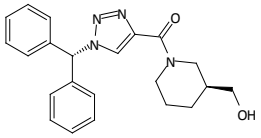	1.97 μM	1.10 μM
SEL101878	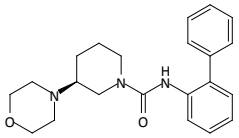	689.69 nM	6.05 μM
SEL101879	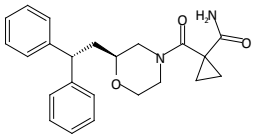	1.81 μM	5.03 μM
SEL101880	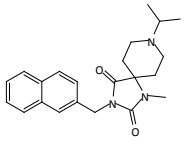	2.03 μM	3.96 μM
SEL101881	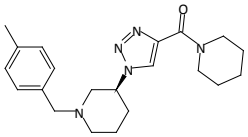	4.41 μM	3.12 μM

Table 4.4 A list of compounds selected from virtual screening.

The compounds were initially screened at a relatively low concentration of 200μM to ensure the compounds did not precipitate in solution. SEL101875, SEL101876 and SEL101880 needed to be further diluted to 50μM due to observed precipitation. The assays were screened at MDM2-N (500nM), MDMX-N (500nM), p53-F (2nM) and 1% DMSO (as described in **Section 4.6.4**). In the assay Nutlin-3 (1μM) was used as a positive control and the results showed Nutlin-3 (1μM) gave 95% inhibition against MDM2-N whereas only 16% inhibition was found against MDMX-N (**Figure 4.26**).

The results of this screen showed that only compound SEL101876 gave a relatively high inhibition of 33% at 50μM while other compounds only showed 1% - 12% inhibition. In the screen against MDMX-N, SEL101876 was also identified as having the highest (84%) inhibition at 50μM.

These data were evaluated using the ANOVA statistical analysis (as described in **Section 4.2**) to determine if effect of the inhibition is significantly different from the control MDM2-N/MDMX-N values. Only SEL101876 showed a significant difference when screening in both MDM2-N and MDMX-N proteins. The other compounds showed no significant difference to the control. Another more sensitive assay using capillary electrophoresis is described in Chapter 5 and validates the SEL101876 hit.

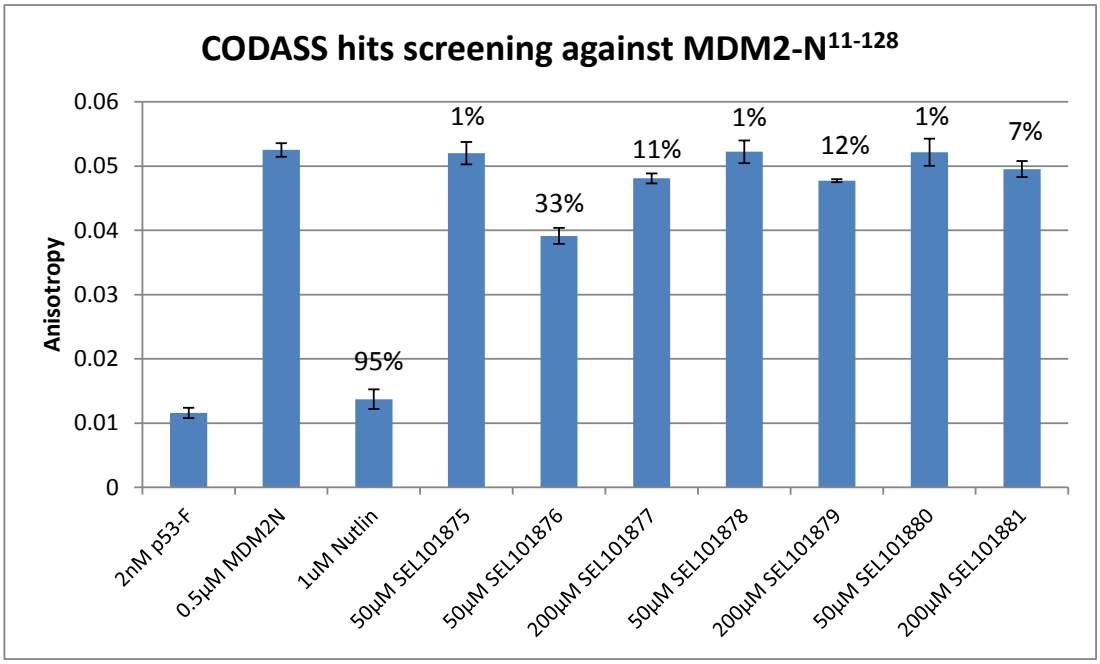

Dunnett's Multiple Comparison Test	Mean Diff.	q	Significant? P < 0.05?	Summary	95% CI of diff
MDM2N vs p53-F	0.04	23	Yes	***	0.04 to 0.05
MDM2N vs 1uM Nutlin	0.04	22	Yes	***	0.03 to 0.04
MDM2N vs SEL101875	-0.0002	0.1	No	ns	-0.005 to 0.005
MDM2N vs SEL101876	0.01	8	Yes	***	0.008 to 0.02
MDM2N vs SEL101877	0.004	3	No	ns	-0.0007 to 0.01
MDM2N vs SEL101878	0.0003	0.2	No	ns	-0.005 to 0.005
MDM2N vs SEL101879	0.005	3	No	ns	-0.0004 to 0.01
MDM2N vs SEL101880	-2e-005	0.01	No	ns	-0.005 to 0.005
MDM2N vs SEL101881	0.003	2	No	ns	-0.002 to 0.008

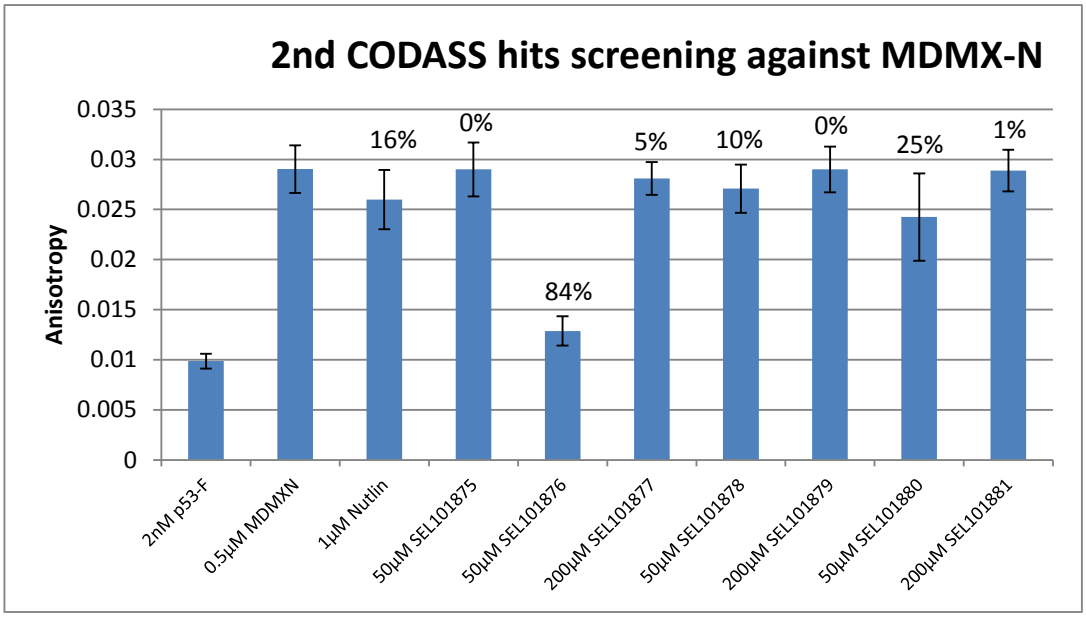

Dunnett's Multiple Comparison Test	Mean Diff.	q	Significant? P < 0.05?	Summary	95% CI of diff
MDMXN vs p53-F	0.02	10	Yes	***	0.01 to 0.02
MDMXN vs 1uM Nutlin	-0.002	1	No	ns	-0.008 to 0.003
MDMXN vs SEL101875	-0.0001	0.06	No	ns	-0.006 to 0.006
MDMXN vs SEL101876	0.02	8	Yes	***	0.01 to 0.02
MDMXN vs SEL101877	0.0009	0.5	No	ns	-0.005 to 0.007
MDMXN vs SEL101878	0.002	1	No	ns	-0.004 to 0.008
MDMXN vs SEL101879	-0.0005	0.3	No	ns	-0.006 to 0.005
MDMXN vs SEL101880	0.005	2	No	ns	-0.0009 to 0.01
MDMXN vs SEL101881	0.0001	0.07	No	ns	-0.006 to 0.006

Figure 4.26 Virtual screening hits were screened against MDM2-N and MDMX-N.

Top panel) Virtual screen hits were screened in the competition FP assay with MDM2-N and MDMX-N. Nutlin-3 (1μM) was used as a positive control. MDM2-N (0.5μM), MDMX-N (0.5μM) and p53-F (2nM) represents the anisotropy of fully bound and unbound. The compounds were screened at 200μM and 50μM depending on the solubility.

Lower panel) ANOVA statistic analysis was performed using one way ANOVA in GraphPad Prism. $P < 0.05$ was considered as significant.

4.10 Discussion

This chapter describes establishing FP as an orthogonal assay to screen weak binding small molecules as protein-protein interaction (PPI) inhibitors. The target of interest is the MDM2-N/p53 interaction and there have been several papers that use FP as a tool to screen for small molecule inhibitors against this interaction (Shangary et al., 2008, Popowicz et al., 2010, Reed et al., 2010). A summary of results generated in this work along with the most relevant published work is given below (**Table 4.5**). There are three known published peptide inhibitors that bind to both MDM2-N and MDMX-N with affinity range of 0.9nM – 216nM and 2.31nM – 229nM respectively (Bernal et al., 2010, Pazgier et al., 2009, Chang et al., 2013). The affinities of these peptide inhibitors were measured using SPR and FP (**Table 4.5**). Apart from peptide inhibitors, there are also numerous known published small molecules inhibitors discovered which inhibit MDM2-N and the most well-known inhibitors are listed in **Table 4.5** (Vassilev et al., 2004, Shangary et al., 2008, Popowicz et al., 2010, Hardcastle et al., 2011, Allen et al., 2009, Grasberger et al., 2005). The first published MDM2-N small molecule inhibitor is Nutlin with an IC_{50} value of 90nM. Many of the MDM2-N inhibitors use the Nutlin-like concept to fill the three hydrophobic pockets in MDM2-N (Phe19, Trp23 and Leu26 pockets) and have affinities in the range of 3nM – 1.2µM (**Table 4.5**). Currently there are only two inhibitors that bind tightly to MDMX-N, namely SJ-172550 and RO-2443 with an EC_{50} value of 2.3µM and an IC_{50} value of 41nM respectively (Reed et al., 2010, Graves et al., 2012). SJ-172550 showed a weaker affinity when interacting to MDM2-N with an EC_{50} value of 26µM and only RO-2443 binds potently to both MDM2-N and MDMX-N (**Table 4.5**). In our work, the first CODASS virtual screening run identified several 5-membered ring compounds that are similar to the known Nutlin-like inhibitors and these compounds bind to MDM2-N with percentage inhibitions between 3% - 37% (**Table 4.5**).

	Structures/Sequences	Inhibitor name	Binding affinity with MDM2	Binding affinity with MDMX	Techniques used	Reference
Known published inhibitors	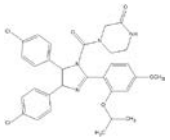	Nutlin-3a	IC50 = 90nM	Ki = 9μM	SPR	(Vassilev L. et al. 2004)
	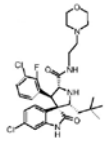	MI63	Ki = 3nM	Ki = 55μM	FP assay	(Shangary S. et al. 2008)
	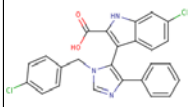	WW298	Ki = 109nM	Ki = 11μM	FP assay	(Popowicz G. M. et al. 2010)
	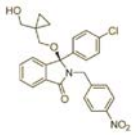	Isoindolinone	IC50 = 170nM		NMR	(Hardcastle I. R. et al. 2011)
	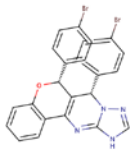	Chromenotriaz-olopyrimidines	IC50 = 1.2μM		FRET	(Allen J. et al. 2009)
	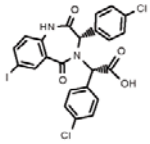	Benzodiazepinedione	Kd = 80nM		ThermoFluor	(Grasberger B L. et al. 2005)
	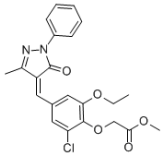	SJ-172550	EC50 = 26μM	EC50 = 2.3μM	FP assay	(Reed D. et al. 2010)
	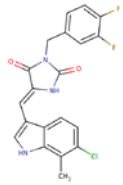	RO-2443	IC50 = 33nM	IC50 = 41nM	TR-FRET	(Graves et al. 2012)
	TSFAEYWNLLSP	PMI peptide	Kd = 3.36nM	Kd = 4.15nM	SPR	(Pazgier et al. 2009)
	Ac-QSQQTF*NLWRLL*QN-NH2	SAH-p53-8	IC_{50} = 216nM	IC_{50} = 229nM	FP assay	(Bernal et al. 2010)
	Ac-LTFR8EYWAQCbaS5SAA	ATSP-7041	Kd = 0.91nM	Kd = 2.31nM	SPR	(Chang et al. 2013)

	Structures/Sequences	Inhibitor name	Binding affinity with MDM2	Binding affinity with MDMX	Assay used
Compounds screened in this work	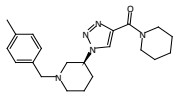	SEL-101881	CE = 72% at 50μM FP = 7% at 200μM	FP = 1% at 200μM	CE assay FP assay
	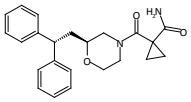	SEL-101879	CE = 59% at 100μM FP = 12% at 200μM	FP = 0% at 200μM	CE assay FP assay
	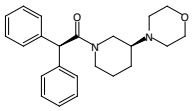	SEL-101876	CE = 58% at 50μM FP = 33% at 50μM	CE = 100% at 50μM FP = 84% at 50μM	CE assay FP assay
	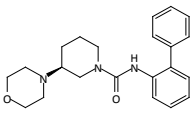	SEL-101878	CE = 58% at 100μM FP = 1% at 50μM	FP = 10% at 50μM	CE assay FP assay
	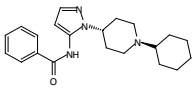	SEL-101875	CE = 40% at 50μM FP = 1% at 50μM	FP = 0% at 50μM	CE assay FP assay
	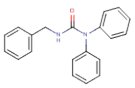	SEL101066	CE = 42% at 300μM FP = 18% at500μM		CE assay FP assay
	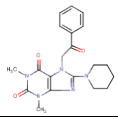	SEL101067	CE = 40% at 300μM FP = 25% at500μM		CE assay FP assay
	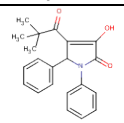	SEL101064	CE = 40% at 300μM FP = 37% at500μM		CE assay FP assay
	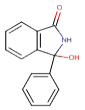	SEL101069	CE = 40% at 300μM FP = 13% at 500μM		CE assay FP assay
	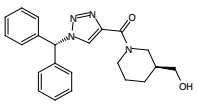	SEL-101877	CE = 18% at 50μM FP = 11% at 50μM	FP = 25% at 50μM	CE assay FP assay
	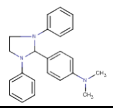	SEL101063	CE = 13% at 50μM FP = 0% at 50μM		CE assay FP assay
	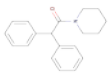	SEL101068	CE = 0% at 50μM FP = 3% at 50μM		CE assay FP assay
	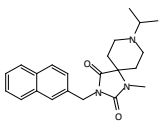	SEL-101880	CE = 0% at 100μM FP = 1% at 50μM	FP = 5% at 200μM	CE assay FP assay

Table 4.5 Summary table of known published MDM2 and MDMX inhibitors along with the compounds screened in this work.

Development of the FP assay: Numerous published papers use an FP assay for screening inhibitors of MDM2, therefore this assay becomes an ideal technique for validating the hits in this work (Shangary et al., 2008, Popowicz et al., 2010, Reed et al., 2010). Initially there was a problem with the low fluorescent signal when running the FP assay. This was found to be caused by p53-F sticking to the plastic tips and Eppendorf tubes which resulted in the use of high concentrations of p53-F and MDM2-N and thus greatly reduce the sensitivity of the assay. This problem was overcome by using siliconised tips/tubes in order to prevent absorption of p53-F to the tips/tubes. This change in plasticware allowed us to greatly reduce the p53-F concentration by a factor of ~1000 and hence significantly improved the sensitivity of the assays.
This improved assay gave excellent and consistent results which matched the published values for standard compounds. For example the published values for Ki and IC_{50} for Nutlin-3 using an FP competition range from 36nM to 2.11µM (Shangary et al., 2008, Bernal et al., 2010, Popowicz et al., 2010). This confers with a value of 266nM from our FP competition assay (using racemic Nutlin-3a and Nutlin-3b mixture). The binding data obtained from our FP is also found to be comparable with the Ki and IC_{50} values determined using other techniques including SPR, ITC and FRET which gave values for Nutlin-3 between 23nM to 263nM (Vassilev et al., 2004, Pazgier et al., 2009, Allen et al., 2009).

Studies from several published papers have shown that MDMX is also a negative regulator of the tumour suppressor p53 protein (Marine and Jochemsen, 2005, Marine et al., 2007). There are a few peptides and small molecules in the literature which show dual activity against both MDM2 and MDMX (Bernal et al., 2010, Chang et al., 2013, Pazgier et al., 2009, Graves et al., 2012). The binding data presented in **Table 4.5** shows significant differences in affinities for the known inhibitors when binding to MDM2 and MDMX. These Nutlin-like inhibitors bind more weakly to MDMX (affinities range of 9 - 55µM) compared with MDM2 (affinities range of 3nM – 1.2µM) which is an average reduction of ~99%. In order to identify small molecule inhibitors to inhibit both MDM2-N and MDMX-N an FP assay was developed for screening compounds on MDMX-N/p53 interaction. Initially, titrations of Nutlin-3 with MDM2-N and MDMX-N were performed to compare the affinity with MDM2-N and MDMX-

N. The Nutlin-3 titrations resulted in Ki values of 266nM and 2.8µM against MDM2-N and MDMX-N respectively. This indicates that Nutlin-3 binds to MDMX-N ten times more weakly than MDM2-N. The results are in agreement with the findings from Shangary S. et al. and Popowicz G. M. et al. where Ki values of 9.3µM and 70µM are determined for the interaction of Nutlin with MDMX-N (Shangary et al., 2008, Popowicz et al., 2010). As can be seen from **Figure 4.24**, MDM2-N contains a deep hydrophobic binding site whereas the binding site in MDMX-N is shallower. This may cause difficulty for the 4-chlorophenyl groups on Nutlin-3 to accommodate into the MDMX-N binding site.

In order to identify dual binding inhibitors that interact with both MDM2-N and MDMX-N, a reduced complexity subset EDULISS library was used to screen against MDM2-N and MDMX-N in CODASS (discussed in **Chapter 3**). The compound screening results for **Table 4.5** showed that only SEL101876 gave a significant inhibition for both MDM2-N and MDMX-N with values of 33% and 84% at 50µM concentration respectively. There is a higher inhibition against MDMX-N which may be due to the flexible conformation of the compound that allows it to fit into the shallow binding site in MDMX-N. The identification of SEL101876 shared little similarity with the known published Nutlin-like inhibitors (**Figure 4.20**). The flexible conformation feature in the SEL101876 (**Figure 4.27 left**) is also present in the new published dual binding inhibitor RO-2443 (**Figure 4.27 right**) (Graves et al., 2012). This may support the idea that compounds with flexible conformations are more suitable for designing dual binding inhibitors. Further validation on these compounds will be carried out using a more sensitive capillary electrophoresis (CE) assay (**Chapter 5**).

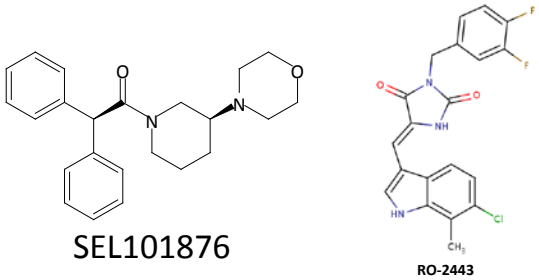

Figure 4.27 Chemical structure of SEL101876 (left) and RO-2443 (right).

Chapter 5 Screening of compounds using capillary electrophoresis (CE)

5.1 Introduction to capillary electrophoresis (CE)

Capillary electrophoresis (CE) has been used as an analytical technique to study the interaction between biomacromolecules. CE was developed by Stellan Hjerten in 1967 and only really became popular in 1981 when James Jorgenson and Krynn Lukacs demonstrated CE using a capillary with internal diameter of 75μm (Jorgenson and Lukacs, 1981).

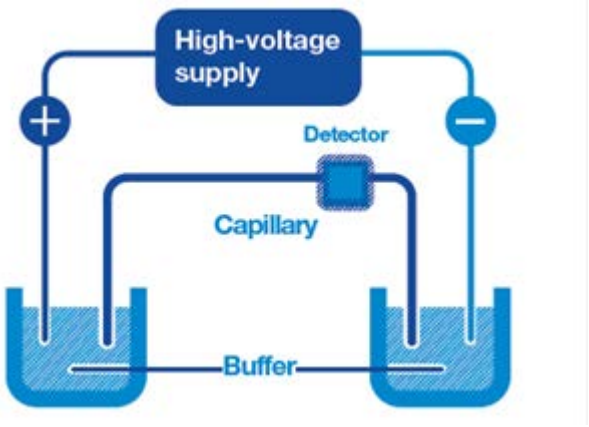

Figure 5.1 A schematic diagram of CE machine

A schematic diagram showing the main components of a CE machine which include the buffer vials, a capillary, electrodes, a detector and a high voltage supply. The capillary and electrodes are placed in the buffer vials. When voltage is applied the molecules will migrate through the capillary according to their charge to mass ratio.

A schematic diagram of CE can be seen in **Figure 5.1**. Two electrodes connected to high voltage supply are dipped into the solution with the ends of the capillary. When voltage is applied the electrodes induce an electric field to initiate the migration of the sample, either from cathode to anode or anode to cathode, through the capillary tube depending on the polarity. The capillary contains a 2mm window which is cut at the end of the capillary depending on the polarity, and this allows the laser induced fluorescence or UV light to pass through the window for fluorescence/UV detection.

The data from the CE is generated into an electropherogram as a plot of time from injection on the x-axis against the detector signal (relative fluorescence unit (RFU)/absorbance unit (AU)) on the y-axis.

CE has the ability to separate ions based on their electrophoretic mobility with the use of the applied voltage. Several factors affect the electrophoretic mobility of the molecule. These include the viscosity, the charge of the molecule and its molecular size.

Equation 5.1 describes the electrophoretic mobility:

$$\mu_e = \frac{q}{6\pi\eta r}$$

Equation 5.1 Electrophoretic mobility equation
q is the charge on the ion, η is the solution viscosity and r is the ion radius.

This equation states that the electrophoretic mobility will be affected by the differences in the charge to size ratio of the analyte ion (Beckman 1994). Therefore it is possible to separate mixtures of various ions by mass and charge ratio under the same electric field strength (**Figure 5.2**).

Another force that can be present in CE is the electroosmotic flow (EOF) that drives the migration of neutral ions in an uncoated capillary (Coulter, 1994). The ionisable silanol group that is present on the surface of the capillary wall provides a negative charge to the wall surface. This negatively charged surface attracts positively charged ions from the buffer and creates a double layer composed of a rigid layer and a diffuse layer. When a voltage is applied the cations in the diffused layer move towards the cathode carrying positive, negative and neutral charged ions. In EOF positive charged ions moved the fastest and negative ions the slowest with neutral ions as intermediates (Coulter, 1994).

In a coated polyvinyl alcohol (PVA) capillary there is little EOF and migration of ions is dependent mainly on the electrophoretic separation. The PVA coating can prevent hydrophobic and electrostatic interaction between the solute and wall surface.

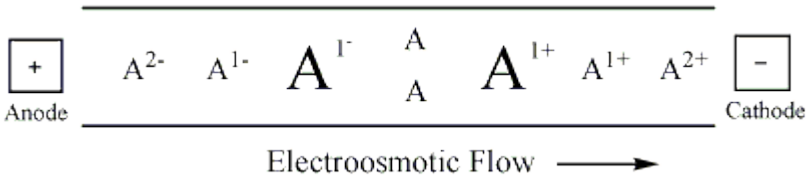

Figure 5.2 Schematic of EOF.

Separation of analytes in CE according to their electrophoretic and electroosmotic flow mobility.

5.1.1 Affinity capillary electrophoresis (ACE)

In order to identify specific binding interaction we have used affinity capillary electrophoresis (ACE) to monitor the migration patterns of the interacting molecules in the capillary. The technique uses the electrophoretic mobility of the molecules to distinguish between the binding and dissociation of formed ligand-receptor complexes during electrophoresis (Pierceall et al., 2004, Espada and Molina-Martin, 2012). ACE has been used in different varieties of interaction studies including protein-ligand, protein-protein or protein-DNA (German et al., 1998, Pierceall et al., 2004, Austin et al., 2012). Using appropriate laser-induced fluorescence (LIF) or UV detection, a fluorescently labelled probe ligand can be monitored as it migrates across the capillary. LIF detection enables CE to be able to detect the probe ligand-target interaction at much lower concentrations (nM to pM) (Pierceall et al., 2004). This is one format of an ACE assay to enable detection of weak affinity ligand (Hughes et al., 2002).

Using the probe ligand (PL), ACE can measure the mobility shift and the peak area of the PL (trace 1 in **Figure 5.3**). In the presence of the protein target in the separation buffer the PL interacts with the protein target during its migration through the capillary resulting in a mobility shift and the peak shape change of the PL (trace 2 in **Figure 5.3**). Addition of an inhibitor in the separation buffer containing the protein target and injection of the probe ligand results in prevention of the PL binding to the target which results in a reduced target dependent mobility shift of the PL (trace 3 in **Figure 5.3**). It is possible to determine the binding affinity of the inhibitor depending on how much the mobility shift is reduced.

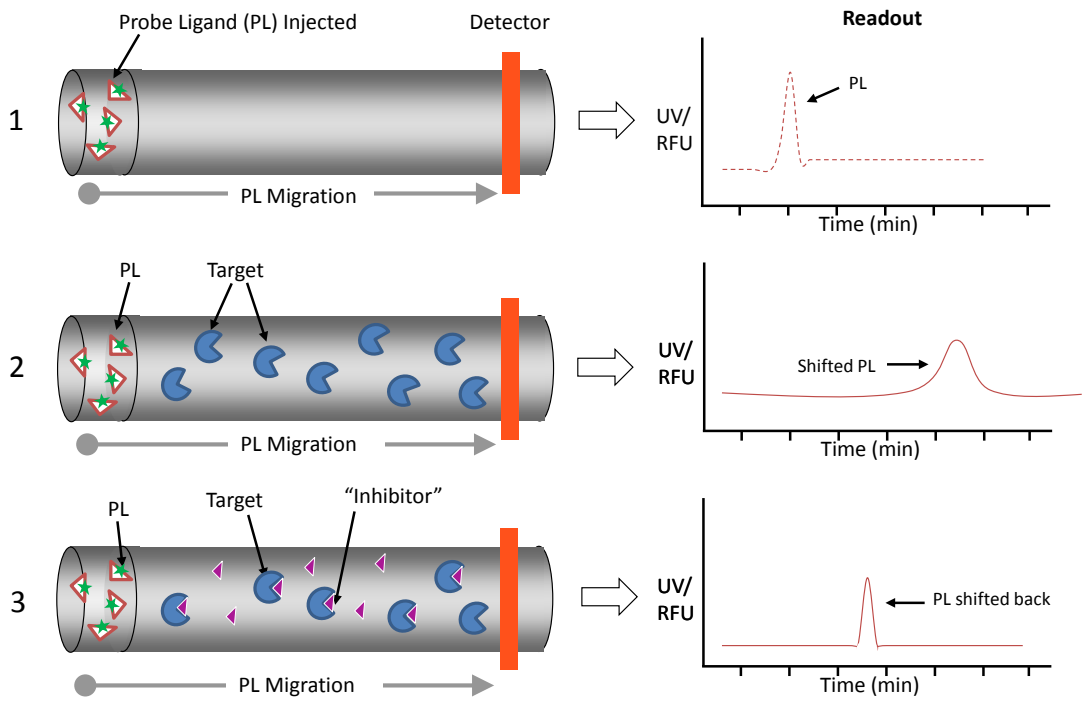

Figure 5.3 Schematic diagram of affinity capillary electrophoresis (ACE)

An example of an ACE experiment involving monitoring of an injected probe ligand (PL) with the protein target and test inhibitor in the separation buffer. The electrophoretic mobility of the probe ligand varies depend on the binding to the protein target. Upon binding to the protein target the mobility of the PL peak will shift from trace 1 to trace 2. Addition of an inhibitor in the separation buffer with the target results in prevention of PL binding resulting in reduction of the target dependent mobility shift (trace 3).

There are several advantages of using a CE assay in compound screening. CE requires only small injection volumes and the analysis cost is low. CE is performed using a high voltage to produce a high resolution profile with a short migration time to separate numerous analytes. The assay provides a high sensitivity through the use of the laser induced fluorescence (LIF) detector. The CE enables the assay to be performed with a low labelled probe concentration which allows compounds to be screened at low concentrations.

5.1.2 Principle of competitive CE assay

A competitive CE assay was developed in this work to detect competition between compounds and fluorescently labelled p53 peptide (p53-F) in MDM2-N/p53 and MDMX-N/p53 binding site.

Figure 5.4 shows an example of how the mobility of p53-F peak shifts in the presence of MDM2-N with and without compounds. The migration times of p53-F peak and p53-F/MDM2-N complex peak have to be determined prior to screening the compounds. These migration times can be used to calculate inhibition (%) of an inhibitor disrupting the p53-F interaction with MDM2-N.

Initially the p53-F is injected into the capillary and the migration time of the p53-F can be monitored by the LIF detector (**Figure 5.4** trace 1). Upon binding to the target protein MDM2-N the mass of p53-F increased due to MDM2-N/p53-F complex formation during the capillary run time. Hence the migration time increased (**Figure 5.4** trace 2).

For screening of compounds the capillary is filled with running buffer containing MDM2-N and the compound. The compound will therefore be bound to MDM2-N before injection of the p53-F. When p53-F is injected into the capillary and a high voltage applied across the capillary, p53-F will move through the capillary and compete with MDM2-N/compound complex. Where there is a compound/MDM2-N interaction the compound prevents p53-F from binding to the binding site. Depending upon how strong the compound/MDM2-N interaction is and how much compound is present the p53-F peak will gradually shift back to its original position (**Figure 5.4** trace 3). When there is no interaction present between the compound and the binding site the p53-F peak will remain at p53-F/MDM2-N peak position.

An optimised condition of MDM2-N/p53 competitive CE assay was developed by Dr. Dallas Hughes, Dr. Yuriy Dunayevskiy, Dr. Alexy Korneev and Dr. Leonid Rashkovetsky in Selcia US (see **Appendix A3** for SOP). The plan was to reproduce the assay, validate with known ligands and use the conditions for subsequent compound screening work.

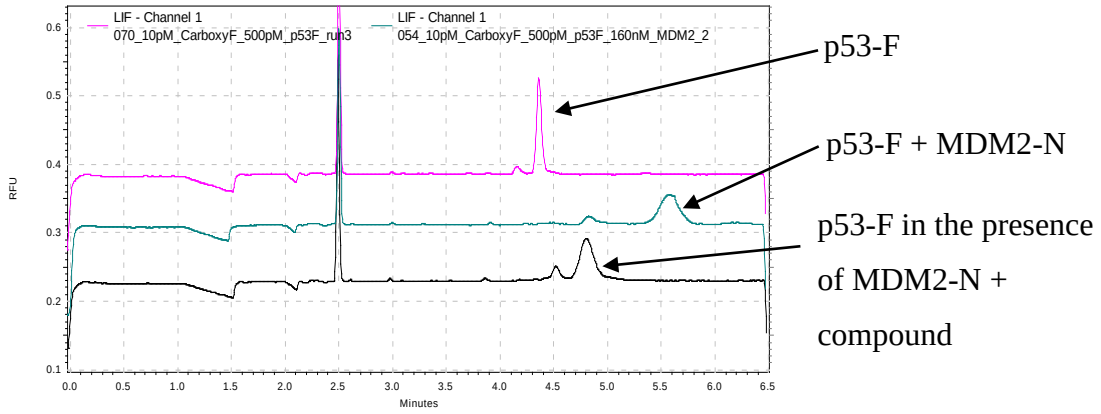

Figure 5.4 Example of CE traces.

LIF detection of injected PL (p53-F (500pM)) when it is alone (first trace), in the presence of MDM2-N (160nM) in the separation buffer with (third trace) and without (second trace) test compound (50µM or 300µM).

5.2 Materials and methods

5.2.1 Materials and methods for MDM2-N CE

A detailed CE standard operation procedure (SOP) can be found in the **Appendix A3**. In the CE the labelled probe used was a fluorescently labelled p53 peptide (p53-F) (Sequence is shown in **section 5.3.3**) which can be detected using a laser induced fluorescence (LIF) detector. The model of the LIF detector used was a Beckman Coulter 488nm laser module and the laser used had an argon ion laser source with excitation/ emission wavelengths of 488nm/520nm. The excitation/ emission wavelengths used in the CE were similar to the p53-F detection in the FP assay where 485nm/530nm were used.

When screening the compound in the CE the injection sample contained Carboxyfluorescein (internal standard (10pM)) and p53-F (500pM) in TAPS/Tris (1mM) pH 8.0, DTT (1mM).

The separation sample buffer contained MDM2-N (160nM), test compound (300µM depending on solubility), TAPS/Tris (200mM) pH 8.0, DMSO (1% f/c) and glycerol (0.25% f/c). In this work Nutlin-3 and unlabeled p53 peptide were used as test inhibitors to validate the assay.

5.2.2 Materials and methods for MDMX-N CE

In the MDMX-N CE assay the same fluorescently labelled p53 peptide (p53-F) was used. The SOP used for MDM2-N CE assay was also used in the MDMX-N CE assay (**Appendix A3**). The injection sample buffer contained Carboxyfluorescein (10pM) and p53-F (500pM) in TAPS/Tris (1mM) pH 8.0, DTT (1mM). The separation sample buffer contained MDMX-N (160nM (requires further optimization)), test compound (concentration depended on the compound solubility), TAPS/Tris (200mM) pH 8.0, DMSO (1% f/c) and glycerol (0.25% f/c).

5.2.3 Sequences of the MDM2-N and MDMX-N

The protein constructs used in the assays contained only N-terminal sequences because the p53 binding site is located at the N-terminal domain of MDM2 and MDMX. It should also be noted that the full length sequence structures of MDM2 and MDMX are highly unstable and prone to precipitation.

The MDM2-N and MDMX-N constructs that were used in the FP and CE assay were:

His_6-tag-MDM2-$N^{11\text{-}130}$

```
10         20         30         40         50         60
MGSSHHHHHH SSGLVPRGSH MDGAVTTSQI PASEQETLVR PKPLLLKLLK SVGAQKDTYT

        70         80         90        100        110        120
MKEVLFYLGQ YIMTKRLYDE KQQHIVYCSN DLLGDLFGVP SFSVKEHRKI YTMIYRNLVV

       130
VNQQESSDSG TSVSENLE
```

His6-tag-$MDMX\text{-}N^{14\text{-}111}$

```
        10         20         30         40         50         60
MGSSHHHHHH SSGLVPRGSH MDSASRISPG QINQVRPKLP LLKILHAAGA QGEMFTVKEV

        70         80         90        100        110
MHYLGQYIMV KQLYDQQEQH MVYCGGDLLG ELLGRQSFSV KNPSPLYDML RKNLVTLAT
```

Upon examining a list of different labelled p53 peptide of MDM2-N used in the literature (See **Chapter 4**) only the labelled p53 peptide (p53-F) from Brown C. et al. has a suitably low affinity for our competition experiment (Brown et al., 2010).
The fluorescently labelled p53 derived peptide (p53-F) used in the CE assay was:

5-FAM-QETFSDLWKLLP-OH
Fluorescein amidite (FAM) is a fluorescein dye that can be detected by the LIF detector at 520nm emission wavelength.

5.2.4 Testing of compounds in the CE assay

Compounds were screened at an initial screening concentration of 300µM or 50µM depending on the compound solubility. **Appendix A3** gives the method for the CE compound screening.
After injection of the sample a voltage of 10kV was applied and separation was carried out for 6.5min. The migration time of the p53-F peak was recorded and the inhibition (%) was calculated using the equation below.

$$\% \text{ Inhibition} = 100(T_H - T_L)/(T_H - T_R)$$

Where: T_H is migration time of p53-F peak in the presence of MDM2-N.
T_R is the migration time of p53-F peak.
T_L is the migration time of p53-F peak in the presence of MDM2-N + compound.

Selected hits shown to be active in CE were titrated to confirm if the compound gave a dose response curve. Where possible an IC_{50} was calculated.

5.2.5 IC_{50} Calculation

Compounds were titrated using ~10 different concentrations and the percentage inhibition was calculated from the migration time. Calculated % inhibition of each concentration was input into GraphPad prism software. Compound concentration was

converted into Molar unit and transformed to $\log_{10}$. A four parameter variable slope was used to fit the curve and the IC_{50} was calculated.
The curve was fitted using the equation:

$Y = Bottom + (Top – Bottom)/(1+10^{((LogIC_{50} - X)*Hillslope)})$

Where: X is log of dose or concentration.

Y is response, decreasing as X increases.

Top and Bottom is Plateaus in same units as Y.

$logIC_{50}$ is same log units as X.

HillSlope is Slope factor.

5.3 Results

Initial experiments using the Selcia US conditions were not reproducible (data not shown) and after discussion with Selcia US they suggested using siliconised tips/vials to prevent p53-F sticking to plastic. The optimised MDM2-N and p53-F condition developed by Selcia US is MDM2-N (160nM) and p53-F (500pM). A new experiment was therefore carried out to confirm the effectiveness of siliconised tips/vials.

5.3.1 Improving sensitivity using siliconised vials/tips

In this study normal pipette tips and PCR vials were replaced with siliconised tips/vials in order to minimise sticking of p53-F to vials and tips. Carboxyfluorescein (4nM) and p53-F (250nM) were first tested and repeated 3 times to confirm if the results were reproducible. It was found that the three repeats overlapped and in fact the p53-F (250nM) peak was saturated (Figure 5.5). These results showed that using siliconised tips/vials can help prevent the p53-F sticking and also improves the reproducibility of the assay.

Due to the p53-F peak being saturated it was possible to decrease the concentration of Carboxyfluorescein and p53-F to find the minimum concentration required. Serial dilution of Carboxyfluorescein and p53-F in Figure 5.6 showed the concentration could be lowered to the pM range and reproduction of the Selcia US conditions becomes possible.

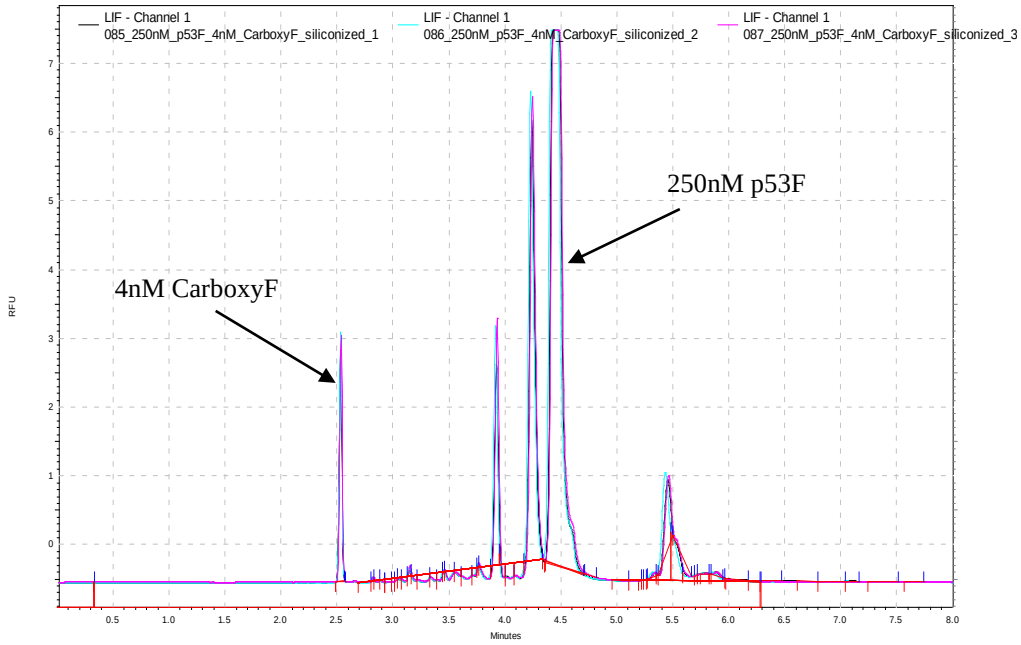

Figure 5.5 Repeating runs of Carboxyfluorescein and p53-F.

Carboxyfluorescein (4nM) and p53-F (250nM) were first tested and repeated 3 times. The results became reproducible after using siliconised tips/vials. The peak was saturated when using p53-F (250nM) and there were other peaks present which may be contaminants that were not removed during the peptide synthesis.

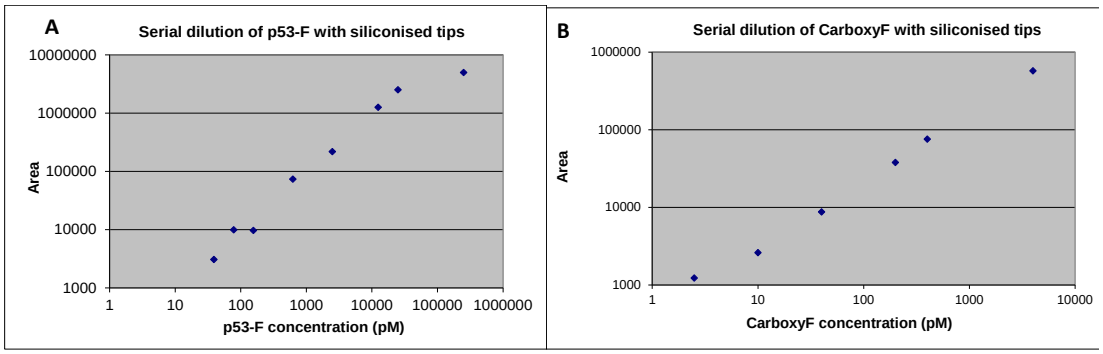

Figure 5.6 A and B Serial dilution of p53-F and Carboxyfluorescein using siliconised tips/vials.

The area of and p53-F (**A**) and Carboxyfluorescein (**B**) peaks were recorded in each dilution and plotted. With decreasing p53-F or Carboxyfluorescein concentration the peak area decreased.

5.3.2 Addition of MDM2-N in the CE assay

In order to carry out compound screening an optimum concentration of MDM2-N has to be determined. The optimum conditions given from Selcia US were p53-F (500pM) and MDM2-N (160nM) using siliconised tips/vials. Using these conditions it was possible to obtain an assay window of one minute between the p53-F peak and the MDM2-N/p53-F complex peak. Assay window is the difference between the minimal and the maximal signal and an adequate window ensures the detection of active inhibitor that disrupts p53-F/MDM2-N interaction. Figure 5.7 shows that with addition of MDM2-N (160nM) in the solution the p53-F peak shifted from 4.32min to 5.36min. This one minute assay window is sufficient for subsequent inhibitor screening.

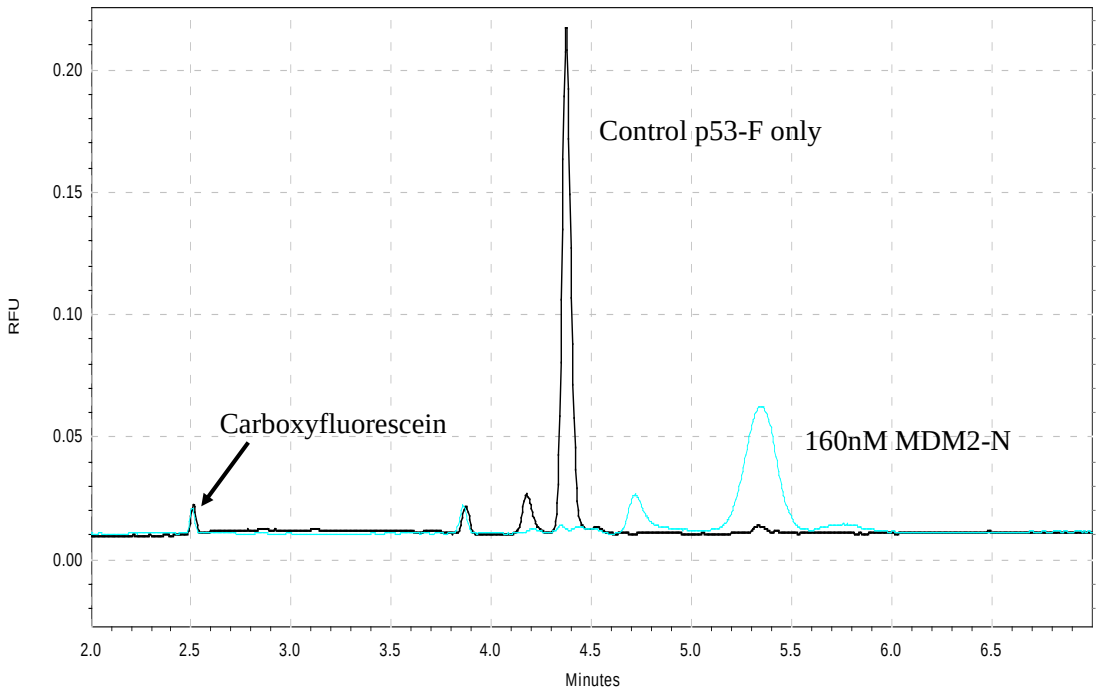

Figure 5.7 CE electropherogram of MDM2-N (160nM) run with Selcia US conditions. The electropherogram shows the migration time of p53-F (500pM) in black colour trace and the migration time of p53-F (500pM)/MDM2-N (160nM) complex in light blue colour trace. Carboxyfluorescein (25pM) was added as an internal standard.

5.3.3 Nutlin-3 titration

Nutlin-3, a known inhibitor of the MDM2-N/p53 interaction, was used in order to confirm if the p53-F/MDM2-N peak shifted back in the presence of an inhibitor of the MDM2-N/p53 interaction. From the literature Nutlin-3 showed IC_{50} values of 90nM and 432nM determined using SPR and FP assay (Vassilev et al., 2004, Ding et al., 2006), while the IC_{50} observed in our FP assay was 266nM (**Chapter 4**). It may be possible to see a full inhibition with the addition of twice the Ki concentration of Nutlin-3. Upon adding Nutlin-3 (100nM) the peak shifted back to the p53-F peak position with a change in peak shape indicating competition between p53-F and Nutlin-3 in the MDM2-N binding site (**Figure 5.8 bottom trace**).

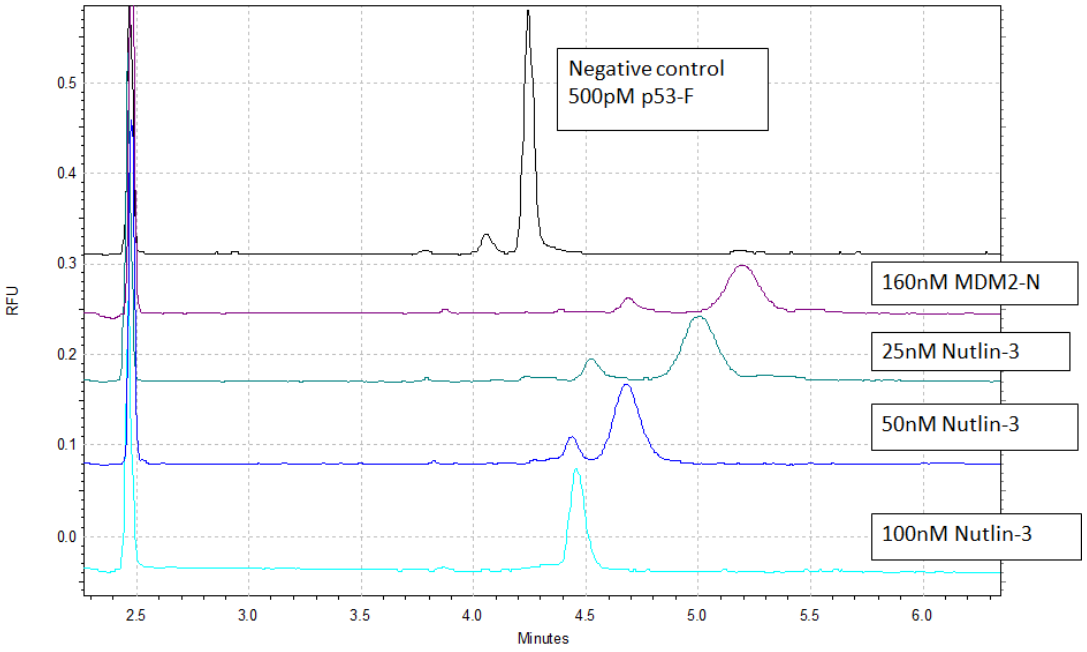

Figure 5.8 Nutlin-3 titration.

As the Nutlin-3 concentration increases the peak shifted back to the p53-F control peak position. In this titration the injection buffer used contains Carboxyfluorescein (internal standard (10pM)) and p53-F (500pM) in TAPS/Tris (1mM) pH 8.0, DTT (1mM). The top trace is the p53-F (500pM) alone and contains TAPS/Tris (200mM) pH 8.0, DMSO (1% f/c) and glycerol (0.25% f/c) in the separation buffer. This is followed by p53-F (500pM) running in the separation buffer containing MDM2-N (160nM), TAPS/Tris (200mM) pH 8.0, DMSO (1% f/c) and glycerol (0.25% f/c). Nutlin-3 was then added into the sample with increasing concentrations (separation buffer: Nutlin-3, MDM2-N (160nM), TAPS/Tris (200mM) pH 8.0, DMSO (1% f/c) and glycerol (0.25% f/c).

With additional titration the IC_{50} of Nutlin-3 could be calculated. Nutlin-3 was titrated from 0.5nM to 400nM and % inhibition was calculated from the migration time of Nutlin-3 (Figure 5.9).

The % inhibition was fitted against Nutlin-3 concentration in Log scale using GraphPad Prism and IC_{50} was calculated to be 37.3nM. The calculated IC_{50} is similar to the literature value of 90nM (Vassilev et al., 2004). This confirms that the CE assay is able to identify inhibitor binding and calculate an accurate IC_{50}.

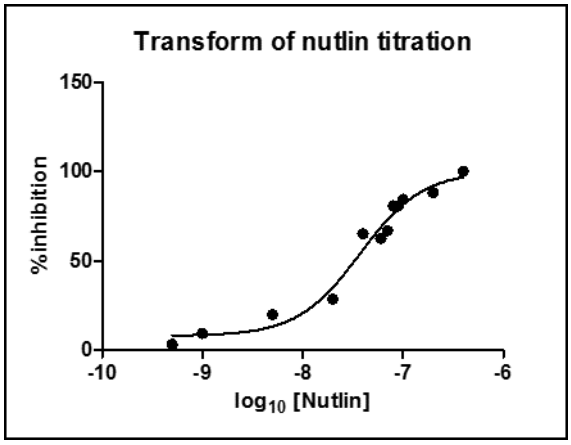

Figure 5.9 Graph showing inhibition (%) plotted against Nutlin-3 concentration.
From the data an IC_{50} of 37.3nM was determined.

5.3.4 Unlabelled p53 peptide titration

To further evaluate the reliability of the CE assay an unlabelled p53 peptide (13amino acid sequence) that is known to bind to the MDM2-N binding site (Kussie et al., 1996) was tested in the assay. A titration of unlabelled p53 peptide was performed to obtain the IC_{50} which can be used to compare with the IC_{50} from the literature.

```
P53-U  ETFSDLWKLLPEN
       ||||||||||||
Phan   ETFSDLWKLLPE
```

An IC_{50} was performed over the range 0.025µM to 40µM. Increasing the concentration of unlabelled p53 peptide showed that the p53-F peak gradually shifted back to its

original position (**Figure 5.10**). This suggests that there was unlabelled p53 peptide/MDM2-N complex formation and p53-F was not able to bind to MDM2-N. A dose response curve was generated using the % inhibition calculated and the IC_{50} was calculated to be 3.1µM (**Figure 5.11**). The IC_{50} of unlabelled p53 peptide from the literature is 2µM (Phan et al., 2010) but only an IC_{50} value of 23µM was observed in our FP assay. This suggest that FP assay is less sensitive and is unable to measure accurate IC_{50}. The IC_{50} obtained from the CE was in good agreement with the IC_{50} from the literature and implies that the CE assay is able to measure accurate IC_{50}.

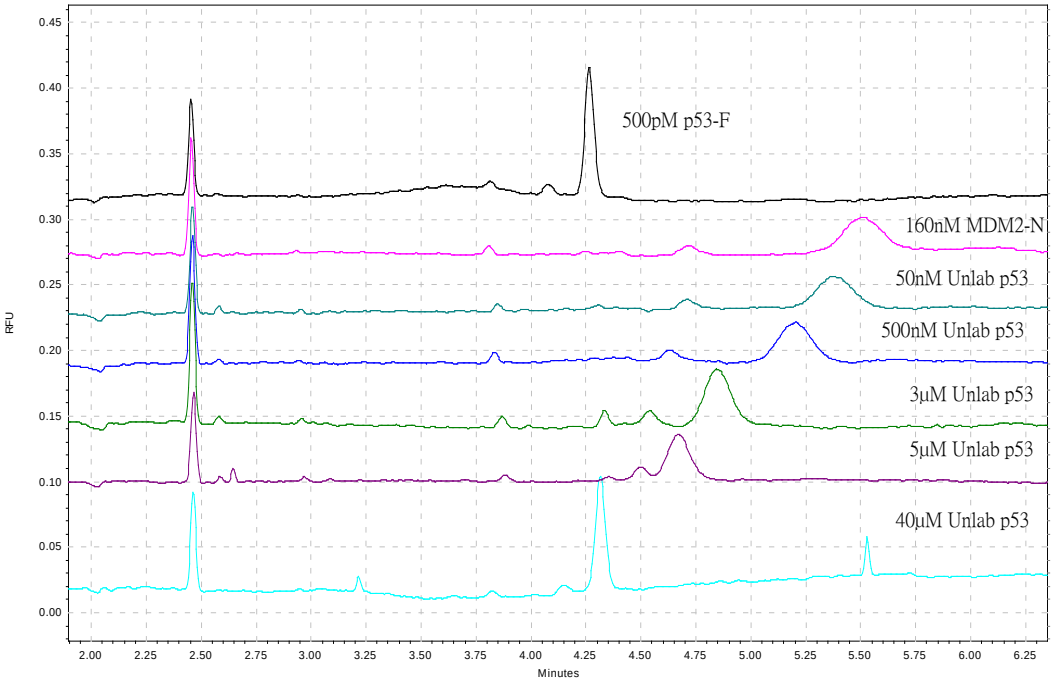

Figure 5.10 Electropherogram of unlabelled p53 peptide titrated against p53-F (500pM). The diagram shows some representative traces of p53-F peak gradually shifting back to its original position with increasing concentration of unlabelled p53 peptide.

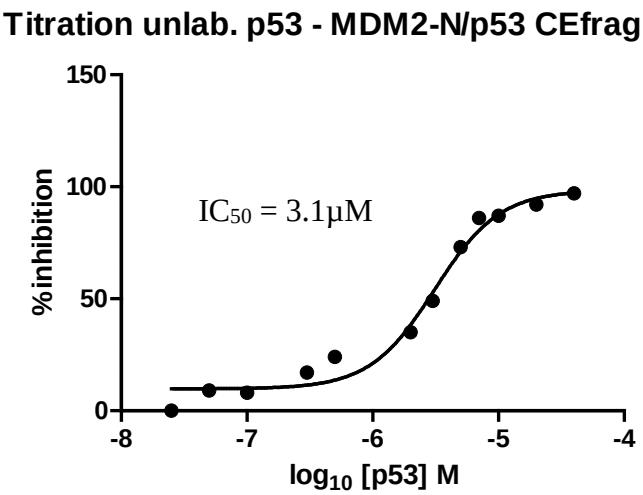

Figure 5.11 Dose response curve for unlabelled p53 peptide (13mer).

Graph showing the % inhibition against the unlabelled p53 peptide concentrations in log scale. An IC_{50} was determined from the curve using GraphPad Prism software (Dose response curve, GraphPad Prism 5).

5.3.5 Validation of virtual screening hits using CE

The six compounds purchased from the initial virtual screening CODASS (See **Chapter 2**) were selected as they had different chemical motifs. Unfortunately there was insufficient amount of the compound to perform solubility tests. Initially they were tested at one concentration (300µM), however SEL101063 and SEL101068 were tested at 50µM because it was discovered the compounds precipitated in the solution at 300µM. Subsequently they were tested at a final concentration of 50µM. **Figure 5.13 – Figure 5.14** presents the CE electropherograms of the compounds. After each compound screen a control run with MDM2-N was carried out to ensure that the p53-F peak shifted back to the original MDM2-N peak position. Percentage inhibition was calculated as previously described and the results are summarised in **Table 5.1**. Of the six virtual screening hits only SEL101068 was found to be inactive. This may be due to screening at the low concentration of 50µM. All other virtual screening hits showed ~40% inhibition at 300µM concentration. SEL101063 was also shown to be active with 13% inhibition at 50µM; however it was not evaluated further due to poor

solubility. The compounds were also shown to be active in the FP assay with only SEL101063 and SEL101068 inactive which may be due to the assay not being sensitive enough to detect weak binding at lower concentration (**Table 5.1**).

From the CE screen SEL101066 was confirmed to be the strongest hit. Analogues of this compound were further explored to find the segment of structure that provides optimum inhibition (See **Chapter 6**).

	% Inhibition from CE	% Inhibition from FP
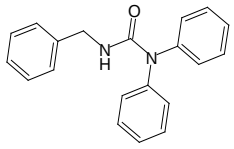 SEL101066	42.0% at 300µM	18% at 500µM
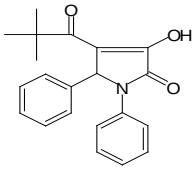 SEL101064	40.6% at 300µM	37% at 500µM
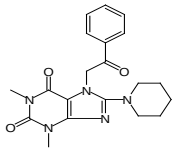 SEL101067	40.6% at 300µM	25% at 500µM
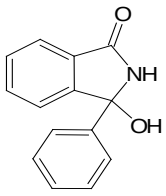 SEL101069	40.1% at 300µM	13% at 500µM

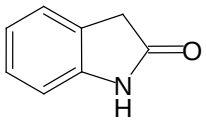 SFL001328	27.67% at 300µM	8% at 500µM
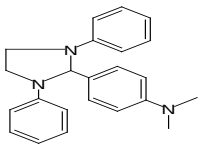 SEL101063	13.2% at 50µM	0% at 50µM
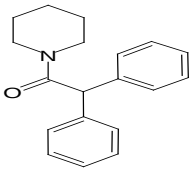 SEL101068	0% at 50µM	3% at 50µM

Table 5.1 Summary results of the CE and FP screen on virtual screening compounds
The compounds were ranked based on the % inhibition from CE.

5.3.6 CE screen on SFL001328 fragment

The Selcia fragment SFL001328 was also screened in CE at 300µM. The solubility of this compound was determined at Selcia to be 1mM with 3% f/c of DMSO as part of a solubility test of the Selcia fragment library.

SFL001328 is a fragment of the Spiro-oxindoles inhibitor Mi63 as shown in **Figure 5.12**. SEL101069 also contains a similar motif as SFL001328. SFL001328 showed a 27% inhibition in CE at 300µM concentration (**Figure 5.13**) which suggests that SFL001328 may be used as a starting point in the fragment optimisation process. Titration was done on SEL101069 and SFL001328 to obtain the IC_{50} and also to confirm that the hits are not due to compound aggregation (See **Section 6.7**). If the inhibition was due to the presence of compound aggregation then a sudden increase in inhibition may occur with increasing compound concentration.

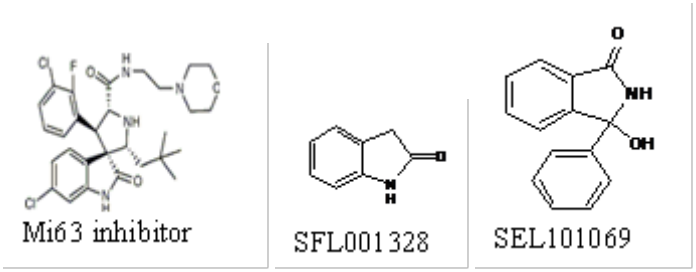

Figure 5.12 Chemical structure of Mi63 inhibitor and the oxindole analogues, SFL001328 and SEL101069.

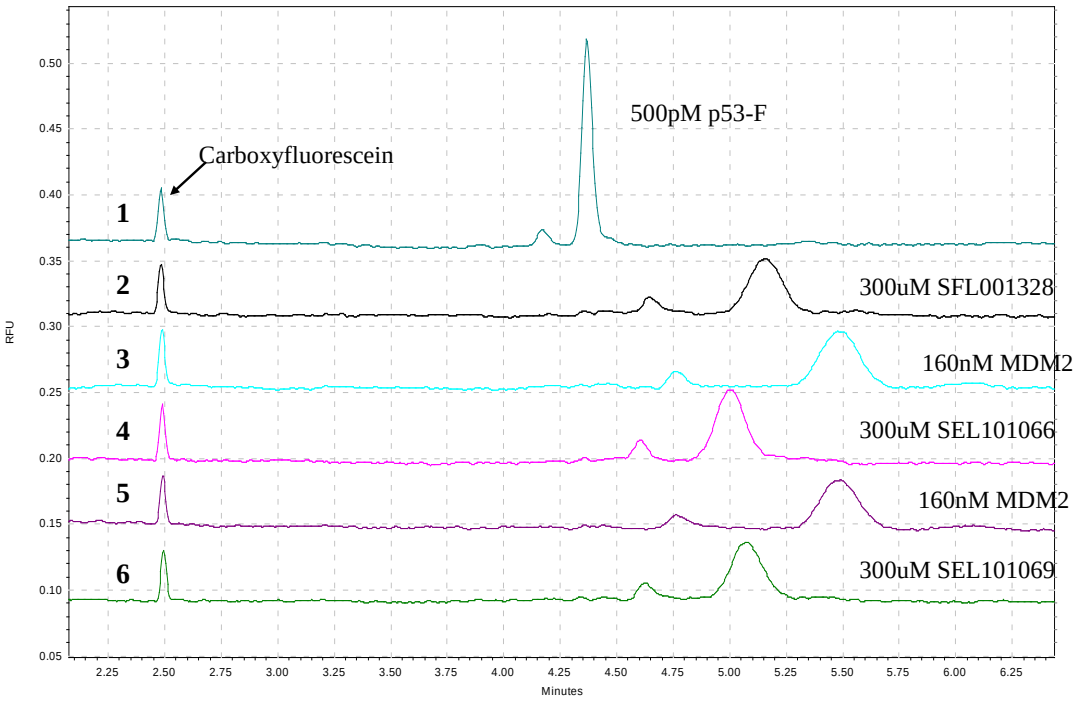

Figure 5.13 Electropherogram of CE screen on virtual screening hits.

All compounds shifted the p53-F peak, which is indicative of an interaction taking place. The first trace is the control of p53-F (500pM). The second trace is the SFL001328 (300µM) fragment. The third and fifth traces are the controls of MDM2-N (160nM) with p53-F (500pM). The fourth trace is SEL101066 (300µM) and the sixth trace is the SEL101069 (300µM).

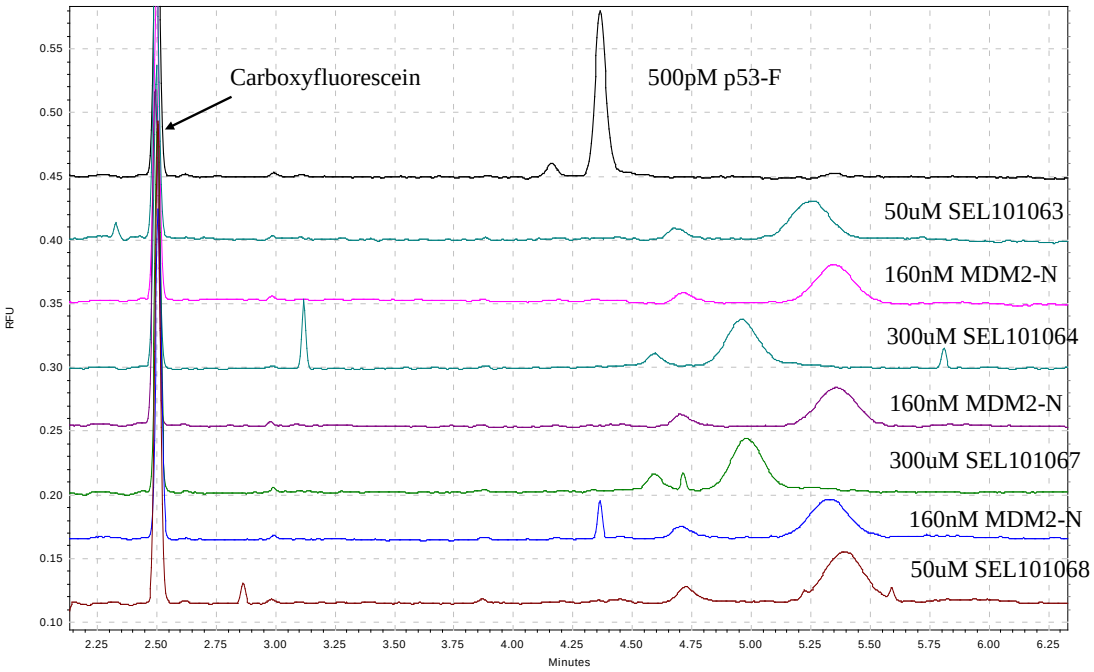

Figure 5.14 Electropherogram of CE screen on virtual screening hit compounds.

The diagram shows the change in migration time of the p53-F peak in the presence of compounds. The control run of p53-F (500pM) running in the separation buffer containing MDM2-N (160nM) was performed in between each compound screen. Only SEL101068 did not shift the p53-F peak which confirms no interaction taking place.

5.3.7 Screening the second set of CODASS hits against MDM2-N in the CE assay

Due to the success of the previous virtual screen a new CODASS run was performed to screen through a reduced complexity subset of EDULISS library containing 518,000 compounds to identify dual inhibitors against the MDM2-N and MDMX-N. The virtual screening results were explained in more detail in **Chapter 2**. From the 1000 hits ~100 compounds from Chembridge were pulled out. Seven compounds containing different chemical classes were purchased (**Table 5.2**).

Solubility tests were performed on the CODASS hits (**Appendix A4**). However it was only performed after screening in the FP assay and SEL101877 and SEL1881 were screened at the solubility limit in the FP assay. SEL101875 – SEL101877 and SEL101881 showed lower solubility so these compounds were screened at 50µM.

There is a similarity between these compounds in which they contain triazole piperidinyl motif in the structure (circled in red) which may be why they have lower solubility. SEL101878 – SEL101880 had higher solubility and were screened at 100µM.

Table 5.2 showed the summary results of the CODASS hits screened against MDM2-N in the CE and FP assays. Percentage inhibition calculation was described as in the methods (**Section 5.2.4**). Of the eight compounds only SEL101880 was found to be inactive in both assays. SEL101875, SEL101876, SEL101878, SEL101879 and SEL101881 were found to be active with inhibition over 40% at either 50µM or 100µM in the CE assay. SEL101877 was also active in the CE assay but with a weaker inhibition of 15%. These compounds however did not show similar inhibition in the FP assay. A possible reason is that SEL101875 and SEL101878 were screened at 50µM in the FP assay which may be at the limit of detection, whereas SEL101879 and SEL101881 were screened at 200µM in the FP assay which is at the solubility limit and the compounds may be aggregated in the solution.

From the screening several compounds were identified with inhibition >50%. The compounds SEL101876, SEL101878, SEL101879 and SEL101881 were selected for titration to obtain the IC_{50} of these hits. These compounds were titrated based upon the solubility (**Appendix A4**) and the % inhibition values obtained (Table 5.2). SEL101876 was titrated from 3.1µM to 100µM, SEL101878 and SEL101879 were titrated from 25µM to 200µM and finally SEL101881 was titrated from 3.1µM to 50µM. The titration curves can be found in the **Appendix A5**.

The IC_{50} values calculated for these compounds are listed in Table 5.2. The result showed SEL101881 was found to have the highest inhibition against MDM2-N with an IC_{50} of 17.6µM.

These compounds showed little similarity with the known MDM2-N inhibitors and have more rotatable bonds, therefore these flexible structure compounds may have a higher chance on binding to the MDMX-N binding site. These compounds were screened in the FP assay (**Chapter 4**) prior to screening in the CE assay and from the FP assay results the compound SEL101876 was binding tightly to MDMX-N with 86% inhibition at 50µM. CE assay for MDMX-N was then set up in order to verify these virtual screening hits against MDMX-N.

	% inhibition from CE assay	% inhibition from FP assay	IC_{50} determined using CE assay
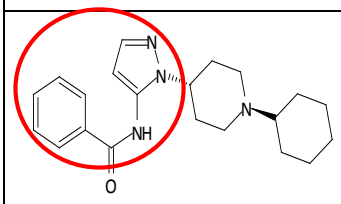 SEL101875	41% At 50µM	1% At 50µM	
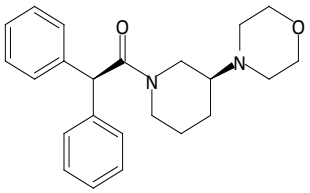 SEL101876	58% At 50µM	33% At 50µM	31.7µM
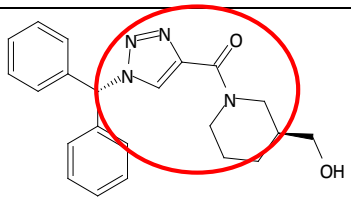 SEL101877	16% At 50µM	11% At 200µM	
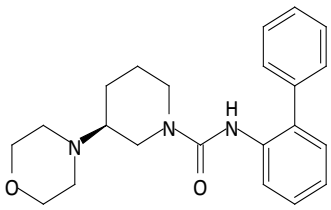 SEL101878	58% At 100µM	1% At 50µM	69µM
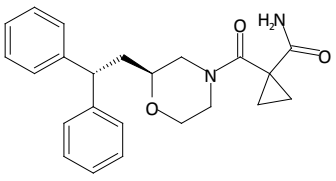 SEL101879	59% At 100µM	12% At 200µM	71µM

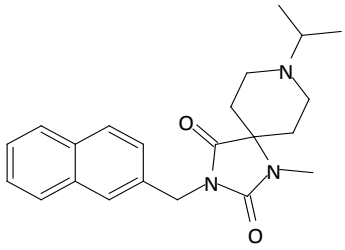 SEL101880	0% At 100µM	1% At 50µM	
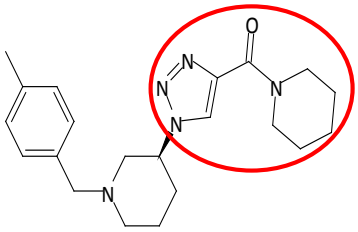 SEL101881	72% At 50µM	7% At 200µM	17µM

Table 5.2 Summary results on the CE and FP assays on second CODASS hits against MDM2-N

The compounds were screened at different concentrations in the CE and FP assays because the solubility test was not performed before running the FP assay. SEL101875, SEL101877 and SEL101881 contained a similar motif in the structure as highlighted by the red circles.

5.3.8 Developing the CE assay for MDMX-N$^{14-111}$

The CODASS hits were also screened against MDMX-N$^{14-111}$ using CE. The materials and methods for MDMX-N CE assay can be found in **section 5.3.2**. MDMX-N was run in the same buffer conditions, using 200mM TAPS/Tris pH 8.0, as that for MDM2-N. MDMX-N has a pI of 9.2 and is consequently positively charged at pH 8.0, whilst p53-F was negatively charged at pH 8.0. Whereas MDM2-N is negatively charged at pH 8.0 and migrates from the negative end to the positive end in the capillary. During the separation MDMX-N will migrate from the positive end to the negative end and p53-F will migrate from the negative to the positive. This migration direction is the opposite of MDM2-N which suggests that there will be more interaction between the MDMX-N and the p53-F.

When the MDMX-N protein concentration was re-measured by Bradford assay before running in the CE assay the concentration was found to be three times less than originally measured. The laser protein concentration in the solution which may be due

to aggregation after storing in the -80°C freezer for one month. A new measured concentration was then used in the assays.

A protein titration was performed to analyse the binding of p53-F with MDMX-N. The titration was performed from 100nM to 1000nM and the p53-F gradually shifted further with increasing concentration of MDMX-N (**Figure 5.15**). From the protein titration 240nM concentration was found to provide the best assay condition with a 1min window for screening compounds. Higher concentration of MDMX-N may provide an even bigger window, however this will lose the sensitivity on detecting ligand binding.

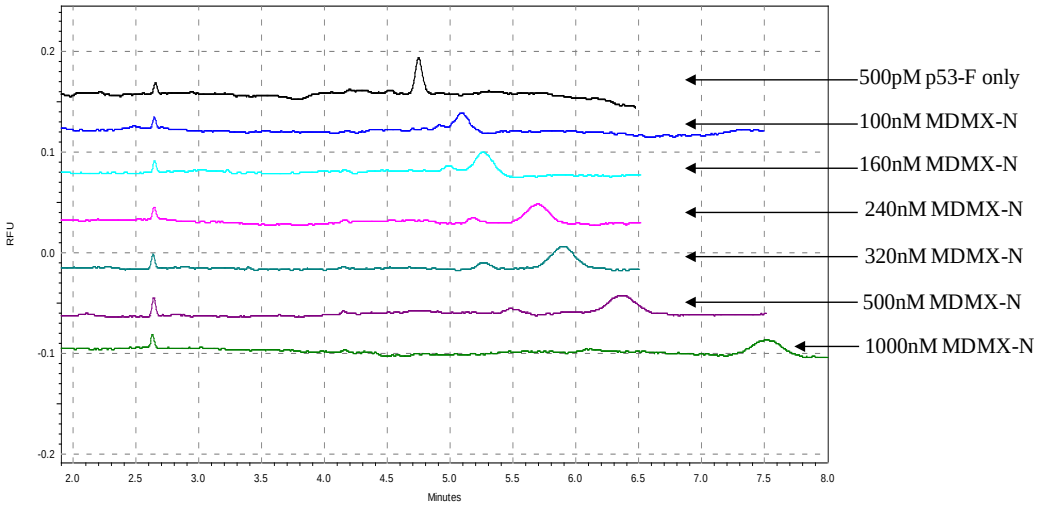

Figure 5.15 MDMX-N titration in the CE.

The titration of MDMX-N was performed from 100nM to 1000nM concentrations. The first trace is the control experiment with p53-F on its own followed by increasing concentration of MDMX-N. The migration time of MDMX-N/p53-F peak gradually increased as the MDMX-N concentration increased.

Nutlin-3 was added into the separation buffer with MDMX-N (240nM) in order to confirm if the p53-F/MDMX-N complex peak will shift back to the p53-F alone peak position.

From the literature (Popowicz et al., 2010) and the previous FP assay result (**Section 4.8.2**), Nutlin-3 binds weakly to MDMX-N with an IC_{50} >3µM. Therefore a higher concentration of Nutlin-3 had to be added into the CE to get full inhibition. Nutlin-3

(10µM) was added and 100% inhibition was seen (Figure 5.16). However when running the MDMX-N run after the Nutlin-3 run the migration time of the MDMX-N/p53-F peak did not shift back to its original position. This indicates that the Nutlin-3 may not have been fully washed away from the capillary. Intense washing was applied to try and remove the Nutlin-3 from the capillary. After the separation run, a 2 min running buffer rinse was added and the H_2O rinse was increased from 0.5 min to 2 min followed by a 3 min BSA (1mg/ml) rinse. After the intense rinse the capillary was regenerated and the migration time of p53-F/MDMX-N (240nM) complex peak was restored to 5.8min (Second peak in **Figure 5.17**).

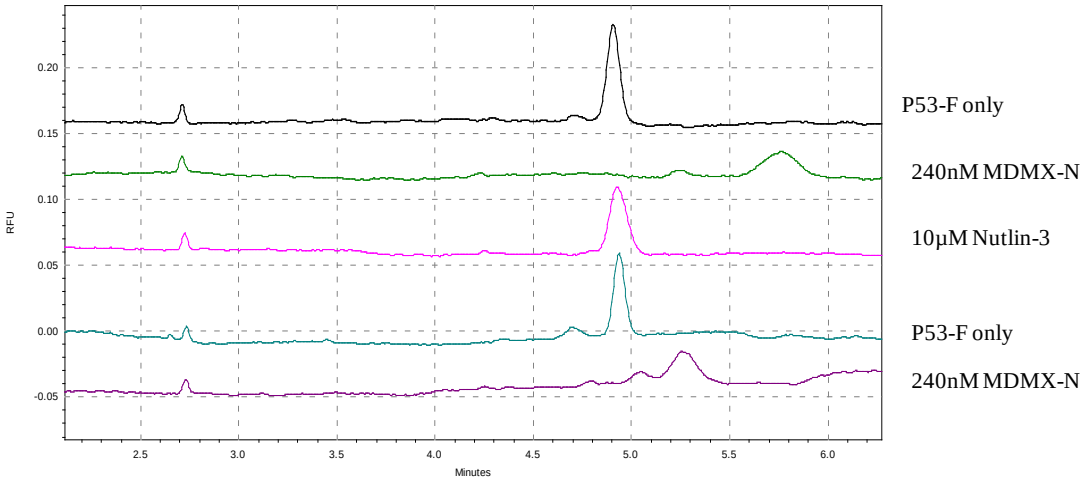

Figure 5.16 CE traces of p53-F peak in the presence of Nutlin-3 (10µM).
The third trace is the competition experiment of Nutlin-3 (10µM) run after the MDMX-N (240nM) control. The p53-F peak has shifted back in the presence of Nutlin-3 (10µM). Control experiments of p53-F and MDMX-N (240nM) were repeated after the competition experiment but the MDMX-N/p53-F complex peak did not shift as far as the first MDMX-N/p53-F run due to the Nutlin-3 remaining in the capillary.

However, when repeat adding Nutlin-3 (10µM) it was discovered that the p53-F peak did not shift back to the original position (third trace from the top in **Figure 5.17**). It is possible that at 10µM Nutlin-3 the concentration may be above the limit of its solubility and the aggregated Nutlin-3 damaged the coating on the capillary wall. After the Nutlin-3 (10µM) run the migration time of the MDMX-N/p53-F peak was not able to migrate back to its original position (Fourth trace in **Figure 5.17**). The migration

time of the MDMX-N/p53-F complex peak was reduced from 1.2min to ~0.65min. It is possible that Nutlin-3 was still not washed away from the capillary even with the additional rinsing steps. To try and remove all the particles and contaminants the capillary was rinsed with 10mM phosphoric acid for 3min followed by H_2O rinse for 5min. Phosphoric acid is used as a rinsing reagent to remove proteins adsorbed on the coated capillary wall. Following the rinses with phosphoric acid the migration time with MDMX-N was partially but not fully recovered (5 and 6th traces from the top in **Figure 5.17**). The migration time of MDMX-N (240nM)/p53-F peak only shifted by 0.65min from the p53-F peak. The migration time of MDMX-N/p53-F peak reduced by half compared to the beginning when Nutlin-3 was not added.

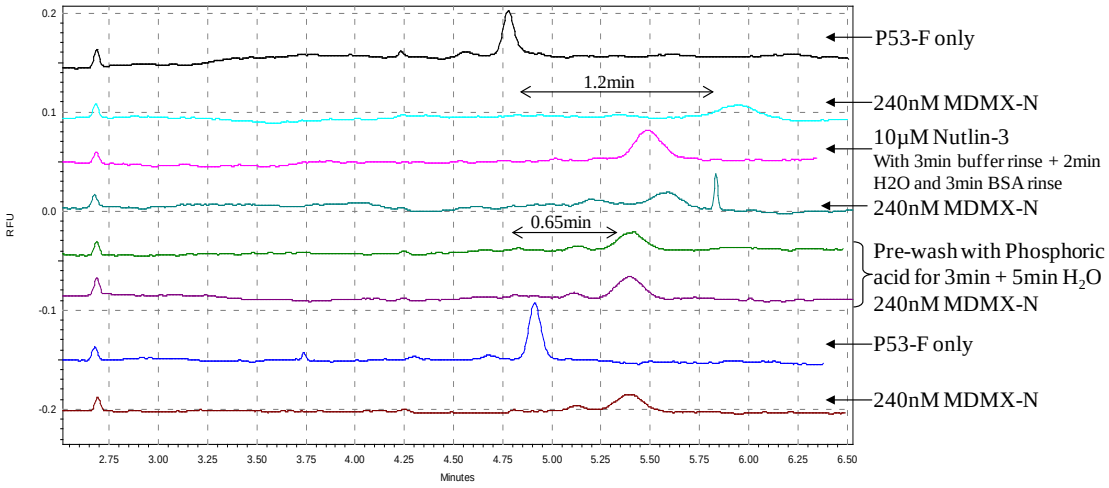

Figure 5.17 CE traces of MDMX-N/p53-F peak.

The MDMX-N/p53-F peak did not shift back to 5.9min after the Nutlin-3 (10µM) run. The capillary was washed and MDMX-N (240nM) run was repeated several times but the migration time of MDMX-N/p53-F peak was not fully recovered.

The migration time of MDMX-N peak was not reproducible which may have been caused by the Nutlin-3 particles damaging the coating on the capillary wall. Therefore a new capillary was inserted into the cartridge and conditioned with the running buffer and H_2O. The internal standard Carboxyfluorescein (20pM) and p53-F (500pM) control were run followed by a MDMX-N (240nM) run. The MDMX-N (240nM) run was repeated twice and p53-F (500pM) was run in between to ensure that the p53-F

peak would migrate back to its original position. As can be seen in Figure 5.18, the first MDMX-N (240nM) run (blue trace), the MDMX-N/p53-F peak migrated to 5.85min and the p53-F peak returned to its original position on the next run. However on the second MDMX-N (240nM) run the MDMX-N/p53-F peak required a longer time to migrate through the capillary (teal trace, 4th trace in **Figure 5.18**). The migration time has increased to over 6.5min with the assay window extended to over 1min.

It may be possible to repeat the CE run with MDMX-N (160nM) concentration and monitor if the migration time of MDMX-N/p53-F complex will change.

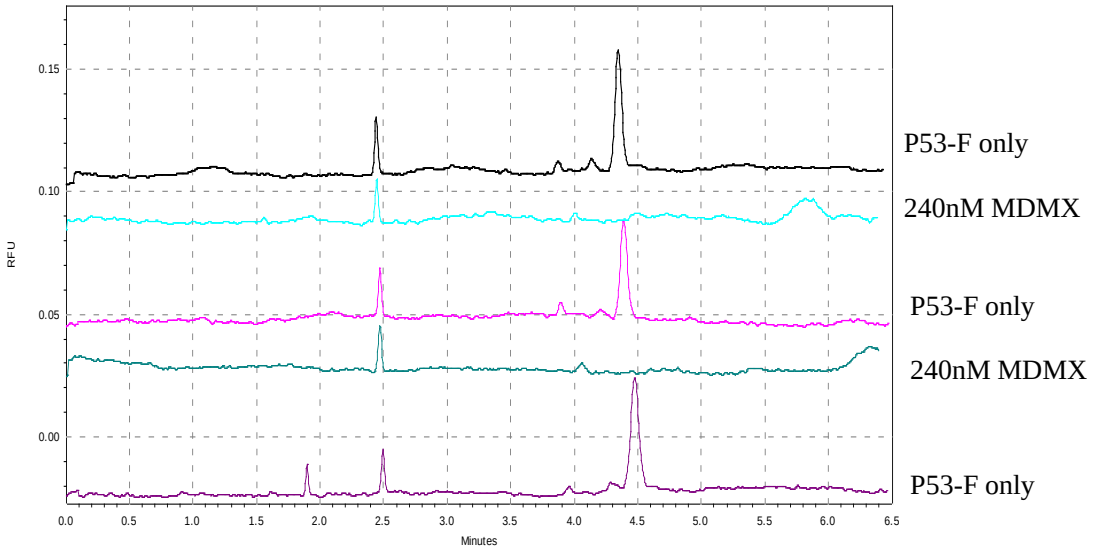

Figure 5.18 CE traces of p53-F peak in the presence of MDMX-N (240nM).

The p53-F peak shifts from ~4.5min to 5.8min when MDMX-N (240nM) was present in the capillary. However the migration time of the MDMX-N/p53-F peak shifted to 6.5min in the repeat run (teal trace). The migration time of p53-F was not affected when run on its own in-between the MDMX-N (240nM) runs.

When running MDMX-N (160nM) the migration time was ~5.3min which was similar to the migration time in **Figure 5.15**. However the migration time of MDMX-N/p53-F peak increased when repeating the run (fourth and sixth in **Figure 5.19**) which may be caused by adsorption of MDMX-N to the capillary. More MDMX-N in the capillary will result in more MDMX-N/p53-F interaction and this increases the p53-F run time.

If the adhered MDMX-N was not washed away then it could interact with the p53-F and increase its migration time during the p53-F control run. However this was not observed in the p53-F run when running in between the MDMX-N run (Third and Fifth traces in **Figure 5.19**).

As discussed in **section 5.3.8** there was aggregated MDMX-N found in the frozen stock. This could suggest that the aggregates adhered in the capillary and interact with MDMX-N to form large aggregates. The aggregates formation in the capillary further increase the migration time of the MDMX-N/p53-F complex. The migration time of p53-F was not affected when running p53-F control run possibly because the aggregates only interact with MDMX-N but not p53-F. To remove these aggregated proteins intense rinse steps were applied by rinsing with H_2O for 5min, running buffer for 10min and H_2O for 2min. Unfortunately, even when applying the intense rinse steps at the end of every MDMX-N run, the aggregated proteins were not completely removed in the capillary and the migration time of MDMX-N/p53-F still fluctuated in every run.

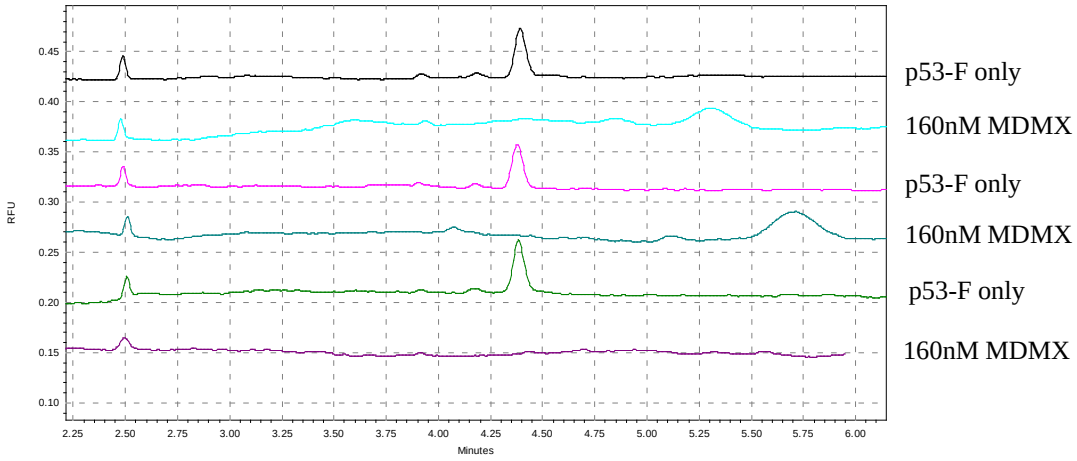

Figure 5.19 Control runs of MDMX-N and p53-F.

MDMX-N (160nM) and p53-F runs were repeated one after the other. The migration time of MDMX-N/p53-F peak shifted further when run several times. The migration time of the p53-F peak was not affected when running in between the MDMX-N (160nM) runs.

5.3.9 CODASS hits screening against MDMX-N$^{14-111}$

Due to the problem with the inconsistent migration time of MDMX-N/p53-F peak compound screening was difficult. It was a challenge to determine how much inhibition the compound had caused. However it was still possible to screen the compounds by monitoring the p53-F peak and observe if the compounds were able to shift the p53-F peak back to its original position. This method could show the displacement of p53-F by the compound but the % inhibition cannot be reliably determined. Further work on assay optimisation is required to confirm the results.

The compounds identified from the CODASS virtual screening were already measured by the FP assay (**section 4.9**) and showed SEL101876 to have a relatively high inhibition against MDMX-N. Therefore it will be interesting to verify SEL101876 in the CE to confirm the inhibition.

SEL101876 (50µM) was screened after the p53-F and MDMX-N (160nM) control runs. When SEL101876 (50µM) was added the p53-F peak shifted back to its original position. This suggested that p53-F was fully competed off from MDMX-N by SEL101876 (**Figure 5.20**). Screening SEL101878 and SEL101881 did not shift the p53-F back so these two compounds were ranked as non-inhibitors (Results not shown). A summary of results for the CODASS hits screened using the FP and CE assays is presented in Table 5.3**.** From the FP and CE assays SEL101876 gave a relatively high inhibition at 50µM concentration. SEL101876 gave even higher inhibition against MDMX-N than against MDM2-N. However SEL101876 titration was not performed against MDMX-N due to the unstable migration time of MDMX-N/p53-F. The MDMX-N CE condition has to be further optimized in order to perform the titration.

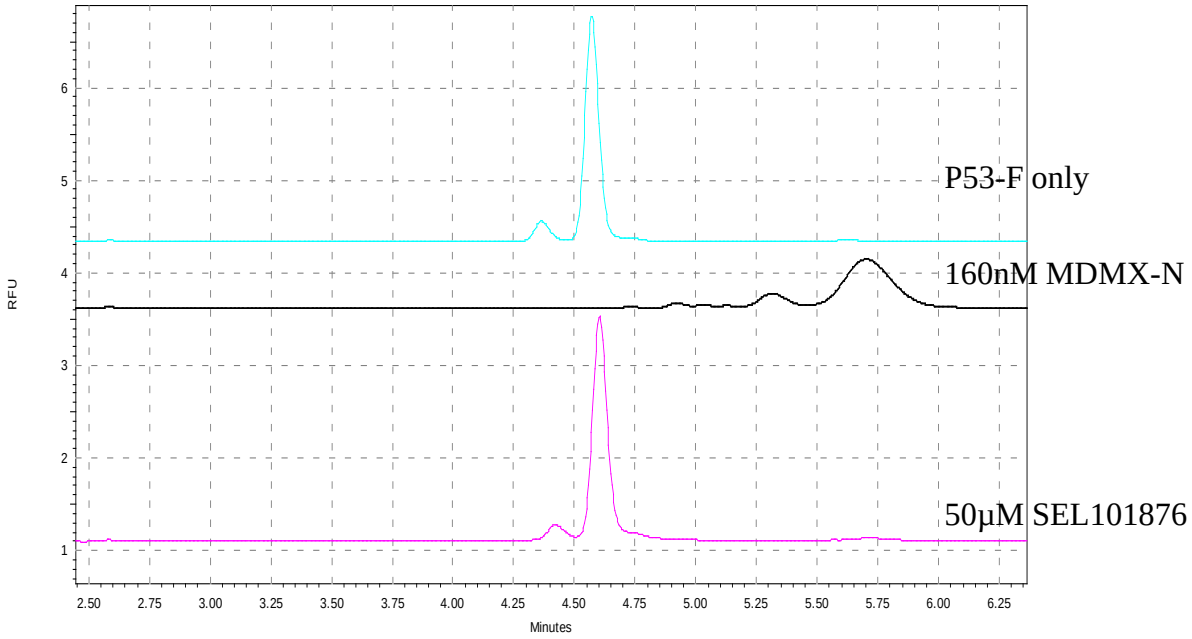

Figure 5.20 CE traces of SEL101876 (50µM) screening against MDMX-N.

The trace in aqua is the sample with p53-F on its own. The black trace is the MDMX-N/p53-F complex peak. The pink trace is the competition experiment containing SEL101876, MDMX-N and p53-F in the solution. The p53-F peak shifted back to its original position when SEL101876 (50µM) was present.

	% inhibition from CE assay	% inhibition from FP assay
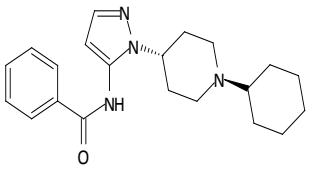 SEL101875	Not tested	0% At 50µM
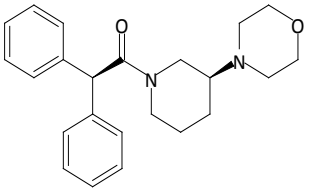 SEL101876	100% At 50µM	84% At 50µM
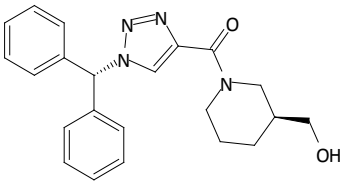 SEL101877	Not tested	5% At 200µM
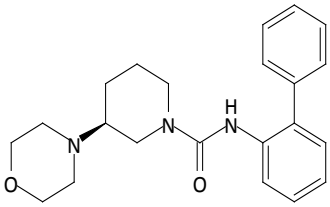 SEL101878	0% At 100µM	10% At 50µM
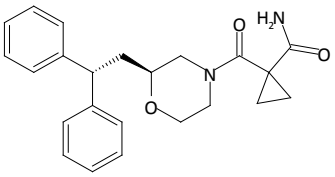 SEL101879	Not tested	0% At 200µM

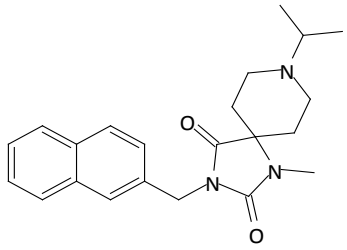 SEL101880	Not tested	25% At 50µM
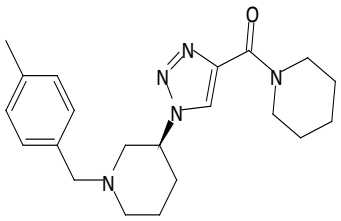 SEL101881	0% At 50µM	1% At 200µM

Table 5.3 Summary table of CODASS hits screened against MDMX-N in the FP and CE assays.

The table shows the % inhibition of the compounds against MDMX-N obtained in CE and FP assays. The concentrations above the bars are the concentrations used in the assays. Only SEL101876, SEL101878 and SEL101881 were screened in the CE assay.

5.4 Discussion

In this study we have employed capillary electrophoresis as an orthogonal assay to confirm the virtual screening results and verify with the FP assay results. The MDM2-N CE assay condition was initially optimised by the scientists in Selcia US and the assay was then reproduced in this work. In the CE assay for MDM2/p53 the p53-F peak migration time increased and the peak shape broadened upon binding to MDM2-N in the separation buffer. This was due to the slower migration of the MDM2-N/p53-F complex while migrating through the LIF detector at the capillary window.

The assay was validated using Nutlin-3 and unlabelled p53 peptide as controls, thus demonstrating that the CE assay is capable of detecting ligand-protein and protein-peptide interactions with high accuracy. The IC_{50} determined by the CE assay showed tighter affinities than determined by the FP assay which gave values for Nutlin-3 and unlabelled p53 peptide of 266nM and 23µM.

5.4.1 CODASS hits verification using the CE assay

The initial virtual screening run using CODASS (**Chapter 2**) identified six hits and these were subsequently screened in the FP and CE assays. The screening results from the CE and FP assays were compared to ensure that the hits identified were active in both assays (FP assay is described in **Chapter 4**). This will confirm whether the hits are genuine and if the results are not comparable then this may suggest that the hits are false positive. Table 5.1 showed the % inhibition from the screenings and SEL101064, SEL101066, SEL101067 and SEL101069 were identified as active in both assays. SEL101068 was however inactive in both assays at 50µM. However we cannot necessarily conclude the compound does not bind. It may have a weak affinity and require a higher concentration to show signs of inhibition. SEL101063 was active in the CE assay but inactive in the FP assay and this was possibly due to screening at too low concentration for detection in the FP assay.

Overall in the comparison (**Table 5.1**) the results from the CE assay and FP assay show a positive correlation and confirmed the hits to be genuine. However the compounds show a weaker inhibition in the FP assay compared with the CE assay. This was also observed in the affinities of Nutlin-3 and unlabelled p53 peptide where FP assay gave weaker affinities than the CE assay. This could suggest that the FP assay is less sensitive than the CE assay and therefore requires a higher concentration of compound

to detect binding. This was also shown in the Austin C. et al. paper where some fragment hits identified by the CE assay were not detected by FP assay against a different target Hsp90 (Austin et al., 2012).

5.4.2 Hits of second CODASS screen were screened against MDM2-N using the CE assay

With the success from the first virtual screening a new virtual screening run was performed using a reduced complexity EDULISS library to screen against MDM2-N and MDMX-N (**Chapter 2**). The structures in these compounds showed a more flexible scaffold than the first virtual screening hits. These compounds were pre-screened in the FP assay prior to screening in the CE assay and the results showed that only SEL101880 was inactive in the CE assay (Table 5.2). When comparing the CE assay result with the FP assay result, SEL101880 was confirmed inactive in both assays while SEL101876 and SEL101877 were found active in both CE and FP assays. However when examining SEL101875 and SEL101878, these compounds showed high inhibitions in the CE assay but no inhibition in the FP assay. These compounds were apparently screened at 50μM in the FP assay and this concentration is probably too low for the FP assay to detect the binding. This problem was already seen in the previous virtual screening hits screening where nearly two times of concentrations were required to detect the binding in the FP assay (**section 5.4.1**). For the SEL101881 compound a strong inhibition in the CE assay was identified with an IC_{50} of 17μM. However there was only a weak inhibition in the FP assay. This may be because SEL101881 was screened at 200μM in the FP assay which was at the limit of its solubility and the compound may have aggregated in the assay, hence low inhibition in the FP assay.

These compounds showed higher binding affinities toward MDM2-N compared to the hits from the first virtual screening (**section 5.3.5**). One possible reason for higher binding affinities may be due to the flexible structures in these new virtual screening hits which enables a stronger interaction into the three hydrophobic grooves in the MDM2-N binding site. These compounds showed little similarity with the known MDM2-N inhibitors and do not contain an imidazoline group as the centre to link multiple aromatic rings.

5.4.3 Screening fragments using the CE assay

In this study the CE assay has also been used to study the weak affinity fragment-protein interaction. Through the use of the known inhibitor structures this work has identified an oxindole fragment (SFL001328) that can be used to test to see whether smaller molecule compounds would inhibit the p53-MDM2 interaction. From the CE assay screening SFL001328 was shown to be active (**Table 5.1**) and this demonstrated that the CE assay is capable of detecting weak fragment interaction and inhibition of the p53-MDM2 interaction with fragments is feasible. The ligand efficiency (LE) for SFL001328 was determined to be 0.5kcal mol^{-1} per non hydrogen atom (**Chapter 6**) which is an acceptable value for drug candidates (Schultes et al., 2010). Further fragment exploration will be carried out to identify more fragments with improved binding efficiency (see **Chapter 6**).

5.4.4 Using the CE assay to identify dual action inhibitors against MDM2 and MDMX

The negative role of MDMX in the regulation of the tumour suppressor p53 has gradually emerged from multiple studies and it has been shown that overexpression of MDMX allows the cancer cell to resist the MDM2 antagonist (Marine and Jochemsen, 2005, Wade and Wahl, 2009). Both MDM2 and MDMX use the N-terminal binding site to bind to the p53 N-terminal transactivation domain. In order to identify a dual binding inhibitor to inhibit both MDM2 and MDMX the CE assay for MDMX-N has to be developed.

In the initial MDMX-N CE assay development it was found that the MDMX-N/p53-F peak was not reproducible and the migration time continuously increased. One possible explanation could be that there was aggregation in the frozen stock after storing in the -80°C freezer for one month. The concentration measured by Bradford assay was three times less than originally measured using a Nanodrop spectrophotometer. In order to reproduce the MDMX-N/p53-F peak fresh MDMX-N protein should be purified and run in the CE assay immediately to prevent aggregation. MDMX-N is a highly unstable protein therefore it is possible that the protein will gradually aggregate after few days of storage. DMSO (100%) wash should also be

added into the cleaning step at the end of each compound screen in order to wash away compound particles that may be present in the capillary.

Even though the assay was not fully optimised it was still possible to screen the compounds by monitoring if the p53-F peak would shift back to its original position in the presence of inhibitors. In this study SEL101876, SEL101878 and SEL101881 were screened in the CE assay against MDMX-N and SEL101876 fully shifted the p53-F peak back to its original position at 50μM concentration. This is consistent with the results obtained from the FP assay (Table 5.3) and may signify that SEL101876 is a dual inhibitor with a low μM affinity against MDM2-N and MDMX-N. However further optimisation on the CE assay condition is required in order to validate this result and confirm the binding affinity. As discussed in **Chapter 4** the structures of these compounds identified from the second CODASS run shared little similarity with the known published inhibitors. However the flexible conformation feature in SEL101876 is also present in the published dual binding inhibitor RO-2443 (see **section 4.10**). Thus this new chemical scaffold allows further optimisation to develop a more potent MDM2/X-N dual inhibitor.

In this study we have demonstrated that CE is a promising tool for characterising protein-ligand, protein-peptide and protein-fragment interactions. The results presented in this work provided the first example of using FP and CE as orthogonal assays for MDM2/X-p53 ligand screening and illustrate the importance of validation with different techniques.

Chapter 6 Identification and validation of small molecule families of MDM2 inhibitors

6.1 Introduction

The CE and FP assays described in Chapters 4 and 5 confirmed active compounds identified using virtual screening. However these virtual screening compounds have a high molecular weight and low solubility. Therefore, finding analogues of the virtual screening hits could help to identify small molecular weight fragments with higher solubility. Ideally we are looking for small molecule fragments which are able to interact in the binding site efficiently and which have good ligand efficiency. In current published literature the known inhibitors identified are complex structures with multiple hydrophobic groups and thus have poor solubility and ligand efficiency.

6.2 Identification of diphenylamine analogue fragments

Analogues of the virtual screening hit SEL101066 were further explored because the structure was novel and different from known published inhibitors. The virtual screening studies (**Table 3.2 in Section 3.2.2**) showed that the diphenylamine group was present in a number of the hits (Compound 3, 5 and 7) which suggests that the diphenylamine group may be responsible for the interaction with the MDM2 binding site. Hence, SEL101066 was further explored by Simon Pettit using the Selcia chemical store substructure search tool in the Selcia compound library to identify compounds containing the diphenylamine motif.

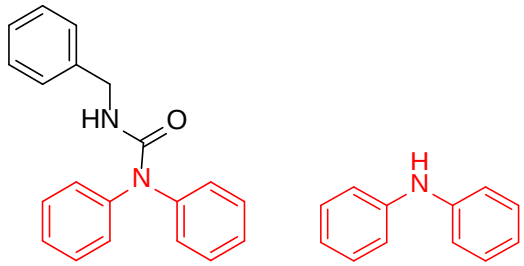

Structure of SEL101066 (left), Diphenylamine (right)

Fluspirilene, phenoxazine, carbamazepine, 2-chlorophenothiazine, phenothiazine, phentolamine HCl, 2-phenylamino-benzoic acid, N-phenyl-p-phenylenediamine, 4-hydroxydiphenylamine, 3-hydroxydiphenylamine and diphenylamine contained a similar motif (shown as red in **Figure 6.1**) and were tested by performing the CE assay. The analogues were validated dependent upon the % inhibition observed.

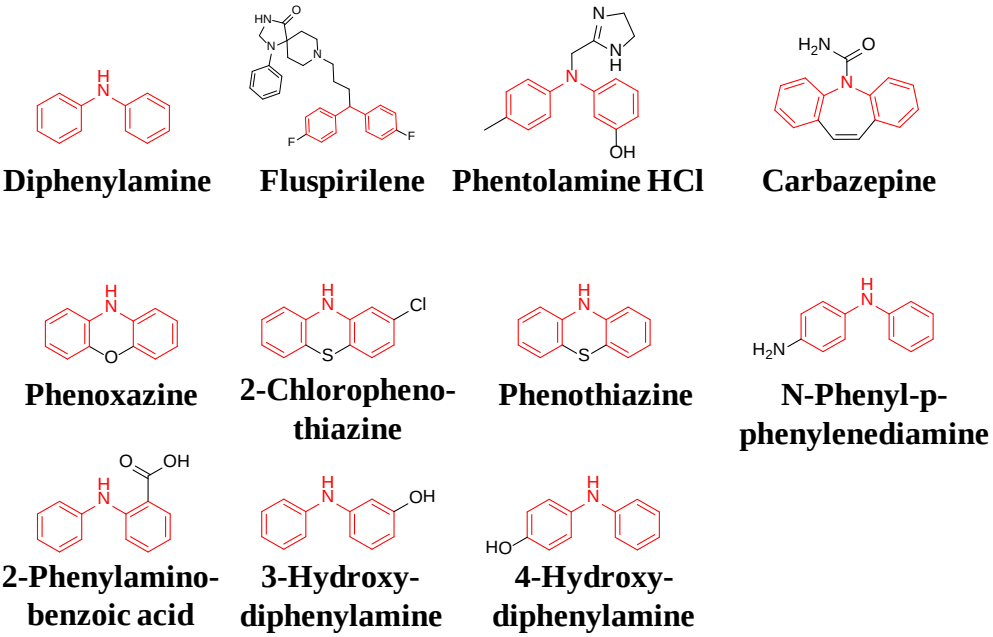

Figure 6.1 Chemical structures of compounds selected with diphenylamine motif. The diphenylamine motif present in the structures is highlighted in red.

6.3 Analogue screen in CE

6.3.1 CE screen on analogues of SEL101066

Solubility tests of the compounds can be found in the **Appendix A4**. Due to low solubility, fluspirilene was screened at 100µM and phenoxazine was screened at 200µM. All others were screened at 300µM. 2-chlorophenothiazine and phenothiazine were ranked as having low solubility (**Appendix A4**) and for this reason not further evaluated by CE assay.

Figure 6.2 shows an electropherogram of the analogues screened using CE assay. In the assay the injection sample contains carboxyfluorescein (10pM) and p53-F (500pM) in TAPS/Tris (1mM) pH 8.0, DTT (1mM). The separation sample contains MDM2-N

(160nM), test compound, TAP/Tris (200mM) pH 8.0, DMSO (1%) and glycerol (0.25%).

Initially p53-F (500pM) was run on its own as a control to record the migration time of p53-F (Trace 1 in **Figure 6.2**). This was then followed by running p53-F in the presence of MDM2-N (160nM) and the migration time of p53-F/MDM2-N was recorded (Trace 3 in **Figure 6.2**). The compounds were then screened and the MDM2-N control was run in between each compound screen. A % inhibition for every compound was calculated using the equation:

$$\% \text{ Inhibition} = 100(T_H - T_L)/(T_H - T_R)$$

T_H is migration time of p53-F peak in the presence of MDM2-N.

T_R is the migration time of p53-F peak.

T_L is the migration time of p53-F peak in the presence of MDM2-N + compound.

The results are summarised in **Table 6.1** with calculated % inhibition. Phentolamine HCl (300µM) showed no inhibition whereas fluspirilene (100µM) showed a high inhibition of ~60%. However, fluspirilene contained a complex structure (see **Table 6.1**) with a low solubility so no further evaluation was carried out on this compound.

Both phenoxazine and carbazepine contained the similar motif of three rings linked together. Carbazepine only gave a 10% inhibition, whereas phenoxazine gave ~40% inhibition. It may be possible that the oxygen atom present in the phenoxazine ring gives rise to a hydrogen bond interaction in the binding site, indicative of the higher inhibition found for phenoxazine.

3-hydroxydiphenylamine, 4-hydroxydiphenylamine and diphenylamine were smaller fragments with high solubility and these fragments gave 40% - 60% inhibition at 300µM.

3-Hydroxydiphenylamine was found to have the highest inhibition of 66%, which was repeatable. This suggests the inhibition was improved when an OH group was in the 3-position. 3-Hydroxydiphenylamine was also a fragment of phentolamine, however phentolamine was found to be inactive in CE (**Table 6.1**). The results suggest that the

extra diazole group present in phentolamine HCl may cause the inactivity of the compound.

Phenothiazine type compounds are rigid in structure and not as flexible when compared to diphenylamine. Therefore the docking positions of phenothiazine type compounds are assumed to be limited. In contrast, the diphenylamine type compounds can freely rotate to fit tighter into the binding site.

Both 3-hydroxydiphenylamine and 4-hydroxydiphenylamine have good solubility as found in the solubility test (**Appendix A4**). Therefore titration was performed on these fragments and IC_{50} determined (**Section 6.3.2**).

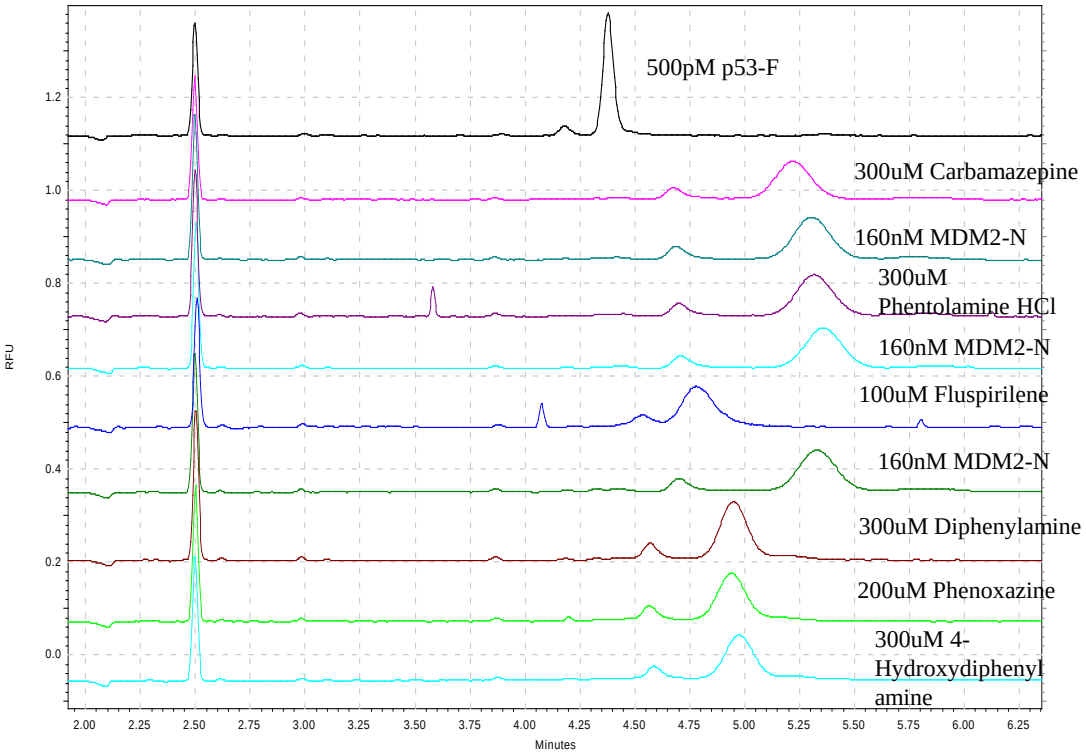

Figure 6.2 Electropherograms of the analogues screening in CE.

The first trace is the control with p53-F alone followed by the individual compound at the curves indicated. Control runs with 160nM MDM2-N were carried out between each compound screen.

		% Inhibition	
	Concentration tested	1st repeat	2nd repeat
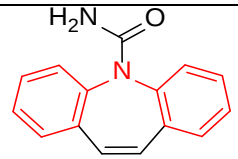 Carbazepine	300µM	10%	
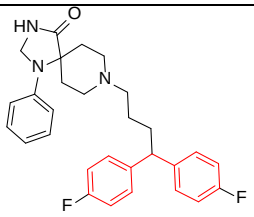 Fluspirilene	100µM	60%	53%
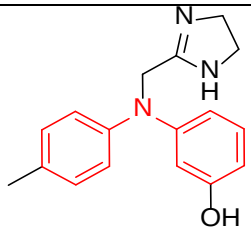 Phentolamine HCl	300µM	0%	0%
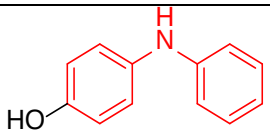 4-Hydroxy-diphenylamine	300µM	40%	65%
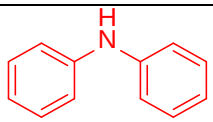 Diphenylamine	300µM	42%	31%
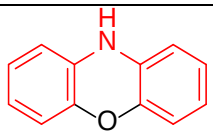 Phenoxazine	200µM	43%	25%

		% Inhibition	
	Concentration tested	1st repeat	2nd repeat
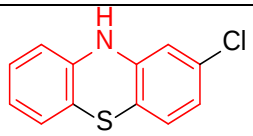 2-Chlorophenothiazine	Not tested		
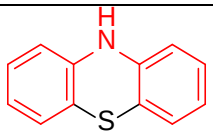 Phenothiazine	Not tested		
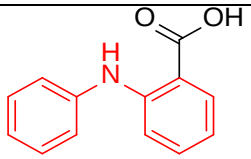 2-Phenylamino-benzoic acid	300µM	58%	28%
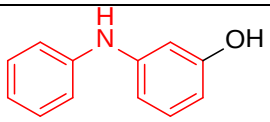 3-Hydroxy-diphenylamine	300µM	66%	67%
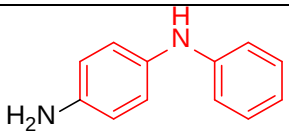 N-Phenyl-p-phenylenediamine	300µM	30%	

Table 6.1 Summary of results of the CE screen of analogues binding to MDM2

6.3.2 Titration of 3-Hydroxydiphenylamine (SEL101266), 4-Hydroxydiphenylamine (SEL101267)

Titrations of 3-hydroxydiphenylamine (SEL101266) and 4-hydroxydiphenylamine (SEL101267) were carried out. They were titrated from 1 – 1000µM and 0.1 – 900µM respectively. From the titration curve the % inhibition was above 90% for both compounds (**Figure 6.3**). This reveals it is possible for both fragments to shift the p53-F peak back to its original position. The diphenylamine fragments contain a rotatable bond, suggesting the off rate may be slower than the rigid structures of SEL101069 and SFL001328 (**Section 6.7**).

From the dose response curve the IC_{50} was calculated to be 362µM for SEL101266 and 116µM for SEL101267 (**Figure 6.3**). The affinity of SEL101267 was found to be higher than SEL101266 and when looking at the docking by AutoDock (**Figure 6.3**), SEL101266 occupied the Leu26 pocket and interacts with Val93 and His96 through hydrogen bonding. Whereas, SEL101267 fragment interacts with MDM2-N by occupying both Leu26 and Trp23 pockets. The models suggest a strong affinity may be obtained by binding deep into the hydrophobic pockets (**Figure 6.4 bottom**).

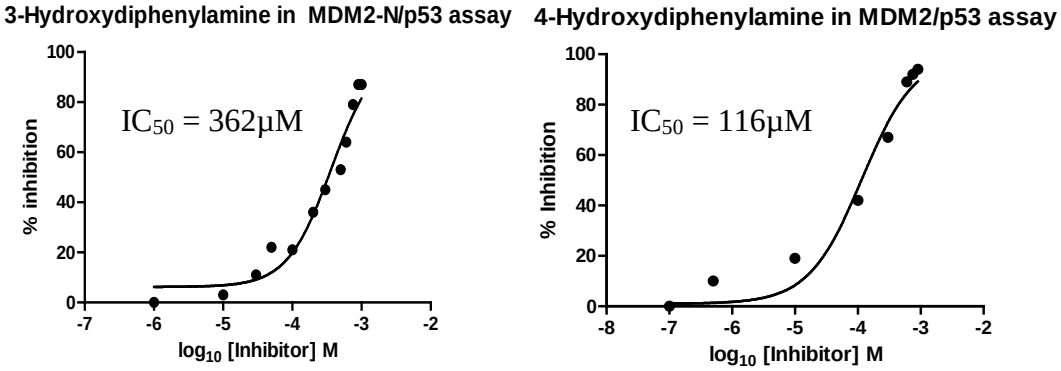

Figure 6.3 Titration of SEL101266 (Left) and SEL101267 (Right).

The fragments were titrated in the CE using MDM2-N (500nM) and p53-F (500pM). The % inhibitions were calculated from the CE traces and plotted into curve.

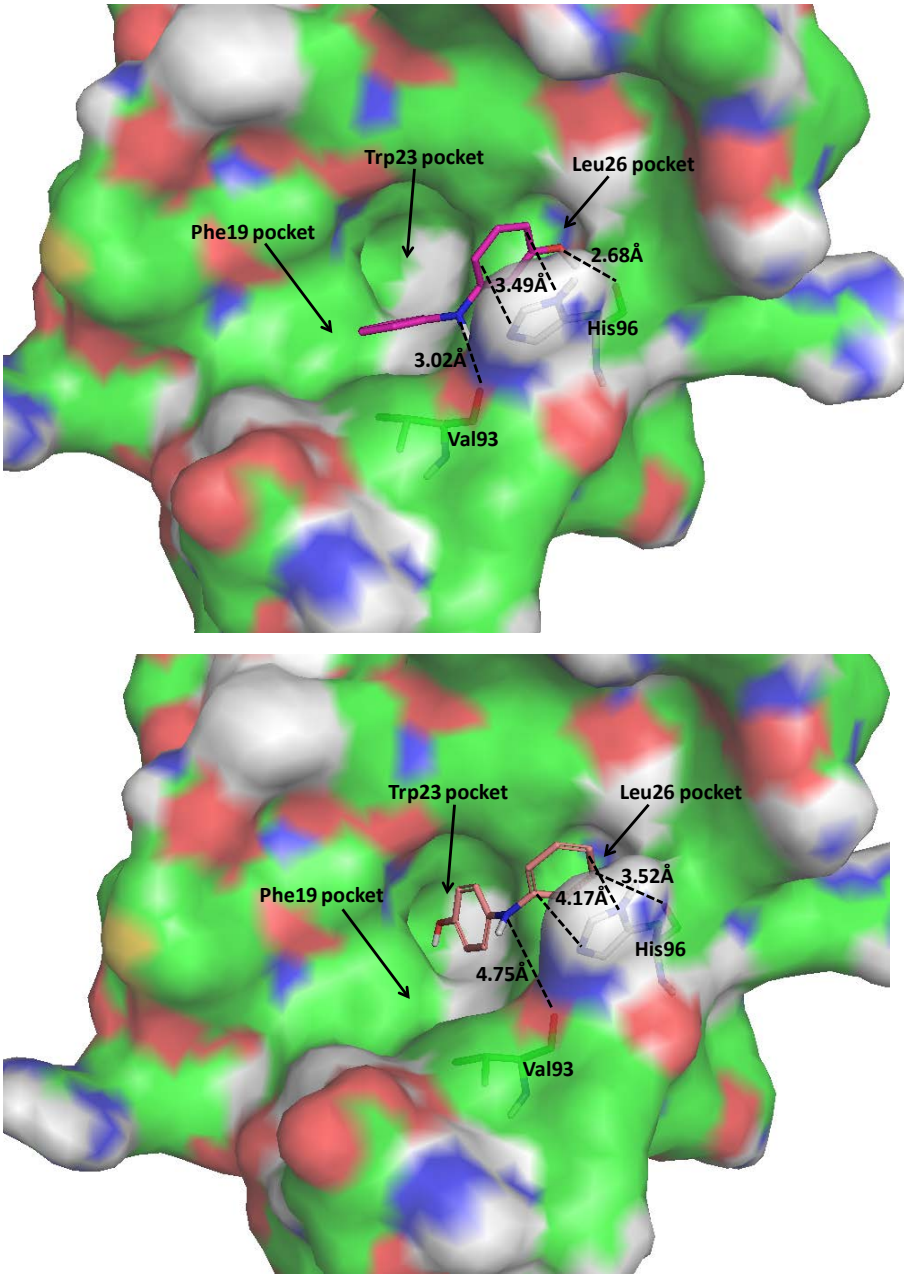

Figure 6.4 Docking models of SEL101266 and SEL101267.

3-Hydroxydiphenylamine (top) and 4-Hydroxydiphenylamine (bottom) are docked using AutoDock software into the MDM2-N binding site. MDM2-N protein structures are displayed in surface and the residues that can interact with the fragments are shown in stick. The interactions involved in fragment binding are indicated by dashed lines in black.

6.4 Analogue validation in FP assay

The diphenylamine fragments measured in the CE assay showed a high affinity and this was mimicked in the FP assay. The sensitivity of the FP assay was previously optimised, which enables the assay to be used in screening weak binding fragments. However, compared to the CE assay, the FP assay required a higher concentration of fragments in order to detect the binding.

The FP assay was performed using the method from the FP assay SOP (See **section 4.6.4**). SEL101267 showed the highest inhibition of 60% and SEL101266 showed an inhibition of 31%. The fragments; SEL101268, SEL101269 and SEL101270 were also validated as active using the FP assay. The data was analysed using ANOVA statistical analysis, which confirmed the fragments were significantly different from the MDM2-N control value (**Figure 6.5 Bottom**). The summary table in **Table 6.2** showed the FP results correlates with the results obtained from the CE.

Ligand efficiency is the binding energy per atom for a ligand and it is a more useful concept to use for examining the druggability of the target (Hopkins et al., 2004). Using the **equation 3.1** from **Section 3.1.8**, we are able to calculate the ligand efficiency for SEL101266 (IC_{50} = 362μM) and SEL101267 (IC_{50} = 116μM). The ligand efficiencies calculated for SEL101266 and SEL101267 are 0.34kcal/mol/atom and 0.38kcal/mol/atom respectively. These are the typical values for the contribution of a fragment like atom (Abad-Zapatero, 2007).

Despite these apparently encouraging results presented in Sections 6.3 and 6.4 using orthogonal assays of FP and CE as described in Section 6.6, it was shown using isothermal titration calorimetry and dynamic light scattering (in the following section) that the inhibitions seen in diphenylamine analogues are actually artefacts due to protein aggregation.

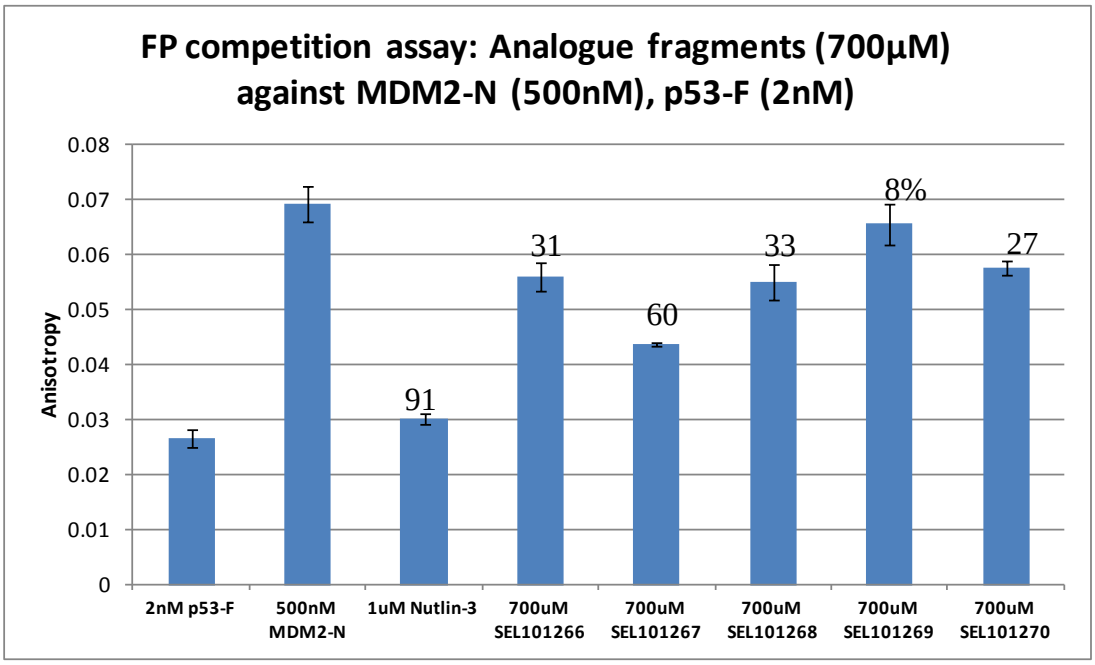

Dunnett's Multiple Comparison Test	Mean Diff.	q	Significant? P < 0.05?	Summary	95% CI of diff
MDM2-N vs p53-F	0.04	24	Yes	***	0.04 to 0.05
MDM2-N vs Nutlin-3	0.04	21	Yes	***	0.03 to 0.04
MDM2-N vs SEL101266	0.01	7	Yes	***	0.007 to 0.02
MDM2-N vs SEL101267	0.02	15	Yes	***	0.02 to 0.03
MDM2-N vs SEL101268	0.01	8	Yes	***	0.008 to 0.02
MDM2-N vs SEL101269	0.003	2	No	ns	-0.002 to 0.008
MDM2-N vs SEL101270	0.01	6	Yes	***	0.006 to 0.02

Figure 6.5 FP competition assay to screen diphenylamine fragments with MDM2-N. Diphenylamine fragments were screened at 700µM in the presence of 500nM MDM2-N and 2nM p53-F. % inhibition was calculated using the equation in the FP assay SOP (Appendix). Bottom table shows the ANOVA analysis and $P < 0.05$ was considered as significant.

		CE results	FP results
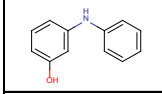	SEL101266	66% at 300uM	31% at 700uM
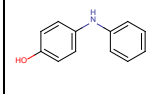	SEL101267	52% at 300uM	60% at 700uM
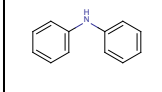	SEL101268	36% at 300uM	33% at 700uM
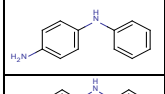	SEL101269	30% at 300uM	8% at 700uM
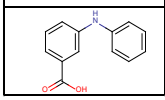	SEL101270	43% at 300uM	27% at 700uM

Table 6.2 Overview of screening results from CE and FP assays.

The diphenylamine fragments were screened in both assays and were summarised in the table with the % inhibition and concentration used.

6.5 Analogue validation in ITC

Even though the CE and FP assay results were consistent, there were doubts about the sensitivity of the FP assay and a further biophysical technique was used to try and validate the binding results.

Isothermal Titration Calorimetry (ITC) is a technique that can study the binding interaction and the thermodynamic properties generated from an interaction between two or more molecules. ITC has the ability to ascertain the association equilibrium constant (K_A) of an interaction at different temperatures and the Gibbs free energy (ΔG_A) correlates with the binding constant. Therefore, from the binding constant obtained, the other relevant thermodynamic parameters can also be determined by the following equations (Okhrimenko and Jelesarov, 2008):

6.1) $\Delta G_A = -RT\ln K_A$

&

6.2) $\Delta G_A = \Delta H_A - T\Delta S_A$

Where ΔG_A is Gibbs free energy, R is the gas constant, T is the absolute temperature in Kelvin, K_A is the association equilibrium constant, ΔH_A is the change in enthalpy and ΔS_A is the change in entropy.

Heat is often generated or absorbed when molecules interact and this can be directly measured by ITC. The enthalpy change (ΔH) is the relationship of the bonds created to bonds broken. If the energy produced by bond formation is greater than the energy required to break the bonds, then this will indicate a negative value of enthalpy change which favours the binding.

6.5.1 Principle of ITC

ITC has become a widely used biophysical technique to measure interaction in solution. The ITC instrument consists of a sample cell and a reference cell which are connected by a thermopile (**Figure 6.6**). During the ITC experiment the temperature in the cells was held constant and the reference cell was used to compare the change in heat occurring in the sample cell through a thermopile.

In the majority of the experiments ligand is injected into the protein and heat effects are observed by the heat of binding, the heat of mixing and the dilution of the protein and ligand.

The temperature differences between two cells are constantly monitored by the cell feedback network. A constant power is applied to the reference cell and this triggers the feedback network to apply the power to the sample cell to maintain the temperature difference caused by the reactions.

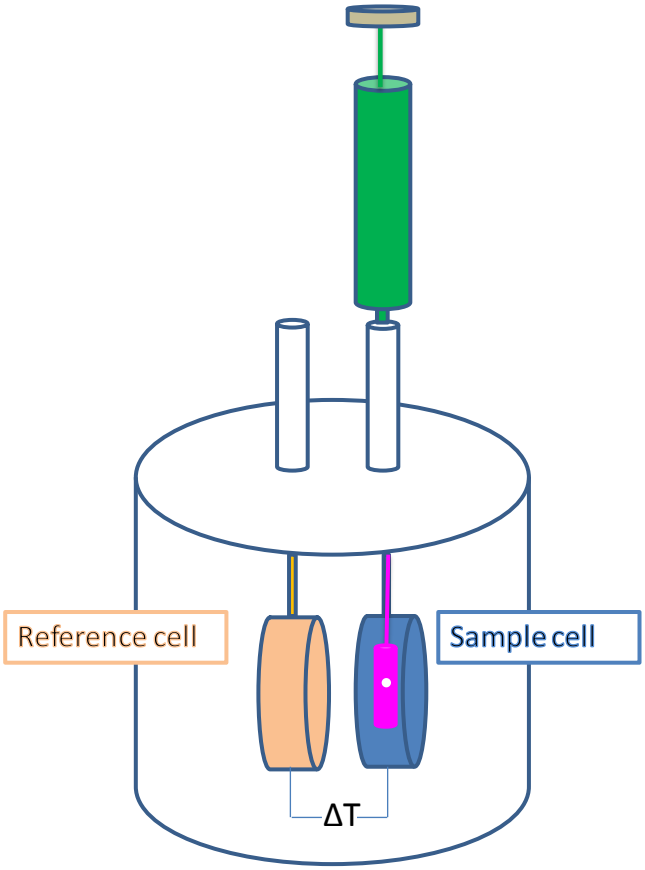

Figure 6.6 Schematic diagram of ITC equipment.

ITC contains the reference cell and sample cell where the temperatures between the cells are maintained by the cell feedback network. The syringe injects the ligand into the cell and the temperature difference between these two cells is constantly monitored.

6.5.2 Materials & Methods for ITC

The instrument model used in the ITC experiment was Auto-ITC HT Microcalorimeter (GE Healthcare). One vial of distilled H_2O was degassed and sonicated and carefully filled into the reference cell prior to the start of the experiment. Freshly prepared 2.5% Decon, degassed H_2O and methanol were added to the appropriate containers. The robot arms and the sample cell were initially washed with H_2O twice followed by Decon (2.5%), water and methanol. The samples were stored in 96 well 2ml round bottom plates in the cold cabinet at 4°C. The buffer solution used in the cell and the syringe were matched to prevent signal to noise problems. Organic solvent can lead to a large heat effect, therefore the DMSO concentration (1%) in both protein and ligand solution was matched. ITC experiments were performed using the parameters in **Table 6.3.**

Cell temp.	No. Inject	Inject Volume	Inject Duration	Inject Spacing	Stirring (RPM)	Reference Power
25°C	19	14.83µl	29.7	200	250	5

Table 6.3 Details of parameters selected for ITC experiment.

6.5.3 Nutlin-3 binding affinity determined by ITC

The interaction of MDM2-N with Nutlin-3 was measured by ITC (**Figure 6.7)**. The interaction was performed at 298K. The interaction was initially performed using 15µM of Nutlin-3 with 1.5µM MDM2-N in the cell (**Left panel in Figure 6.7**). The data shown in **Figure 6.7 (left panel)** demonstrates decent signal levels using this condition (-5kcal/mole$_{(injectant)}$). However the isotherm gave an incomplete sigmoidal curve with increasing molar ratio, which may be due to the low Nutlin-3 concentration used in the ITC experiment. Therefore, the ITC experiment was repeated using a more concentrated Nutlin-3 (25µM). The isotherm shown in **Figure 6.7 (Right panel)** for Nutlin-3 (25µM) gave a complete sigmoidal curve with increasing molar ratio. The determined value of the Kd is calculated based on the midpoint of the curve. The interaction of the Nutlin-3 gave a Kd of 52nM (**Figure 6.7 Right panel**). This is very

similar to the IC_{50} (37.3nM) obtained by the CE assay (**Section 5.4.1.2**) and the Ki value (36nM) from published literature (Shangary et al., 2008).

From the isotherm the enthalpy of the interaction between MDM2-N and the racemic mixture Nutlin-3 is -5.1kcal/mol (**Figure 6.7 Right panel**). The enthalpy change is a negative value which indicates the enthalpy of the interaction favours the binding. The entropy of interaction between MDM2-N and Nutlin-3 is 16.3cal/mol/degree. The free energy of binding calculated using equation 6.2 gives -9.9kcal/mol at 298K in which the reaction is driven by both enthalpy and entropy.

In the Michelsen K. *et al.* paper, they have performed ITC experiments on the Nutlin-3a (Michelsen et al., 2012). Their results showed the interaction of the Nutlin-3a gave a Kd of 24nM which is half of the Kd that we have obtained for the racemic mixture Nutlin-3 (Kd = 52nM). The enthalpy of the Nutlin-3a interaction with MDM2-N is -10.2kcal/mol and entropy is 0.67cal/mol/degree. The free energy of binding is -10.4kcal/mol which suggests that the reaction is driven by enthalpy.

A higher entropy value in the ITC experiment of racemic mixture Nutlin-3 is caused by the inactive Nutlin-3 being present in the system. As discussed in **section 1.5**, there is a lid present at the MDM2/p53 binding site that is responsible for controlling the stability of the MDM2/p53 complex. In our ITC studies, the lid at the N-terminal domain of MDM2 may be in an open state which resulted in an increase of entropy to the system. The Nutlin-3a on the other hand may be stabilizing the lid by allowing the lid to interact with the side of the hydrophobic cleft which had been suggested by Showalter *et al.* paper and thereby reducing the entropy of the system (Showalter et al., 2008).

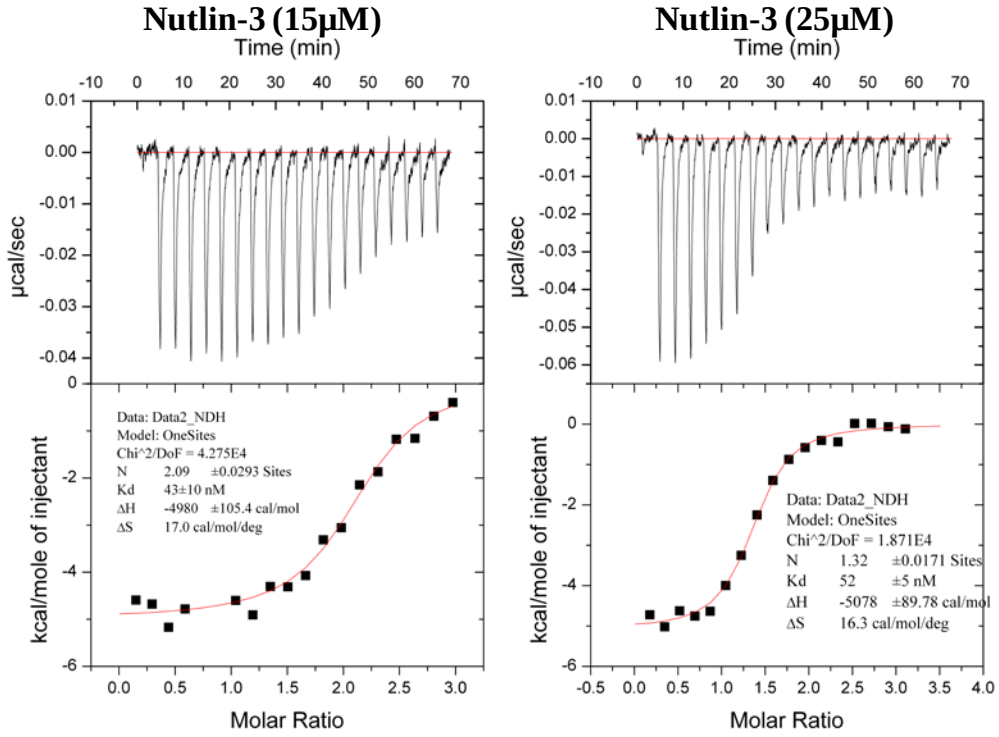

Figure 6.7 The ITC isotherm of MDM2-N/Nutlin-3 interaction.

The ITC experiments of Nutlin-3 titration were performed in two concentrations (15µM and 25µM). Top panel shows the energy data of the baseline sample against time. The bottom panel shows the ITC injection fit and plotted in kcal/mol against Molar ratio of protein and Nutlin-3.

6.5.4 Fragments screening by ITC

The ITC method developed for MDM2-N was then used to verify the interaction with the diphenylamine analogues. **Figure 6.8** shows the raw data of the diphenylamine analogues screened in ITC. The fragments were injected at 1mM concentrations, with no significant heat signal present with increasing molar ratio. The heat signal level in the control of injecting buffer into buffer (**Figure 6.8 bottom trace**) is equivalent to heat signals seen in fragment screening.

One possibility for the lack of heat signal may be caused by the low fragment concentrations used, since these fragments are of weak affinity. Therefore, a much higher concentration of fragments will be required in order to detect the heat of binding. However it is not possible to further increase the fragment concentration in ITC due to the limit of solubility. An alternative competition assay was developed in order to identify the fragment/protein interaction at a lower concentration.

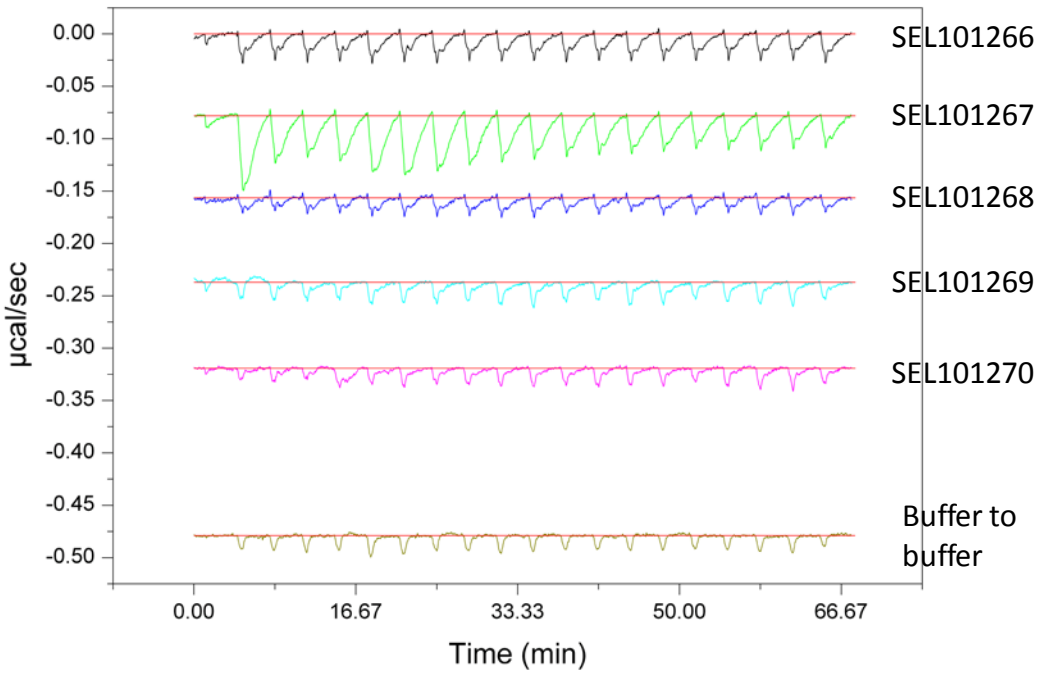

Figure 6.8 ITC analysis on diphenylamine fragments interaction with MDM2-N.
The image shows the energy data of the diphenylamine fragments (1mM) interaction with MDM2-N. Bottom trace shows the energy data of the control buffer into buffer. The energy data was plotted in sample against time.

6.5.5 ITC competition assay to detect fragment interaction

When using ITC for direct measurement of MDM2-N and fragment binding the data indicates no heat change in the cell. This is caused by the low concentration of the fragments used, which could not be increased due to the solubility issue of the fragments. The ideal conditions to determine low affinity ligand sometimes cannot be met. Low affinity binding often requires a high concentration of protein to obtain a detectable heat change, however this will result in a high ligand concentration.

Here, we describe the use of ITC to perform the competition experiments to study the weak binding affinity fragments. This involves injecting a known inhibitor in the presence of a fixed concentration of weak binding fragment. The fragment is incubated with the protein to pre-form the complex. The presence of known inhibitor will displace the fragment from the complex with protein. The difference between the thermodynamic of known ligand and the thermodynamic coupling of two ligands can be used to obtain the thermodynamic of the weak binding fragment. The fragment binding can be determined by the apparent binding constant obtained.

In this experiment the syringe containing Nutlin-3 (25μM) and SEL101267 (350μM) was injected into the cell with MDM2-N (1.5μM) and SEL101267 (350μM). The raw data in **Figure 6.9 top** shows that injecting SEL101267 with Nutlin-3 gave no signal. The **Figure 6.9 bottom** shows the control experiment of Nutlin-3 titration. In the presence of SEL101267 (350μM), there was no heat signal present upon the first injection and with increasing molar ratio. However the heat signal was present in the control experiment of Nutlin-3 titration when SEL101267 (350μM) is absent (**Figure 6.9 bottom**). The Kd and ΔH obtained from the control experiment showed no significant difference (**Figure 6.10**) compared with the data obtained from the previous ITC titration (**Figure 6.7**). From this result we can confirm that MDM2-N is still active and has not aggregated. The surprising result that showed no binding for the SEL101267/Nutlin-3 suggests that the fragment may have aggregated the protein during the incubation in the 96 well plate.

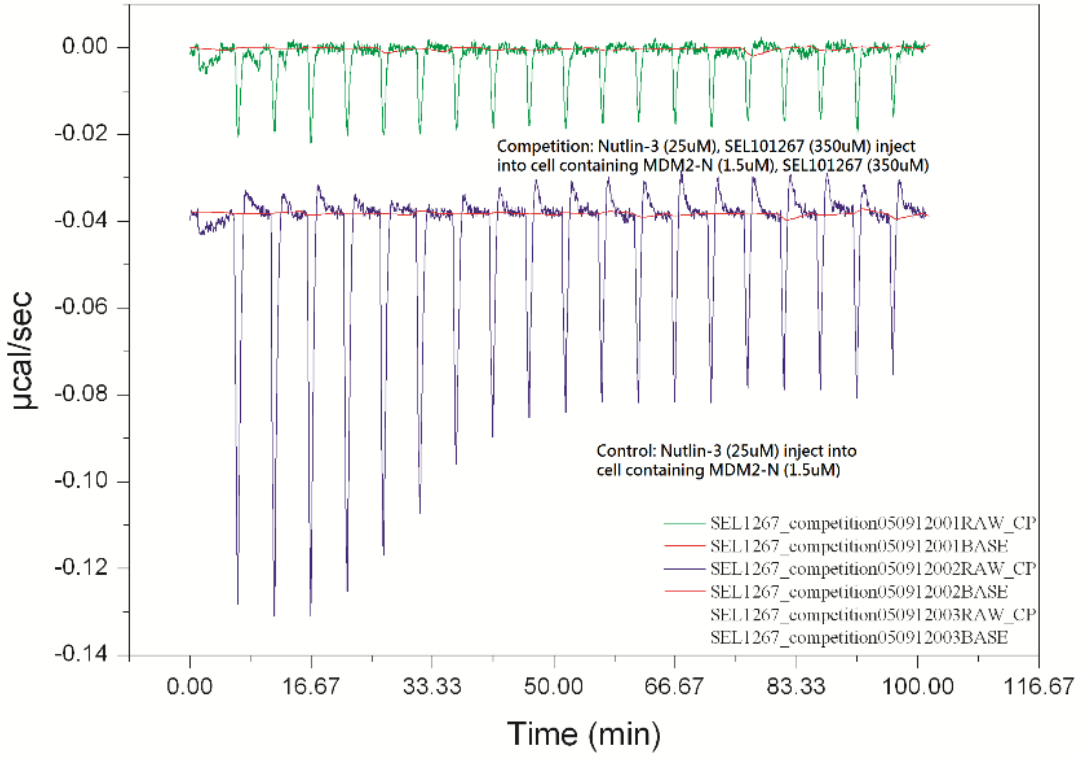

Figure 6.9 Raw data of (top) SEL101267 (350µM) carried out in ITC competition assay. Green trace shows the competition ITC assay with Nutlin-3 injected into the cell containing MDM2-N and SEl101267 (350µM).

Purple trace is the energy data of the ITC control experiment of Nutlin-3 interaction with MDM2-N.

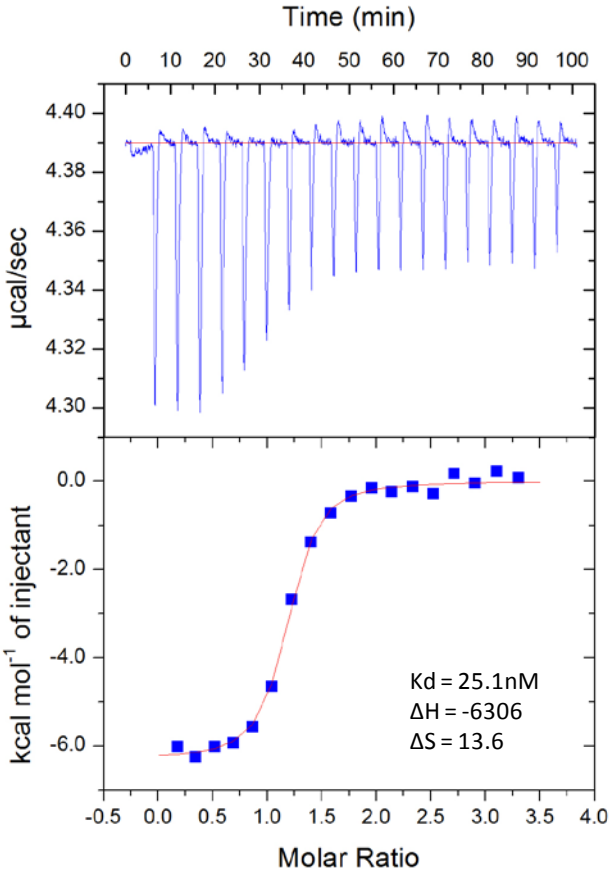

Figure 6.10 ITC binding isotherm of the control experiment with Nutlin-3.

Top panel) Shows the energy data of the baseline sample against time.

Bottom panel) The ITC injection fit plotted in kcal/mol against Molar ratio of MDM2-N and Nutlin-3.

To monitor if the aggregation may be caused by the high concentration of the fragments, the concentration of SEL101267 was reduced from 350µM to 100µM for the ITC competition experiment. A clear heat signal can be seen in the presence of Nutlin-3 (25µM) and SEL101267 (100µM) in **Figure 6.11**. There is a clear difference in the heat signals between the ITC titration in the presence and absence of SEL101267 (100µM). The isotherm shows that when SEL101267 (100µM) is present the heat signals reach saturation at a higher rate with lower molar ratio. However it is quite surprising that the fragment is able to displace the tight binding inhibitor Nutlin-3 with only 100µM concentration. The most likely explanation for this shift in the saturation

curve (**Figure 6.11**) is again that the protein is partially aggregated by SEL101267 and the available concentration of MDM2 has been reduced. The protein aggregation rate will increase with increasing fragment concentrations (**Figure 6.9)**.

The same effect was also seen when assessing the related ligand SEL101266 (100µM) in the ITC competition assay. In **Figure 6.12** the saturation binding curves in the presence of SEL101266 (100µM) could also be explained by aggregation of MDM2-N.

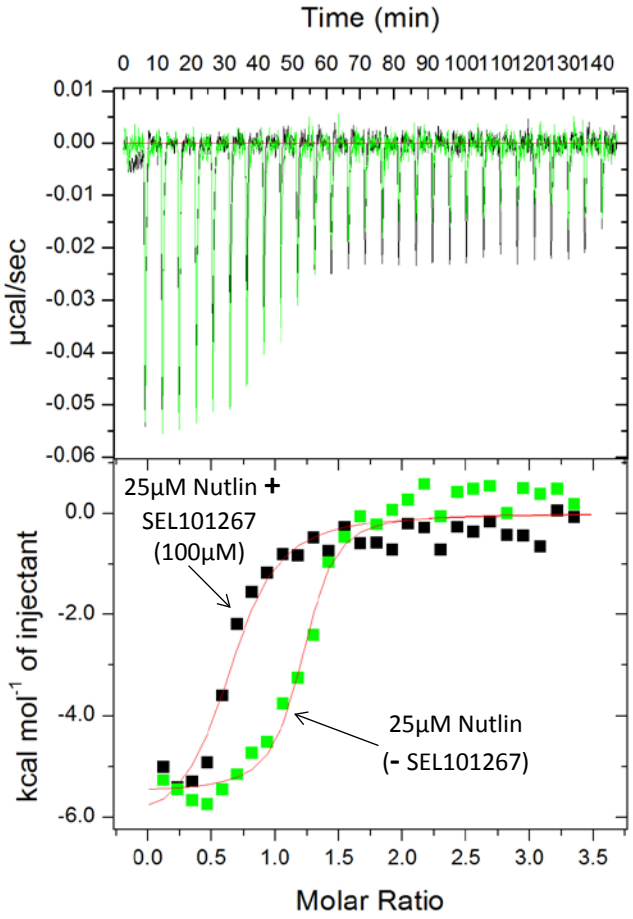

Figure 6.11 ITC isotherm of the MDM2-N/SEL101267 (100µM) interaction in competition form.

Black trace is the ITC competition experiment. Nutlin-3 was titrated into the cell containing SEL101267 (100µM) and MDM2-N.

Green trace is the ITC control experiment of Nutlin-3 titration in the absence of SEL101267 (100µM).

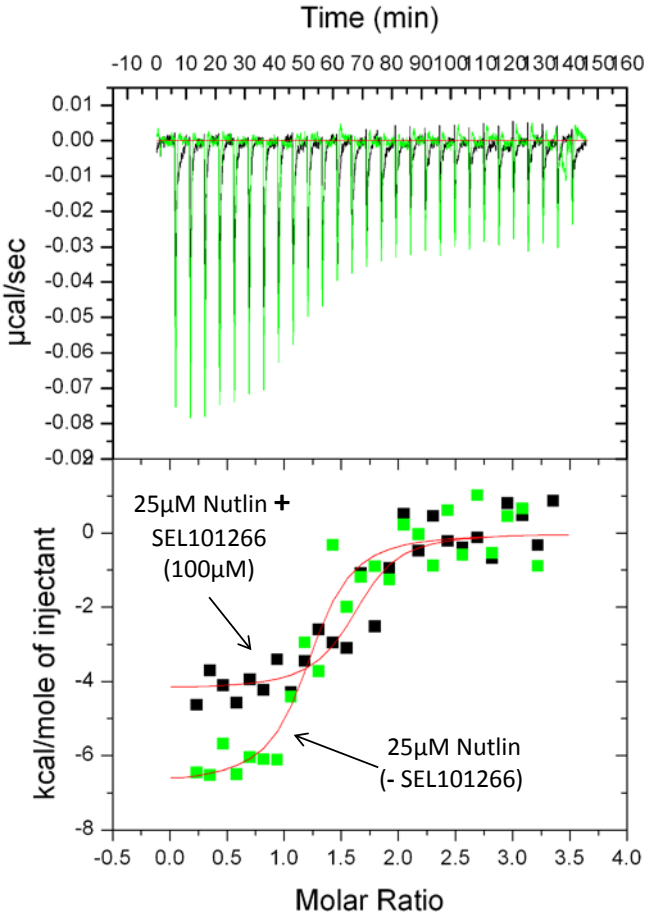

Figure 6.12 ITC isotherm of the MDM2-N/SEL101266 (100µM) interaction in competition form.

Black trace is the ITC competition experiment. Nutlin-3 was titrated into the cell containing SEL101266 (100µM) and MDM2-N.

Green trace is the ITC control experiment of Nutlin-3 titration in the absence of SEL101266 (100µM).

6.6 Study of MDM2-N aggregation caused by diphenylamine fragments in the DLS

In order to examine protein aggregation caused by the fragments, Dynamic Light Scattering (DLS) can be used.

DLS is a technique that can determine the hydrodynamic size of macromolecules in solution. The phenomenon of protein aggregation caused by diphenylamine analogues was studied in the DLS. SEL101266 and SEL101267 were incubated with MDM2-N (64μM) in protein buffer (50mM HEPES pH 7.5, 100mM NaCl, 1mM DTT) at various concentrations for 30 minutes on ice. Control experiments were also set up using the negative control SFL001328 and the published inhibitor Nutlin-3 as a positive control. If we first look at the control experiments in **Figure 6.13**, the DLS profile of size distribution shows a peak at 5.3nm hydrodynamic radius representing the dominant species. A radius of 5.3nm is consistent with the hydrodynamic radius of monomer MDM2-N. In the profile, the hydrodynamic radii of the peaks for these samples was also shown to be 5.3nm when SFL001328 and Nutlin-3 were incubated with MDM2-N.

MDM2-N is stable when incubated with various concentrations of SFL001328 (**Figure 6.13 top**) or Nutlin-3 (**Figure 6.13 bottom**). There is no change in the hydrodynamic size of the protein, however an increase of size is seen when 10μM Nutlin-3 was added which suggests aggregation of Nutlin-3 at 10μM concentration.

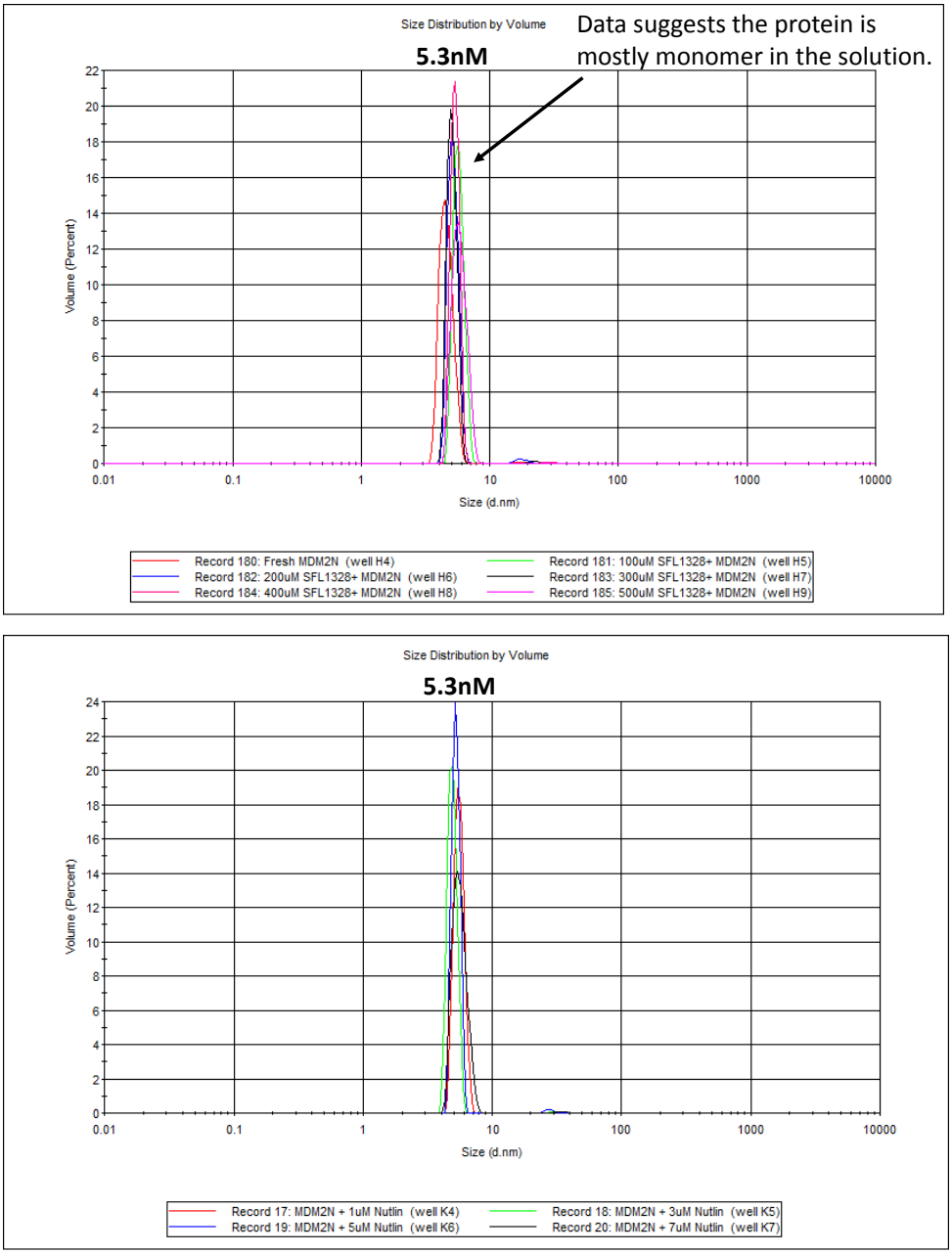

Figure 6.13 DLS size distribution by mass profile of MDM2-N incubated with various concentrations of SFL1328 fragment (Top) and Nutlin-3 (Bottom).

The profile shows the hydrodynamic size of the molecules present in the solutions. MDM2-N is displayed as monomer in the solutions with 5.3nm size after incubating with SFL001328 (Top) and Nutlin-3 (Bottom).

Figure 6.14 top and bottom shows the size distribution by mass for MDM2-N incubated with SEL101266 and SEL101267 in the protein buffer on ice. In the absence of the fragments the hydrodynamic radii of MDM2-N were ~5.3nm. However when the diphenylamine fragments were present, large molecules are formed in the solution with hydrodynamic radii over 50nm. The molecules with radii of over 50nm indicate that large molecules are present in the solution. There were only small molecules with 0.1 – 0.3nm hydrodynamic radii present when running SEL101267 on its own in DLS (**Figure 6.15**). This means that the diphenylamine analogues alone do not form large molecules. These results have validated the hypothesis of MDM2-N forming large molecules by the diphenylamine analogues in the solution.

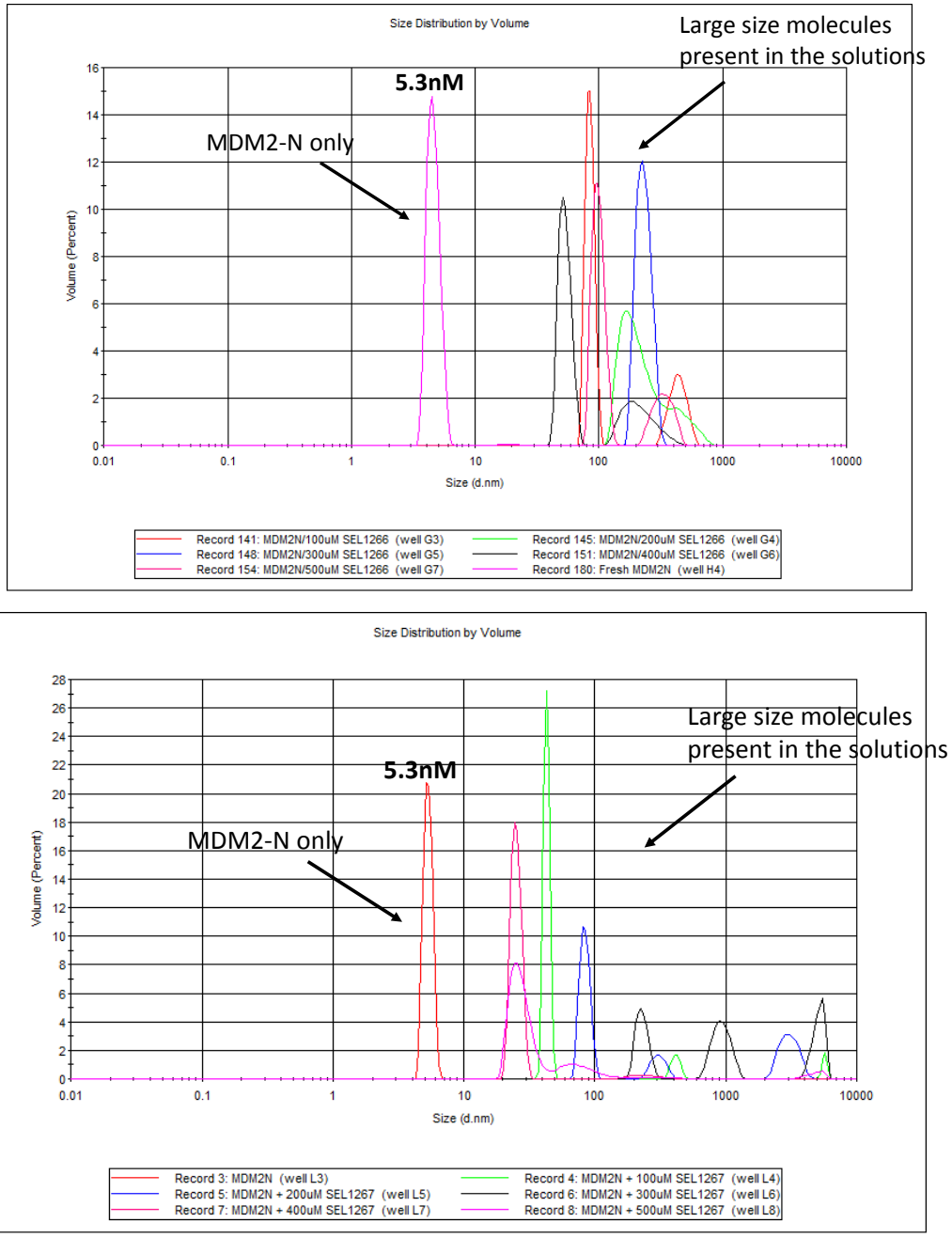

Figure 6.14 DLS size distribution by volume profile of MDM2-N incubated with various concentrations of SEL101266 (Top) and SEL101267 (Bottom) fragments.

The profiles are shown in volume (%) against hydrodynamic size (d.nm). Large hydrodynamic size molecules are formed after incubating with SEL101266 and SEL101267.

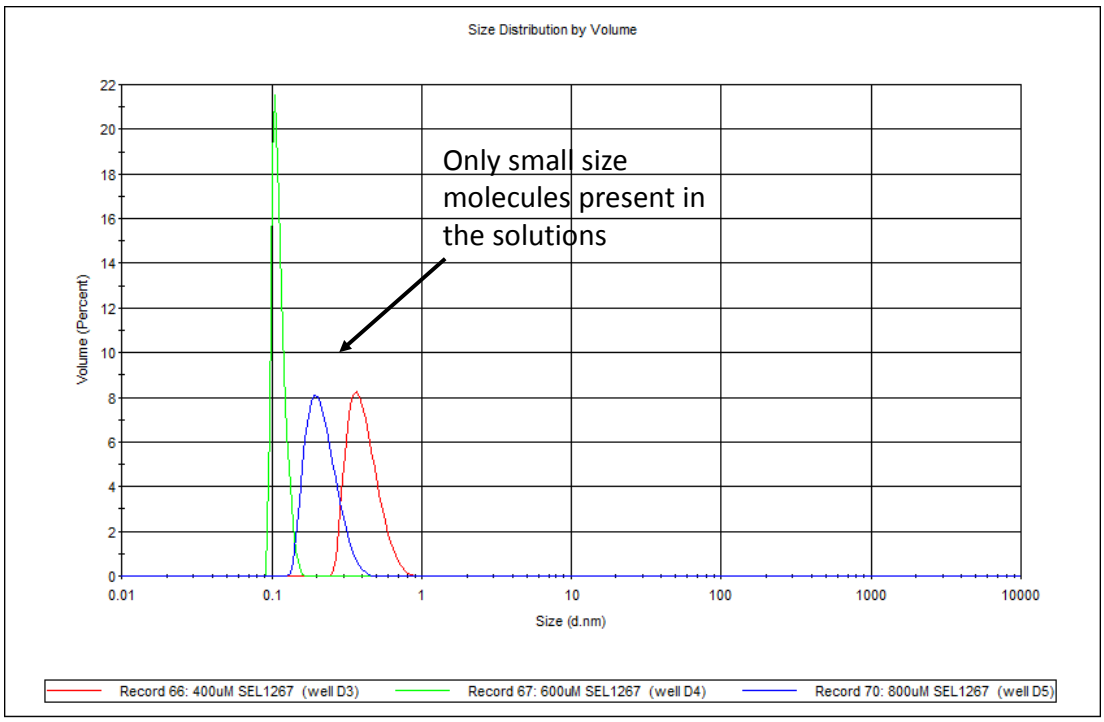

Figure 6.15 DLS mass distribution by volume profile of SEL101267 fragment.

The profile shows the hydrodynamic radius of molecules present in the solution. Only small size molecules are present when dissolving SEL101267 at concentrations of 400µM to 800µM.

6.7 Identification and characterisation of oxindole analogues

There are different potent inhibitors available for MDM2-N with structures having common features. The structures are mainly composed of multiple hydrophobic rings that occupy the three hydrophobic pockets in the MDM2-N binding site. In Mi63 inhibitor there is an oxindole present in the structures and it is also present in the isoindolinone and WW298 inhibitors (**Figure 6.16**) (Shangary et al., 2008, Hardcastle et al., 2011, Popowicz et al., 2010).

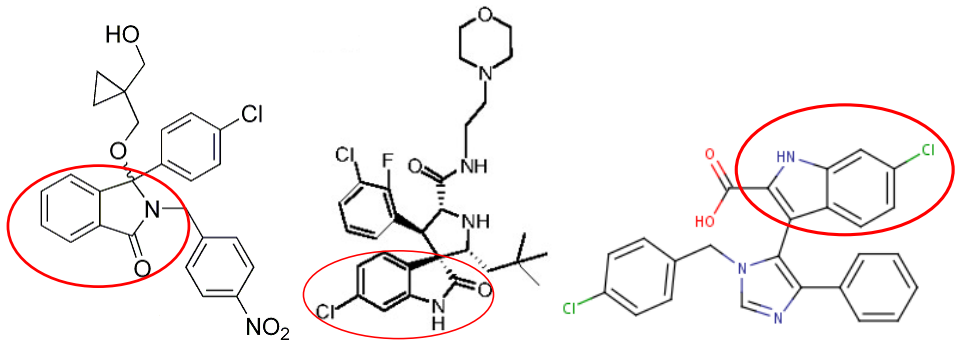

Figure 6.16 Structure of isoindolinone (left), Mi63 (middle) and WW298 inhibitors.
The structures are composed of multiple hydrophobic rings to occupy the hydrophobic pockets in the MDM2-N. An oxindole sub-structure (circle in red) is present in both inhibitors.

From the previous FP and CE assays (**Section 5.4.1.5**), we have identified two oxindole analogue fragments that showed an interaction with MDM2-N (**Figure 6.17**). These fragments showed 40% inhibition (SEL101069 (300μM)) and 27% inhibition (SFL001328 (300μM)) in the CE assay (**Chapter 5**). Additionally the DLS data shows SFL001328 did not aggregate MDM2-N (**Figure 6.13**). Therefore, we can confirm the oxindole analogues as genuine hits.

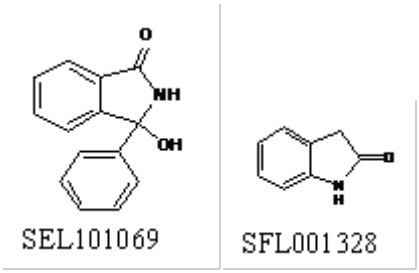

Figure 6.17 Structure of oxindole analogues SEL101069 (Left) and SFL001328 (Right).

Additional CE experiments were performed to further evaluate the affinity of these fragments.

SEL101069 was titrated from 0.01µM – 1000µM and SFL001328 was titrated from 25µM - 750µM. The results of both Nutlin-3 and unlabelled p53 peptide titrations showed that the p53-F peak shifted all the way back to its original position and gave an inhibition of ~90% (**Chapter 5 Figure 5.8 & Figure 5.11**). However, in both SFL001328 and SEL101069 titration curves the maximum inhibition found was ~40% (**Figure 6.18 top and bottom**). The curve reached a plateau at ~40% inhibition and the inhibition did not increase any further when the compound concentration was further increased.

Two factors may contribute to this partial inhibition:

1. The compounds may aggregate at higher concentration. The aggregated compound may have sequestered around the binding site to cause inhibition. Alternatively the compounds may simply aggregate in solution at higher concentrations.
2. Every compound has a different binding kinetic when binding to the binding site. The molecular properties of compound may affect the kinetics of the compound (Miller et al., 2012). SEL101069 and SFL001328 are low molecular weight compounds with no rotatable bonds so these compounds may have a fast off rate.

The IC_{50} was calculated to be 352µM for SEL101069, whereas SFL001328 was calculated to be 242µM. SFL001328 is a fragment of SEL101069 but the affinity of SFL001328 was higher than SEL101069. It is possible that the nitrogen atom in the oxindole is required to be positioned at the 2-indolinone position to give tighter binding. The nitrogen in SEL101069 is at the 2-indolinone position which could be a reason for it being less potent than SFL001328.

The Hill slope in the SEL101069 titration curve was found to be steep with a value of 9.8. This indicates a rapid increase in inhibition which can be indicative of aggregating compounds (Feng and Shoichet, 2006). Aggregation can be inhibited using detergents. Therefore further controls need to be run to confirm if the inhibition is due to colloidal aggregation. A trial experiment was carried out by adding 0.005% Tween-20 into the separation solution with MDM2-N plus compound. However no

change in the dose response curve was observed (data not shown). An experiment was also carried out by adding Nutlin-3 (40nM) along with SFL001328 (700µM) and MDM2-N (160nM) and a further increase of inhibition was found (Results not shown). This increase in inhibition suggests the SFL001328 did not fully occupy the protein binding site and there was still unbound protein present in the solution.

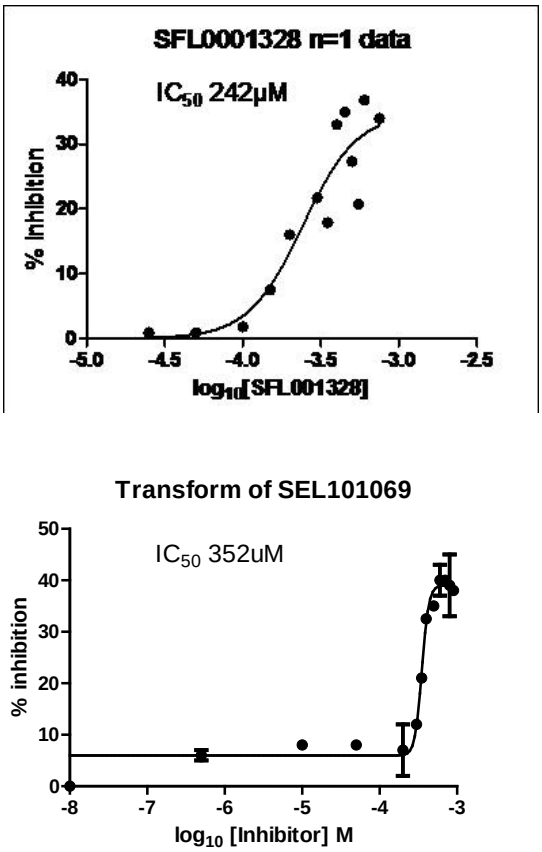

Figure 6.18 Dose response curve of SFL001328 (top) and SEL101069 (bottom).
The titration curves of SFL001328 and SEL101069 were fitted using GraphPad prism and IC_{50}s were calculated from the titration curves.

In order to analyse whether these fragments are worth developing into leads, the ligand efficiency (LE) was calculated using the **equation 3.1** from **Chapter 3** and the IC_{50} was calculated from **Figure 6.18**. SEL101069 contains 17 non-hydrogen atoms and SFL001328 contains 10 non-hydrogen atoms. LE calculated for SEL101069 and

SFL001328 are 0.28kcal mol^{-1} per non-hydrogen atom and 0.5kcal mol^{-1} per non-hydrogen atom respectively. There is no improved ligand efficiency with the additional phenyl ring in the SEL101069. Further analogue exploration on the oxindole fragment will require further chemistry to identify analogues with improved ligand efficiency.

6.8 Oxindole analogue exploration

Further analogue exploration was carried out to identify more analogues of the oxindole fragment. Oxindole analogues were searched using eMolecules (http://www.emolecules.com/) and there were many compounds identified containing a similar motif.

Some analogues found are listed in **Table 6.4,** these analogues contain different heavy atoms on the side chain. Compounds **1** and **6** contains an extra methyl group at the 7 and 2 positions, compound **2** contains fluorine at 5 position, compounds **3** and **5** contain nitrate positions at 5 and 6, compound **4** has introduced a nitro group at 5 position, compound **7** contains a OH group at 5 position and compound 8 contains a chlorine atom at 6 position. Different heavy atoms were selected at different positions on the oxindole group to assist in understanding the change in the affinity and help in identifying a higher affinity oxindole analogue.

Only compound 8, 6-chloro-2-oxindole, was available in the Selcia Compound Library and could be used for analysis in the CE and FP assays immediately (Selcia number SEL101884). It should be noted that SEL101884 contains the same structure as the substructure in the published Mi63 inhibitor which has an Ki of 3nM (**Figure 6.16**) (Shangary et al., 2008).

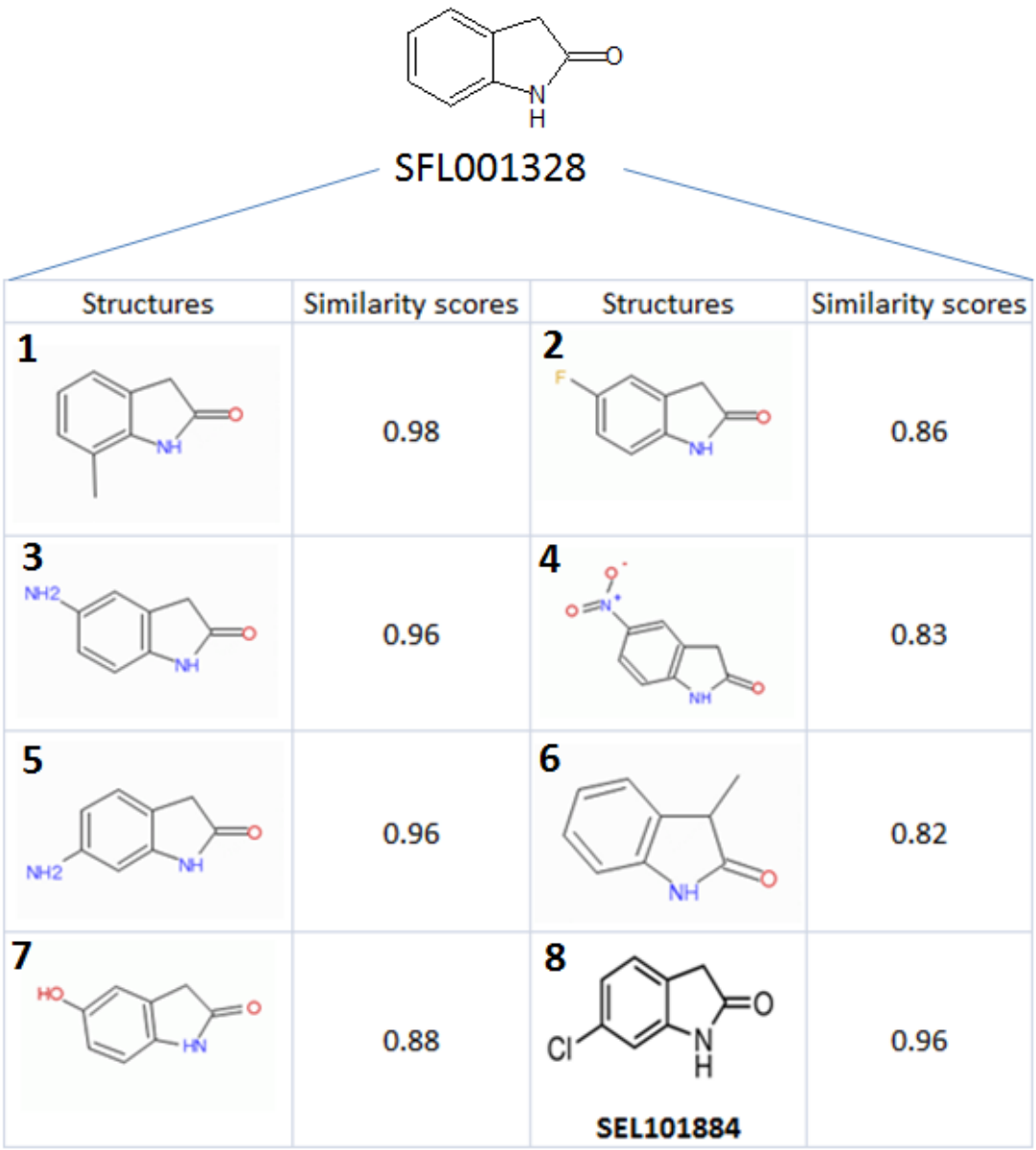

Table 6.4 Analogues of SFL001328 identified using eMolecules.

Analogue of SFL001328 was explored using online similarity search tool eMolecules (http://www.emolecules.com). The structures of the SFL001328 analogues were listed in the table with the similarity score.

The solubility of SEL101884 was examined using a turbidimetric test and a solubility > 500µM was confirmed (**Appendix A4**). Initially the fragment was tested in the FP assay at 200µM and showed an 8% inhibition. When screening the fragment in the CE assay 24% inhibition was found at 100µM concentration (**Table 6.5**). Compared with SFL001328, which was tested at 300µM, SEL101884 achieved a similar inhibition with a concentration of 100µM (**Table 6.5**). A similar result was also discovered when screening the fragments in the FP assay (**Table 6.5**). This suggests the efficiency of interaction has been improved by three fold with the addition of a chlorine atom at 6 position.

	% Inhibition	
	CE assay	FP assay
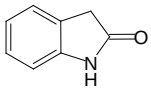 SFL001328	27.7% at 300µM	8% at 500µM
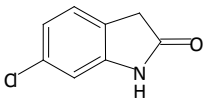 SEL101884	24% at 100µM	8% at 200µM

Table 6.5 Results of SEL101884 in CE and FP assays.

6.9 Discussion

This chapter describes the use of fluorescence polarization (FP), capillary electrophoresis (CE) and isothermal titration calorimetry (ITC) to validate the interaction of fragments with MDM2-N. Fragments possess weak binding affinities and hence require multiple orthogonal techniques for validation. Initial studies on the diphenylamine series fragments in the FP and CE assays showed convincing results. However, when studying the diphenylamine fragments in the DLS and ITC, the results showed that the diphenylamine compounds appear to aggregate the MDM2-N protein in solution (**section 6.6**). This fragment induced protein aggregation can be difficult to detect by the competition studies in both the CE and FP assays.

In further tests to examine this aggregation effect isothermal titration calorimetry (ITC) and dynamic light scattering (DLS) were used. However it should be noted that there is a difference in the protein concentration used in ITC and DLS. In ITC the MDM2-N concentration used is 1.5µM, however the concentration used in the DLS is 64µM which is 42 times higher. The higher protein concentration used in the DLS may result in an increase of aggregation. The percentage of aggregation present in the DLS profile is unclear because if there are large aggregates present in the solution then this can mask the signals of the small molecules.
Currently, how these diphenylamine analogues aggregate the MDM2-N protein is still unclear. One hypothesis could be that the diphenylamine fragments first interact with the MDM2-N binding site and then the phenyl ring of the fragment stacks with phenyl rings of other fragments molecules, thereby creating an aggregate. The phenyl rings on the diphenylamine fragment can adopt different conformations and therefore may be able to interact with each other at different angles leading to protein aggregation (Baell and Holloway, 2010).

It was however possible to identify genuine fragment inhibitors which did not show this protein aggregation effect. When examining different potent published (mainly Nutlin-like) inhibitors for MDM2-N a similar motif in the structures was identified. One of the features is that the MI series, isoindolinone and WW298 inhibitors (**Figure 6.16**) all contain an oxindole group in the structure to mimic the Trp23 side chain on

p53 peptide. Consequently the oxindole analogues SEL101069 and SFL001328 were tested in the FP and CE assays and it was confirmed that they interacted with MDM2-N (**Chapter 4 and 5**). Further titrations of SEL101069 and SFL001328 were performed and IC_{50} values of 352µM and 242µM respectively were obtained.

SEL101069 and SFL001328 were docked into the MDM2-N binding site using AutoDock. The docking poses of SEL101069 and SFL001328 are shown in **Figure 6.19 and Figure 6.20** respectively. The best docked pose for SEL101069 shows the phenyl ring inside the Trp23 pocket forming hydrophobic interactions with Phe86, while the oxindole ring sits in the Phe19 pocket and forms van der Waals interaction with Ile61. There are two oxygen atoms on SEL101069 that also forms van der Waals interactions with Leu54 and Val93.

The best docked poses for SFL001328 with MDM2-N (**Figure 6.20**) shows the oxindole docked into the Trp23 pocket, forming a hydrophobic interaction with Phe86. The NH atom on the SFL001328 also forms a hydrogen bond interaction with Leu54. This additional hydrogen bond may explain why SFL001328 binds more tightly in the Trp23 pocket than SEL101069. From the published structure of MDM2-N with Mi63 (**Figure 6.21**), the oxindole substructure also fits in the Trp23 pocket and interacts in the same position as predicted by AutoDock.

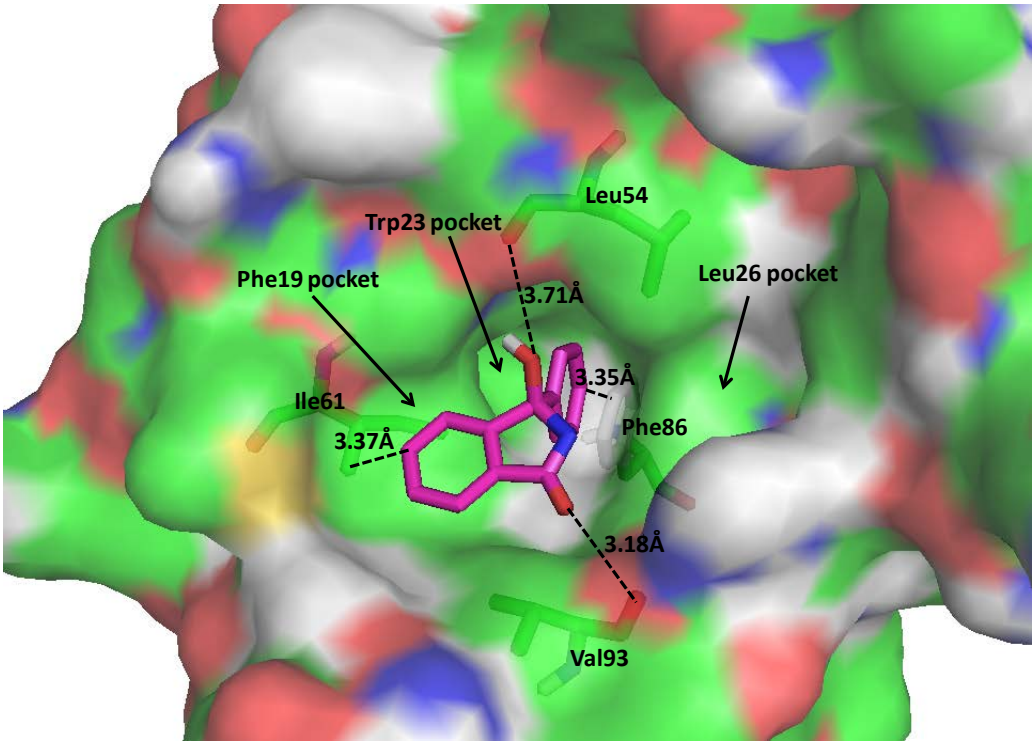

Figure 6.19 Docking poses of SEL101069 in MDM2-N.

SEL101069 was docked into MDM2-N binding site using AutoDock. The arrows indicate the name for each hydrophobic groove. The black dashed lines show the distance between the compound and the residues.

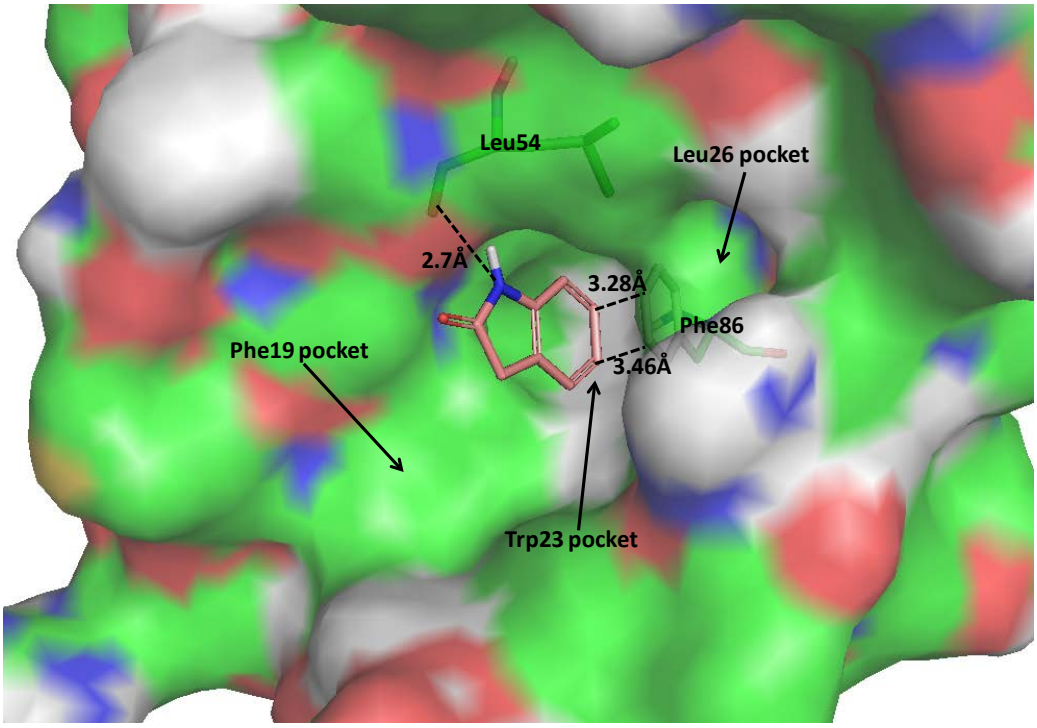

Figure 6.20 Docking poses of SFL001328 in MDM2-N.

SFL001328 (pink stick) is docked into Trp23 pocket in MDM2-N binding site. The distance between the fragment and the residues are shown in black dashed lines.

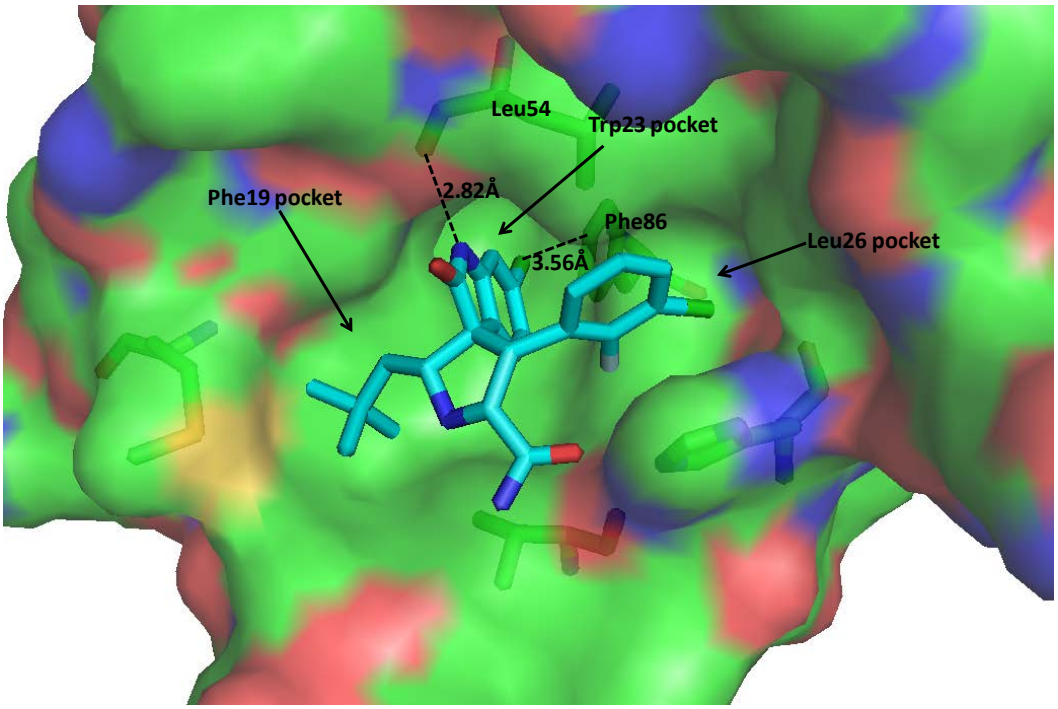

Figure 6.21 Interaction of Mi63 with MDM2-N

The diagram shows the X-ray crystal structure of MDM2-N with Mi63 inhibitor bound (3LBL; (Popowicz et al., 2010)).

Further analysis of 6-chloro-2-oxindole showed the binding efficiency has been improved by three fold and this suggests that the addition of chlorine atom at the 6 position allows the fragment to bind deeply into the Trp23 pocket as shown in **Figure 6.22**.

These are encouraging results and provide a useful starting point for the design and synthesis of tighter binding analogues.

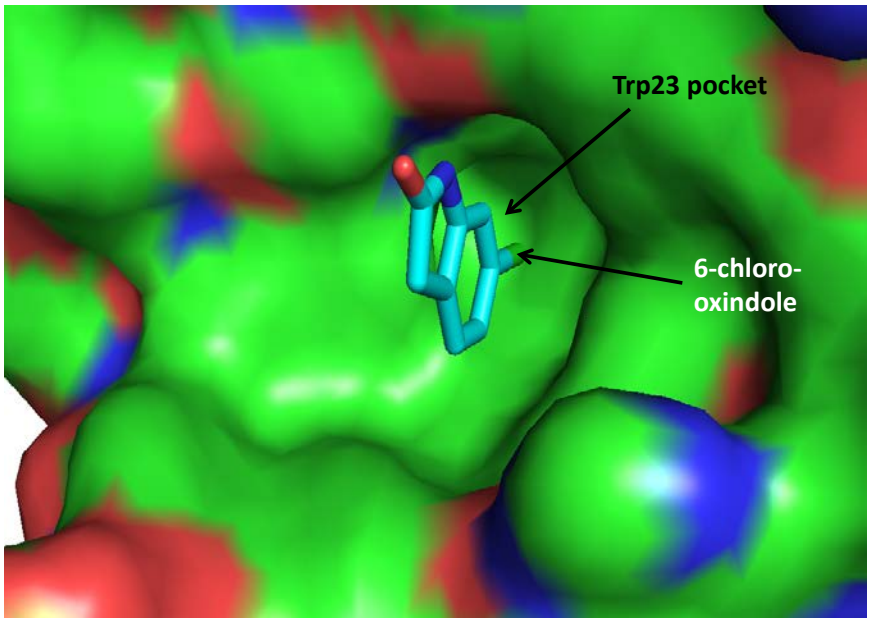

Figure 6.22 Interaction of 6-chloro-2-oxindole with MDM2

The diagram shows the 6-chloro-2-oxindole bind into the MDM2-N Trp23 pocket and the chlorine atom binds deeply into the pocket.

Chapter 7 Conclusion and forward look

7.1 Overall conclusions of the work

The original aim of this work was to look into the feasibility of identifying small molecule inhibitors to inhibit protein-protein interactions (PPI). Currently as described in **Chapter 1** there are a handful of examples demonstrating the design of PPI inhibitors. However the PPI inhibitors designed are often large complex structures and designing small molecules to bind to PPI sites holds many challenges. The PPI sites are often large and shallow which make them difficult to target by small molecules. This leaves an open question on whether low molecular weight fragments are too small to inhibit protein-protein interactions and whether fragment based drug design is possible for designing PPI inhibitors.

The PPI system selected for study is the MDM2/p53 interaction. In several cancer models MDM2 has been discovered to be overexpressed and inhibits the tumour suppressor activity in p53. Huge efforts have been put into restoring the p53 activities by the use of small molecules to inhibit MDM2 from binding. There are numerous inhibitors identified to target MDM2/p53 interaction and high resolution crystal structures of MDM2 with inhibitors bound are available (Zhao et al., 2013). These structures provided useful information that allowed us to select potential fragments to test whether smaller molecule compounds would inhibit the p53-MDM2 interaction.

A series of orthogonal assays were designed. In order to validate the interaction of small molecule inhibitors with the PPI of interest a series of assays had to be established. It has been known that fragment hits need to be validated by more than one method, thus different methods had to be set up to validate hits. In this work the assays which were applied for ligand studies are fluorescence polarization (FP), capillary electrophoresis (CE) and isothermal calorimetry (ITC). There are only a few techniques that are capable of screening fragments against PPIs and CE is one of the few techniques that offers fragment based drug discovery on PPIs (Austin et al., 2012). CE is a solution based technique that uses low sample consumptions to detect weak affinity interactions and the technique is emerging in the small molecule drug discovery (Austin et al., 2012, Espada and Molina-Martin, 2012, Rauch et al., 2013). This work is one of the few published studies that have used a CE assay for the

identification of small molecular ligand-receptor interactions. As far as we know this is the first reported study using CE assay on MDM2/MDMX drug discovery. When screening the small molecules against MDM2-N/p53 in the FP and CE assays it was shown that the FP assay requires an approximately 2 fold higher concentration of compound in order to detect the inhibition (see **section 5.4.1**). This indicates that the FP assay is less sensitive than the CE assay in detecting weak ligand binding which has also been shown in Austin et al. paper where the FP assay was not able to pick up weak affinity interactions (Austin et al., 2012). The IC_{50} of Nutlin-3 calculated from the CE titration is in agreement with the published value, demonstrating its high accuracy. The high sensitivity and accurate results obtained using the CE assay indicates that it is a very promising tool for ligand discovery. The results presented in the thesis provided the first example of combining the FP and CE assays for p53-MDM2 and p53-MDMX ligand screening and demonstrate the importance of validation with different techniques.

Problems with assay sensitivity and low signal. When developing the assays there were several issues that needed to be tackled. The fluorescently labelled p53 peptide (p53-F) showed a low fluorescent signal when running in the FP and CE assays. This required the use of high concentrations of p53-F and MDM2-N and greatly reduced the sensitivity of the assays. It was eventually discovered that the main reason for low signal was that the p53-F was sticking to the pipette tips and Eppendorf tubes. In order to improve the fluorescent signal of p53-F siliconised vials/tips were used which prevent absorption of p53-F onto the plastic. This improved the effective concentration by a factor of ~1000 and hence significantly improved the sensitivity of the assays.

A related problem that often arises during ligand screening is compound interference that can mask genuine hits as well as result in false positives especially when screening at high concentration of weak fragments. Compound interference can arise from intrinsic fluorescence of the compound, especially when a low concentration of fluorophore was used in the screen (e.g. 2nM p53-F) with a high concentration of compound (e.g. 500µM). In this work it was particularly important to test and account for any compound fluorescence. Another problem that can arise during ligand screening is compound induced protein aggregation which can result in false positive

hits. Above certain concentrations some compounds appear to have the ability to and aggregate protein through an unknown mechanism (McGovern et al., 2003).

Select fragment based on known inhibitors. There are different potent inhibitors available for MDM2-N with structures having common features. In Mi63 inhibitor there is an oxindole motif present in the structure and it is also present in the WW298 and isoindolinone inhibitors (Shangary et al., 2008, Popowicz et al., 2010, Hardcastle et al., 2011). Using the CE and FP assays the oxindole fragment (SFL001328) was identified with 28% (300µM) and 8% (500µM) inhibitions respectively and using the CE assay an IC_{50} of 242µM was determined. Docking model of SFL001328 showed the fragment buried deeply into the Trp23 pocket in MDM2-N and forms a hydrogen bond interaction with the Leu54 (**Figure 7.1**). This binding interaction mimics the binding mode of the oxindole subgroup in the Mi63 and WW298 inhibitors.

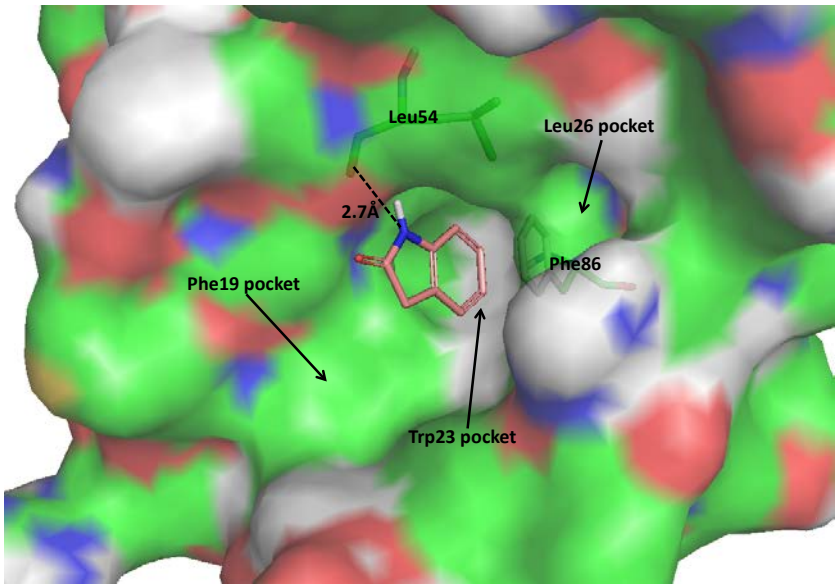

Figure 7.1 Binding conformation of oxindole fragment (SFL001328)

Oxindole fragment was docked into the MDM2-N binding site using AutoDock (Morris et al., 2009). MDM2-N binding site is represented using surface form and the name for the three hydrophobic grooves are pointed by the arrows. The oxindole fragment is shown as pink stick and the hydrogen bond interaction is displayed using black dash.

Further fragment studies using 6-chloro-2-oxindole (SEL101884) showed that the addition of a chlorine atom at 6-position improves the efficiency of interaction by three fold.

Virtual screening to identify small molecule inhibitors. In these studies we have employed virtual screening as an approach for ligand discovery and the hits identified were further evaluated by fragment identification. Virtual screening is a computational approach that is able to analyse millions of compounds stored in databases using high throughput computational docking. As part of the project an integrated virtual screening script CODASS, that combines multiple virtual screening programs to reduce the run time and maximises the enrichment, was used. Initially 1.1 million compounds in the EDULISS library were screened against MDM2-N (PDB: 3LBL) and the top 266 compounds from the rank were kept. These top scoring hits were then screened "visually" by Dr. Simon Pettit (Chemist at Selcia) and 6 compounds were selected based on the criteria listed in **section 3.2.2**. However this is a biased approach and a better approach would be to screen top hits blind but there is a cost implication with screening too many compounds.

Subsequent screening of these compounds in MDM2-N/p53 FP and CE assays showed 5 out of 6 compounds were active in both assays indicating the high hit rate of CODASS. The inactive compound was screened at 50µM only, therefore we cannot conclude that the compound does not bind. It may have weak interaction and requires a higher concentration to detect. This MDM2 study therefore provides an excellent example of the power of virtual screening using the CODASS routine. In this case showing a hit rate of 80%. This is well above the expected "industry standard" (Houston and Walkinshaw, 2013). The docking models were generated by AutoDock to provide the insight into the binding conformation of these hits. The compounds shared a common property of using a core imidazoline group as centre to stretch three hydrophobic rings into the Phe19, Trp23 and Leu26 pockets **(Figure 7.2**). This is generally caused by the hydrophobic pocket of MDM2-N and results in compounds being less soluble which is also evident in the well-known MDM2 inhibitors such as Nutlin-3 and MI219. The virtual screening hits showed no hydrogen bond interaction with the MDM2-N and the interactions are mainly driven by hydrophobic bonds.

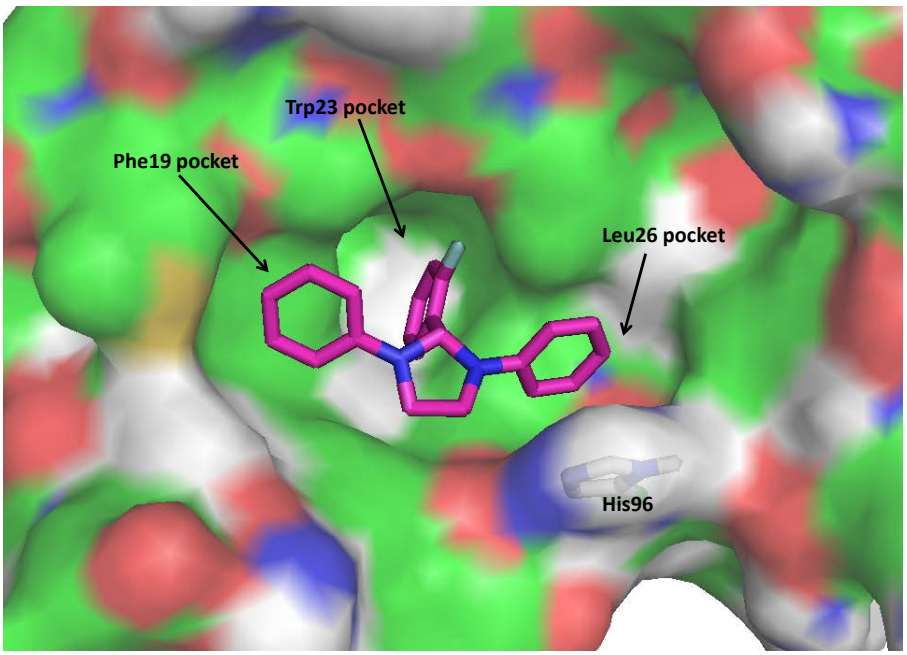

Figure 7.2 Virtual screening hits showed similar binding conformation with the well-known inhibitors.

This is one of the virtual screening hits that showed similar binding conformation with the well-known inhibitors. MDM2-N is represented in surface form and the virtual screening compound is shown in red stick.

Fragments exploration identified false positive hits. Protein forming large molecules was found to be a particular problem with the family of diphenylamines described in **Chapter 6**. In both the FP and CE assays convincing dose-response curves were obtained. However it was not until dynamic light scattering (DLS) and isothermal titration calorimetry (ITC) studies were carried out that it was apparent that the compounds were causing protein to form large molecules and the apparent low FP signal was due to large molecules and not because of specific protein binding. Similarly the shift of the p53 peak in the CE assay was caused by release of p53-F upon protein multimerization. It is likely that the diphenyl fragment binds non-specifically with MDM2-N and intermolecular aromatic stacking between diphenyl molecules causes large molecules formation. Protein aggregation caused by compounds is often inevitable and incurs wasted resources when followed up in lead design. This problem often arises during high throughput screening (HTS) and fragment based drug discovery (FBDD) and efforts have been put in to minimise the

false positives. There are filters developed which filter out functional groups that are reactive or prone to aggregate (Rishton, 1997, Baell and Holloway, 2010). During compound screening it is always important to run DLS on protein with compound as a control to rule out compounds that cause protein aggregation.

MDMX as a target to design a dual inhibitor. It has been confirmed that MDM2 and MDMX are both negative regulators of the tumour suppressor p53 (Marine and Jochemsen, 2004). These proteins use their highly similar N-terminal domain to bind to the N-terminal transactivation domain of p53 and inhibit p53 transcriptional activity. In order to identify a dual binding inhibitor to inhibit both MDM2 and MDMX, we used a reduced complexity subset EDULISS library comprising of 518,000 compounds to screen against MDM2-N and MDMX-N in the CODASS. The chemical structures of the top 1000 ranked hits showed they do not possess the chemical scaffold that was seen in the published MDM2 inhibitors. In fact these compounds are more flexible and do not contain the imidazoline centre to link multiple hydrophobic rings. It was also noted that most of these compounds do not bind into MDMX-N Leu26 pocket where the discrepancy between MDM2 and MDMX is. Using a specific set of criteria discussed in **section 3.2.2**, there were 7 compounds selected from the top 1000 ranked hits to validate the binding against MDM2-N and MDMX-N. Using the FP and CE assays SEL101876 showed a relatively high inhibition against MDM2-N and MDMX-N. This result still needs to be repeated using a fully optimised MDMX-N CE assay condition. Unfortunately there was not enough time to optimise the assay and test all the compounds. The identification of the novel dual action inhibitor SEL101876 shared little similarity with Nutlin-3 and MI-63 inhibitors. The binding model showed the piperidinyl morpholine group in SEL101876 occupies the Leu26 pocket in the MDM2-N binding site to provide stacking interaction with the His96 ring (**Figure 7.3 left**), while the two phenyl rings bind into Phe19 and Trp23 pockets. However a different binding approach of SEL101876 was found when binding into the MDMX-N binding site (**Figure 7.3 right**). The phenyl rings in SEL101876 bind into the Trp23 pocket and interact with MDMX-N Met53 residue. The piperidinyl morpholine group does not interact in the MDMX-N Leu26 pocket. Instead it interacts with the MDMX-N Phe19 pocket to form hydrogen bond interaction with Gln71 residue. This is absent in MDM2-N which may explain the reason of stronger

inhibition seen in the assays. The data presented in this work suggests that evading the interaction with Leu26 pocket and providing hydrogen bond interaction between the compound and MDMX-N are required for developing a higher affinity dual inhibitor. Besides the peptide inhibitor found by Chang et al. there are only two examples of dual MDM2/X small molecule inhibitors in the literature (Graves et al., 2012, Popowicz et al., 2010, Chang et al., 2013). This new chemical scaffold allows further optimisation to develop a more potent MDM2/X-N inhibitor.

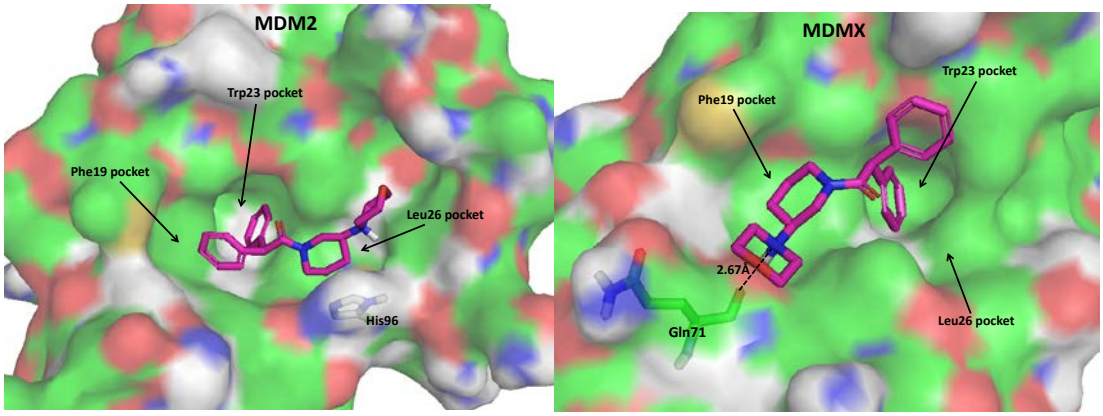

Figure 7.3 Binding conformation of SEL101876 in MDM2 (left) and MDMX (right). The docking models of SEL101876 with MDM2-N (PDB structure 3LBL) and MDMX-N (PDB structure 3LBJ) showed that SEL101876 does not bind to the Leu26 pocket when it interacts with MDMX-N. There is a hydrogen bond formation (black dash line) on the piperidinyl morpholine group with Gln71-MDMX-N.

7.2 Forward look

In this work a dual action inhibitor SEL101876 was identified. In order to understand how SEL101876 interacts in the MDM2-N and MDMX-N binding site, X-ray co-crystal structures should be obtained. This was originally planned as part of the study, however there was not enough time to complete. As described in **Chapter 2** the MDM2-N$^{11-130}$ construct used in the assays contains an unstructured tail and also extra residues at the N-terminal that causes crystallisation to be impossible. Sequence alignment of MDMX-N$^{14-111}$ with the published crystal structures' sequences (**Figure**

2.2) showed that MDMX-N^{14-111} contains extra residues at the N-terminal that may affect the crystallisation.

Attempts on expression and purification of truncated MDM2-N^{18-111} and MDMX-N^{23-109} constructs were unsuccessful. In the MDM2-N^{18-111} construct the N-terminal His-tag linked by the TEV cleavage site was discovered to be difficult to cleave. It is possible that the His-tag is buried into the binding site and hides the cleavage site. If the His-tag on the protein is not cleavable then this will cause difficulty in crystallising the protein. Therefore untagged or C-terminal His-tag constructs should be designed for crystallisation trials.

The dual action inhibitor SEL101876 identified using the CE and FP assays showed that this compound is novel and different from known published inhibitors. Quantitative structure-activity relationship (QSAR) should be carried out to characterise the activities in every subgroup. This will assist in the identification of the subgroup in SEL101876 required for MDM2/X-N interaction and more potent fragments can be developed. In addition, with the combination of X-ray crystallography it is possible to add in hydrophilic subgroup into the fragment to improve the solubility of the compound. In the MDM2-N crystal structure there is a hydrophilic region between Gln72 and Lys94. Therefore extending to this region will provide additional interaction as well as improving the solubility and water accessibility.

MDM2/p53 is a typical PPI example representing a deep hydrophobic binding site. In this work the results have proven that virtual screening in combination with CE and FP assays can be used as a tool for fragment development and the small fragments can be active against PPI.

References

ABAD-ZAPATERO, C. 2007. Ligand efficiency indices for effective drug discovery. *Expert Opin Drug Discov,* 2**,** 469-88.

ACCELRYS 2013. Discovery Studio Modeling Environment, Release 4.0. *San Diego: Accelrys Software Inc.*

ALARCON-VARGAS, D. & RONAI, Z. E. 2002. p53–Mdm2—the affair that never ends. *Carcinogenesis,* 23**,** 541-547.

ALEXEI, D., ALEXEY, L., MICHAEL, C., BRADLEY, M., GERHARD, W., TIMOTHY, M. & JUNYING, Y. 2001. Identification of small-molecule inhibitors of interaction between the BH3 domain and Bcl-xL. *Nature Cell Biology,* 3**,** 173-182.

ALLEN, J. G., BOURBEAU, M. P., WOHLHIETER, G. E., BARTBERGER, M. D., MICHELSEN, K., HUNGATE, R., GADWOOD, R. C., GASTON, R. D., EVANS, B., MANN, L. W., MATISON, M. E., SCHNEIDER, S., HUANG, X., YU, D., ANDREWS, P. S., REICHELT, A., LONG, A. M., YAKOWEC, P., YANG, E. Y., LEE, T. A. & OLINER, J. D. 2009. Discovery and Optimization of Chromenotriazolopyrimidines as Potent Inhibitors of the Mouse Double Minute 2−Tumor Protein 53 Protein−Protein Interaction. *Journal of Medicinal Chemistry,* 52**,** 7044-7053.

ANIL, B., RIEDINGER, C., ENDICOTT, J. A. & NOBLE, M. E. M. 2013. The structure of an MDM2-Nutlin-3a complex solved by the use of a validated MDM2 surface-entropy reduction mutant. *Acta Crystallographica Section D,* 69**,** 1358-1366.

ARKIN, M. R. & WELLS, J. A. 2004. Small-molecule inhibitors of protein-protein interactions: progressing towards the dream. *Nat Rev Drug Discov,* 3**,** 301-317.

AUSTIN, C., PETTIT, S. N., MAGNOLO, S. K., SANVOISIN, J., CHEN, W., WOOD, S. P., FREEMAN, L. D., PENGELLY, R. J. & HUGHES, D. E. 2012. Fragment Screening Using Capillary Electrophoresis (CEfrag) for Hit Identification of Heat Shock Protein 90 ATPase Inhibitors. *Journal of Biomolecular Screening,* 17**,** 868-876.

AZAM, S., ABRO, A., TANVIR, F. & PARVAIZ, N. 2014. Identification of unique binding site and molecular docking studies for structurally diverse Bcl-xL inhibitors. *Medicinal Chemistry Research,* 23**,** 3765-3783.

BABA, M., NISHIMURA, O., KANZAKI, N., OKAMOTO, M., SAWADA, H., IIZAWA, Y., SHIRAISHI, M., ARAMAKI, Y., OKONOGI, K., OGAWA, Y., MEGURO, K. & FUJINO, M. 1999. A small-molecule, nonpeptide CCR5 antagonist with highly potent and selective anti-HIV-1 activity. *Proceedings of the National Academy of Sciences,* 96**,** 5698-5703.

BAELL, J. B. & HOLLOWAY, G. A. 2010. New Substructure Filters for Removal of Pan Assay Interference Compounds (PAINS) from Screening Libraries and for Their Exclusion in Bioassays. *Journal of Medicinal Chemistry,* 53**,** 2719-2740.

BAJORATH, J. 2002. Integration of virtual and high-throughput screening. *Nat Rev Drug Discov,* 1**,** 882-894.

BARKER, J., HESTERKAMP, T. & WHITTAKER, M. 2008. Integrating HTS and fragment-based drug discovery. *DDW DRUG DISCOVERY WORLD,* 9**,** 69.

BERNAL, F., WADE, M., GODES, M., DAVIS, T. N., WHITEHEAD, D. G., KUNG, A. L., WAHL, G. M. & WALENSKY, L. D. 2010. A stapled p53 helix overcomes HDMX-mediated suppression of p53. *Cancer cell,* 18**,** 411-422.

BEUTLER, J. A. 2001. Natural Products as a Foundation for Drug Discovery. *Current Protocols in Pharmacology.* John Wiley & Sons, Inc.

BRAISTED, A. C., OSLOB, J. D., DELANO, W. L., HYDE, J., MCDOWELL, R. S., WAAL, N., YU, C., ARKIN, M. R. & RAIMUNDO, B. C. 2003. Discovery of a Potent Small Molecule IL-2 Inhibitor through Fragment Assembly. *Journal of the American Chemical Society,* 125**,** 3714-3715.

BROWN, C. J., CHEOK, C. F., VERMA, C. S. & LANE, D. P. 2011. Reactivation of p53: from peptides to small molecules. *Trends in Pharmacological Sciences,* 32**,** 53-62.

BROWN, C. J., DASTIDAR, S. G., SEE, H. Y., COOMBER, D. W., ORTIZ-LOMBARDIA, M., VERMA, C. & LANE, D. P. 2010. Rational design and biophysical characterization of thioredoxin-based aptamers: insights into peptide grafting. *J Mol Biol,* 395**,** 871-83.

BROWN, C. J., LAIN, S., VERMA, C. S., FERSHT, A. R. & LANE, D. P. 2009. Awakening guardian angels: drugging the p53 pathway. *Nature Reviews Cancer,* 9**,** 862-873.

BURKE, T. J., LONIELLO, K. R., BEEBE, J. A. & ERVIN, K. M. 2003. Development and application of fluorescence polarization assays in drug discovery. *Comb Chem High Throughput Screen,* 6**,** 183-94.

CAHILLY-SNYDER, L., YANG-FENG, T., FRANCKE, U. & GEORGE, D. L. 1987. Molecular analysis and chromosomal mapping of amplified genes isolated from a transformed mouse 3T3 cell line. *Somat Cell Mol Genet,* 13**,** 235-44.

CARR, R. A. E., CONGREVE, M., MURRAY, C. W. & REES, D. C. 2005. Fragment-based lead discovery: leads by design. *Drug Discovery Today,* 10**,** 987-992.

CHANG, Y. S., GRAVES, B., GUERLAVAIS, V., TOVAR, C., PACKMAN, K., TO, K.-H., OLSON, K. A., KESAVAN, K., GANGURDE, P., MUKHERJEE, A., BAKER, T., DARLAK, K., ELKIN, C., FILIPOVIC, Z., QURESHI, F. Z., CAI, H., BERRY, P., FEYFANT, E., SHI, X. E., HORSTICK, J., ANNIS, D. A., MANNING, A. M., FOTOUHI, N., NASH, H., VASSILEV, L. T. & SAWYER, T. K. 2013. Stapled α−helical peptide drug development: A potent dual inhibitor of MDM2 and MDMX for p53-dependent cancer therapy. *Proceedings of the National Academy of Sciences,* 110**,** E3445-E3454.

CONGREVE, M., CARR, R., MURRAY, C. & JHOTI, H. 2003. A 'Rule of Three' for fragment-based lead discovery? *Drug Discovery Today,* 8**,** 876-877.

CONGREVE, M., CHESSARI, G., TISI, D. & WOODHEAD, A. J. 2008. Recent developments in fragment-based drug discovery. *J Med Chem,* 51**,** 3661-80.

COULTER, B. 1994. Introduction to Capillary to Electrophoresis.

DANDLIKER, W. B. & DE SAUSSURE, V. A. 1970. Fluorescence polarization in immunochemistry. *Immunochemistry,* 7**,** 799-828.

DELANO, W. L. 2002. The PyMOL Molecular Graphics System.

DING, K., LU, Y., NIKOLOVSKA-COLESKA, Z., QIU, S., DING, Y., GAO, W., STUCKEY, J., KRAJEWSKI, K., ROLLER, P. P., TOMITA, Y., PARRISH, D. A., DESCHAMPS, J. R. & WANG, S. 2005. Structure-Based Design of Potent Non-Peptide MDM2 Inhibitors. *Journal of the American Chemical Society,* 127**,** 10130-10131.

DING, K., LU, Y., NIKOLOVSKA-COLESKA, Z., WANG, G., QIU, S., SHANGARY, S., GAO, W., QIN, D., STUCKEY, J., KRAJEWSKI, K., ROLLER, P. P. & WANG, S. 2006. Structure-Based Design of Spiro-oxindoles as Potent, Specific Small-Molecule Inhibitors of the MDM2−p53 Interaction. *Journal of Medicinal Chemistry,* 49**,** 3432-3435.

ESPADA, A. & MOLINA-MARTIN, M. 2012. Capillary electrophoresis and small molecule drug discovery: a perfect match? *Drug Discovery Today,* 17**,** 396-404.

FENG, B. Y. & SHOICHET, B. K. 2006. A detergent-based assay for the detection of promiscuous inhibitors. *Nat. Protocols,* 1**,** 550-553.

GADEK, T. R. & NICHOLAS, J. B. 2003. Small molecule antagonists of proteins. *Biochemical Pharmacology,* 65**,** 1-8.

GALLICCHIO, E., DENG, N., HE, P., WICKSTROM, L., PERRYMAN, A., SANTIAGO, D., FORLI, S., OLSON, A. & LEVY, R. 2014. Virtual screening of integrase inhibitors by large scale binding free energy calculations: the SAMPL4 challenge. *Journal of Computer-Aided Molecular Design,* 28**,** 475-490.

GERMAN, I., BUCHANAN, D. D. & KENNEDY, R. T. 1998. Aptamers as Ligands in Affinity Probe Capillary Electrophoresis. *Analytical Chemistry,* 70**,** 4540-4545.

GHOSH, S., NIE, A., AN, J. & HUANG, Z. 2006. Structure-based virtual screening of chemical libraries for drug discovery. *Current Opinion in Chemical Biology,* 10**,** 194-202.

GRASBERGER, B. L., LU, T., SCHUBERT, C., PARKS, D. J., CARVER, T. E., KOBLISH, H. K., CUMMINGS, M. D., LAFRANCE, L. V., MILKIEWICZ, K. L., CALVO, R. R., MAGUIRE, D., LATTANZE, J., FRANKS, C. F., ZHAO, S., RAMACHANDREN, K., BYLEBYL, G. R., ZHANG, M., MANTHEY, C. L., PETRELLA, E. C., PANTOLIANO, M. W., DECKMAN, I. C., SPURLINO, J. C., MARONEY, A. C., TOMCZUK, B. E., MOLLOY, C. J. & BONE, R. F. 2005. Discovery and Cocrystal Structure of Benzodiazepinedione HDM2 Antagonists That Activate p53 in Cells. *Journal of Medicinal Chemistry,* 48**,** 909-912.

GRAVES, B., THOMPSON, T., XIA, M., JANSON, C., LUKACS, C., DEO, D., DI LELLO, P., FRY, D., GARVIE, C., HUANG, K.-S., GAO, L., TOVAR, C., LOVEY, A., WANNER, J. & VASSILEV, L. T. 2012. Activation of the p53 pathway by small-molecule-induced MDM2 and MDMX dimerization. *Proceedings of the National Academy of Sciences*.

GREER, J. & BUSH, B. L. 1978. Macromolecular shape and surface maps by solvent exclusion. *Proceedings of the National Academy of Sciences,* 75**,** 303-307.

GRIBBON, P. & ANDREAS, S. 2005. High-throughput drug discovery: What can we expect from HTS? *Drug Discovery Today,* 10**,** 17-22.

GU, J., KAWAI, H., NIE, L., KITAO, H., WIEDERSCHAIN, D., JOCHEMSEN, A. G., PARANT, J., LOZANO, G. & YUAN, Z.-M. 2002. Mutual Dependence of MDM2 and MDMX in Their Functional Inactivation of p53. *Journal of Biological Chemistry,* 277**,** 19251-19254.

HAJDUK, P. J. & GREER, J. 2007. A decade of fragment-based drug design: strategic advances and lessons learned. *Nat Rev Drug Discov,* 6**,** 211-9.

HANAHAN, D. & WEINBERG, R. A. 2000. The hallmarks of cancer. *Cell,* 100**,** 57-70.

HANN, M. M. & OPREA, T. I. 2004. Pursuing the leadlikeness concept in pharmaceutical research. *Current Opinion in Chemical Biology,* 8**,** 255-263.

HARDCASTLE, I. R., LIU, J., VALEUR, E., WATSON, A., AHMED, S. U., BLACKBURN, T. J., BENNACEUR, K., CLEGG, W., DRUMMOND, C., ENDICOTT, J. A., GOLDING, B. T., GRIFFIN, R. J., GRUBER, J., HAGGERTY, K., HARRINGTON, R. W., HUTTON, C., KEMP, S., LU, X., MCDONNELL, J. M., NEWELL, D. R., NOBLE, M. E. M., PAYNE, S. L., REVILL, C. H., RIEDINGER, C., XU, Q. & LUNEC, J. 2011. Isoindolinone Inhibitors of the Murine Double Minute 2 (MDM2)-p53 Protein−Protein Interaction: Structure−Activity Studies Leading to Improved Potency. *Journal of Medicinal Chemistry,* 54**,** 1233-1243.

HARTSHORN, M. J., MURRAY, C. W., CLEASBY, A., FREDERICKSON, M., TICKLE, I. J. & JHOTI, H. 2004. Fragment-Based Lead Discovery Using X-ray Crystallography. *Journal of Medicinal Chemistry,* 48**,** 403-413.

HERNYCHOVA, L., MAN, P., VERMA, C., NICHOLSON, J., SHARMA, C.-A., RUCKOVA, E., TEO, J. Y., BALL, K., VOJTESEK, B. & HUPP, T. R. 2013. Identification of a second Nutlin-3 responsive interaction site in the N-terminal domain of MDM2 using hydrogen/deuterium exchange mass spectrometry. *PROTEOMICS,* 13**,** 2512-2525.

HOE, K. K., VERMA, C. S. & LANE, D. P. 2014. Drugging the p53 pathway: understanding the route to clinical efficacy. *Nat Rev Drug Discov,* 13**,** 217-236.

HOPKINS, A. L., GROOM, C. R. & ALEX, A. 2004. Ligand efficiency: a useful metric for lead selection. *Drug Discovery Today,* 9**,** 430-431.

HOUSTON, D. R. & WALKINSHAW, M. D. 2013. Consensus Docking: Improving the Reliability of Docking in a Virtual Screening Context. *Journal of Chemical Information and Modeling,* 53**,** 384-390.

HSIN, K. Y., MORGAN, H. P., SHAVE, S. R., HINTON, A. C., TAYLOR, P. & WALKINSHAW, M. D. 2011. EDULISS: a small-molecule database with data-mining and pharmacophore searching capabilities. *Nucleic Acids Res,* 39**,** D1042-D1048.

HUANG, S.-Y., GRINTER, S. Z. & ZOU, X. 2010. Scoring functions and their evaluation methods for protein-ligand docking: recent advances and future directions. *Physical Chemistry Chemical Physics,* 12**,** 12899-12908.

HUGHES, D. E., KARGER, B. L., WATERS, J. L. & DUNAYEVSKIY, Y. M. 2002. Method to detect and analyze tight-binding ligands in complex biological samples using capillary electrophoresis and mass spectrometry. Google Patents.

HUMPHREY, W., DALKE, A. & SCHULTEN, K. 1996. VMD: visual molecular dynamics. *Journal of molecular graphics,* 14**,** 33-38.

INVITROGEN 2006. Technical Resource Guide Fourth Edition Fluorescence Polarization.

IVANOV, A. A., KHURI, F. R. & FU, H. 2013. Targeting protein protein interactions as an anticancer strategy. *Trends in pharmacological sciences,* 34**,** 393-400.

JACHIMSKA, B., WASILEWSKA, M. & ADAMCZYK, Z. 2008. Characterization of globular protein solutions by dynamic light scattering, electrophoretic mobility, and viscosity measurements. *Langmuir,* 24**,** 6866-72.

JONES, S. N., HANCOCK, A. R., VOGEL, H., DONEHOWER, L. A. & BRADLEY, A. 1998. Overexpression of Mdm2 in mice reveals a p53-independent role for Mdm2 in tumorigenesis. *Proceedings of the National Academy of Sciences,* 95**,** 15608-15612.

JORGENSON, J. W. & LUKACS, K. D. 1981. Free-zone electrophoresis in glass capillaries. *Clinical Chemistry,* 27**,** 1551-3.

KARAS, M. & HILLENKAMP, F. 1988. Laser desorption ionization of proteins with molecular masses exceeding 10,000 daltons. *Analytical Chemistry,* 60**,** 2299-2301.

KELLY, T. A., JEANFAVRE, D. D., MCNEIL, D. W., WOSKA, J. R., REILLY, P. L., MAINOLFI, E. A., KISHIMOTO, K. M., NABOZNY, G. H., ZINTER, R., BORMANN, B.-J. & ROTHLEIN, R. 1999. Cutting Edge: A Small Molecule Antagonist of LFA-1-Mediated Cell Adhesion. *The Journal of Immunology,* 163**,** 5173-5177.

KUNTZ, I. D., BLANEY, J. M., OATLEY, S. J., LANGRIDGE, R. & FERRIN, T. E. 1982. A GEOMETRIC APPROACH TO MACROMOLECULE-LIGAND INTERACTIONS. *Journal of Molecular Biology,* 161**,** 269-288.

KUSSIE, P. H., GORINA, S., MARECHAL, V., ELENBAAS, B., MOREAU, J., LEVINE, A. J. & PAVLETICH, N. P. 1996. Structure of the MDM2 Oncoprotein Bound to the p53 Tumor Suppressor Transactivation Domain. *Science,* 274**,** 948-953.

LAI, Z., AUGER, K. R., MANUBAY, C. M. & COPELAND, R. A. 2000. Thermodynamics of p53 Binding to hdm2(1–126): Effects of Phosphorylation and p53 Peptide Length. *Archives of Biochemistry and Biophysics,* 381**,** 278-284.

LANE, D. P. 1992. Cancer. p53, guardian of the genome. *Nature,* 358**,** 15-6.

LAST-BARNEY, K., DAVIDSON, W., CARDOZO, M., FRYE, L. L., GRYGON, C. A., HOPKINS, J. L., JEANFAVRE, D. D., PAV, S., QIAN, C., STEVENSON, J. M., TONG, L., ZINDELL, R. & KELLY, T. A. 2001. Binding Site Elucidation of Hydantoin-Based Antagonists of LFA-1 Using Multidisciplinary Technologies: Evidence for the Allosteric Inhibition of a Protein−Protein Interaction. *Journal of the American Chemical Society,* 123**,** 5643-5650.

LAZARENO, S. & BIRDSALL, N. J. M. 1993. Estimation of competitive antagonist affinity from functional inhibition curves using the Gaddum, Schild and Cheng-Prusoíf equations. *British Journal of Pharmacology,* 109**,** 1110-1119.

LEPRE, C. A., MOORE, J. M. & PENG, J. W. 2004. Theory and Applications of NMR-Based Screening in Pharmaceutical Research. *Chemical Reviews,* 104**,** 3641-3676.

LEVINTHAL, C., WODAK, S. J., KAHN, P. & DADIVANIAN, A. K. 1975. Hemoglobin interaction in sickle cell fibers. I: Theoretical approaches to the molecular contacts. *Proceedings of the National Academy of Sciences,* 72**,** 1330-1334.

LIPINSKI, C. A., LOMBARDO, F., DOMINY, B. W. & FEENEY, P. J. 1997. Experimental and computational approaches to estimate solubility and permeability in drug discovery and development settings. *Advanced Drug Delivery Reviews,* 23**,** 3-25.

MARINE, J.-C. & JOCHEMSEN, A. G. 2005. Mdmx as an essential regulator of p53 activity. *Biochemical and Biophysical Research Communications,* 331**,** 750-760.

MARINE, J.-C. W., DYER, M. A. & JOCHEMSEN, A. G. 2007. MDMX: from bench to bedside. *Journal of Cell Science,* 120**,** 371-378.

MARINE, J. C. & JOCHEMSEN, A. G. 2004. Mdmx and Mdm2: brothers in arms? *Cell Cycle,* 3**,** 900-4.

MCCOY, M. A., GESELL, J. J., SENIOR, M. M. & WYSS, D. F. 2003. Flexible lid to the p53-binding domain of human Mdm2: Implications for p53 regulation. *Proceedings of the National Academy of Sciences,* 100**,** 1645-1648.

MCGOVERN, S. L., HELFAND, B. T., FENG, B. & SHOICHET, B. K. 2003. A Specific Mechanism of Nonspecific Inhibition. *Journal of Medicinal Chemistry,* 46**,** 4265-4272.

MCINNES, C. 2007. Virtual screening strategies in drug discovery. *Current Opinion in Chemical Biology,* 11**,** 494-502.

MICHELSEN, K., JORDAN, J. B., LEWIS, J., LONG, A. M., YANG, E., REW, Y., ZHOU, J., YAKOWEC, P., SCHNIER, P. D., HUANG, X. & POPPE, L. 2012. Ordering of the N-Terminus of Human MDM2 by Small Molecule Inhibitors. *Journal of the American Chemical Society,* 134**,** 17059-17067.

MILLER, D. C., LUNN, G., JONES, P., SABNIS, Y., DAVIES, N. L. & DRISCOLL, P. 2012. Investigation of the effect of molecular properties on the binding kinetics of a ligand to its biological target. *MedChemComm,* 3**,** 449-452.

MOLL, U. M. & PETRENKO, O. 2003. The MDM2-p53 Interaction. *Molecular Cancer Research,* 1**,** 1001-1008.

MOMAND, J., ZAMBETTI, G. P., OLSON, D. C., GEORGE, D. & LEVINE, A. J. 1992. The mdm-2 oncogene product forms a complex with the p53 protein and inhibits p53-mediated transactivation. *Cell,* 69**,** 1237-1245.

MORRIS, G. M., HUEY, R., LINDSTROM, W., SANNER, M. F., BELEW, R. K., GOODSELL, D. S. & OLSON, A. J. 2009. AutoDock4 and AutoDockTools4: Automated docking with selective receptor flexibility. *Journal of Computational Chemistry,* 30**,** 2785-2791.

NEIDLE, S. & HUBBARD, R. E. 2006. *Structure-Based Drug Discovery,* Cambridge, Royal Society of Chemistry.

OKHRIMENKO, O. & JELESAROV, I. 2008. A survey of the year 2006 literature on applications of isothermal titration calorimetry. *Journal of Molecular Recognition,* 21**,** 1-19.

OLINER, J. D., KINZLER, K. W., MELTZER, P. S., GEORGE, D. L. & VOGELSTEIN, B. 1992a. Amplification of a gene encoding a p53-associated protein in human sarcomas. *Nature,* 358**,** 80-83.

OLINER, J. D., KINZLER, K. W., MELTZER, P. S., GEORGE, D. L. & VOGELSTEIN, B. 1992b. Amplification of a gene encoding a p53-associated protein in human sarcomas. *Nature,* 358**,** 80-3.

OWICKI, J. C. 2000. Fluorescence Polarization and Anisotropy in High Throughput Screening: Perspectives and Primer. *Journal of Biomolecular Screening,* 5**,** 297-306.

PAGLIARO, L., FELDING, J., AUDOUZE, K., NIELSEN, S. J., TERRY, R. B., KROG-JENSEN, C. & BUTCHER, S. 2004. Emerging classes of protein–protein interaction inhibitors and new tools for their development. *Current Opinion in Chemical Biology,* 8**,** 442-449.

PARKER, G. J., LAW, T. L., LENOCH, F. J. & BOLGER, R. E. 2000. Development of High Throughput Screening Assays Using Fluorescence Polarization: Nuclear Receptor-Ligand-Binding and Kinase/Phosphatase Assays. *Journal of Biomolecular Screening,* 5**,** 77-88.

PAZGIER, M., LIU, M., ZOU, G., YUAN, W., LI, C., LI, C., LI, J., MONBO, J., ZELLA, D. & TARASOV, S. G. 2009. Structural basis for high-affinity peptide inhibition of p53 interactions with MDM2 and MDMX. *Proceedings of the National Academy of Sciences,* 106**,** 4665-4670.

PENTA, A., CHANDER, S., GANGULY, S. & MURUGESAN, S. 2014. De novo design and in-silico studies of novel 1-phenyl-2,3,4,9-tetrahydro-1H-pyrido[3,4-b]indole-3-carboxylic acid derivatives as HIV-1 reverse transcriptase inhibitors. *Medicinal Chemistry Research,* 23**,** 3662-3670.

PERRIN, F. 1926. Polarisation de la lumière de fluorescence. Vie moyenne des molécules dans l'etat excité. *J. Phys. Radium,* 7**,** 390-401.

PETITJEAN, A., MATHE, E., KATO, S., ISHIOKA, C., TAVTIGIAN, S. V., HAINAUT, P. & OLIVIER, M. 2007. Impact of mutant p53 functional properties on TP53 mutation patterns and tumor phenotype: lessons from recent developments in the IARC TP53 database. *Human Mutation,* 28**,** 622-629.

PHAN, J., LI, Z., KASPRZAK, A., LI, B., SEBTI, S., GUIDA, W., SCHÖNBRUNN, E. & CHEN, J. 2010. Structure-based Design of High Affinity Peptides Inhibiting the Interaction of p53 with MDM2 and MDMX. *Journal of Biological Chemistry,* 285**,** 2174-2183.

PIERCEALL, W. E., ZHANG, L. & HUGHES, D. E. 2004. Affinity Capillary Electrophoresis Analyses of Protein—Protein Interactions in Target-Directed Drug Discovery. *Protein-Protein Interactions.*

POPOWICZ, G., CZARNA, A. & HOLAK, T. 2008. Structure of the human Mdmx protein bound to the p53 tumor suppressor transactivation domain. *Cell Cycle,* 7**,** 2441-2443.

POPOWICZ, G. M., CZARNA, A., ROTHWEILER, U., SZWAGIERCZAK, A., KRAJEWSKI, M., WEBER, L. & HOLAK, T. A. 2007. Molecular Basis for the Inhibition of p53 by Mdmx. *Cell Cycle,* 6**,** 2386-2392.

POPOWICZ, G. M., CZARNA, A., WOLF, S., WANG, K., WANG, W., DÖMLING, A. & HOLAK, T. A. 2010. Structures of low molecular weight inhibitors bound to MDMX and MDM2 reveal new approaches for p53-MDMX/MDM2 antagonist drug discovery. *Cell Cycle,* 9**,** 1104-1111.

PRIVES, C. & HALL, P. A. 1999. The p53 pathway. *The Journal of Pathology,* 187**,** 112-126.

RAUCH, J. N., NIE, J., BUCHHOLZ, T. J., GESTWICKI, J. E. & KENNEDY, R. T. 2013. Development of a Capillary Electrophoresis Platform for Identifying Inhibitors of Protein–Protein Interactions. *Analytical Chemistry,* 85**,** 9824-9831.

REDDY, A. S., PATI, S. P., KUMAR, P. P., PRADEEP, H. N. & SASTRY, G. N. 2007. Virtual Screening in Drug Discovery - A Computational Perspective. *Current Protein and Peptide Science,* 8**,** 329-351.

REED, D., SHEN, Y., SHELAT, A., ARNOLD, A., FERREIRA, A., ZHU, F., MILLS, N., SMITHSON, D., REGNI, C., BASHFORD, D., CICERO, S., SCHULMAN, B., JOCHEMSEN, A. G., GUY, K. & DYER, M. A. 2010. Identification and characterization of the first small-molecule inhibitor of MDMX. *Journal of Biological Chemistry*.

REIFENBERGER, G., LIU, L., ICHIMURA, K., SCHMIDT, E. E. & COLLINS, V. P. 1993. Amplification and Overexpression of the MDM2 Gene in a Subset of Human Malignant Gliomas without p53 Mutations. *Cancer Research,* 53**,** 2736-2739.

RISHTON, G. M. 1997. Reactive compounds and< i> in vitro</i> false positives in HTS. *Drug Discovery Today,* 2**,** 382-384.

SALEMME, F. R. 1976. An hypothetical structure for an intermolecular electron transfer complex of cytochromes c and b5. *Journal of Molecular Biology,* 102**,** 563-568.

SCHON, O., FRIEDLER, A., FREUND, S. & FERSHT, A. R. 2004. Binding of p53-derived Ligands to MDM2 Induces a Variety of Long Range Conformational Changes. *Journal of Molecular Biology,* 336**,** 197-202.

SCHULTES, S., DE GRAAF, C., HAAKSMA, E. E. J., DE ESCH, I. J. P., LEURS, R. & KRÄMER, O. 2010. Ligand efficiency as a guide in fragment hit selection and optimization. *Drug Discovery Today: Technologies,* 7**,** e157-e162.

SCHULZ, M. N. & HUBBARD, R. E. 2009. Recent progress in fragment-based lead discovery. *Current Opinion in Pharmacology,* 9**,** 615-621.

SCOTT, D. E., COYNE, A. G., HUDSON, S. A. & ABELL, C. 2012. Fragment-Based Approaches in Drug Discovery and Chemical Biology. *Biochemistry,* 51**,** 4990-5003.

SHANGARY, S., QIN, D., MCEACHERN, D., LIU, M., MILLER, R. S., QIU, S., NIKOLOVSKA-COLESKA, Z., DING, K., WANG, G., CHEN, J., BERNARD, D., ZHANG, J., LU, Y., GU, Q., SHAH, R. B., PIENTA, K. J., LING, X., KANG, S., GUO, M., SUN, Y., YANG, D. & WANG, S. 2008. Temporal activation of p53 by a specific MDM2 inhibitor is selectively toxic to tumors and leads to complete tumor growth inhibition. *Proceedings of the National Academy of Sciences,* 105**,** 3933-3938.

SHAVE, S. 2010. The Development of High Performance Structure and Ligand Based Virtual Screening Techniques.

SHIMIZU, H. & HUPP, T. R. 2003. Intrasteric regulation of MDM2. *Trends Biochem Sci,* 28**,** 346-9.

SHOICHET, B. K. 2004. Virtual screening of chemical libraries. *Nature,* 432**,** 862-865.

SHOWALTER, S. A., BRUSCHWEILER-LI, L., JOHNSON, E., ZHANG, F. & BRUSCHWEILER, R. 2008. Quantitative lid dynamics of MDM2 reveals

differential ligand binding modes of the p53-binding cleft. *J Am Chem Soc,* 130**,** 6472-8.

STOLL, R., RENNER, C., HANSEN, S., PALME, S., KLEIN, C., BELLING, A., ZESLAWSKI, W., KAMIONKA, M., REHM, T., MÜHLHAHN, P., SCHUMACHER, R., HESSE, F., KALUZA, B., VOELTER, W., ENGH, R. A. & HOLAK, T. A. 2001. Chalcone Derivatives Antagonize Interactions between the Human Oncoprotein MDM2 and p53†. *Biochemistry,* 40**,** 336-344.

TANAKA, K., WAKI, H., IDO, Y., AKITA, S., YOSHIDA, Y., YOSHIDA, T. & MATSUO, T. 1988. Protein and polymer analyses up to m/z 100 000 by laser ionization time-of-flight mass spectrometry. *Rapid Communications in Mass Spectrometry,* 2**,** 151-153.

TANIMURA, S., OHTSUKA, S., MITSUI, K., SHIROUZU, K., YOSHIMURA, A. & OHTSUBO, M. 1999. MDM2 interacts with MDMX through their RING finger domains. *FEBS Letters,* 447**,** 5-9.

TAYLOR, P., BLACKBURN, E., SHENG, Y. G., HARDING, S., HSIN, K. Y., KAN, D., SHAVE, S. & WALKINSHAW, M. D. 2008. Ligand discovery and virtual screening using the program LIDAEUS. *British Journal of Pharmacology,* 153**,** S55-S67.

TEODORO, J., EVANS, S. & GREEN, M. 2007. Inhibition of tumor angiogenesis by p53: a new role for the guardian of the genome. *Journal of Molecular Medicine,* 85**,** 1175-1186.

TILLEY, J. W., CHEN, L., FRY, D. C., EMERSON, S. D., POWERS, G. D., BIONDI, D., VARNELL, T., TRILLES, R., GUTHRIE, R., MENNONA, F., KAPLAN, G., LEMAHIEU, R. A., CARSON, M., HAN, R.-J., LIU, C. M., PALERMO, R. & JU, G. 1997. Identification of a Small Molecule Inhibitor of the IL-2/IL-2Rα Receptor Interaction Which Binds to IL-2. *Journal of the American Chemical Society,* 119**,** 7589-7590.

TOVAR, C., ROSINSKI, J., FILIPOVIC, Z., HIGGINS, B., KOLINSKY, K., HILTON, H., ZHAO, X., VU, B. T., QING, W., PACKMAN, K., MYKLEBOST, O., HEIMBROOK, D. C. & VASSILEV, L. T. 2006. Small-molecule MDM2 antagonists reveal aberrant p53 signaling in cancer: Implications for therapy. *Proceedings of the National Academy of Sciences of the United States of America,* 103**,** 1888-1893.

TROTT, O. & OLSON, A. J. 2010. AutoDock Vina: Improving the speed and accuracy of docking with a new scoring function, efficient optimization, and multithreading. *Journal of Computational Chemistry,* 31**,** 455-461.

UHRINOVA, S., UHRIN, D., POWERS, H., WATT, K., ZHELEVA, D., FISCHER, P., MCINNES, C. & BARLOW, P. N. 2005. Structure of free MDM2 N-terminal domain reveals conformational adjustments that accompany p53-binding. *J Mol Biol,* 350**,** 587-98.

VAN GUNSTEREN, W. F., BAKOWIES, D., BARON, R., CHANDRASEKHAR, I., CHRISTEN, M., DAURA, X., GEE, P., GEERKE, D. P., GLATTLI, A., HUNENBERGER, P. H., KASTENHOLZ, M. A., OOSTENBRINK, C., SCHENK, M., TRZESNIAK, D., VAN DER VEGT, N. F. & YU, H. B. 2006. Biomolecular modeling: Goals, problems, perspectives. *Angew Chem Int Ed Engl,* 45**,** 4064-92.

VASSILEV, L. T., VU, B. T., GRAVES, B., CARVAJAL, D., PODLASKI, F., FILIPOVIC, Z., KONG, N., KAMMLOTT, U., LUKACS, C., KLEIN, C., FOTOUHI, N. & LIU, E. A. 2004. In Vivo Activation of the p53 Pathway by Small-Molecule Antagonists of MDM2. *Science,* 303**,** 844-848.

VEBER, D. F., JOHNSON, S. R., CHENG, H.-Y., SMITH, B. R., WARD, K. W. & KOPPLE, K. D. 2002. Molecular Properties That Influence the Oral Bioavailability of Drug Candidates. *Journal of Medicinal Chemistry,* 45**,** 2615-2623.

VELEC, H. F. G., GOHLKE, H. & KLEBE, G. 2005. DrugScoreCSDKnowledge-Based Scoring Function Derived from Small Molecule Crystal Data with Superior Recognition Rate of Near-Native Ligand Poses and Better Affinity Prediction. *Journal of Medicinal Chemistry,* 48**,** 6296-6303.

VOGELSTEIN, B., LANE, D. & LEVINE, A. J. 2000. Surfing the p53 network. *Nature,* 408**,** 307-310.

WADE, M. & WAHL, G. M. 2009. Targeting Mdm2 and Mdmx in Cancer Therapy: Better Living through Medicinal Chemistry? *Molecular Cancer Research,* 7**,** 1-11.

WANG, R., LAI, L. & WANG, S. 2002. Further development and validation of empirical scoring functions for structure-based binding affinity prediction. *Journal of Computer-Aided Molecular Design,* 16**,** 11-26.

WHITE, A. W., WESTWELL, A. D. & BRAHEMI, G. 2008. Protein–protein interactions as targets for small-molecule therapeutics in cancer. *Expert Reviews in Molecular Medicine,* 10**,** null-null.

WODAK, S. J. & JANIN, J. 1978. Computer analysis of protein-protein interaction. *Journal of Molecular Biology,* 124**,** 323-342.

WYATT, P. G., WOODHEAD, A. J., BERDINI, V., BOULSTRIDGE, J. A., CARR, M. G., CROSS, D. M., DAVIS, D. J., DEVINE, L. A., EARLY, T. R., FELTELL, R. E., LEWIS, E. J., MCMENAMIN, R. L., NAVARRO, E. F., O'BRIEN, M. A., O'REILLY, M., REULE, M., SAXTY, G., SEAVERS, L. C. A., SMITH, D.-M., SQUIRES, M. S., TREWARTHA, G., WALKER, M. T. & WOOLFORD, A. J. A. 2008. Identification of N-(4-Piperidinyl)-4-(2,6-dichlorobenzoylamino)-1H-pyrazole-3-carboxamide (AT7519), a Novel Cyclin Dependent Kinase Inhibitor Using Fragment-Based X-Ray Crystallography and Structure Based Drug Design†. *Journal of Medicinal Chemistry,* 51**,** 4986-4999.

ZHANG, R., MAYHOOD, T., LIPARI, P., WANG, Y., DURKIN, J., SYTO, R., GESELL, J., MCNEMAR, C. & WINDSOR, W. 2004. Fluorescence polarization assay and inhibitor design for MDM2/p53 interaction. *Analytical Biochemistry,* 331**,** 138-146.

ZHAO, Y., BERNARD, D. & WANG, S. 2013. Small molecule inhibitors of MDM2-p53 and MDMX-p53 interactions as new cancer therapeutics. *BioDiscovery,* 8.

ZOR, E., ESAD SAGLAM, M., ALPAYDIN, S. & BINGOL, H. 2014. A reduced graphene oxide/[small alpha]-cyclodextrin hybrid for the detection of methionine: electrochemical, fluorometric and computational studies. *Analytical Methods,* 6**,** 6522-6530.

Appendix

Appendix A1. Protparam details

A1.1 His-tag MDM2-N$^{11-130}$

```
        10         20         30         40         50         60
MGSSHHHHHH SSGLVPRGSH MDGAVTTSQI PASEQETLVR PKPLLLKLLK SVGAQKDTYT
        70         80         90        100        110        120
MKEVLFYLGQ YIMTKRLYDE KQQHIVYCSN DLLGDLFGVP SFSVKEHRKI YTMIYRNLVV
       130
VNQQESSDSG TSVSENLE
```

Number of amino acids: 138

Molecular weight: 15601.7

Theoretical pI: 7.13

Extinction coefficients:

Extinction coefficients are in units of M^{-1} cm^{-1}, at 280 nm measured in water.

Ext. coefficient 10430

Abs 0.1% (=1 g/l) 0.669, assuming all pairs of Cys residues form cystines

A1.2 MDM2-N$^{11-130}$

```
        10         20         30         40         50         60
GSHMDGAVTT SQIPASEQET LVRPKPLLLK LLKSVGAQKD TYTMKEVLFY LGQYIMTKRL
        70         80         90        100        110        120
YDEKQQHIVY CSNDLLGDLF GVPSFSVKEH RKIYTMIYRN LVVVNQQESS DSGTSVSENL

E
```

Number of amino acids: 121

Molecular weight: 13719.6

Theoretical pI: 6.33

Extinction coefficients:

Extinction coefficients are in units of M^{-1} cm^{-1}, at 280 nm measured in water.

Ext. coefficient 10430

Abs 0.1% (=1 g/l) 0.760, assuming all pairs of Cys residues form cystines

A1.3 His-tag MDM2-N$^{18\text{-}111}$

```
        10          20          30          40          50          60
MSYYHHHHHH DYDIPTTENL YFQGMQIPAS EQETLVRPKP LLLKLLKSVG AQKDTYTMKE
        70          80          90         100         110
VLFYLGQYIM TKRLYDEKQQ HIVYCSNDLL GDLFGVPSFS VKEHRKIYTM IYRNLVVVN
```

Number of amino acids: 119

Molecular weight: 14153.3

Theoretical pI: 7.88

Extinction coefficients:

Extinction coefficients are in units of M^{-1} cm^{-1}, at 280 nm measured in water.

Ext. coefficient 16390

Abs 0.1% (=1 g/l) 1.158, assuming all pairs of Cys residues form cystines

A1.4 MDM2-N$^{18\text{-}111}$

```
        10          20          30          40          50          60
GMQIPASEQE TLVRPKPLLL KLLKSVGAQK DTYTMKEVLF YLGQYIMTKR LYDEKQQHIV
        70          80          90
YCSNDLLGDL FGVPSFSVKE HRKIYTMIYR NLVVVN
```

Number of amino acids: 96

Molecular weight: 11185.1

Theoretical pI: 9.24

Extinction coefficients:

Extinction coefficients are in units of M^{-1} cm^{-1}, at 280 nm measured in water.

Ext. coefficient 10430

Abs 0.1% (=1 g/l) 0.932, assuming all pairs of Cys residues form cystines

A1.5 His-tag MDMX-N$^{14-111}$

```
        10          20          30          40          50          60
MGSSHHHHHH SSGLVPRGSH MDSASRISPG QINQVRPKLP LLKILHAAGA QGEMFTVKEV
        70          80          90         100         110
MHYLGQYIMV KQLYDQQEQH MVYCGGDLLG ELLGRQSFSV KNPSPLYDML RKNLVTLAT
```

Number of amino acids: 119

Molecular weight: 13313.3

Theoretical pI: 9.17

Extinction coefficients:

Extinction coefficients are in units of M^{-1} cm^{-1}, at 280 nm measured in water.

Ext. coefficient 7450

Abs 0.1% (=1 g/l) 0.560, assuming all pairs of Cys residues form cystines

A1.6 MDMX-N$^{14-111}$

```
        10          20          30          40          50          60
GSHMDSASRI SPGQINQVRP KLPLLKILHA AGAQGEMFTV KEVMHYLGQY IMVKQLYDQQ
        70          80          90         100
EQHMVYCGGD LLGELLGRQS FSVKNPSPLY DMLRKNLVTL AT
```

Number of amino acids: 102

Molecular weight: 11431.3

Theoretical pI: 8.81

Extinction coefficients:

Extinction coefficients are in units of M^{-1} cm^{-1}, at 280 nm measured in water.

Ext. coefficient 7450

Abs 0.1% (=1 g/l) 0.652, assuming all pairs of Cys residues form cystines

A1.7 His-tag MDMX-N$^{23-109}$

```
        10          20          30          40          50          60
MSYYHHHHHH DYDIPTTENL YFQGQINQVR PKLPLLKILH AAGAQGEMFT VKEVMHYLGQ

        70          80          90         100         110
YIMVKQLYDQ QEQHMVYCGG DLLGELLGRQ SFSVKDPSPL YDMLRKNLVT L
```

Number of amino acids: 111

Molecular weight: 13001.9

Theoretical pI: 6.48

Extinction coefficients:

Extinction coefficients are in units of M^{-1} cm^{-1}, at 280 nm measured in water.

Ext. coefficient 13410

Abs 0.1% (=1 g/l) 1.031, assuming all pairs of Cys residues form cystines

A1.8 MDMX-N$^{23-109}$

```
        10          20          30          40          50          60
GQINQVRPKL PLLKILHAAG AQGEMFTVKE VMHYLGQYIM VKQLYDQQEQ HMVYCGGDLL

        70          80
GELLGRQSFS VKDPSPLYDM LRKNLVTL
```

Number of amino acids: 88

Molecular weight: 10033.7

Theoretical pI: 8.07

Extinction coefficients:
Extinction coefficients are in units of M^{-1} cm^{-1}, at 280 nm measured in water.
Ext. coefficient 7450
Abs 0.1% (=1 g/l) 0.742, assuming all pairs of Cys residues form cystines

Appendix A2. SOP of optimised FP assay

A2.1 Equipment

LJL Biosystems Analyst AD

A2.2 Materials

* Siliconised polypropylene microcentrifuge tubes volume 0.65ml: Sigma-Aldrich T3281-500EA.

* HEPES: Sigma H4034

* Sodium Chloride: Fisher Scientific S/3160/63

* DTT: Melford MB1015

* 384 well, low volume, flat bottom, non-binding surface, black polystyrene plate: Corning cat No: 3820

* Nutlin-3: Tocris 3984

MW = 590.5

* Fluorescently labelled p53 derived peptide (p53-F)

5-FAM-QETFSDLWKLLP-OH

MW = 1835.03

Custom synthesis by Biomatiks.

A2.3 Preparation of stock solutions

Always use siliconised pipette tips and siliconised vials when working with p53-F and MDM2-N

1M DTT

1M stock of DTT was prepared by dissolving 5g of DTT into 32.4ml of H_2O. Aliquots of 1ml were prepared and frozen in -20˚C freezer.

Running Buffer (50mM HEPES pH 7.5, 100mM NaCl, 1mM DTT)

Weigh 5.95g HEPES, 2.92g NaCl and dissolve in 490ml of distilled H_2O and adjust pH using 5M NaOH. Adjust final volume to 500ml with distilled H_2O and degas/ filter using 0.2µm filter membrane and filter on a degas station. Add 500µl of DTT (1M) into the solution prior to the experiment.

Preparation of p53-F stock

Use siliconised pipette tips and siliconised vials when working with p53-F.

Weigh 2mg of p53-F powder and dissolve in 150µl of running buffer (Final concentration p53-F = 7.3mM). 70µl of p53-F (7.3mM) was diluted in 70µl running buffer to obtain 3.65mM stock. Wrap the vials with tinfoil and store in the -20°C freezer.

Preparation of p53-F (10µM) stock

Dilute p53-F stock (2.7µl, 3.65mM) with running buffer (997µl). Store aliquots of 5µl in siliconised tubes in the dark -80°C freezer.

Analyst multi-plate reader setting

Excitation/Emission filter: Fluorescein 485nm/530nm

G factor: 0.94

Z height: Middle of well

Detector counting: Smart read

Sensitivity setting: 2

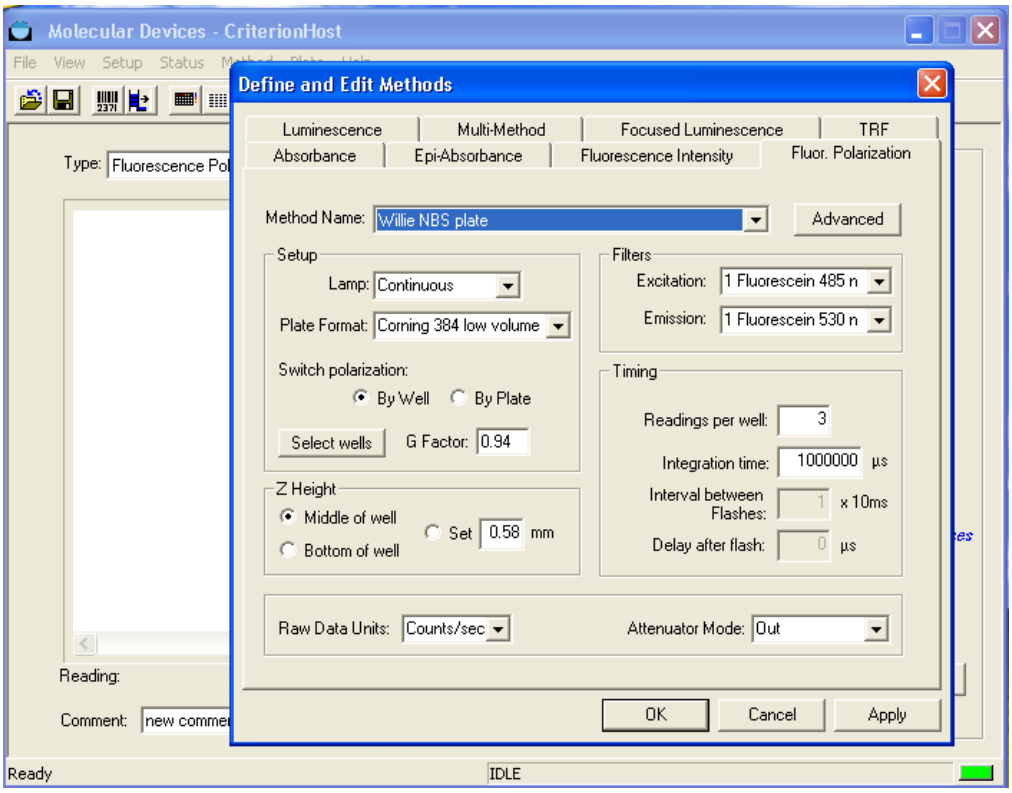

Parameters for Analyst FP assay setting

A2.4 Sample preparation and plate set up for FP MDM2-N/small molecules screening

Initially MDM2-N, p53-F and compounds were diluted into the siliconised vials using the following steps:

Dilution for p53-F

Using siliconised tube and tips, add 1µl of 10µM stock into 9µl assay buffer (f/c = 1µM). Dilute 6µl of 1µM p53-F into 1494µl assay buffer to get f/c = 4nM.

Dilution for MDM2-N

Use siliconised pipette tips and siliconised vials when working with MDM2-N. Thaw frozen 1mg/ml MDM2-N (64µM) and dilute 12µl MDM2-N (64µM) with 738µl assay buffer (f/c = 1.02µM).

Compounds stock

Make 100mM compound DMSO stock from ~1mg dry powder. Add 5µl of 100mM stock into 5µl DMSO (f/c compound = 50mM in 100% DMSO). Screen the fragments at 500µM as the initial screening concentration depends upon the compound solubility.

Assay plate set up

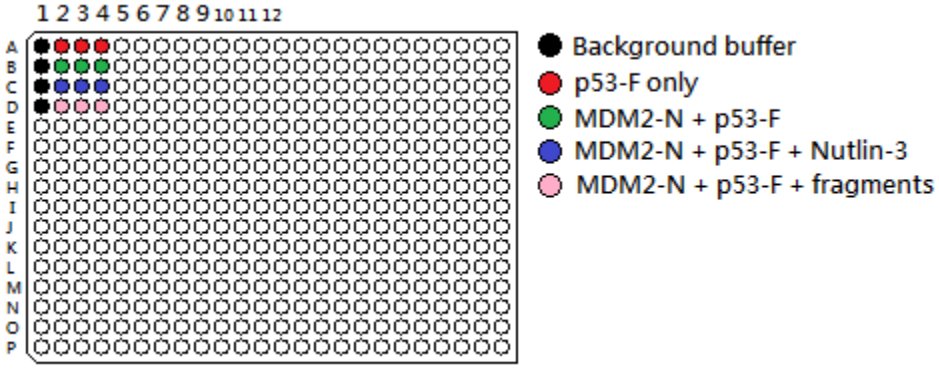

Samples set up in the non-binding surface plate

For screening compounds against MDM2-N the samples were set up in the 384 wells plate using the following protocol:

A1 – Background buffer (50mM HEPES, 100mM NaCl, 1mM DTT, 1% DMSO). Add 0.5µl DMSO (100%) into 49.5µl assay buffer. Use a pipette to mix the mixture.

B1 – Background buffer (50mM HEPES, 100mM NaCl, 1mM DTT, 1% DMSO). Add 0.5µl DMSO (100%) into 49.5µl assay buffer. Use a pipette to mix the mixture.

C1 – Background buffer (50mM HEPES, 100mM NaCl, 1mM DTT, 1% DMSO, 1µM Nutlin-3). Add 0.5µl Nutlin-3 (100µM) into 49.5µl assay buffer. Use a pipette to mix the mixture.

D1 – Background buffer (50mM HEPES, 100mM NaCl, 1mM DTT, 1% DMSO, 700µM compound). Add 0.5µl compound (70mM) into 49.5µl assay buffer. Use a pipette to mix the mixture.

A2:A4 – p53-F only (50mM HEPES, 100mM NaCl, 1mM DTT, 2nM p53-F, 1% DMSO). 24.5µl assay buffer was first added into the well then followed by 0.5µl DMSO (100%). 25µl p53-F (4nM) was added last into the well and mix the mixture using a pipette.

B2:B4 – MDM2-N + p53-F (50mM HEPES, 100mM NaCl, 1mM DTT , 2nM p53-F, 500nM MDM2-N, 1% DMSO). 24.5µl MDM2-N (1.02µM) was added into the well then followed by 0.5µl DMSO (100%). 25µl p53-F (4nM) was added last into the well and mix the mixture using a pipette.

C2:C4 – MDM2-N + p53-F + Nutlin-3 (50mM HEPES, 100mM NaCl, 1mM DTT , 2nM p53-F, 500nM MDM2-N, 1µM Nutlin-3, 1% DMSO). 24.5µl MDM2-N (1.02µM) was added into the well then followed by 0.5µl Nutlin-3 (100µM). 25µl p53-F (4nM) was added last into the well and mix the mixture using a pipette.

D2:D4 – MDM2-N + p53-F + fragments (50mM HEPES, 100mM NaCl, 1mM DTT , 2nM p53-F, 500nM MDM2-N, 700µM fragment, 1% DMSO). 24.5µl MDM2-N (1.02µM) was added into the well then followed by 0.5µl fragment (70mM). 25µl p53-F (4nM) was added last into the well and mix the mixture using a pipette.

A2.5 Results interpretation

Background subtraction

Background was subtracted manually by subtracting parallel and perpendicular values with the background buffer values.

Background subtraction:

Parallel - background reading

Perpendicular - background reading

% Inhibition equation

Percentage of inhibition will be calculated for each compound screen.

The equation used is:

% Inhibition = $100(A_F - A_U) / (A_F - A_I)$

A_F is the anisotropy value of p53-F in the presence of MDM2-N.

A_U is the anisotropy value of p53-F.

A_I is the anisotropy value of p53-F in the presence of MDM2-N + compound.

Appendix A3. MDM2-N CE SOP

A3.1 Equipment

P/ACE^{TM}MDQ Capillary Electrophoresis System/ Beckman Coulter

Beckman Coulter 488nm laser module

A3.2 Materials

* Siliconised 200µl pipette tips: VWR Europe Cat No. 613-0279

* Siliconised 10µl pipette tips: VWR Europe Cat No. 613-0337

* Siliconised polypropylene microcentrifuge tubes volume 0.65ml: Sigma-Aldrich T3281-500EA.

* 0.2µM Single use syringe membrane filter: Satorius stedim ref: 17597

* Bovine Serum Albumin (BSA): Sigma A2153

* TAPS: Sigma T5130

* Tris base: Sigma T1503

* DTT: Melford MB1015

* Nutlin-3: Tocris 3984

MW = 590.5

* Fluorescently labelled p53 derived peptide (p53-F)

5-FAM-QETFSDLWKLLP-OH

MW = 1835.03

Custom synthesis by Biomatiks.

* Carboxy-fluorescein (Sigma Aldrich 447293)

MW = 376.33

* MDM2-N

MW = 15600

```
          20           30           40           50           60
DGAVTTSQIP ASEQETLVRP KPLLLKLLKS VGAQKDTYTM KEVLFYLGQY
          70           80           90          100          110
120
IMTKRLYDEK QQHIVYCSND LLGDLFGVPS FSVKEHRKIY TMIYRNLVVV NQQESSDSGT
         130
SVSENRCHLE
```

Sequence of His-tag with thrombin cleavage site at N-terminus of MDM2-N:

MGSSHHHHHHSSGLVPRGSH

His-tag MDM2-N was purified in University of Edinburgh. It was expressed from E. coli BL21 STAR strain. MDM2-N was purified using AKTA purifier. MDM2-N was loaded onto a 5ml Ni^{2+} HisTrap column followed by a polishing step through a S200 16/60 Gel filtration column.

A3.3 Preparation of stock solutions

*Always use siliconised pipette tips and siliconised vials when working with

p53-F and MDM2-N*

1mg/ml BSA

Dissolve 1.5mg of BSA in 1.5ml H_2O. Make up 1mg/ml BSA fresh every day.

100mM DTT

1M stock of DTT was prepared in Edinburgh by dissolving 5g of DTT into 32.4ml of H_2O. Aliquots of 1ml were prepared and frozen in -20˚C freezer. Thaw 1ml of 1M stock of DTT and dilute into 9ml of H2O (DTT f/c = 100mM concentration). Prepare aliquots of 8µl (~300 aliquots) and 105µl (~80 aliquots) and frozen in –80˚C freezer. 105µl aliquot will be used for adding into Running Buffer and 8µl aliquot will be used for adding into injection sample.

Working Buffer (200mM TAPS/Tris pH 8.0)

Weigh 4.87g TAPS and dissolve in 90ml UHQ H_2O and adjust pH to 8.0 by adding dry Tris base. Adjust final volume to 100ml with UHQ H_2O and filter using a 0.2µm syringe filter and store at room temperature. Working buffer can be stored for ~3 weeks after which a new working buffer should be made up.

Running Buffer (200mM TAPS/Tris pH 8.0, 1mM DTT)

Mix 9.9ml of working buffer with 100µl of 100mM DTT and store at room temperature.

Tris Buffer (200mM Tris pH 8.0) for diluting Carboxyfluorescein and peptide

Add 2.42g Tris base into 100ml UHQ H_2O and adjust pH to 8.0 using HCl. Filter buffer solution through 0.2µm syringe filter and stored at room temperature. Fresh Tris buffer should be re-made after ~4 weeks.

Preparation of p53-F stock

Use siliconised pipette tips and siliconised vials when working with p53-F.

Dissolve 1.5mg of p53-F in 400µl of 200mM Tris pH 8.0 (final concentration p53-F= 2.04mM). Store aliquots of 20µl in the dark at –80˚C freezer in siliconised vials.

Preparation of 150µM stock of p53-F

Dilute p53-F stock (20µl, 2.04mM) with buffer (252µl, 200mM Tris pH 8.0). Store aliquots of 10µl in siliconised tubes in the dark at –80˚C freezer. Prepare new aliquots from the stock (2.04mM) every 3-4 weeks.

Internal standard Carboxy-fluorescein (CarboxyF)

Dissolve 1mg of Carboxy-fluorescein in 1ml of DMSO (f/c 1mg/ml). 1mg/ml = 2.6mM. Dilute 2.6mM CarboxyF to 30µM by adding 4.6µl of 2.6mM stock to 395µl DMSO. Put 2.6mM and 30µM CarboxyF stock into a box and keep in the dark in the drawer at room temperature. New stock was made up after 4 weeks.

His tag-MDM2-N

Use siliconised pipette tips and siliconised vials when working with MDM2-N. Thaw frozen 1mg/ml MDM2-N (64µM) and dilute 1:1 (v/v) with 80% glycerol (f/c = 32µM). Final buffer solution contains 25mM HEPES pH 7.5, 50mM NaCl, 0.5mM DTT and 40% glycerol. Put aliquots (10µl) into siliconised tubes and keep in –80˚C freezer.

A3.4 CE setting:

The capillary was prepared using the following protocol:

Capillary: Polyvinyl alcohol (PVA) coated capillary as per Cetek method with 30cm total length, 50µm internal diameter. A capillary window (2mm) was cut at 10cm from the outlet end to the detection window. Set temperature of the coolant at 15˚C.

Inject: Outlet injection 0.5psi for 5sec.

Separation: Normal polarity (+ to -), 10kV for 6.50min.

Detection: Laser Induced Fluorescence (LIF) detector.

Excitation/emission: 488nm/520nm

Filter: Normal.

Dynamic range: 10 RFU.

Temperature: Sample tray 4˚C.

Inlet and Outlet trays 20-24˚C.

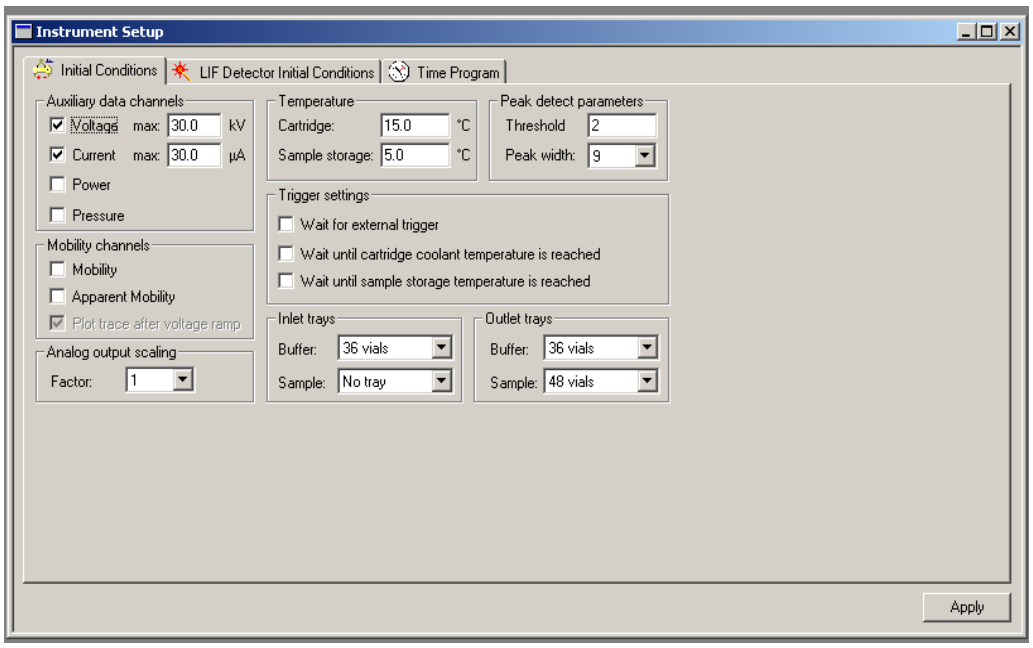

Initial condition set up

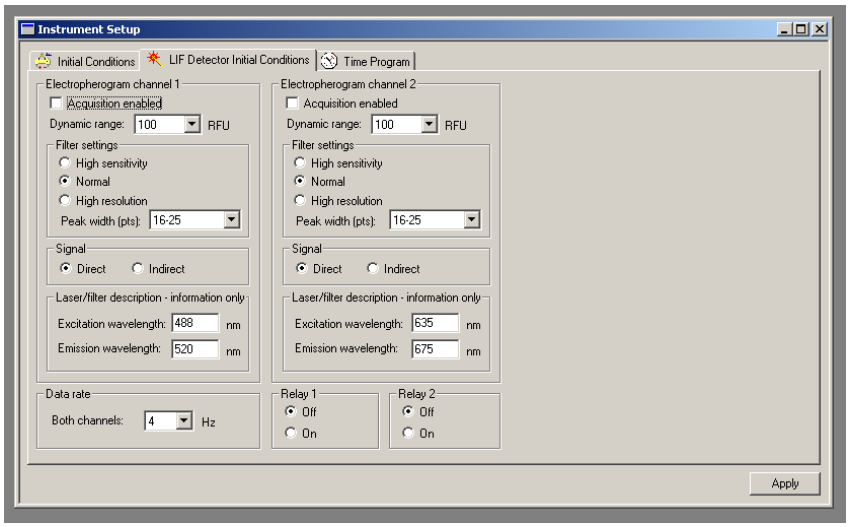

LIF Detection condition set up

A3.5 Coated capillary condition Run setup

Method and buffer tray set up for coated capillary condition method

BI = Buffer Inlet tray

BO = Buffer Outlet tray

BO: A2 – Waste vial (empty glass vial, red cap).

BO: A6 – Home position (Add 1.5ml filtered water into 2ml glass vial with red cap).

BI: A2 –Water rinse vial (Add 1.5ml filtered water into 2ml glass vial with red cap).

BI: A3 – Running buffer rinse vial (Add 1.5ml running buffer into 2ml glass vial with red cap).

BI: A6 – Home position (Add 1.5ml filtered water into 2ml glass vial with red cap).

Table of Inlet and Outlet Buffer Trays layout

6	Home					
5						
4						
3	RB					
2	H_2O					
1						
	A	B	C	D	E	F

Inlet Tray

Home					
Waste					

Outlet Tray

<u>Instrument set up for the coated capillary condition run</u>

1. Rinse with H_2O for 5min at 20psi pressure.
2. Rinse with running buffer for 10min at 20psi pressure.
3. Rinse with H_2O for 2min at 20psi pressure.

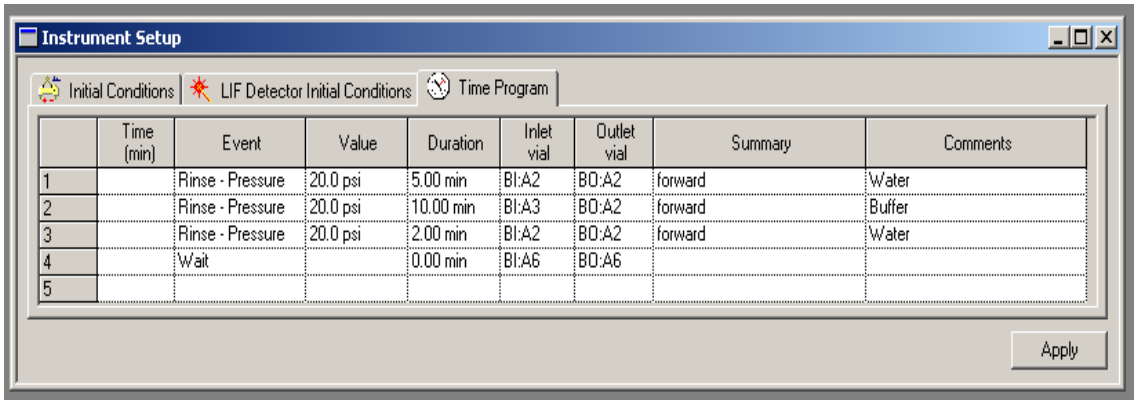

	Time (min)	Event	Value	Duration	Inlet vial	Outlet vial	Summary	Comments
1		Rinse - Pressure	20.0 psi	5.00 min	BI:A2	BO:A2	forward	Water
2		Rinse - Pressure	20.0 psi	10.00 min	BI:A3	BO:A2	forward	Buffer
3		Rinse - Pressure	20.0 psi	2.00 min	BI:A2	BO:A2	forward	Water
4		Wait		0.00 min	BI:A6	BO:A6		
5								

A3.6 Method and buffer tray set up for coated capillary p53-F control run method

<u>Dilution for CarboxyF</u>

Add 4µl of 30µM stock into 396µl of TB (200mM Tris pH 8.0) (f/c CarboxyF = 300nM). Dilute 10µl of 10nM stock into 290µl of TB (f/c = 10nM). Add 10µl of 10nM stock into 190µl TB (f/c = 500pM).

Dilution for p53-F

Using siliconised vials and tips, add 10µl of 150µM stock into 65µl Tris Buffer (f/c p53-F = 20uM). Add 10µl of 20µM into 390µl TB (f/c p53-F = 500nM). Add 4µl of 500nM stock into 396µl TB to get f/c = 5nM.

Buffer tray set up for p53-F control run

SO = Sample Outlet tray

SO: A2 – Injection sample (1mM TAPS/Tris pH 8.0, 1mM DTT, 10pM CarboxyF, 500pM p53-F). Cut the siliconised vials at 0.4ml mark position to be able to fit into plastic vial with spring. Add 1µl of Working Buffer, 2µl of 100mM DTT, 4µl of 500pM CarboxyF, 20µl of 5nM p53-F and make volume to 200µl by adding 173µl of H_2O.

BO: A6 – Home position (Add 1.5ml filtered water into 2ml glass vial with red cap).

BO: A3 – BSA rinse vial (Add 1.5ml of 1mg/ml BSA into 2ml glass vial with red cap).

BO: A1 – Water rinse vial (Add 1.5ml filtered water into 2ml glass vial with red cap).

BO: B1 – Running buffer rinse (Add 200µl running buffer into PCR vial and place in plastic vial with spring and grey cap).

BO: C2 – Separation buffer (200mM TAPS/Tris pH 8.0, 160nM MDM2-N, 1% DMSO, 0.2% Glycerol). Add 197µl of Working Buffer, 1µl of 32µM MDM2-N and 2µl of DMSO into siliconised vial and place in plastic vial with spring and plastic cap. Then transfer 100µl of this solution to vial in BI: C2 position as balance.

BI: C2 – Separation Buffer (200mM TAPS/Tris pH 8.0, 160nM MDM2-N, 1% DMSO, 0.2% Glycerol).

BI: E2 – Running Buffer balance (Add 200µl running buffer into PCR vial and place in glass vial with spring and grey cap).

BI: F2 – Waste vial (Add 0.75ml filtered water into 2ml glass vial with red cap).

Table of Inlet and Outlet Buffer Trays layout

Home					
		Separation Sample		RB	Waste

Home					
BSA					
		Separation Sample			
H_2O	RB				

Instrument set up for p53-F control run

1. Rinse with running buffer for 2min at 20psi pressure in reverse direction from BO:B1 vial to BI:F2 vial.
2. Rinse with separation sample for 1min at 20psi pressure to equilibrate capillary in reverse direction from BO:C2 vial to BI:F2 vial.
3. Inject sample from injection sample vial using pressure inject at 0.5psi for 5sec in reverse direction from SO:A2 vial to BI:E2 vial.
4. Separate sample at 10kV for 6.5min using normal polarity from BO:C2 vial to BI:C2 vial.
5. Rinse with H_2O for 0.5min with 20psi pressure in reverse direction from BO:A1 vial to BI:F2 vial.
6. Rinse with 1mg/ml BSA for 3min with 20psi pressure in reverse direction from BO:A3 vial to BO:F2 vial.

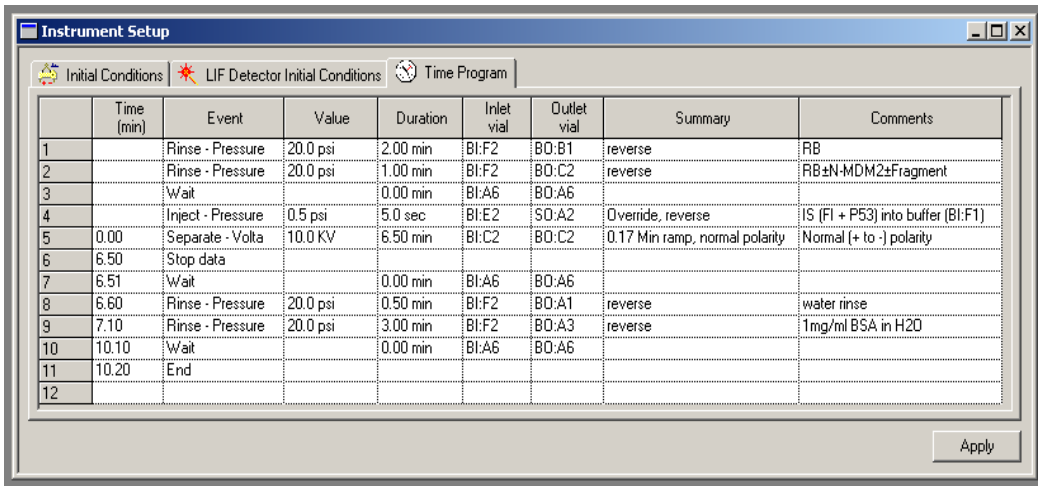

	Time (min)	Event	Value	Duration	Inlet vial	Outlet vial	Summary	Comments
1		Rinse - Pressure	20.0 psi	2.00 min	BI:F2	BO:B1	reverse	RB
2		Rinse - Pressure	20.0 psi	1.00 min	BI:F2	BO:C2	reverse	RB±N-MDM2±Fragment
3		Wait		0.00 min	BI:A6	BO:A6		
4		Inject - Pressure	0.5 psi	5.0 sec	BI:E2	SO:A2	Override, reverse	IS (FI + P53) into buffer (BI:F1)
5	0.00	Separate - Volta	10.0 KV	6.50 min	BI:C2	BO:C2	0.17 Min ramp, normal polarity	Normal (+ to -) polarity
6	6.50	Stop data						
7	6.51	Wait		0.00 min	BI:A6	BO:A6		
8	6.60	Rinse - Pressure	20.0 psi	0.50 min	BI:F2	BO:A1	reverse	water rinse
9	7.10	Rinse - Pressure	20.0 psi	3.00 min	BI:F2	BO:A3	reverse	1mg/ml BSA in H2O
10	10.10	Wait		0.00 min	BI:A6	BO:A6		
11	10.20	End						
12								

Coated capillary p53-F control run setup

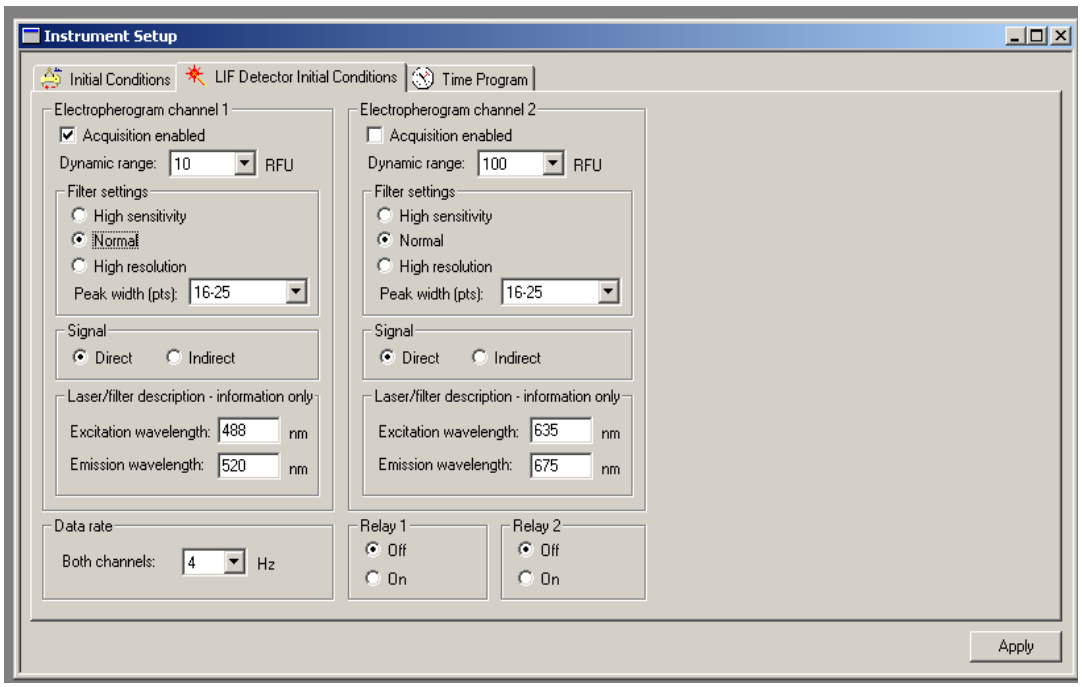

LIF Detector set up

A3.7 Method and buffer tray set up for coated capillary MDM2-N/fragment run method

Compounds stock

Make 100mM DMSO stock from ~1mg dry powder. Add 3µl of 100mM stock into 7µl DMSO (f/c compound = 300µM in 100% DMSO). Screen the fragments at 300µM as the initial screening concentration depends upon the compound solubility.

Buffer tray set up for MDM2-N/compound screening

SO: A2 – Injection sample (1mM TAPS/Tris pH 8.0, 1mM DTT, 10pM CarboxyF, 500pM p53-F). Cut the siliconised vials at 0.4ml mark position to be able to fit into the plastic vial with spring. Add 1µl of Working Buffer, 2µl of 100mM DTT, 4µl of 500pM CarboxyF, 20µl of 5nM p53-F and make volume to 200µl by adding 173µl of H_2O.

BO: A6 – Home position (Add 1.5ml filtered water into 2ml glass vial with red cap).

BO: A3 – BSA rinse vial (Add 1.5ml of 1mg/ml BSA into 2ml glass vial with red cap).

BO: A1 – Water rinse vial (Add 1.5ml filtered water into 2ml glass vial with red cap).

BO: B1 – Running buffer rinse (Add 200µl running buffer into PCR vial and place in plastic vial with spring and grey cap).

BO: C1 – Separation buffer (200mM TAPS/Tris pH 8.0, 160nM MDM2-N, 300µM compound, 1% DMSO, 0.2% Glycerol). Add 197µl of Working Buffer, 1µl of 32uM MDM2-N and 2µl of 30mM compound into siliconised vial and place in plastic vial with spring and grey cap. Transfer 100µl of this solution to a siliconised vial in BI: C2 position as balance.

BI: C2 – Separation Buffer (200mM TAPS/Tris pH 8.0, 160nM MDM2-N, 300µM compound, 1% DMSO, 0.2% Glycerol).

BI: E2 – Running Buffer balance (Add 200µl running buffer into PCR vial and place in plastic vial with spring and grey cap).

BI: F2 – Waste vial (Add 0.75ml filtered water into 2ml glass vial with red cap).

Table of Inlet and Outlet Buffer Trays layout

Home					
				Buffer	Waste
		Separation Sample			

Home					
BSA					
H_2O	Buffer	Separation Sample			

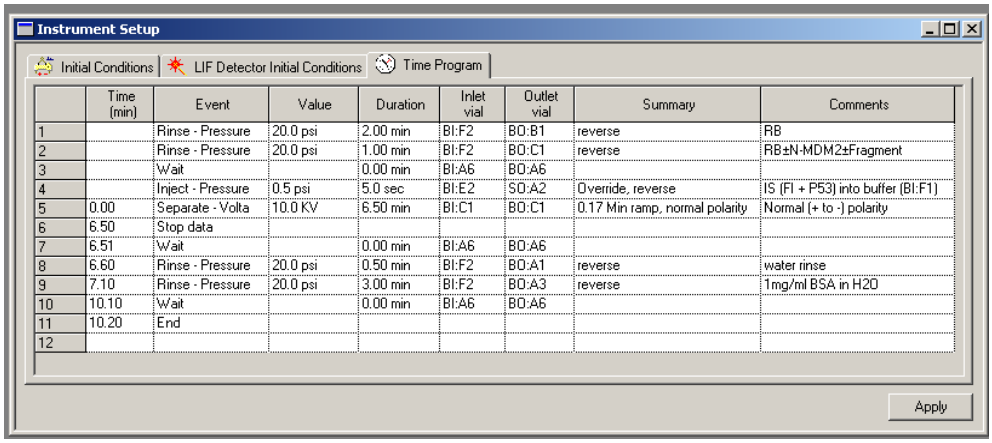

	Time (min)	Event	Value	Duration	Inlet vial	Outlet vial	Summary	Comments
1		Rinse - Pressure	20.0 psi	2.00 min	BI:F2	BO:B1	reverse	RB
2		Rinse - Pressure	20.0 psi	1.00 min	BI:F2	BO:C1	reverse	RB±N-MDM2±Fragment
3		Wait		0.00 min	BI:A6	BO:A6		
4		Inject - Pressure	0.5 psi	5.0 sec	BI:E2	SO:A2	Override, reverse	IS (FI + P53) into buffer (BI:F1)
5	0.00	Separate - Volta	10.0 KV	6.50 min	BI:C1	BO:C1	0.17 Min ramp, normal polarity	Normal (+ to -) polarity
6	6.50	Stop data						
7	6.51	Wait		0.00 min	BI:A6	BO:A6		
8	6.60	Rinse - Pressure	20.0 psi	0.50 min	BI:F2	BO:A1	reverse	water rinse
9	7.10	Rinse - Pressure	20.0 psi	3.00 min	BI:F2	BO:A3	reverse	1mg/ml BSA in H2O
10	10.10	Wait		0.00 min	BI:A6	BO:A6		
11	10.20	End						
12								

Coated capillary MDM2-N/fragment run set up

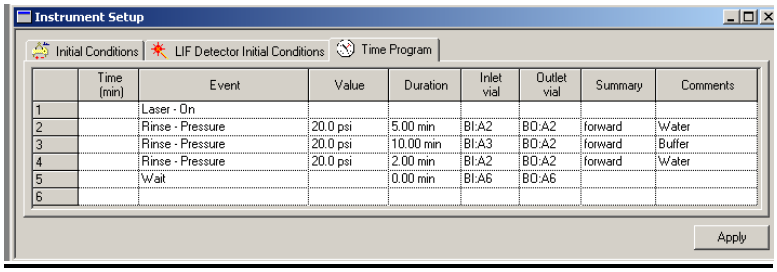

	Time (min)	Event	Value	Duration	Inlet vial	Outlet vial	Summary	Comments
1		Laser - On						
2		Rinse - Pressure	20.0 psi	5.00 min	BI:A2	BO:A2	forward	Water
3		Rinse - Pressure	20.0 psi	10.00 min	BI:A3	BO:A2	forward	Buffer
4		Rinse - Pressure	20.0 psi	2.00 min	BI:A2	BO:A2	forward	Water
5		Wait		0.00 min	BI:A6	BO:A6		
6								

Laser on method

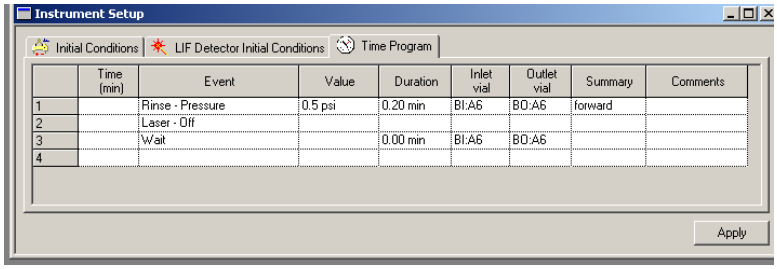

	Time (min)	Event	Value	Duration	Inlet vial	Outlet vial	Summary	Comments
1		Rinse - Pressure	0.5 psi	0.20 min	BI:A6	BO:A6	forward	
2		Laser - Off						
3		Wait		0.00 min	BI:A6	BO:A6		
4								

Laser off method

A3.8 Results

Calculation of % Inhibition

Percentage of inhibition will be calculated for each compound screen.

The equation used is:

% Inhibition = $100(T_H - T_L)/(T_H-T_R)$

T_H is migration time of p53-F peak in the presence of MDM2-N.

T_R is the migration time of p53-F peak.

T_L is the migration time of p53-F peak in the presence of MDM2-N + compound.

For example:

SEL101066 at 300μM has a migration time of 4.97min (T_L). The MDM2-N control peak migration time is 5.34min (T_H) and p53-F peak migration time is 4.37min (T_R).

To calculate % Inhibition of SEL101066:

% Inhibition = $100(5.34 - 4.97)/(5.34 - 4.37) = 38.1\%$

Criteria

<20% inhibition at 300μM	Weak hits
>20% inhibition at 300μM	Strong hits
>40% inhibition at 300μM	Very strong hits

Weak hits will not be evaluated further.

Titrations will be performed on the strong and very strong hits and the IC_{50} determined.

Quality control for MDM2-N CE runs

- Fresh buffer and filtered UHQ H_2O will be added into the vials every morning.
- A condition run should be carried out at the beginning of each day to wash the capillary and wash away anything left in the capillary.
- The laser should be switched on and left for 30min to allow the laser to warm up before starting the control run. This can be performed automatically by setting laser on method before operator arrives.
- Before starting to screen the fragments, CarboxyF/p53-F control run should be run in triplicate to make sure that the migration time, peak height and area are reproducible.
- MDM2-N control run should be run after confirming the CarboxyF and p53-F peaks were reproducible. The migration time of p53-F/MDM2-N peak, p53-F peak and CarboxyF peak will vary by ~0.2min. The migration time will also vary if changing capillary.
- After screening each compound, MDM2-N control should be run to make sure that the peak shifts back to the MDM2-N migration time.
- If screening a large number of compounds then additional control runs will be run at the start of a compound screen after every 4-5 compounds and at the end of compound screen to confirm that the peak shifts back to the MDM2-N migration time.
- At the end of the day, a condition run should be carried out to wash the capillary.
- Laser should be switched off at the end of the day using the laser off method.

A3.9 Troubleshooting

Indication of broken capillary/ reduced coating
Smeary peak present

This indicates the PVA coating in the capillary has probably deteriorated. Try a condition run followed by 10min rinse with BSA and 10min rinse with UHQ filtered H_2O. If this does not improve peak shape then a new capillary has to be installed.

Example of smeared peak

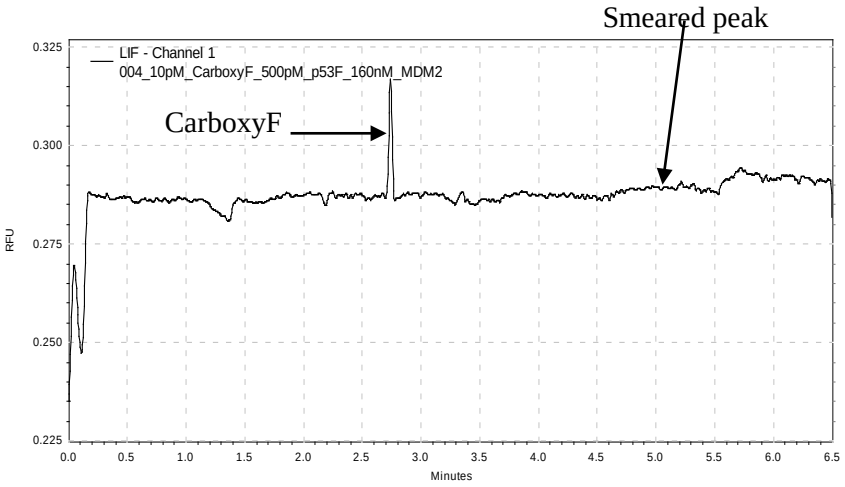

Check the current during control run.

Usually current error or a sudden drop in current if a capillary is broken. Check capillary window for a crack or sign of coolant leak.

What if the p53-F/ MDM2-N peak did not shift back?

During the compound screen, if the control p53-F/ MDM2-N peak did not shift back then extensive washing is required to remove any compound left in the capillary. Rinse capillary with 1mg/ml BSA at 20psi pressure for 5min followed by 5min rinse with UHQ filtered H_2O at 20psi pressure. Then rinse with running buffer at 20psi pressure for 2min.

What happens if the peak area is smaller than normal while running p53-F control run?

If the peak area is smaller than normal in the control run then repeat the control run continuously. It is possible the laser is still warming up and requires several control runs to regain the normal peak area. If necessary, repeat the run with fresh sample.

If this fail then try switch off the laser module and let the laser module to cool down for ~5-10min and switch on again and run the control to see if peak area becomes normal. The laser should be switched on before the operator arrives using automated method to turn laser on.

Appendix A4. Turbidimetric test

Turbidimetric solubility standard assay was carried out by Sarah to confirm the solubility of the compounds from 1mM to 0.0625mM.

Equiment: V-bottomed PP 96 well plate (Costar)

400ul flat bottomed clear 96 well plate (Matrix)

Heated plate shaker (Grant-Bio PHMP, Glas-Col LLC or equivalent)

SpectraMax M5

100mM DMSO stocks of test compounds (200ul)

100mM DMSO stocks pyrene & aspirin (200ul)

DMSO

Assay buffer

Tecan liquid handling system (optional)

1. Perform appropriate 100x f/c dilution series compounds in DMSO as per Table 2.1 Add DMSO to row A and B for use as blanks.

Table 2.1 Dilution series of compounds in DMSO

	Stock (mM)	Volume (ul)	DMSO (ul)	Stock final conc (mM)	Checksum
A	0	0	100	0	0
B	0	0	100	0	0
C	100	15	0	100	100
D	100	15	5	75	75
E	100	15	15	50	50
F	50	15	15	25	25
G	25	15	15	12.5	12.5
H	12.5	15	15	6.25	6.25

2. Add 247.5ul filtered assay buffer to all required wells.

3. Transfer 2.5ul 100x DMSO dilution series in triplicate into assay plates, note locations.

4. Seal plates with adhesive plate seal and ensure no gaps for evaporative loss. Shake the plate at 250rpm for ~18hours overnight.

5. After shaking, remove plate seal and check for any bubbles and remove if present.
6. Put the plate into SpectraMax M5 with 5sec pre-shake and read plate at OD_{650}.
7. Results were export to excel spreadsheet for analysis.

A4.1 Turbidimetric test result

	Solubility cut-off	Rank
SFL001290	0.75mM<x<1mM	High
SFL001675	> 2mM	High
SFL000577	> 2mM	High
SFL001303	0.75mM<x<1mM	High
SFL000829	> 2mM	High
SFL000134	> 2mM	High
SFL000576	> 2mM	High
SFL000866	> 2mM	High
SFL001502	> 2mM	High
SFL001397	> 2mM	High
SFL001328	> 2mM	High
SFL001542	> 2mM	High

	Solubility cutoff (mM)	Rank
2-Chlorophenothiazine	<0.0625	Low
Phenothiazine	0.0625<x<0.125	Medium
N-Phenyl-p-phenylenediamine	0.0625<x<0.125	Medium
2-Phenylamino-benzoic acid	>1	High
3-Hydroxydiphenylamine	0.25<x<0.5	High

	Solubility cutoff (mM)	Rank
SEL101069	>1	High solubility
4-Hydroxydiphenylamine	0.25<x<0.5	High solubility
Diphenylamine	0.75<x<1	High solubility
Phenoxazine	0.0625<x<0.125	Medium solubility

#	Compound:	Solubility cut-off:	Rank	Project:
1	Pyrene	<0.0625mM	Medium	Positive Control
2	Aspirin	>1mM	High	Negative Control
3	SEL101875	0.125mM<x<0.25mM	High	
4	SEL101876	0.125mM<x<0.25mM	High	
5	SEL101877	0.125mM<x<0.25mM	High	
6	SEL101878	0.25mM<x<0.5mM	High	
7	SEL101879	0.25mM<x<0.5mM	High	
8	SEL101880	>0.5mM	High	
9	SEL101881	0.125mM<x<0.25mM	High	
10	SEL101884	>0.5mM	High	

Appendix A5. CODASS hits titration against MDM2-N in the CE

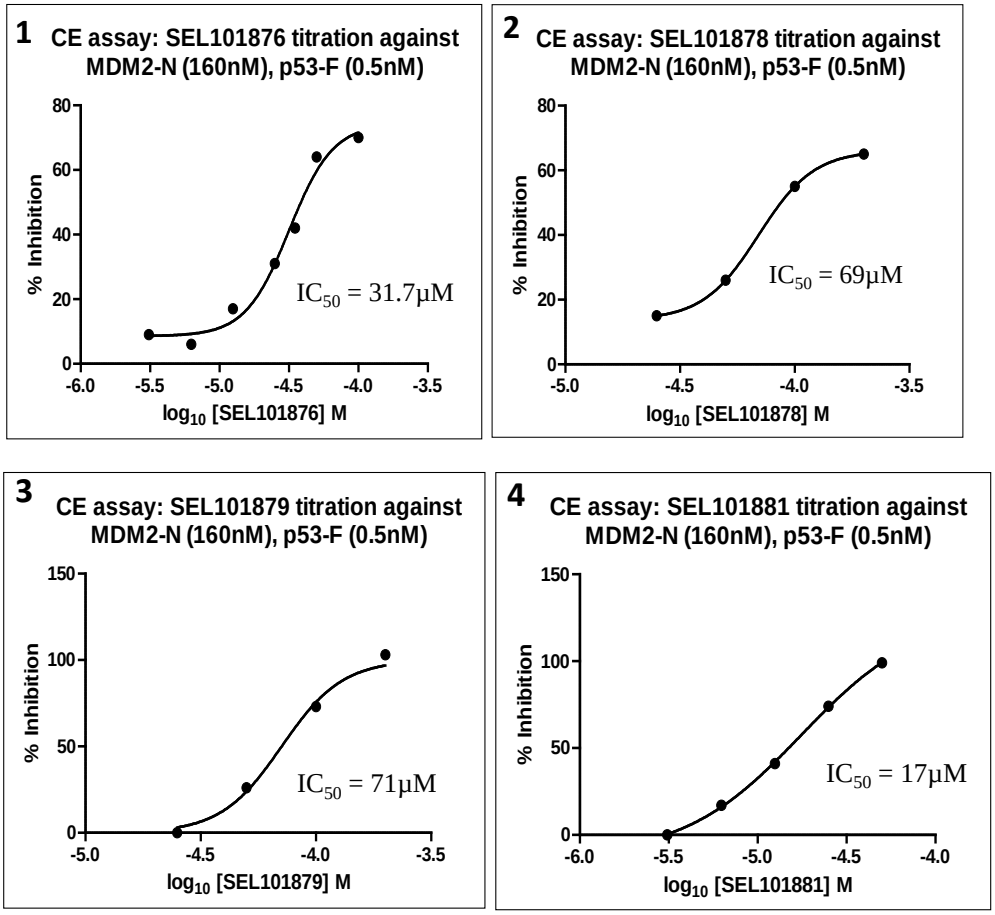

Titration was performed on four CODASS hits against MDM2-N using CE assay. The % inhibitions were fitted into the curve against compound concentrations in log scale. IC_{50} was determined for each hits.

Appendix A6. Crystal plates set up for MDM2-N^{11-130}

The crystal plates were set up using hanging drop method and SEL101266 and SEL101267 were co-crystallised with MDM2-N^{11-130}. The final concentration in the drop for MDM2-N^{11-130} and fragments are 5mg/ml and 1.6mM respectively.

The crystallisation conditions used are as follow:

PEG200	AS 60%	58%	56%	54%	52%	50%
4%						
3%						
2.5%						
2%						
1%						

54% saturated ammonium sulfate, 100 mM Tris, pH 7.8, 2.5 % PEG200, 50 mM glucose and 5 mM DTT.

	AS 1%	1.5%	2%	2.5%	3%	3.5%

2-2.2% ammonium sulfate, 100mM Bicine pH 9.5